# Understanding the Influence of Fluorine in Crystal Packing of Organic Molecules in the Presence and in the Absence of Other Strong/Weak Hydrogen Bonds: A Structural Analysis

*A thesis submitted for the Degree of*

**DOCTOR of PHILOSOPHY**

*By*

***Hare Ram Yadav***

*Department of Chemical Sciences*
*Indian Institute of Science Education and Research (IISER) Mohali*
*Sector 81, Knowledge City, S. A. S. Nagar, Manauli PO, Mohali, 140306*
*Punjab, India*

**July 2017**

*Dedicated to*

# My family…

# DECLARATION

The work presented in this thesis entitled "***Understanding the Influence of Fluorine in Crystal Packing of Organic Molecules in the Presence and in the Absence of Other Strong/Weak Hydrogen Bonds: A Structural Analysis***" has been carried out by me under the supervision of **Dr. Angshuman Roy Choudhury** in the Department of Chemical Sciences, Indian Institute of Science Education and Research (IISER) Mohali, Mohali.

This work has not been submitted in part or full for a degree, diploma or a fellowship to any other university or institute.

Whenever contributions of others are involved, every effort is made to indicate this clearly with due acknowledgements of collaborative work and discussions. This thesis is a bona fide record of original work done by me and all sources listed within have been detailed in the bibliography.

**Hare Ram Yadav**

Date: 28-07-2017
Place: IISER Mohali

In my capacity as the supervisor of the candidate's thesis work, I certify that the above statements by the candidate are true to the best of my knowledge.

**Dr. Angshuman Roy Choudhury**
*Assistant Professor*
*Department of Chemical Sciences*
*Indian Institute of Science Education and Research Mohali*

Date: 28-07-2017
Place: IISER Mohali

# ACKNOWLEDGEMENTS

*This thesis has been kept on track and been seen through to completion with the support and encouragement of numerous people including my well-wishers, my friends, colleagues and various institutions. At this moment of thesis submission, I would like to thank all those people who made this thesis possible and an unforgettable experience for me.*

*It is difficult to express my gratitude to my doctoral supervisor* ***Dr. Angshuman Roy Choudhury*** *for giving me this wonderful opportunity to explore the exciting field of X-ray crystallography and for inspiring me with his guidance to solve interesting research problems. I consider it as my distinct honour and rare privilege to express my deepest sense of gratitude to my venerable supervisor* ***Dr. Angshuman Roy Choudhury.*** *This project would never have been possible without his guidance.*

*I would like to acknowledge our director,* ***Prof. N. Sathyamurthy****, for providing the opportunity and all the research and infrastructural facilities at IISER Mohali to conduct my research without any hindrance.*

*I acknowledge IISER Mohali for central X-ray diffraction and NMR facilities. A special thanks to the X-ray facility committee members* ***Prof. Sanjay Mandal****,* ***Dr. Sanjay Singh*** *and* ***Dr. Angshuman Roy Choudhury*** *for their training and support during my initial days in IISER Mohali. I gratefully acknowledge the training received from* ***Dr. Kavita Dorai*** *to operate the NMR spectrophotometer.*

*I sincerely thank* ***Prof. K. S. Vishwanathan*** *for his continuous support, encouragement, and guidance in my difficult times in IISER Mohali. I also express my gratitude to* ***Prof. Ramesh Kapoor*** *for his continuous support and encouragement and all other faculty members of the Department of Chemical Sciences for facilitating the use of various departmental instruments including UV-VIS and FTIR spectrophotometers, DSC instrument, XtaLABmini table top X-ray diffractometer etc.*

*I would like to gratefully acknowledge continuous help, support and guidance of my doctoral committee members,* ***Dr. Santanu Kumar Pal*** *and* ***Dr. Sanjay Singh****, for fruitful*

*and encouraging discussions during the yearly assessment and also otherwise. I also acknowledge* ***Prof. P. Venugopalan*** *of Panjab University for his comments and suggestions during my SRF review meeting. I express my sincere appreciations for* ***Prof. T. N. Guru Row*** *for enriching my knowledge about crystallography during his short visit to IISER Mohali.*

*I thank* ***Dr. Sagarika Dev*** *for her support in theoretical calculations and encouragement and hospitality throughout my PhD journey.*

*I am grateful to* ***Dr. Deepak Chopra*** *and his students for collaborative work and useful discussions during meetings at various conferences.*

*My sincere thanks to* ***Dr. Gurpreet Kaur****, my laboratory senior for teaching me different aspects of research including single crystal data collection from Brukar and XtaLAB mini, PXRD recording using Rigaku diffractometer and for teaching me the data processing structure solution by using various software packages.*

*I thank* ***Mr. Maheswararao Karanam*** *for his management of the lab and lab notes, usage of different instruments and their software. I am also thankful to my current lab-mate* ***Dr. Prasanta Bhowmik*** *and* ***Mr. Mayank Joshi*** *for their help and cooperation. Other lab members, who were there in the lab for a one year project or summer project,* ***Shivcharan Dudi*** *and* ***Sandhya Singh Patel*** *are also acknowledged for the support and help for organic synthesis.*

*I also thank all the staff members of stores, purchase office, administrative office, account section, library, and computing facility of IISER Mohali for their help and co-operation. I would like to specially thank* ***Prof. Purnananda Guptasarma*** *for his help and support in resolving the matters related to my fellowship between IISER and UGC, without affecting my financial situations.*

*I take this opportunity to acknowledge all faculty members of BHU Varanasi, for their encouragement to pursue research.*

*I cannot forget the contribution of my school teachers towards building my character. My warm regards to them for their love, affection, and teaching during my school*

*days. Without their teaching and encouragement, it was not possible for a village boy like me to come to this stage of my life.*

*I sincerely acknowledge my parents* ***Mr. Ramdev Yadav*** *and* ***Mrs. Surashati Devi*** *for their care throughout my life for my welfare. I deeply express my gratitude to my elder brothers* ***Mr. Ramasharai, Ramashish*** *and* ***Radheshyam*** *and Sisters* ***Mrs. Lalmati*** *and* ***Bhanamati*** *for standing by me all the time in my life. I like to thank my wife* ***Mrs. Reena Yadav*** *and my* ***son*** *for their love, support, encouragement.*

*I can never forget all my friends to name a few for their constant support, encouragement, patience, love and affection for me. I thank my friends* ***Vinesh****,* ***Debmalya, Nayyar****,* ***Vinod Kumar, Ramniwas, Dinesh Singh*** *and* ***Shivshundar Yadav*** *for their cheerful companionship.*

*I acknowledge* ***MHRD****,* ***India*** *for research fellowship and* ***IISER Mohali*** *for financial support to carry out my experimental work and for providing all the research facilities that enabled me to complete my Ph. D in time.*

# SYNOPSIS

The thesis entitled "***Understanding the Influence of Fluorine in Crystal Packing of Organic Molecules in the Presence and in the Absence of Other Strong/Weak Hydrogen Bonds: A Structural Analysis***" consists of **four chapters**. **Chapters 1** is a brief introduction to the field of intermolecular forces including the conventional strong and weak hydrogen bonds, other weaker interactions like C–H···π and π···π, and interactions involving halogens like C–H···X, C–X···X, and C–X···π (X = F, Cl, Br). **Chapter 2** evaluates the importance of organic fluorine in altering the crystal packing in the presence of strong N–H···O hydrogen bond in a series of *mono and di-fluorinated phenylacetamides*. **Chapter 3** describes the structural features of *tetrafluoro N-[2-(3-methoxyphenyl)ethyl]benzamide*, in the absence of strong N–H···O hydrogen bond but with the possibility of weak C–H···O=C hydrogen bonds. **Chapter 4** depicts the structural variations in *tetrafluoro* derivatives of *diphenyl tetrahydroisoquinolines* in the absence of strong hydrogen bonds like N–H···O hydrogen bond and weak hydrogen bonds like C–H···O=C.

The intermolecular interactions are responsible for the state of existence of a compound at a given temperature and pressure. A combination of strong and weak intermolecular forces is known to dictate the physical properties of various compounds and materials. Therefore, the understanding of such forces is necessary to understand the properties of materials and compounds. Strong and weak hydrogen bonds are well known in the literature and its influence in guiding crystal structure has been established beyond doubt. The understanding of the role of weaker interactions in controlling the crystal packing is still a gray area in crystal engineering. Especially, the influence of fluorine in in small organic molecules in guiding the packing leading to its crystallization has remained controversial, though few studies to understand the interactions involving fluorine have been made in the past. The systematic analysis of weak interactions involving *organic fluorine* based on three different but related molecular systems of *fluorinated* organic molecules is the theme of this thesis. The selected molecular framework allows us for the

evaluation of the effect of the changes of the number and the position of fluorine substitution in the aromatic rings on the crystal packing. Based on this molecular structure, we are interested to systematically analyze the much weaker and hence considered insignificant intermolecular interactions like C–H···F, C–F···F–C, and C–F···π etc. A brief introduction to strong and weak interactions is provided in the **Chapter 1** of this thesis.

**Chapter 2** describes the structural analyses of ten molecules (derivatives of phenylacetamide) contain a strong hydrogen bond donor (N–H group) and a strong hydrogen bond acceptor (O=C group) in addition to one or two C–F groups and a –OMe group (Scheme 1). The role of C–F group(s) in altering the crystal structures of these molecules in the presence of strong conventional N–H···O=C hydrogen bond has been illustrated in this chapter. The influence of aromatic fluorine in bringing structural variation in these molecules has been highlighted.

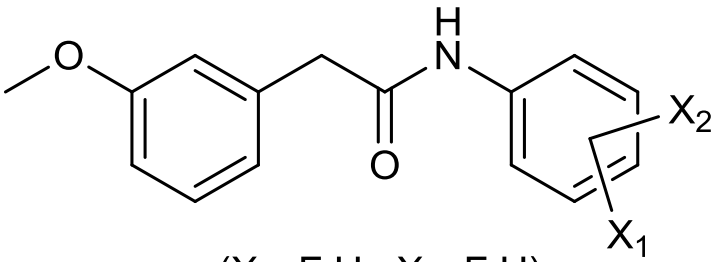


($X_1$=F,H ; $X_2$=F,H)

Scheme 1.1

**Chapter 3** illustrates the structural features arising due to the presence of four C–F groups in the molecule in the presence of C=O and –OMe groups as hydrogen bond acceptors without the strong donor like N–H group (Scheme 2). These structures highlighted the cooperative effects of weak hydrogen bonds (C–H···O=C, C–H···OMe and C–H···F–C), C–H···π and halogen···halogen (C–F···F–C) interactions. Various supramolecular synthons have been identified and rationalized in the thesis.

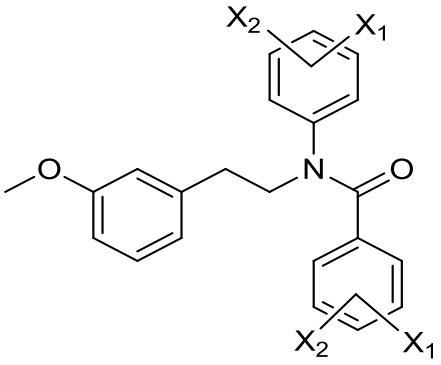


($X_1$=F,H ; $X_2$=F,H)

Scheme 1.2

**Chapter 4** encompasses the structural variations of *tetrafluoro* derivatives of *diphenyl tetrahydroisoquinolines* (Scheme 3). These molecules are devoid of any strong hydrogen bond donor like N–H group and strong hydrogen bond acceptor like a C=O group. Therefore, crystal structures of all the compounds are governed majorly by weak interactions involving fluorine (C–H···F–C and C–F···F–C) and a few weak hydrogen bonds like C–H···OMe and much weaker C–H···π interaction(s). Based on the observed structural features an attempt has been made to rationalize the interactions involving fluorine in the absence of strong hydrogen bonds in this chapter.

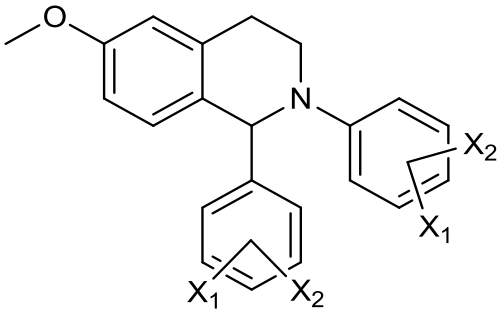


($X_1$ = $X_2$ = F, H)

Scheme 1.3

In addition to the above chapters, **Appendix** contains the structural analyses of *trifluorinated phenylacetamides* and *tetrafluorinated* bridge-flipped isomeric *bis-benzylidineanilines*, which are closely related to the compounds reported in the thesis.

# Contents

# Chapter 1

## Intermolecular interactions

# Chapter 1

## 1.1 Overview of Intermolecular Interactions

The intermolecular interactions are responsible for physical and chemical properties of all the materials in any state of its existence. Intermolecular interactions and molecular recognition patterns are important aspects to understand the physical properties of mater in the gaseous, liquid and most importantly in the solid state. Intermolecular interactions range from very strong (15-40 kcal/mol) to strong hydrogen bonds (4-15 kcal/mol), to weak (1-4 kcal/mol) and very weak (<1 kcal/mol) hydrogen bonds, interactions involving π systems, and as weak as van der Waals' interactions.[1] Very strong hydrogen bonds are known to play a significant role in determining the physical properties of molecular compounds. HF exists as liquid at ambient temperature due to very strong ···H–F···H–F··· hydrogen bonds while HCl is a gas under similar conditions due to weaker hydrogen bonds than in HF. Similarly, $H_2O$ is liquid while $H_2S$ is gas at ambient conditions of temperature and pressure as the hydrogen bond in water is much stronger than those in $H_2S$. Therefore, the nature of hydrogen bond and the stability that is gained by a strong hydrogen bond is the key feature in the determination of physical properties of mater.

Hydrogen bonds were first characterized by Linus Pauling in 1939.[2] Though the definition of hydrogen bond has been modified,[3] the most widely accepted definition of hydrogen bond by Pauling[2] reads as

*"A hydrogen bond is an interaction that dictates association of a covalently bound hydrogen atom with one or more atoms, groups of atoms or molecules into an*

*aggregate structure that is sufficiently stable to make it convenient for the chemist to consider it as an independent chemical species."*

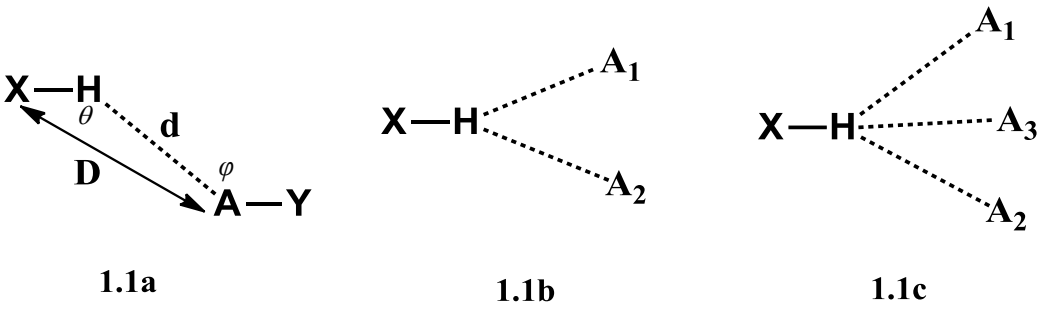


**1.1a** **1.1b** **1.1c**

**Figure 1.1: (a)** Hydrogen bond with one acceptor. **(b)** Bifurcated hydrogen bond with two acceptors. **(c)** Trifurcated hydrogen bond with three acceptors.

The group X–H in a hydrogen bond is termed as the hydrogen bond donor and the group A–Y is called as an acceptor. The physical parameters *D*, *d* and $\theta$ define the geometry of a hydrogen bond (Figure 1.1). In the past, before the advancement in the X-ray diffraction techniques, the hydrogen atom position could not be ascertained or located by X-ray diffraction data. Therefore, in those days, the parameter 'D' was used to determine the geometry of hydrogen bonds.[4] The parameter *d* has gained importance recently after the advancement in X-ray diffraction data collection techniques and in conjunction with neutron diffraction experiments, wherein, it became possible to locate the position of H atoms with a reasonable degree of accuracy and is more talked about than *D*. The hydrogen bonds can be of two, three or four center hydrogen bonds[1] as shown in figure 1.1. These are called bifurcated/trifurcated hydrogen bonds. This bifurcation/trifurcation may be observed at both the acceptor and donor sites.

The definition of hydrogen bond has been modified a few times in the past and the definition by Pimentel and McClellan[5] does not enforce any restriction on the nature of the donor and acceptor groups and the definition reads as

*"A hydrogen bond is said to exist when (1) there is evidence of a bond, and (2) there is evidence that this bond sterically involves a hydrogen atom already bonded to another atom."*

As this definition involves van der Waals' contact within its limit, which is also a bond and may involve hydrogen in it this definition needed further

modification. Steiner and Saenger redefined hydrogen bond as "Any cohesive interaction where H carries a positive charge and A, a negative charge (partial or full) and the charge on H is more positive than on X" in 1993.[6]

The most recent and widely accepted definition of the hydrogen bond[7] reads as

"*'The hydrogen bond is an attractive interaction between a hydrogen atom from a molecule or a molecular fragment X–H in which X is more electronegative than H, and an atom or a group of atoms in the same or a different molecule, in which there is evidence of bond formation*."

This definition un-restricted about the nature of atoms involved, their strength and the evidences of hydrogen bond formation. Therefore, this definition is broad and it encompasses different kinds of hydrogen bonds. Hydrogen bonds can be classified in many ways, but, in view of physical properties, these can be differentiated in terms of their stabilization energies as very strong, strong and weak hydrogen bonds.[1] The tables 1.4 and 1.5 of the book entitled "The Weak Hydrogen Bond In Structural Chemistry and Biology" by Desiraju[1] summarized the properties of different kinds of hydrogen bonds.

### 1.2 Hydrogen Bonds in the Solid State Chemistry

Supramolecular assemblies in solution and in the solid state are generally guided by various very strong and strong hydrogen bonds (O–H···O, N–H···O, N–H···N, O–H···N). The highly directional nature and large negative stabilization energy make them predictable often.[8] These hydrogen bonds are regarded as "strong" and "directional" because of higher stabilization energy (4-15 kcal/mol) and the angle $\theta$ (Figure 1.1) becoming close to 180$^{o}$. Various supramolecular assemblies, also termed as synthons by Desiraju, have been designed based on the strength and directionality of these strong hydrogen bonds.[9] Development of various co-crystals[10] based on these strong hydrogen bonds are known in the literature.[11] But, the manipulation of supramolecular organization of small organic molecules in a crystals lattice through weak hydrogen bonds (C–H···O=C, C–H···O–C, C–H···N, C–H···F–C etc.) is non-trivial. The uncertainty associated with the various possible modes of association of molecules through weak hydrogen bond donors and acceptors results in different supramolecular assemblies under various experimental conditions. As the

stabilization energy of weak hydrogen bond is generally < 4 kcal/mol, they offer a variety of different geometrical possibilities for the formation of supramolecular synthons.[12] These weak hydrogen bonds are usually electrostatic in nature and are directional to some extent based on the acceptor. Due to lower stabilization energy, their directionality can be influenced by the availability of other interactions offered by some other active functional grope(s) present in the concerned molecule.[13] The necessity in considering intermolecular interactions through weak and very weak hydrogen bonding may seem unimportant, but the cumulative contribution of a large number of weak intermolecular interactions in building a crystalline architecture cannot be refuted, even though the individual contribution of such interactions may be small while calculating the stabilization energy. Hence their influence in altering the crystal structures can become useful in various cases. A number of studies have been reported in the literature exploring and explaining more about their utilization in the field of solid state chemistry. Desiraju in 2002 have classified these interactions as weak donor and strong acceptors (C–H···O, P–H···O, C–H···N), strong donors and weak acceptors (O–H···F–C, N–H···F–C, O–H···π, N–H···π), and weak donor and weak acceptors C–H···F–C, C–H···Cl–C.[14]

The C–H···O hydrogen bonds were first identified by Glasstone[12(a)] in 1937, while studying the reasons for unusual physical properties of the mixture of chloroform with acetone. This was illustrated by the directional electrostatic hydrogen bond like interactions as shown in the figure 1.2.

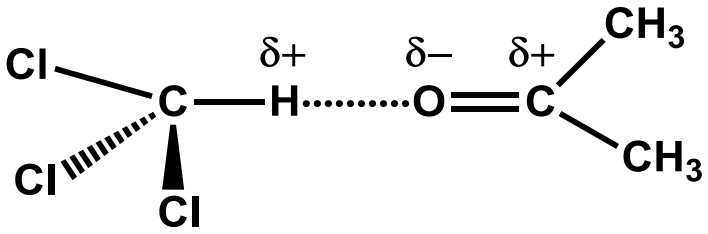


**Figure 1.2**: C–H···O interactions described by Glasstone. This figure has been re-drawn based on the figure from reference no. 12(a).

Since then a large number of research groups across the world have explored extensively the role of this type of weak interaction in building crystal lattices.[12] Taylor and Kennard[12(g)] utilized Cambridge Structural Database (CSD)[15] to study weak hydrogen bonds based on 113 high quality organic crystal structures determined

by neutron diffraction. These studies elucidated the evidences for the attractive nature of C–H···N, C–H···Cl, C–H···O and C–H···S contacts and termed these as hydrogen bonds. The importance of such hydrogen bonds has been illustrated elaborately in the recent literature.[16] The significance of these hydrogen bonds (C–H···X (X = O, N, S, Cl) in supramolecular chemistry,[17] crystal engineering[18] and in biological systems[19] has been well documented.

### 1.3 Weak interactions involving π acceptor

The weak hydrogen bonds involving strong donor (O–H, N–H etc.) and π acceptors (π = Ph, C=C, C≡C) have been illustrated in the past.[20] Whether the C–H···π interactions having a very weak donor like C–H group should be designated as hydrogen bond or not has been debated in the past.[21] It has been demonstrated that C–H···π interactions have structure directing ability based on the acidity of the proton on the C–H group. These interactions are just strong enough to alter or modulate the conformation of molecules and packing modes in 3D in the organic solids. The C–H···π interactions have been systematically investigated by Nishio and Hirota to establish its involvement in molecular recognition.[22] Nishio demonstrated that the influence of C–H···π interactions don't reduce rapidly with distance unlike the hydrogen bonds and their effect is observed much beyond the van der Waals' radii cut-off limit.[23] The significance of C–H···π interactions in controlling the shape (conformation) and packing of molecules has been highlighted in a review by Nishio.[24] The important role played by these interaction to stabilize the peptides is also documentd.[25] C–H···π interactions is a significant factor in stabilizing the 3D structure of proteins,[26] in the field of optical and electronic devices,[27] supramolecular chemistry,[28] and drug designing.[29] In addition to these C–H···π interactions, instances of C–F···π interactions in organic and biological molecules have also been demonstrated.[30]

### 1.4 Weak interactions involving halogens

The C–X (X = F, Cl, Br or I) bonds are expected to be reasonably polar because of the high electronegativity of the halogens. Heavier halogens (Cl, Br and I) are reported to form short intermolecular contacts with electron donors as well as

electron acceptors.[31] The anisotropic distribution of electron density around the C–X bond is thought to be responsible for this feature. Theoretical calculations and experimental evidences indicated that the electrostatic potential around heavier halogen atoms (Cl, Br, I) is electropositive along the C–X bond and electronegative in its perpendicular direction, while it remains negative everywhere around the C–F bond.[32] Therefore, it is expected that an electron acceptor will approach the C–X (X = Cl, Br, I) group in a perpendicular direction to the C–X bond, and an electron donor will interact along the C–X bond. Hence, halogen will interact with nucleophiles in a nearly linear geometry, while interactions with electrophiles will occur in side on manner (figure 1.3).[33] consequently, these groups (C–X) should be very good acceptors of hydrogen bond in a C–H···X–C interaction in the electrophilic direction of C–X bond.[33f] However, the formation of C–H···Cl hydrogen bonds has always been debated,[34] while van den Berg and Seddon[35] based on CSD analysis have indicated the role of C–H···X hydrogen bonds in the crystal packing.

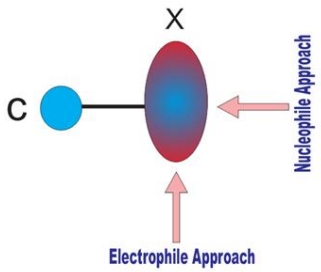


**Figure 1.3:** Direction for the approach of nucleophile and electrophile in a C–X bond. This figure has been re-drawn based on the figure from reference number 33(e).

The presence of both electron deficient and electron rich sites over the C–X bond offers the possibility of interhalogen bonding. Sakurai *et al.*, proposed the geometrical categorization of C–Cl···Cl–C interactions in 1963 as type I and Type II.[36] Ramasubbu *et al.*,[37] later characterized the inter halogen interactions of the type C–$X_1$···$X_2$–C, into three types based on the two angles $\theta_1$ and $\theta_2$, where $\theta_1$ = ∠C–$X_1$···$X_2$ and $\theta_2$ = ∠$X_1$···$X_2$–C.

- *Type I* inter halogen interactions, $\theta_1$ or $\theta_2$ = 90°,
- *Type II* inter halogen interactions, $\theta_1$ or $\theta_2$ = 180° and

- *Type III* inter halogen interactions, $\theta_1 = \theta_2$ and the two halogen atoms are related by crystallographic center of inversion.

Later Desiraju and Parthasarathy, categorized C–$X_1$···$X_2$–C contacts were in a simpler manner into two types[38] (figure 1.4) as

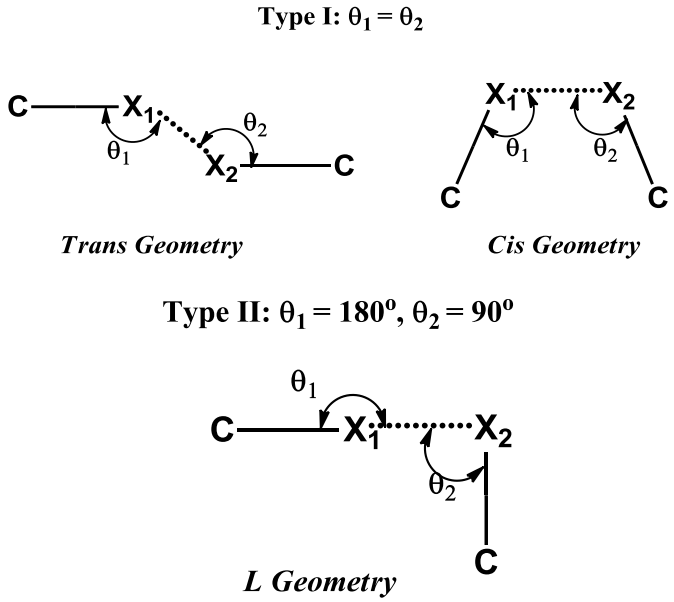


**Figure 1.4:** Different possible geometries through which halo···halo interactions are possible. Figure has been re-drawn based on the figure from reference number 37(b).

- *Type I* (cis or trans geometry) and
- *Type II* (L geometry)

Recently, Thotadi *et al*., proposed homohalogen (X···X) contacts to be of three types based on their CSD analysis on such contacts.[39] Their new classification criterion is based on the difference between angles $\theta_1$ and $\theta_2$, as identified in the Figure 1.4.

- $0° \leq |\theta_1 - \theta_2| \leq 15°$ -contacts will be classified as *type I*,
- $30° \leq |\theta_1 - \theta_2|$ -contacts will be classified as *type II*,
- $15° \leq |\theta_1 - \theta_2| \leq 30°$-contacts will be classified as *quasi type I/type II* interactions.

The X···X interactions involving heavier halogens (X = Cl, Br, I) have demonstrated to be significant in crystal engineering.[40] The review by Metrangolo *et*

*al*., published in 2008 described in-depth understanding of halogen bonding interaction in terms of energetic and geometric requirements, donor and acceptor characteristics, their importance in building various 1D, 2D and 3D architectures to form supramolecular assemblies and their importance in material and biological Chemistry.[40(e)]

Therefore it has been accepted that interactions involving halogens are significant in the crystal packing both in the absence as well as in the presence of other relatively stronger intermolecular interactions.[41]

Among the halogens, apparently, fluorine is reported to behave differently in solution and in the solid state. The low polarizability and small size of fluorine compared to other halogens is believed to be responsible for this different behaviour. While other halogens mostly preferred to interact through $C–X_1\cdots X_2–C$ interactions or R–X···Y (X = Cl, Br, I; Y = O, N, S) halogen bond, but F preferably interacts through C–H···F hydrogen bond.[42] Hence, the interactions involving F are treated separately in the literature.

### 1.5 An Outline on Interactions Involving Fluorine

Fluorine being the most electronegative element in the periodic table, it offers strongest hydrogen bonds as is seen in HF. The single bond between C and F is the strongest among all such bonds C and any other element. Therefore, the substitution of H by F in an organic compound introduces significant changes in its physical properties (melting and boiling points, refractive index, surface tension, lipophilicity, acidity, basicity etc. to name a few) as well as its chemical reactivity.[42] Due to the unusual behaviour of F when introduced in a compound, Schlosser[42(a)] has commented about F in his article as:

"*Fluorine leaves nobody indifferent; it inflames emotions be that affections or aversions. As a substituent, it is rarely boring, always good for a surprise, but often completely unpredictable*."

This comment about F is also valid for intermolecular interactions involving F. Fluorine bonded to a carbon was termed as 'organic fluorine',[43] by Dunitz and the intermolecular interactions offered by a C–F group have remained controversial in the literature.[41,43] But, it is very important to understand them due to its crucial role not

only in the crystal packing, but also in protein-ligand interactions.[44] The inherent nature of C–H···F hydrogen bond makes it important and interesting to explore further. Several studies have been done to analyse and understand the impact of interactions involving 'organic fluorine' in the crystal packing.

In a tutorial review, O'Hagan explained the fundamental aspects related to the C–F bond and explored the rationale for the geometry conformation and reactivity of fluorinated organic compounds.[45]The consequence of high electronegativity of fluorine leads to the polarization of the C–F bond thereby making it less covalent and more electrostatic in nature. This offers relatively large dipole-dipole interaction in fluorinated organic compounds and hence these can be interprets as electrostatic interactions. But, unexpectedly the polarised C–F bond does not have good donor ability as the three lone pairs of electrons on fluorine are tightly held because of high electronegativity of F. Unlike O and N, the lone pairs of F are reluctant to participate in resonance and act as hydrogen bond acceptor. O'Hagan also pointed out in 2008 that the X–H···F–C (X = O, N) hydrogen bonds are less frequent and are about 75% weaker strength compare to the corresponding X–H···X–C (X = O, N) hydrogen bonds.

A tutorial review by Berger *et al,*. published in 2011 indicated the importance of fluorinated organic compounds in the enhancement of various useful properties of such materials.[33f] The author summarised the importance of C–F group in the crystal engineering in the view of various weak intermolecular interactions like $\pi\cdots\pi_F$, C–F···F–C, C–F···H–C, C–F···$\pi$, C–F···$M^+$, C–F···C=O and anion···$\pi$ etc.

The intermolecular interactions involving fluorine has been in the forefront of structural studies since 1990s. Shimoni and Glusker in 1994 through their CSD analysis based on a hand full number of crystal structures of fluorinated molecules inferred that X–H···F–C interactions are very weak and hence insignificant, compared to the C=O···H–X interactions.[46] Dunitz and Taylor in 1997 also denied the significance of these interactions in crystal packing based on their combined CSD and *ab-initio* studies and claimed that "Organic Fluorine Hardly Ever Accepts Hydrogen Bonds".[43(a)] Howard *et al*., at the same time once again used the poorly populated CSD had stated that "the predominant C–F···H–C contacts in the Database appear to have very little significance in energy terms and are essentially van der Waals'

complexes".[47] In 1998, for the first time, C–H···F–C hydrogen bonds received due recognition in crystal packing through the report by Thalladi *et al*., based on their systematic structural study on fluorobenzenes.[48] They indicated that the C–H···F–C interactions can be as important as the C–H···O or C–H···N hydrogen bonds for structure directing abilities to pack molecules in a particular array in its crystal structure.[48] After this, a number of studies have been done on different fluorinated model systems like indole derivatives,[49] isoquinolines,[50] halogenated benzamides,[51] and also with trifluoromethyl group as a substituent,[52] aromatic azo compounds,[53] *N*-benzylideneanilines[54] and many more to elucidate the importance of fluorine mediated interactions in crystal packing. Through all these studies, it can be concluded that C–H···F interactions are weak hydrogen bonds and these can be utilized for building a supramolecular architecture.

Recently we have conducted a search for X–H···F–C (X = O, N) hydrogen bonds with the H···F distance ranging between 1.8 Å and 2.7 Å and ∠X–H···F ranging between 90° and 180° using the 2017 edition of the CSD restricted to only covalent structures with R factor less than 10%, without disordered molecule, only with organic molecules and without polymers.[55] The number of such interactions involving O–H donor has been found to be only 296 (121entries for distance range 1.8-2.5 Å) while the same involving N–H donor is 425 (207 entries for the distance range 1.8-2.5 Å). Unlike conventional strong hydrogen bonds, the preference for ∠X–H···F in case of these interactions are found to be centred between 130° and 160° (Figure 1.5) for shorter contacts (d = 1.8-2.5 Å).

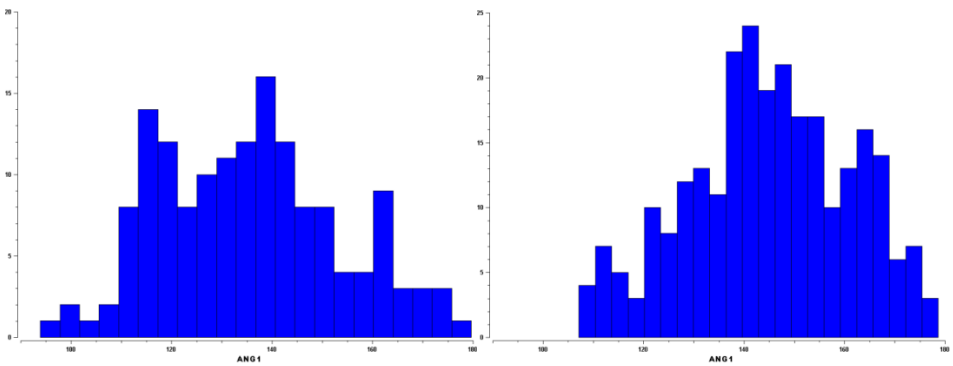

**(a)** **(b)**

**Figure 1.5**: (a) Histogram of ∠O–H···F–C for contacts with d = 1.8-2.5 Å, (b) Histogram of ∠N–H···F–C for contacts with d = 1.8-2.5 Å.

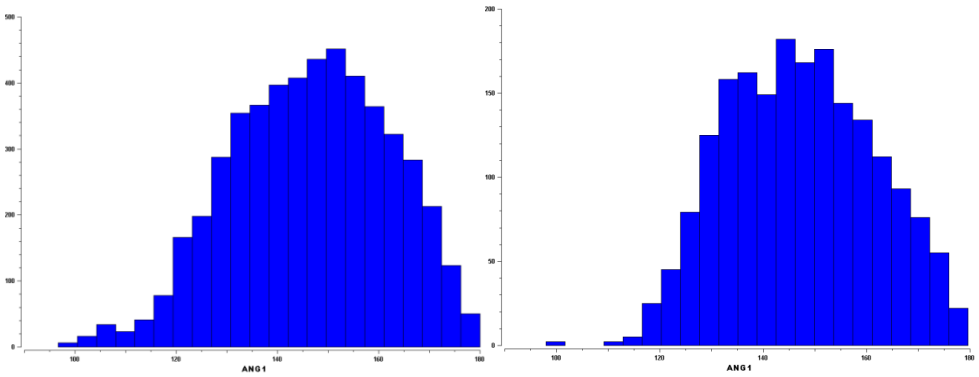

**Figure 1.6**: (a) Histogram of ∠C–H···F–C for contacts with all C–H irrespective of the hybridization of the C atom d = 1.8-2.5 Å, (b) Histogram of ∠C–H···F–C for contacts with aromatic C–H groups and d = 1.8-2.5 Å.

A similar search for C–H···F–C hydrogen bonds have been also done using the same search criteria in the 2017 version of CSD. The number of hits of such interactions involving C–H groups irrespective of the hybridization of the C atom is 12157 (3643 entries for d = 1.8-2.5 Å), 6786 entries for aromatic C–H groups (1575 entries for d = 1.8-2.5 Å), and 26 entries with acetylinic C–H groups (10 entries for d = 1.8-2.5 Å). The histograms provided in the figure 1.6 clearly show that these interactions with d = 1.8-2.5 Å indicates the preference for the ∠C–H···F–C between 140-160$^{o}$. These observations probably indicate that the directional preference for fluorine mediated hydrogen bonds is centred around $\theta$ = 150$^{o}$ and fluorine prefers aromatic and sp$^{2}$ hybridised C–H groups for the formation of C–H···F–C hydrogen bonds.

Although the interaction between two heavier halogens is accepted in the literature, whether the short F···F contacts are attractive or repulsive in natures and whether they are at all significant or not in altering the crystal packing or these are merely the result of close packing, is yet to be confirmed. The statistical survey by Desiraju and Partasarathy have claimed that X···X interactions are attractive in nature except the F···F interactions.[38(a)] Generally these contacts are considered to be the consequence of close packing and hence ignored.[56] Choudhury *et al*. has also emphasized the importance of F···F contacts in the structural analysis of a series of fluorine substituted Isoquinolines.[50(a)-(b)] We have also conducted a database search on the short C–F···F–C contacts with the F···F distance ranging between 1.80 Å and 2.96 Å and ∠C–F···F ranging between 90$^{o}$ and 180$^{o}$ using the 2017 edition of the

CSD restricted to only covalent structures with R factor less than 10%, excluding the disordered molecule, among only organic molecules and without polymers. The number of hits of such interactions involving C–F groups irrespective of the hybridization of the C atom is 4199 (1942 entries for aromatic C–F groups). It is interesting to note that the number of hits with two angles, namely ∠C–F···F ($\theta_1$) and ∠F···F–C ($\theta_2$) being equal ($\theta_1 = \theta_2$) is only 194 (484 with the criteria $0° \leq |\theta_1 - \theta_2| \leq 15°$) irrespective of the hybridization of the C atom while 237 entries belong to type II based on the criteria $30° \leq |\theta_1 - \theta_2|$ and 3478 entries belong to quasi Type I/Type II ($15° \leq |\theta_1 - \theta_2| \leq 30°$). This indicates that the F···F contacts do not prefer to be of the type I or type II rather they prefer to form quasi Type I/Type II contacts. This observation is exactly opposite in comparison to the report by Thotadi *et al.*,[39] on $X_1 \cdots X_2$ ($X_1$, $X_2$ = Cl, Br, I, $X_1 = X_2$ and $X_1 \neq X_2$).

Additionally, fluorinated molecules with aromatic ring are candidates to have weak C–F···π contacts as well. Prasanna and Guru Row has establish the impact of C–F···π interactions in determining the molecular conformation and its role in the crystal packing through their CSD analysis in 2000.[57]

### 1.6 Recent developments on fluorine mediated interactions

In the past decade, a number of research groups across the globe have contributed in the development of the area related to fluorine mediated interactions in the solid state. An highlight by Chopra and Guru Row[58] and a perspective by Chopra[59] have summarized the developments in a concise manner. The importance of C–H···F hydrogen bond has been pointed out by Parsch and Engels in their structural investigation of ribonucleic acids in 2002.[60] Frohlich *et al.*, concluded from there structural comparison of a series of 2-fluoro-2-phenyl cyclopropane derivatives and there non fluorinated analogues that the packing of fluorinated molecules where through various C–H···F hydrogen bond and not only due to the close packing of molecules.[61] The significance of C–H···F hydrogen bond was further demonstrated by Lee *et.al.*, Abad *et.al.*, and also by Mehta and Sen.[62] Nayak *et.al.*, in 2011 and 2012 analysed the structural variations in an exhaustive series of halogens (F, Cl, Br and I) substituted benzanilides.[51(b,c)] Although the structure of all the molecules had N–H···O hydrogen bond in common, the geometry of this hydrogen bond has been

found to vary significantly (H···O distance varied from 2.04 Å to 2.68 Å and ∠N–H···O between 142° and 169°). A variety of space groups ($P\bar{1}$, $P2_1$, *Pc*, *Pn*, $P2_1/c$, $Pna2_1$, $P2_12_12_1$, and *Pbca*) were also observed among these structures. These structural variations are the consequence of different weak interactions involving halogens (C–H···F, C–X···X and C–X···X′, X, X′ = F, Cl, Br and I). Another interesting structural analysis of a series of benzanilides containing one or two $CF_3$ groups in the molecules by Panini and Chopra in 2012 highlighted the significance of the contribution of one or more C–H···F hydrogen bond(s) in stabilizing each structure in the presence of a strong N–H···O hydrogen bond.[52] In addition to C–H···F and C–H···O hydrogen bonds, some of the structures also had one or more short C–F···F contacts (6 type I, 6 type II and 3 quasi type I/type II). It is not worthy that the H···O distance varied between 1.89 Å and 2.31 Å and ∠N–H···O varying between 138° and 166° in these structures indicating that the weaker interactions acting in a cooperative fashion altered the geometry of the N–H···O hydrogen bond, which is otherwise highly directional (linear). Panini and Chopra further extended their earlier study[52(a)] in 2013 and analysed structure variations in F/$CF_3$ substituted N-phenyl acetamides and N-methyl benzamides through structural and computational methods.[52(b)] They further emphasised that a number of weaker interactions together can influence the crystal packing and alter the geometry feature of a strong N–H···O hydrogen bond. Shukla and Chopra reported the structural variations due to fluorine mediated interactions in terms of the hybridization of the C atoms associated with C–H···F–C hydrogen bonds using CSD and a combination of computational methods.[63] Based on their result they concluded that C–H···F–C interactions should be considered as hydrogen bonds based on Koch and Popelier[64] criteria for hydrogen bonds.

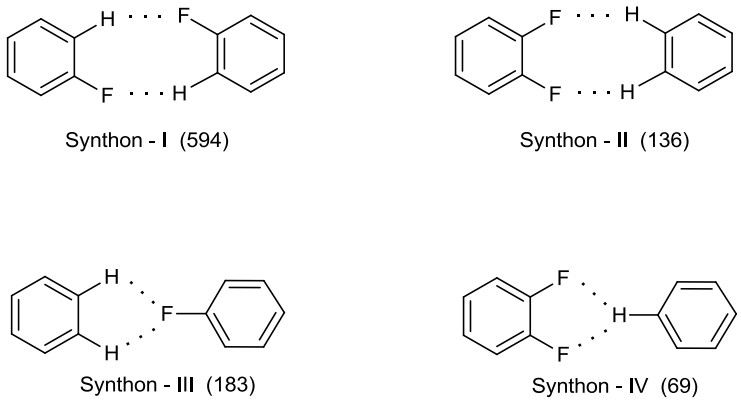


Figure - 1.7

Recent structural analysis on a library of halogenated aromatic imines has indicated that in the absence of any strong hydrogen bonds fluorine mediated interactions lead the formation of crystalline architecture by a few robust supramolecular synthon involving organic fluorine.[54] Kaur and Roy Choudhury demonstrated that when a non-interactive fluorine is replace by Cl or Br to make a new molecule the crystal structure remains unchanged while the replacement of an interactive fluorine by Cl or Br completely changes the crystal packing.[54(b,c)] Four most commonly observed supramolecular synthon involving aromatic C–H and aromatic C–F connected by C–H···F–C hydrogen bonds represented in the figure 1.7. The number of such synthon found in the 2017 edition of CSD is mentioned in the figure 1.7.

Based on the literature reports available on fluorine mediated interaction and our interest to understand the interaction involving organic fluorine in both presence and in the absence of strong hydrogen bonds and its implications in biological activity we intended to synthesise a series of fluorinated isoquinoline derivatives using the reaction scheme (figure 1.8) reported by Nagarajan *et al.*[65]

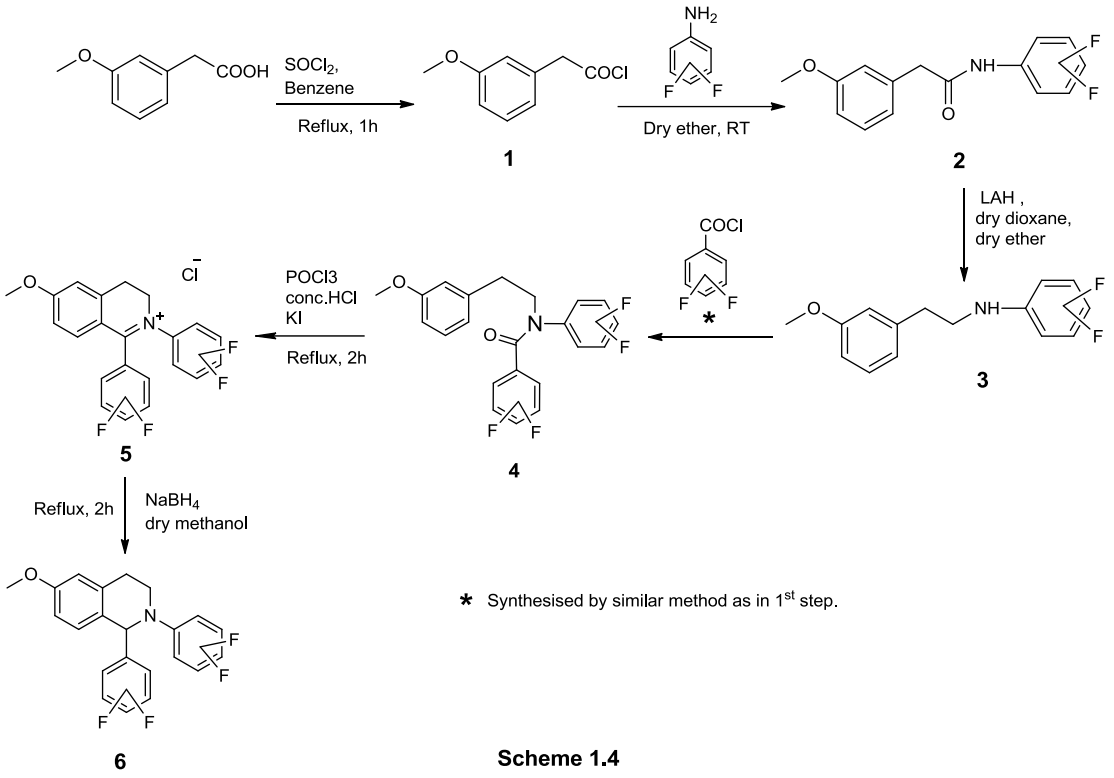


**Scheme 1.4**

Following this scheme we synthesis a series of mono and difluorinated amides (**2**), tetrafluorinated amides (**4**) and tetrafluorinated tetrahydroisoquinolines (**6**) and their corresponding non fluorinated analogues. The mono and difluorinated amides (**1**) enabled us to evaluate the intermolecular interactions involving fluorine in the presence of strong hydrogen bond while the structural analysis of tetrafluorinated amides (**4**) provided scope for such analysis in the absence of strong hydrogen bonds buy with the possibility of other weaker hydrogen bonds involving the C=O group. The third library of molecules (**6**) offered a platform to understand fluorine mediate interaction in the absence of other intermolecular interactions involving oxygen. All the secondary amines formed by the reduction of 1 were dense liquid and hence their structural analyses were not attempted. It is noteworthy that some of the final products of this scheme as synthesized by Nagarajan *et al.*, were found to have anti-implantation activity in rats. Therefore, we also expect that some of the final products containing four fluorine atoms could have similar biological importance. The synthetic strategies reported by Nagarajan *et al.*, were appropriately modified to achieve better yield of some of the compounds reported in this thesis. These modifications will be discussed in the respective chapters.

## 1.7 Foreword

The non-covalent interactions directly influence the crystal nucleation and growth through molecular recognition. To design a targeted supramolecular assembly in the solid state, one needs to gain knowledge about these intermolecular non-covalent interactions. With rich literature reports on the significance of weak hydrogen bonds in building desired crystalline lattice it is still not possible to predict the result of a crystallization experiment to an extent, where one may achieve definite control over these intermolecular interactions. Therefore there are lot more to explore in this area. We are specifically enthusiastic to explore the guiding ability of fluorine to control and alter the packing of molecules in the crystal lattice because of its importance in pharmaceutical industries. As discussed in the earlier sections in detail, organic fluorine participates in the formation of various intermolecular interactions through a number of supramolecular synthons. Even though a number of systematic studies on fluorine substituted organic molecules have overflown the scientific literature, a complete understanding of the structure directing role of fluorine is yet to be achieved.

To improve the current understanding of fluorine mediated interactions in small organic molecules, a systematic study has been performed on model systems in the following chapters. The selected models serve as to gain insights into the fluorine mediated interactions both in the presence and in the absence of other strong and weak hydrogen bonds. Additionally, these systems also enable us to analyse the effect of the variation in the number and positions of the F atom on the selected molecular systems on the crystal packing. The interactions involving fluorine in these crystal structures have been found to be of utmost importance.

**Chapter 2** elucidates the structural analyses of ten derivatives of phenylacetamide containing a strong hydrogen bond donor (N–H group) and a strong hydrogen bond acceptor (O=C group) in addition to one or two C–F groups and a –OMe group (Scheme 1.1). The significance of C–F group(s) in directing the crystal structures of these molecules in the presence of strong conventional N–H···O=C hydrogen bond has been documented in this chapter. The influence of

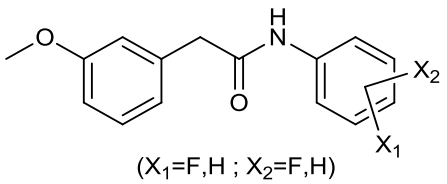


($X_1$=F,H ; $X_2$=F,H)

Scheme - 1.1

aromatic fluorine in introducing structural variation in these molecules has been highlighted.

**Chapter 3** highlight the structural features arising due to the presence of four C–F groups in the molecule in the presence of C=O and –OMe groups as hydrogen bond acceptors without the strong donor like N–H group (Scheme 1.2). These structures demonstrated the cooperative effects of weak hydrogen bonds (C–H···O=C, C–H···OMe and C–H···F–C), C–H···π and halogen···halogen (C–F···F–C) interactions. Various supramolecular synthons have been identified and rationalized in this chapter.

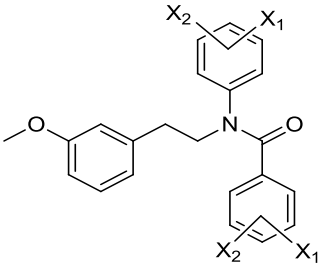

($X_1$=F,H ; $X_2$=F,H)

Scheme - 1.2

**Chapter 4** demonstrates the structural variations of *tetrafluoro* derivatives of *diphenyl tetrahydroisoquinolines* (Scheme 1.3). These molecules do not have strong hydrogen bond donor like N–H group and strong hydrogen bond acceptor like a C=O group. Therefore, structural feature of all the compounds are governed mainly by weak intermolecular interactions involving fluorine (C–H···F–C and C–F···F–C) and a few weak hydrogen bonds like C–H···OMe and much weaker C–H···π interaction(s). Based on the observed structural features an attempt has been made to rationalize the role of fluorine in the absence of strong hydrogen bonds in this chapter.

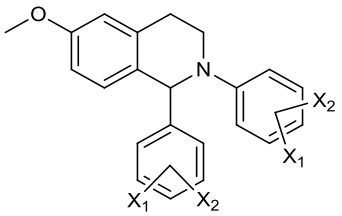

($X_1$ = $X_2$ = F, H)

Scheme - 1.3

# Chapter 2

## Understanding of the Role of Weak C–H···F Hydrogen Bond(s) in the Presence of Strong Hydrogen Bond in a Series of Fluorinated 2-(3-methoxyphenyl)-N-phenylacetamide Derivatives

# Chapter 2

## 2.1 Introduction

The understanding of different intermolecular interactions involving fluorine in small organic molecules has been the theme of contemporary research both in the presence and in the absence of other strong/weak interactions.[46-54] The structural analysis of halogenated benzamides has been extensively studied by a couple of research groups in last few years. Chopra and Row in their structural comparison of four halogen (F/Cl) substituted benzamides noted that the combination of strong O–H···O and N–H···O hydrogen bonds leads the crystal structure thereby resulting into isostructural pair for fluoro and chloro derivatives containing a –OH group in the molecule. When the –OH group is replaced with a $-CH_3$ group, the weaker interactions involving F and Cl became important in altering the 3D packing of molecules thereby leading to two different structures ($P2_1/n$ vs $C2/c$).[67] It was indicated that F prefers C–H···F hydrogen bond while Cl prefers C–Cl···Cl interaction. Chopra and Row in their report in 2008 further emphasized that the crystal structures of a series of mono/di-fluorinated benzamides were mostly guided by the strong N–H···O=C hydrogen bond and minor structural variations were observed due to the varying positions of the F atom.[68] Nayak *et al.,* in their structural analyses in 2011 and 2012 demonstrated that the halogen-mediated interactions can play a significant role in packing of halogenated molecules containing strong hydrogen bond donor and acceptor groups thereby leading to structural variation in molecules, which are otherwise isomeric in nature.[51(b,c)] Panini and Chopra thereafter in 2012 and 2013 extended

the structural analyses of fluorinated benzamides to structural analysis of $–CF_3$ substituted benzamides.[64,52] In another study by Chopra *et al.,* on the structural variation of fluoro anilines, significance of weak C–H···F hydrogen bond in the preference to the classical N–H···N hydrogen bond was highlighted.[67] In this chapter we would like to demonstrate the influence of weak intermolecular interactions offered by organic fluorine in the presence of N–H···O=C hydrogen bond through a detailed structural analysis of a series of fluorinated phenylacetamide. This target molecule contains one additional $–CH_2–$ group, which offers conformational flexibility to the molecule and we believe that this additional flexibility may result into and enhancement of fluorine mediated interactions thereby lead to a larger variety of crystal structures of a series of isomeric molecules.

## 2.2 Experimental

### 2.2.1 Synthesis and Characterization

All the starting materials were purchased from Sigma-Aldrich and were used without further purification. All the compounds (Scheme 2.2.1) were synthesized from their corresponding aniline and 3-methoxyphenylacetic acid initially following the procedure reported by Nagarajan *et al.,*[65] and later based on poor yield of some of our target molecule we followed a different synthetic procedure for better yield with the use of less hazardous chemicals.[68] 3-methoxy-phenyl-acetic acid **2a** (1.0 equivalent), fluorine substituted aniline **2b** (1.10 equivalent), *N*-(3-Dimethylaminopropyl)-*N′*-ethylcarbodiimide hydrochloride (EDC.HCl) (1.10 molar equivalent) and hydroxybenzotriazole (HOBt) (0.50 equivalent) were mixed in a round bottom flask and *N*-methylpyrrolidin-2-one (NMP) solvent was added at room temperature (25 ˚C) under $N_2$ environment. The reaction mixture was stirred at room temperature for 18 hours. After the reaction was over, water and ethyl acetate were added and mixture was stirred for 15 mins. The mixture was allowed to settle in a separating funnel, and the lower aqueous phase was removed and discarded. The organic phase was washed a few times with water and brine solution to remove the unreacted water-soluble compounds and to achieve better separation of organic and

aqueous layers. Then the organic phase was collected over excess anhydrous sodium sulfate to remove traces of moisture in the organic phase. Then the organic solvent was removed under reduced pressure on a rotary evaporator to extract the solid target compound. The crude product was purified by column chromatography using ethyl acetate/hexane mixture as the mobile phase. All the pure compounds were characterized by $^{1}H$, $^{13}C$ and $^{19}F$ NMR (400 MHz, Bruker Biospin Avance-III NMR spectrometer), FTIR (Perkin Elmer Spectrum 2) and the melting point of all the compounds were determined by differential scanning calorimetry (DSC) (Perkin Elmer Diamond 8000 DSC). All the characterization details (NMR, IR, DSC and PXRD) are provided as electronic supporting information (ESI) in the enclosed CD. Representative characterization data is reported here for immediate reference.

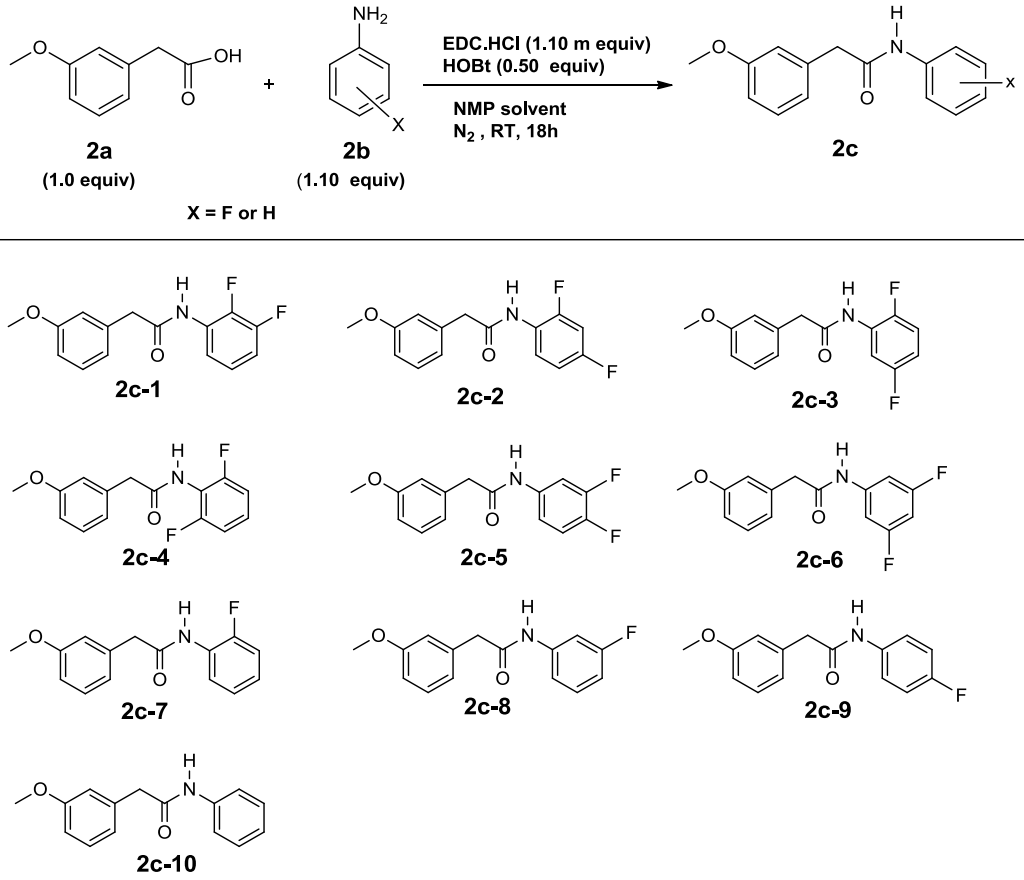


**Scheme 2.2.1**

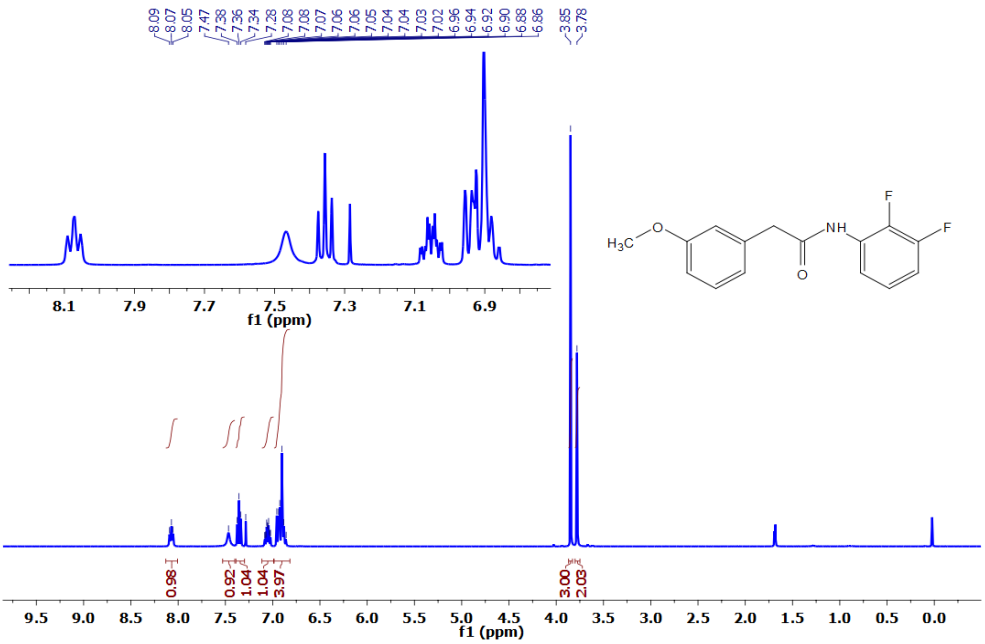


**$^{1}$H - NMR Spectra of 2c-1 (400 MHz, $CDCl_3$) : δ (ppm)** = 3.78 (s, 3H), 3.85 (s, 2H), 6.86 - 6.96 (m, 4H), 7.02 – 7.08 (m, 1H), 7.36 (t, 1H), 7.47(s, 1H), 8.07 (t, 1H).

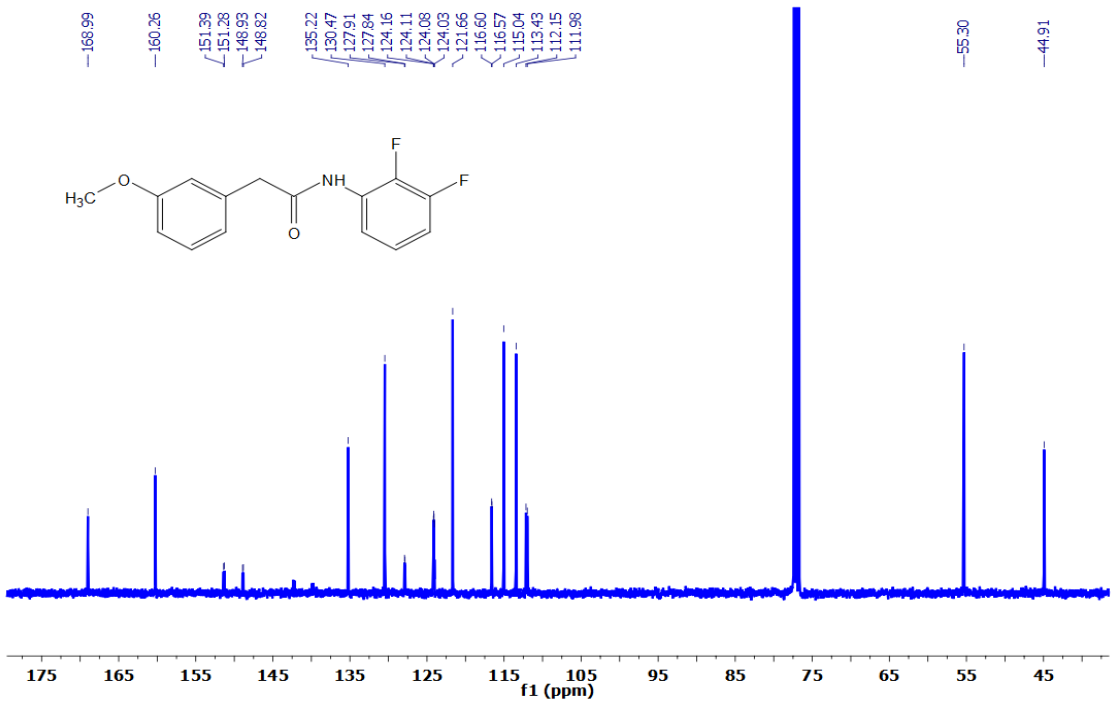


**$^{13}$C- NMR Spectra of 2c-1 ( 125 MHz, $CDCl_3$) : δ (ppm)** = 169.01, 160.28, 151.40, 151.29, 148.95, 48.84, 135.27, 130.48, 127.94, 127.93, 127.87, 127.86, 124.17, 124.12, 124.10, 124.05, 121.67, 16.62, 116.58, 115.05, 113.44, 112.16, 112.00, 55.31, 44.92.

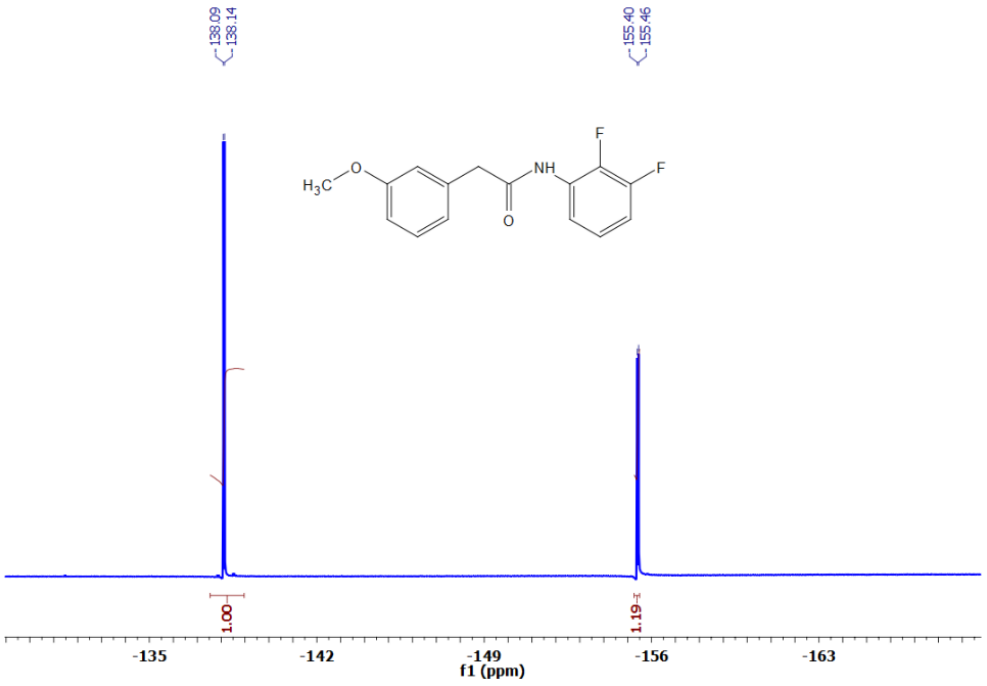


**$^{19}$F- NMR Spectra of 2c-1 (376 MHz, $CDCl_3$): δ (ppm)** = -155.43 (d, 1F), -138.11 (d, 1F)

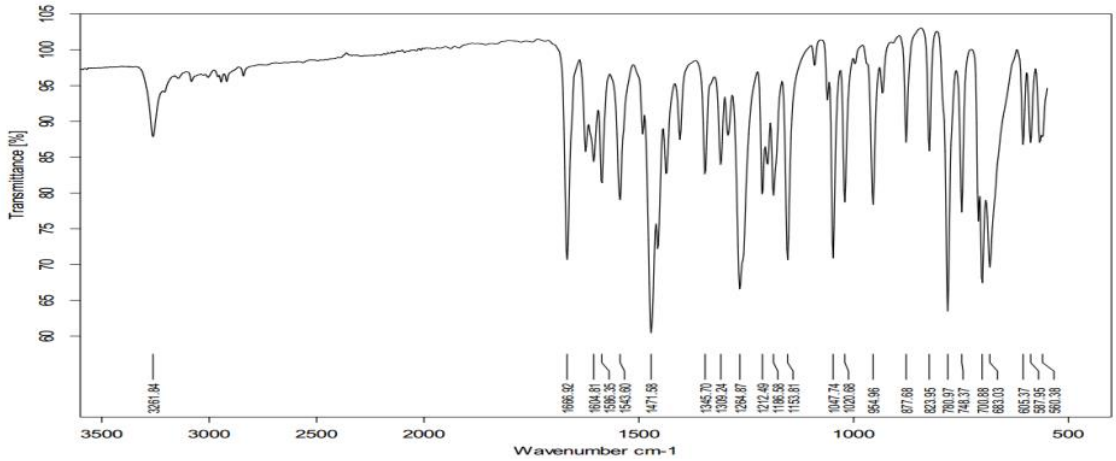


**FT-IR Spectrum of 2c-1**

### 2.2.2 Structural Study

#### 2.2.2.1 Powder X-ray Diffraction (PXRD) Analysis

PXRD patterns of all the pure compounds were recorded on a Rigaku Ultima IV diffractometer using parallel beam geometry equipped with a Cu – Kα radiation, 2.5° Primary and secondary solar slits, 0.5° divergence slit with 10 mm height limit slit, sample rotation stage (120 rpm) attachment and DTex Ultra detector. The tube voltage and current applied were 40 kV and 40 mA. The data were collected over an

angle range 5 to 50° with a scanning speed of 2° per minute with 0.02° step. The observed PXRD patterns have been compared (using WINPLOTR) with the simulated PXRD patterns generated from the crystal coordinates using Mercury.

### 2.2.2.2 Crystal Growth, Single Crystal Data Collection, Structure Solution and Refinement

Single crystals of desired size and quality were grown by slow evaporation by dissolving compound in different solvents like acetone, methanol, ethanol, ethyl acetate, dichloromethane, acetonitrile, toluene or a mixture of solvents such as DCM/hexane, chloroform/hexane, ethyl acetate/hexane, methanol/hexane and acetone/hexane etc.

Single crystal X-ray diffraction data were collected using a Rigaku XtaLABmini X-ray diffractometer equipped with Mercury CCD detector with graphite monochromated Mo-Kα radiation (λ=0.71073 Å) at 100.0(2)K using ω scans. The data were reduced using Crystal Clear suite 2.0.[69] and the space group determination was done using Olex2.[70] The crystal structures were solved by using SHELXS97[71] or SHELXT[72] and were refined using SHELXL97[71] through Olex2 suite. All the hydrogen atoms were geometrically fixed and refined using the riding model. Absorption correction was done by Multi-scan method. Data collection, crystal structure solution and refinement details for all the compounds are listed in the Table 2.2.1-2.2.2. All the packing and interaction diagrams have been generated using Mercury 3.5.[73] Geometric calculations have been done using PARST[74] and PLATON.[75]

**Table 2.2.1: Single crystal X-ray diffraction data of compounds 2c-1 to 2c-5**

| **Identification code** | **2c-1** | **2c-2** | **2c-3** | **2c-4** | **2c-5** |
|---|---|---|---|---|---|
| **CCDC Number** | 1540707 | 1540709 | 1540710 | 1540711 | 1540712 |
| **Formula** | $C_{15}H_{13}F_2NO_2$ | $C_{15}H_{13}F_2NO_2$ | $C_{15}H_{13}F_2NO_2$ | $C_{15}H_{13}F_2NO_2$ | $C_{15}H_{13}F_2NO_2$ |
| **Formula weight** | 277.26 | 277.26 | 277.26 | 277.26 | 277.26 |
| **Temperature (K)** | 100.0 | 100.0 | 100.0 | 100.0 | 100.0 |
| **Crystal system** | Monoclinic | Monoclinic | Monoclinic | Monoclinic | Monoclinic |
| **Space group** | $P2_1/c$ | $P2_1/c$ | $P2_1/c$ | $C2/c$ | $P2_1/c$ |
| **a (Å)** | 11.6788(17) | 10.9903(6) | 11.0509(16) | 22.3996(16) | 5.8400(12) |
| **b (Å)** | 4.8674(7) | 4.6917(2) | 12.231(3) | 4.7464(4) | 26.820(5) |
| **c (Å)** | 27.251(4) | 28.1963(13) | 9.4633(17) | 25.2796(16) | 10.960(2) |
| **α (°)** | 90 | 90 | 90 | 90 | 90 |
| **β (°)** | 124.699(9) | 118.451(3) | 96.740(7) | 103.356(4) | 131.45(3) |
| **γ (°)** | 90 | 90 | 90 | 90 | 90 |
| **V (Å$^3$)** | 1273.6(3) | 1278.30(11) | 1270.2(4) | 2615.0(3) | 1286.7(5) |
| **Z** | 4 | 4 | 4 | 8 | 4 |
| **Z′** | 1 | 1 | 1 | 2 | 1 |
| **$\rho_{calc}$ (g cm$^{-3}$)** | 1.446 | 1.441 | 1.450 | 1.409 | 1.431 |
| **μ/ mm$^{-1}$** | 0.116 | 0.115 | 0.116 | 0.113 | 0.114 |
| **$2\theta_{min,max}$ (°)** | 3.636 - 50.04 | 3.92 - 58.26 | 6.316 - 54.97 | 3.312 - 56.56 | 3.038 - 50.08 |
| **F(000)** | 576 | 576 | 576 | 1152 | 576 |
| **$h_{min,max}$; $k_{min,max}$; $l_{min,max}$;** | -13, 13; -5, 4; -31, 32 | -15, 14; -5, 6;-38 ,38 | -14, 14; -13, 15; -12 ,12 | -26, 29; -6, 6; -30, 33 | -6, 4; -31, 31; -12, 12 |
| **No. of observed reflections** | 8518 | 12235 | 8207 | 6649 | 5567 |
| **$R_{int}$** | 0.0201 | 0.0539 | 0.0319 | 0.0272 | 0.0486 |
| **No. of unique reflections** | 2242 | 3454 | 2892 | 3235 | 2189 |
| **$R_1$ [I > 2σ(I)]** | 0.0366 | 0.0484 | 0.0424 | 0.0447 | 0.0491 |
| **w$R_2$ (all data)** | 0.1037 | 0.1242 | 0.1203 | 0.1122 | 0.1181 |
| **GooF** | 1.043 | 1.023 | 1.035 | 1.016 | 1.036 |
| **$\Delta\rho_{max,min}$/eÅ$^{-3}$** | 0.61, -0.28 | 0.27, -0.25 | 0.28, -0.26 | 0.31, -0.36 | 0.22, -0.29 |

**Table 2.2.2: Single crystal X-ray diffraction data of compounds 2c-6 to 2c-10**

| **Identification code** | **2c-6** | **2c-7** | **2c-9** | **2c-10** |
|---|---|---|---|---|
| **CCDC Number** | 1540713 | 1540714 | 1540715 | 1540708 |
| **Formula** | $C_{15}H_{13}F_2NO_2$ | $C_{15}H_{14}FNO_2$ | $C_{15}H_{14}FNO_2$ | $C_{15}H_{15}NO_2$ |
| **Formula weight** | 277.26 | 259.26 | 259.26 | 241.26 |
| **Crystal system** | Monoclinic | Monoclinic | Monoclinic | Monoclinic |
| **Space group** | $P2_1/c$ | $P2_1/c$ | $P2_1/c$ | $P2_1/c$ |
| **a (Å)** | 10.989(2) | 4.729(3) | 5.0169(14) | 9.5059(16) |
| **b (Å)** | 12.176(3) | 11.406(5) | 12.106(4) | 10.8524(17) |
| **c (Å)** | 9.5202(19) | 23.474(12) | 20.553(9) | 24.154(4) |
| **α (°)** | 90 | 90 | 90 | 90 |
| **β (°)** | 97.740(12) | 93.85(2) | 95.217(16) | 96.267(7) |
| **γ (°)** | 90 | 90 | 90 | 90 |
| **V (Å$^3$)** | 1262.3(5) | 1263.4(11) | 1243.1(8) | 2476.9(7) |
| **Z** | 4 | 4 | 4 | 8 |
| **Z′** | 1 | 1 | 1 | 2 |
| **$\rho_{calc}$ (g cm$^{-3}$)** | 1.459 | 1.363 | 1.385 | 1.294 |
| **Temperature (K)** | 100.0 | 100.0 | 100.0 | 100.0 |
| **μ/ mm$^{-1}$** | 0.117 | 0.100 | 0.102 | 0.086 |
| **$2\theta_{min,max}$ (°)** | 6.284 - 55.02 | 6.324 - 55.056 | 6.732 - 55.226 | 6.096 - 50.052 |
| **F(000)** | 576 | 544 | 544 | 1024 |
| **$h_{min,max}$; $k_{min,max}$; $l_{min,max}$;** | -14, 14; -15, 15; -12, 12 | -4, 6; -14, 14; -30, 30 | -6, 6; -15, 15; -26, 26 | -11, 10; -12, 12; -28, 28 |
| **No. of observed reflections** | 13420 | 11536 | 8716 | 17289 |
| **$R_{int}$** | 0.0532 | 0.0636 | 0.0658 | 0.0700 |
| **No. of unique reflections** | 2905 | 2889 | 2833 | 4332 |
| **$R_1$ [I > 2σ(I)]** | 0.0478 | 0.0560 | 0.0475 | 0.0594 |
| **$wR_2$ (all data)** | 0.1239 | 0.1537 | 0.1213 | 0.1505 |
| **GooF** | 1.091 | 1.056 | 0.986 | 1.110 |
| **$\Delta\rho_{max,min}$/eÅ$^{-3}$** | 0.30, -0.21 | 0.27, -0.23 | 0.30, -0.31 | 0.21, -0.25 |

## 2.3 Results

**2-(3-methoxyphenyl)-N-(2,3-difluorophenyl)acetamide (2c-1):** Compound **2c-1** was crystallized in monoclinic centrosymmetric $P2_1/c$ space group with Z = 4 (Table 2.2.1 and Figure 2.3.1a). In this series, all the compounds have amide group therefore that all the crystal structures discussed in this chapter exhibit the strong N–H···O=C hydrogen-bonded chain as a common feature. This strong hydrogen bond is responsible for making one-dimensional catameric chain along the crystallographic *b* direction (Figure 2.3.1b) with all the molecule aligned in parallel (↑↑↑↑) orientation in **2c-1**. Although there are two fluorine atoms i.e. F1 and F2 corresponding to *ortho*- and *para*- positions but none of these fluorine atoms participated in the C–H···F hydrogen bond and hence there is no significant contribution of fluorine in crystal packing. It is noteworthy that the experimental powder X-ray diffraction (PXRD) pattern (Figure 2.3.1c) recorded on purified crude product **2c-1** does not exactly match with the PXRD pattern simulated using Mercury package from the CIF of the single crystal data. It may have a different polymorph in the crude product.

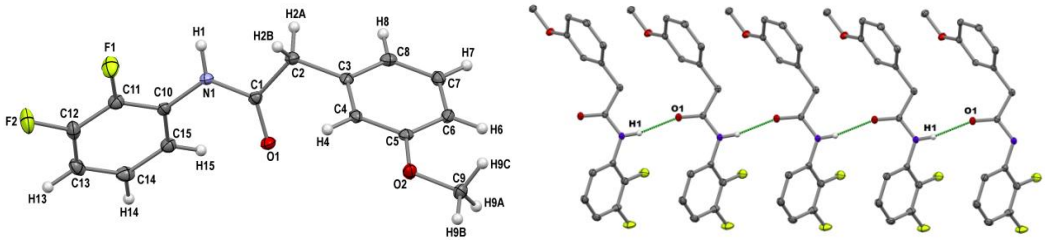


**(a)** **(b)**

**Figure 2.3.1: (a)** ORTEP of **1** drawn with 50% ellipsoidal probability, **(b)** N1–H1···O1 Hydrogen bond in one-dimensional catameric chain along *b*-axis.

**Table 2.3.1: Intermolecular interactions in 2c-1**

| D–H···A/(Å) | (D···H)/Å | *D*(D···A)/Å | *d*(H···A)/Å | ∠D–H···A/º | SYMMETRY |
|---|---|---|---|---|---|
| **N1–H1···O1** | 1.030 | 2.976(2) | 1.97 | 164 | x, y-1, z |
| **C4–H4···O2** | 1.080 | 3.374(3) | 2.38 | 153 | 1-x, y-½, $^3/_2$ -z |
| **C15–H15···O1** | 1.080 | 3.380(2) | 2.60 | 129 | - x, 1- y, 1- z |

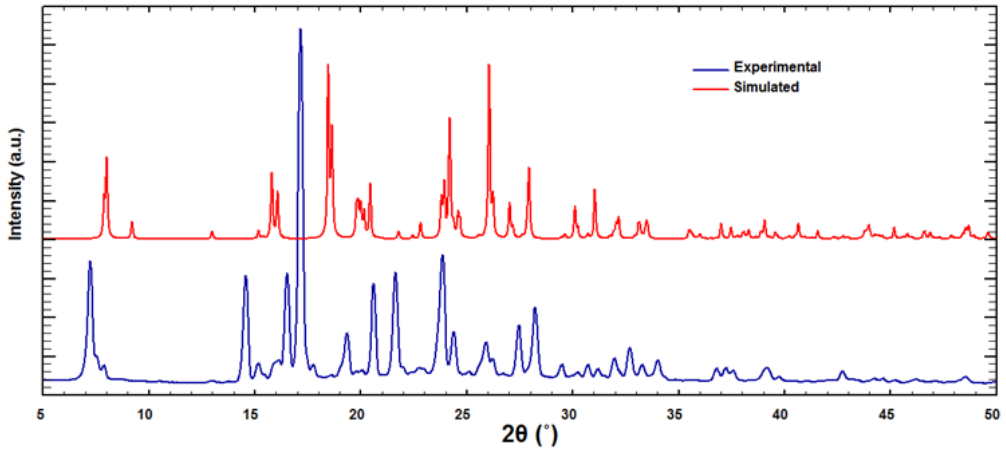


**Figure 2.3.1: (c)** Comparison of experimental and Simulated PXRD patterns of **2c-1**.

**2-(3-methoxyphenyl)-N-(2,4-difluorophenyl)acetamide (2c-2):** This compound was crystallized in the centrosymmetric monoclinic space group $P2_1/c$ with Z = 4 (Figure 2.3.2a). In this amide compound, strong hydrogen N1–H1···O1 bond propagates along the *b* axis with all molecule aligned in parallel (↑↑↑↑) orientation. Fluorine atoms were not involved in any C–H···F hydrogen bond. The experimental PXRD pattern is found to match with the simulated PXRD pattern from the CIF of the single crystal structure solution indicating that the raw material and the recrystallized phases were same (Figure 2.3.2c).

**Table 2.3.2: Intermolecular interactions in 2c-2**

| **D–H···A/(Å)** | **(D···H)/Å** | ***D*(D···A)/Å** | ***d*(H···A)/Å** | **∠D–H···A/º** | **SYMMETRY** |
|---|---|---|---|---|---|
| **N1–H1···O1** | 1.030 | 2.806(2) | 1.85 | 154 | x, y - 1, z |
| **C4–H4···O2** | 1.080 | 3.510(3) | 2.62 | 139 | 1 - x, ½ - y, $^3/_2$ -z |
| **C2–H2B···O2** | 1.080 | 3.377(2) | 2.67 | 122 | 1 - x, y - ½, $^3/_2$ -z |

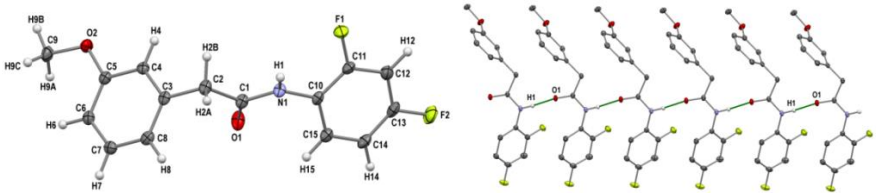

**(a)** **(b)**

**Figure 2.3.2: (a)** ORTEP of **2c-2** drawn with 50% ellipsoidal probability, **(b)** Strong N1–H1···O1 Hydrogen bond and C2–H2A···π interaction in one-dimensional catameric chain along *b*-axis and bond both are parallel.

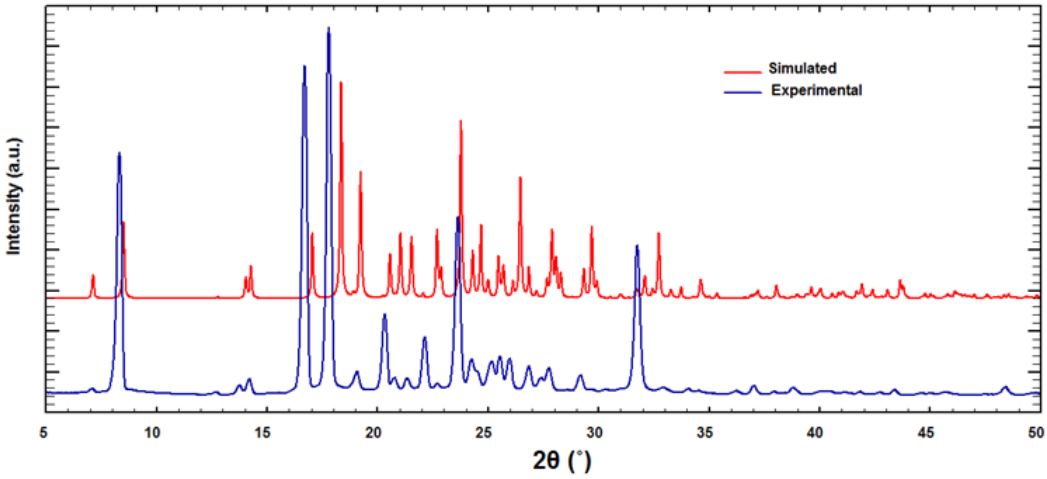


**Figure 2.3.2: (c)** Comparison of experimental and simulated PXRD patterns of **2c-2**.

**N-(2,5-dichlorophenyl)-3-methoxyphenylacetamide (2c-3):** Compound **2c-3** was crystallized in monoclinic centrosymmetric $P2_1/c$ space group with Z = 4 (Figure 2.3.3a). In crystal structure mainly three type of interactions have been found-(1) N–H···O, (2) C-H···O and (3) C–H···F hydrogen bonds. Strong N–H···O hydrogen bond is responsible for making one-dimensional infinite catameric chain with molecules arranged in anti-parallel (↑↓↑↓↑↓) orientation along the crystallographic *c* direction (Figure 2.3.3b). The experimental PXRD pattern of **2c-3** is found to match with the simulated PXRD pattern from the CIF of the single crystal structure solution indicating that the raw material and the recrystallized phases were same (Figure 2.3.3c).

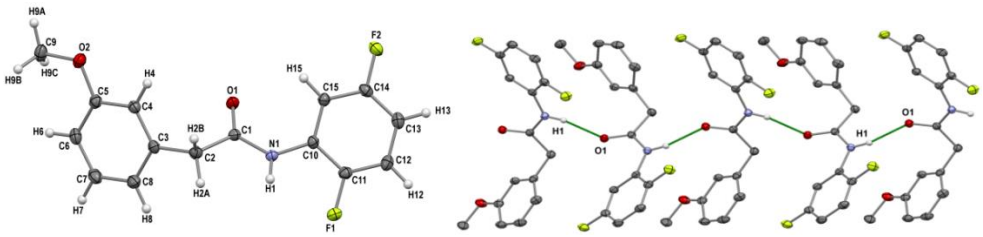


**(a)** **(b)**

**Figure 2.3: (a)** ORTEP of **2c-3** drawn with 50% ellipsoidal probability, **(b)** Strong N1–H1···O1 Hydrogen bond generating one-dimensional alternate antiperiplanar infinite catameric chain along *c*-axis.

*Ortho*-fluorine (F1) of amine ring is found to act as a bifurcated acceptor. The hydrogen bond involving C13–H13···F1 and C7–H7···F2 leads to the formation 2-

dimentional net-like structure (Figure 2.3.3c). Further, through C12–H12···F1 hydrogen bond, centrosymmetric dimers have been identified. These dimers are once again connected to each other by C7–H7···F2 hydrogen bond forming a ribbon-like structure (Figure 2.3.3d).

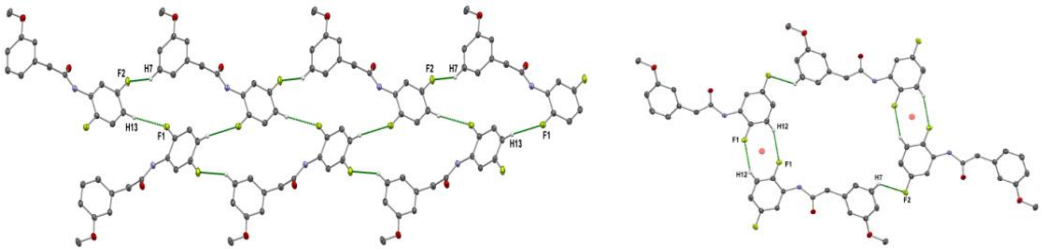


**(c)** **(d)**

**Figure 2.3.3: (c)** a 2-dimentional sheet-like structure **(d)** head to head 8-membered supramolecular synthon in which aromatic C–H···F interactions are involved (a dimer form).

**Table 2.3.3: Intermolecular interactions in 2c-3**

| D–H···A/(Å) | (D···H)/Å | *D*(D···A)/Å | *d*(H···A)/Å | ∠D–H···A/º | SYMMETRY |
|---|---|---|---|---|---|
| **N1–H1···O1** | 1.030 | 2.876(1) | 1.87 | 166 | x, ½ -y , ½ +z |
| **C2–H2A···O1** | 1.080 | 3.236(2) | 2.32 | 142 | x, ½ -y, ½+z |
| **C7–H7···F2** | 1.080 | 3.294(2) | 2.56 | 124 | x, y -1, z |
| **C12–H12···F1** | 1.080 | 3.380(2) | 2.46 | 143 | 1-x, 1-y, 2-z |
| **C13–H13···F1** | 1.080 | 3.602(2) | 2.53 | 170 | 1-x, ½+y, $^3/_2 - z$ |

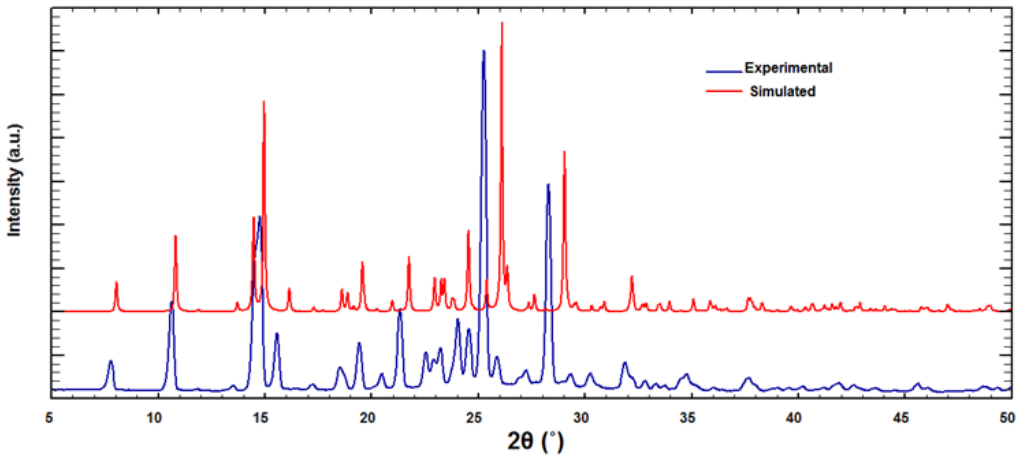


**Figure 2.3.3: (e)** Comparison of experimental and simulated PXRD patterns of **2c-3**.

**2-(3-methoxyphenyl)-N-(2,6-difluorophenyl)acetamide (2c-4):** The compound (**2c-4**) crystallizes in the centrosymmetric monoclinic space group *C*2/*c* with Z = 4. Needless to mention that all the crystal structures discussed in this series exhibits the strong N–H···O hydrogen-bonded chains as a common feature. Here the molecules are found to form catameric chain along the *b* direction involving N1–H1···O1 hydrogen bond (Figure 2.3.4a). Weak C2–H2···π interactions (2.88 Å), like in **2c-2**, are also observed here.

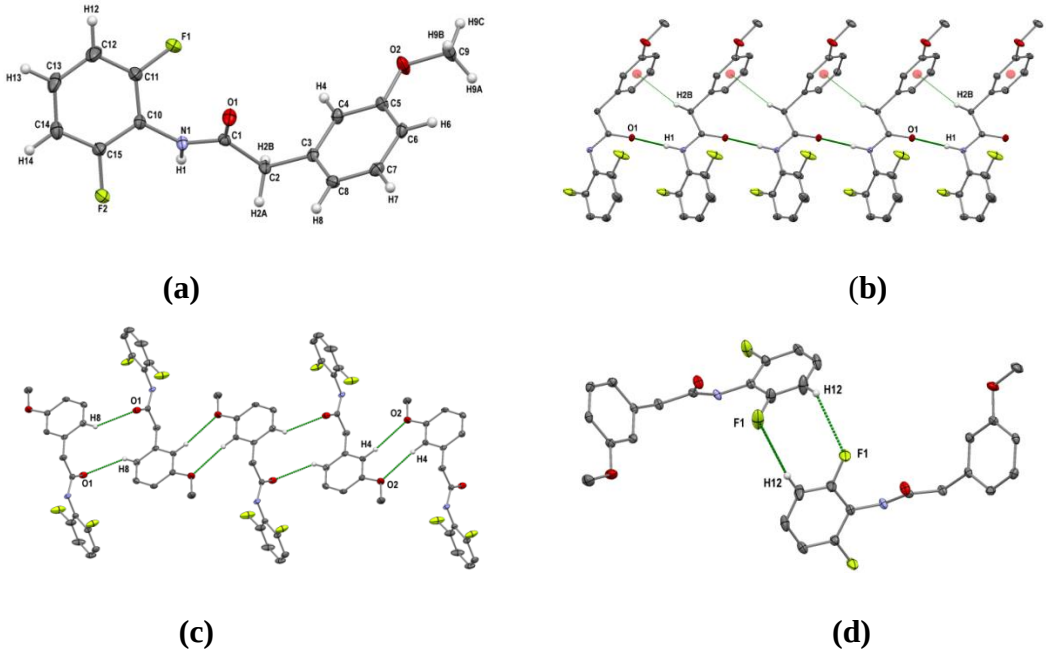


**(a)** (**b)**

**(c)** **(d)**

**Figure 2.3.4: (a)** ORTEP of **2c-4** drawn with 50% ellipsoidal probability, **(b)** Strong N1–H1···O1 Hydrogen bond and aromatic C–H···π interactions both parallel generating one-dimensional infinite catameric chain along *b*-axis. **(c)** Two different type of homo synthon via inversion center by utilization of C–H···O hydrogen bond and creating a tap like structure. **(d)** C12–H12···F1 hydrogen bond that generate 8-member non-planar supramolecular synthon.

Both *ortho*- hydrogens of the methoxyphenyl ring are individually involved in two different C–H···O hydrogen bonds *via* inversion center. The carbonyl oxygen is the acceptor in one hydrogen bond while the oxygen of the methoxy group in another is acting as the acceptor thereby generating a ribbon-like structure (Figure 2.3.4c). The *m*-hydrogen (H12) of the aniline ring forms a dimer through C–H···F hydrogen bond involving F1, and that second fluorine (F2) does not participate in any type of interactions (Figure 2.3.4d). The experimental PXRD pattern of **2c-4** is

found to match with the simulated PXRD pattern from the CIF of the single crystal structure solution indicating that the raw material and the recrystallized phases were same (Figure 2.3.4e).

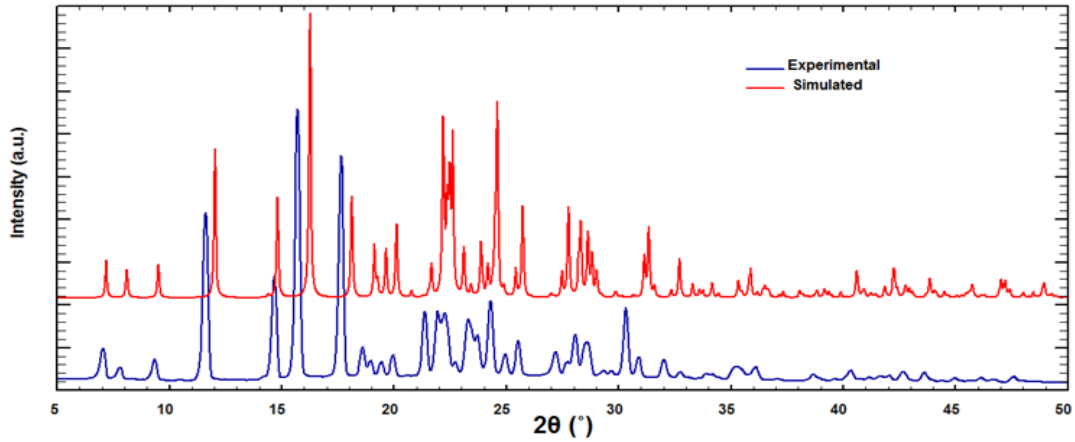


**Figure 2.3.4: (e)** Comparison of experimental and simulated PXRD patterns of **2c-4**.

**Table 2.3.4: Intermolecular interactions in 2c-4**

| **D–H···A/(Å)** | **(D···H)/Å** | ***D*(D···A)/Å** | ***d*(H···A)/Å** | **∠D–H···A/º** | **SYMMETRY** |
|---|---|---|---|---|---|
| **N1–H1···O1** | 1.030 | 2.767(2) | 1.75 | 167 | x, 1+y, z |
| **C8–H8···O1** | 1.080 | 3.417(2) | 2.58 | 134 | ½ -x, ½ -y, 1+z |
| **C4–H4···O2** | 1.080 | 3.598(2) | 2.56 | 160 | 1-x, 1-y, 1-z |
| **C12–H12···F1** | 1.080 | 3.384(2) | 2.65 | 125 | 1-x, y, $^{3}/_{2}$ - z |
| C2–H2B···π | 1.080 | 3.499 | 2.92 | 118 | x, y -1, z |

**2-(3-methoxyphenyl)-N-(3,4-difluorophenyl)acetamide (2c-5):** This compound crystallizes in the centrosymmetric monoclinic space group $P2_1/c$ with Z = 4 (Figure 2.3.5a). Unlike other amides discussed above, the carbonyl oxygen is found to act as a bifurcated acceptor (Figure 2.3.5b). In addition to the bifurcated hydrogen bonds (N1–H7···O1 and C8–H8···O1), weak C7–H7···F1 hydrogen bonds are also identified in the same synthon (Fig. 2.5b). Herein the molecules are arranged in the opposite directions (↑↓↑↓↑↓). The experimental PXRD pattern of **2c-5** is found to match with the simulated PXRD pattern from the CIF of the single crystal structure solution indicating that the raw material and the recrystallized phases were same (Figure 2.3.5c).

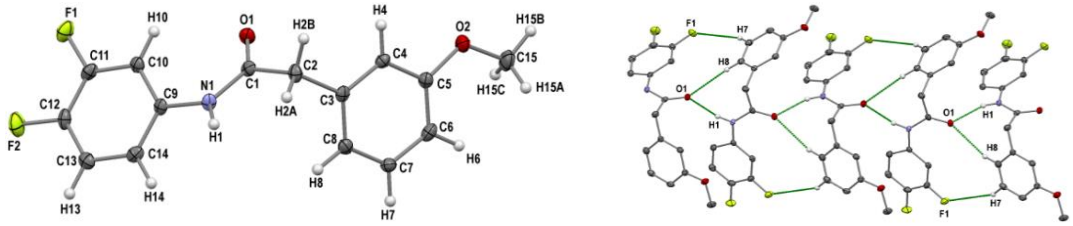


**(a)** **(b)**

**Figure 2.3.5: (a)** ORTEP of **2c-5** drawn with 50% ellipsoidal probability, **(b)** Strong N1–H1···O1 Hydrogen bond along with weak C7–H7···F1 and C8–H8···O1 hydrogen bonds in one dimensional catameric chain type structure.

**Table 2.3.5: Intermolecular interactions in 2c-5**

| **D–H···A/(Å)** | **(D···H)/Å** | ***D*(D···A)/Å** | ***d*(H···A)/Å** | **∠D–H···A/º** | **SYMMETRY** |
|---|---|---|---|---|---|
| **N1–H1···O1** | 1.030 | 2.828(3) | 1.89 | 152 | x-1, $^{1}/_{2}$-y, z-$^{1}/_{2}$ |
| **C8–H8···O1** | 1.080 | 3.531(3) | 2.58 | 147 | x-1, $^{1}/_{2}$-y, z-$^{1}/_{2}$ |
| **C14–H14···O2** | 1.080 | 3.307(3) | 2.34 | 148 | x-2, $^{1}/_{2}$-y, z-$^{1}/_{2}$ |
| **C7–H7···F1** | 1.080 | 3.624(3) | 2.68 | 145 | x-1, $^{1}/_{2}$-y, z-$^{1}/_{2}$ |

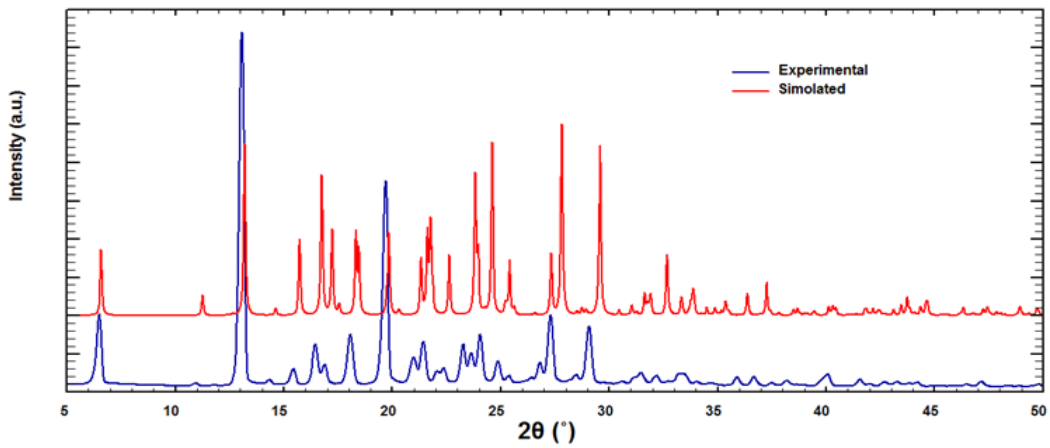


**Figure 2.3.5: (c)** Comparison of experimental and simulated PXRD patterns of **2c-5**.

**2-(3-methoxyphenyl)-N-(3,5-difluorophenyl)acetamide (2c-6):** This compound (Figure 2.3.6a) crystallized in the $P2_1/c$ space group with Z = 4. Similar molecular chains involving N1–H1···O1, C2–H2A···O1 and C8–H8···F1 hydrogen bonds have been identified in **2c-6** just as was seen in **2c-5** (Figure 2.3.6b). The molecules in this chain are arrange in opposite directions (↑↓↑↓↑↓) like **2c-3** and **2c-4**. Like the compound **2c-3**, this molecule also forms a symmetrical 8-membered dimer by the utilization of C15–H15···F2 hydrogen bonds (Figure 2.3.6c). The experimental PXRD pattern of **2c-6** is found to match with the simulated PXRD pattern from the CIF of the single crystal structure solution indicating that the raw material and the recrystallized phases were same (Figure 2.3.6d).

**Table 2.3.6: Intermolecular interactions in 2c-6**

| D–H···A/(Å) | (D···H)/Å | *D*(D···A)/Å | *d*(H···A)/Å | ∠D–H···A/º | SYMMETRY |
|---|---|---|---|---|---|
| **N1–H1···O1** | 1.030 | 2.879(2) | 1.89 | 161 | x, ½ -y, ½ +z |
| **C2–H2A···O1** | 1.080 | 3.282(2) | 2.39 | 139 | x, ½ -y, ½ +z |
| **C8–H8···F1** | 1.080 | 3.455(2) | 2.52 | 145 | x, ½ -y, ½ +z |
| **C7–H7···F1** | 1.080 | 3.358(2) | 2.61 | 125 | x, y-1, z |
| **C15–H15···F2** | 1.080 | 3.448(2) | 2.40 | 163 | 1-x, 1-y, 2-z |

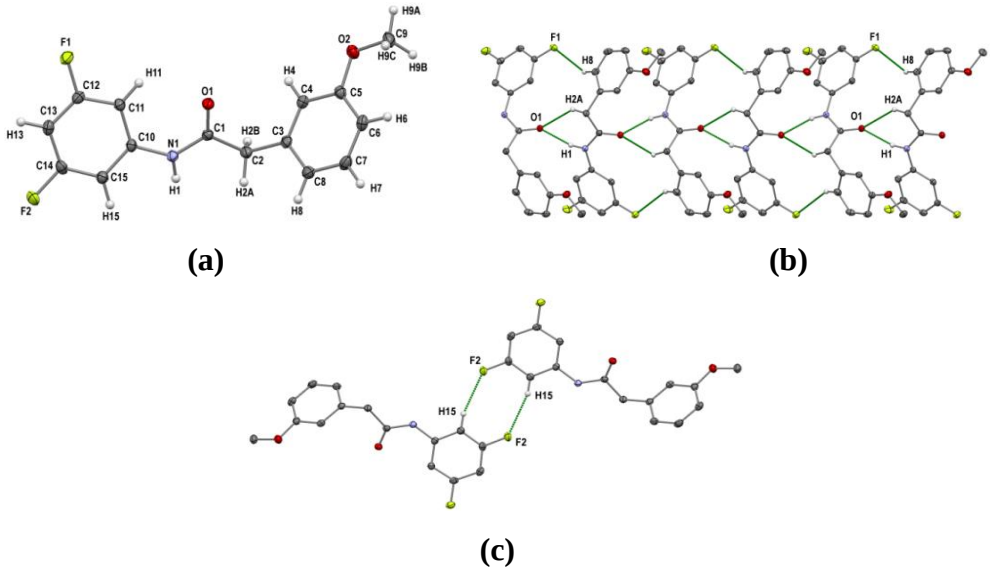


**Figure 2.3.6: (a)** ORTEP of **2c-6** drawn with 50% ellipsoidal probability, **(b)**: Strong N–H···O hydrogen bond and weak C8–H8···F1 hydrogen bond involved in formation of one-dimensional band like structure in crystal packing. **(c)** Inversion center related 8-member head to head supramolecular homo synthon.

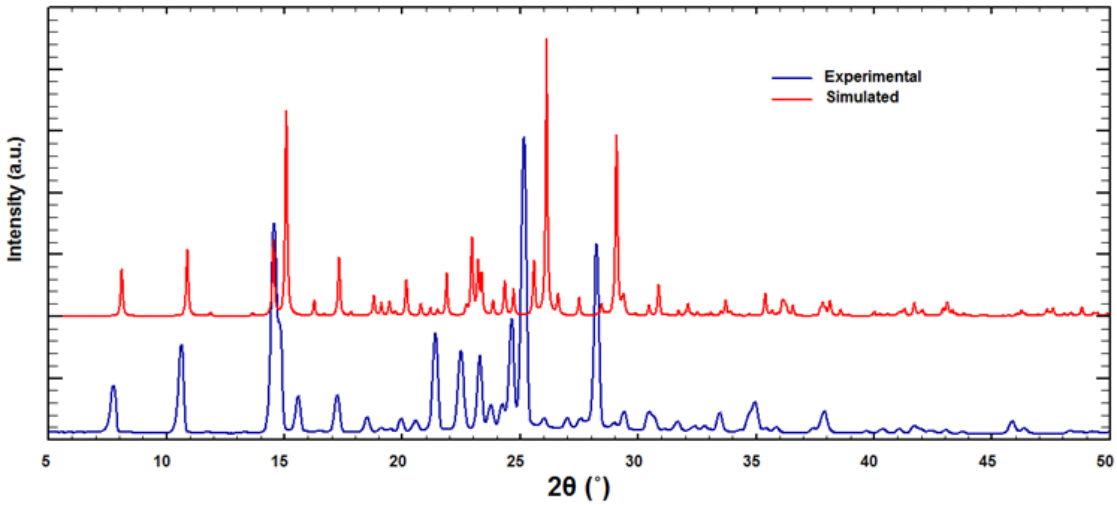


**Figure 2.3.6: (d)** Comparison of experimental and simulated PXRD patterns of **2c-6**.

**2-(3-methoxyphenyl)-N-(2,-fluorophenyl)acetamide (2c-7):** This mono-fluorinated acetamide (**2c-7**) crystallizes in the centrosymmetric monoclinic space group $P2_1/c$ with Z = 4. Amide functional group facilitates the formation of strong N–H···O hydrogen bond along *a* axis forming an infinite chain. Due to this strong hydrogen bond molecules packed parallel (↑↑↑) *via* translational symmetry only (fig2.3.7a)

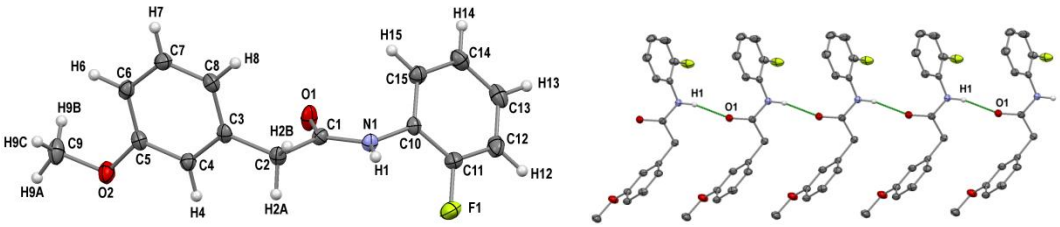


**(a)** **(b)**

**Figure 2.3.7: (a)** ORTEP of **2c-7** drawn with 50% ellipsoidal probability, **(b)** A symmetrical one-dimensional linear chain of strong N1–H1···O1 hydrogen bond along a-axis.

Simultaneously with the strong hydrogen bond, 4 molecules are connected by weak C–H···O hydrogen bonds and generate a tetramer in which methoxy oxygen behave as a bifurcated acceptor and this tetrameric unit propagates in a direction perpendicular to the strong hydrogen bond i.e. in the *b* direction (Fig2.3.7c). In addition, the o*rtho*- fluorine and *meta*- hydrogen participates in the formation of a centrosymmetric dimer through C12–H12···F1 hydrogen bond (Fig. 2.3.7d). The experimental PXRD pattern of **2c-7** is found to match with the simulated PXRD pattern

from the CIF of the single crystal structure solution indicating that the raw material and the recrystallized phases were same (Figure 2.3.7e).

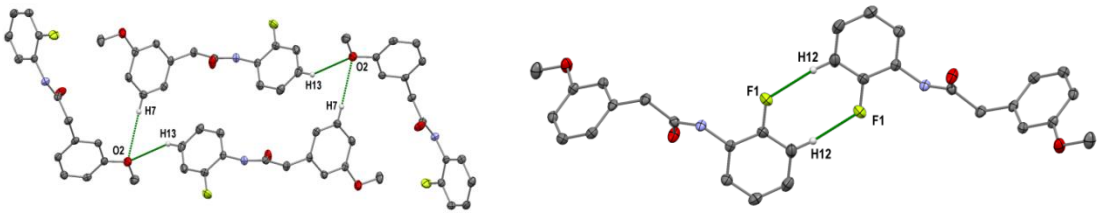


**(c)** **(d)**

**Figure 2.3.7: (c)** A tetramer synthon unit held by bifurcated C–H···O hydrogen bond, **(d)** Inversion center related 8-member head to head supramolecular homo synthon via C12–H12···F1 hydrogen bond.

**Table 2.3.7: Intermolecular interactions in 2c-7**

| D–H···A/(Å) | (D···H)/Å | *D*(D···A)/Å | *d*(H···A)/Å | ∠D–H···A/º | SYMMETRY |
|---|---|---|---|---|---|
| **N1–H1···O1** | 1.030 | 2.856(3) | 1.86 | 164 | 1-x, y, z |
| **C13–H13···O2** | 1.080 | 3.585(3) | 2.62 | 149 | x, ½ -y, ½ +z |
| **C7–H7···O2** | 1.080 | 3.609(3) | 2.53 | 174 | 2-x, ½ +y, ½ -z |
| **C12–H12···F1** | 1.080 | 3.393(3) | 2.50 | 140 | 1-x, -y, 1-z |
| **C14–H14···O1** | 1.080 | 3.604(3) | 2.70 | 142 | 2-x, 1-y, 1-z |

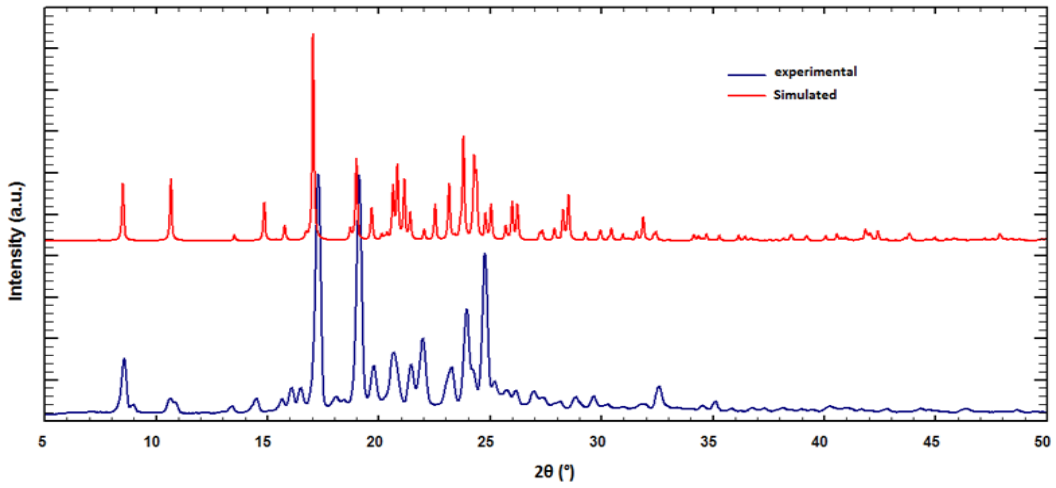


**Figure 2.3.7: (e)** Comparison of experimental and simulated PXRD patterns of **2c-7**.

**2-(3-methoxyphenyl)-N-(4,-fluorophenyl)acetamide (2c-9):** The space group of this compound (2c-9) is $P2_1/c$ with Z = 4 (Figure 2.3.8a). Strong N–H···O hydrogen bond is the guiding feature in packing and is found to propagate along *a*-axis (Figure

2.3.8b). Two molecules are found to form a *head-to-tail* dimer through C8–H8···F1 hydrogen (Figure 2.3.8c). Since fluorine behaves as a bifurcated acceptor here, it also forms a zig-zag chain by C4–H4···F1 hydrogen bond by c-glide (Figure 2.3.8d). The experimental PXRD pattern of **2c-vii** is found to match with the simulated PXRD pattern from the CIF of the single crystal structure solution indicating that the raw material and the recrystallized phases were same (Figure 2.3.8e).

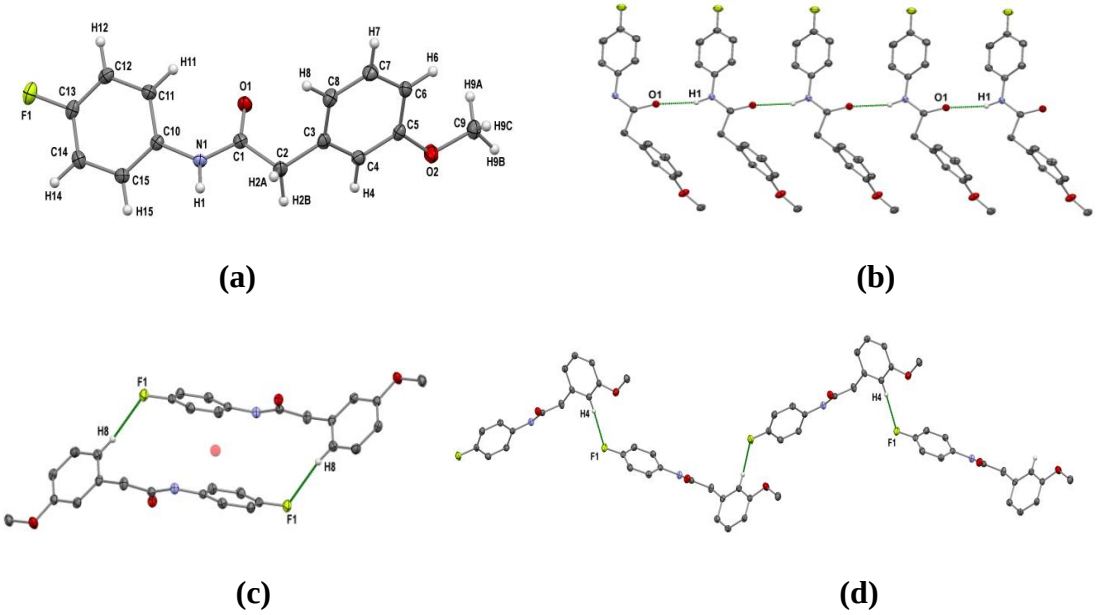


**(a)** **(b)**

**(c)** **(d)**

**Figure 2.3.8: (a)** ORTEP of **2c-9** drawn with 50% ellipsoidal probability, **(b)** A symmetrical one-dimensional linear chain of strong N1–H1···O1 hydrogen bond along a-axis. **(c)** Inversion center related dimer synthon through the C8–H8···F1 hydrogen bond **(d)** C4–H4···F1 hydrogen bond in zig-zag chain.

**Table 2.3.8: Intermolecular interactions in 2c-9**

| **D–H···A/(Å)** | **(D···H)/Å** | ***D*(D···A)/Å** | ***d*(H···A)/Å** | **∠D–H···A/º** | **SYMMETRY** |
|---|---|---|---|---|---|
| **N1–H1···O1** | 1.030 | 2.897(2) | 1.94 | 154 | 1+x, y, z |
| **C12–H12···O1** | 1.080 | 3.531(2) | 2.60 | 144 | 1-x, 1-y, 1-z |
| **C14–H14···O2** | 1.080 | 3.631(2) | 2.64 | 152 | 1+x, $^{3}/_{2}$ - y, ½ -z |
| **C4–H4···F1** | 1.080 | 3.367(2) | 2.29 | 175 | x, $^{3}/_{2}$ - y, ½ +z |
| **C8–H8···F1** | 1.080 | 3.380(2) | 2.38 | 154 | 2-x, 1-y, 1-z |

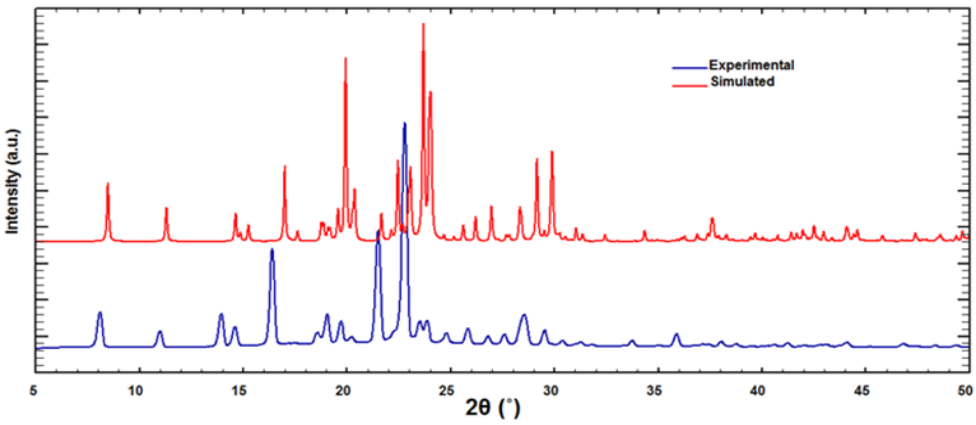


**Figure 2.3.8: (e)** Comparison of experimental and simulated PXRD patterns of **2c-9**.

**2-(3-methoxyphenyl)-N-phenylacetamide (2c-10)**: The compound **2c-10** crystallizes in the centrosymmetric monoclinic space group $P2_1/c$ with $Z = 8$ ($Z' = 2$) (Figure 2.3.9a). Two molecules (A and B) in the asymmetric differ in conformation. The torsion angle between the –CONH group and the –NPh ring are 54º and 33º respectively. These two crystallographically independent molecules are connected by strong N–H···O hydrogen bond and weak aromatic C–H···π interactions (Figure 2.3.9b). Interestingly, the two molecules of the asymmetric unit pack in the lattice by ···A···B···A···B···A···B··· fashion through strong N–H···O hydrogen bonds (Figure 2.3.9c). This is a unique feature, which was not observed in any of the fluorinated molecules discussed before.

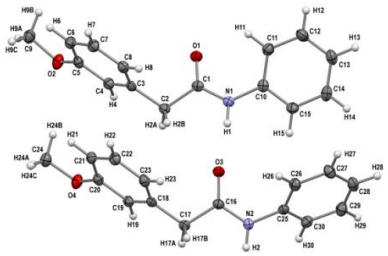

**(a)**

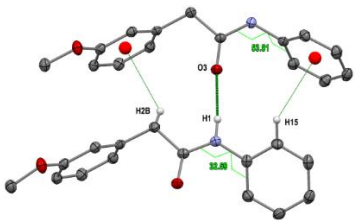

**(b)**

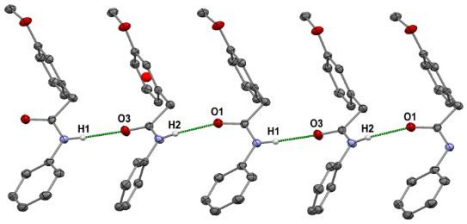


**(c)**

**Figure 2.3.9: (a)** ORTEP of **2c-10** drawn with 40% ellipsoidal probability, **(b)** Two molecules in one asymmetric unit (Z'=2) which are symmetry independent with different torsion angle and connected by strong hydrogen bond. **(c)** Strong

hydrogen bonded chain involving N1–H1···O3 hydrogen bond (within asymmetric unit) and N2–H2···O1 hydrogen bond (by translational symmetry).

**Table 2.3.9: Intermolecular interactions in 2c-10**

| D–H···A/(Å) | (D···H)/Å | *D*(D···A)/Å | *d*(H···A)/Å | ∠D–H···A/º | SYMMETRY |
|---|---|---|---|---|---|
| **N1–H1···O3** | 1.030 | 2.855(3) | 1.83 | 173 | x, y, z |
| **N2–H2···O1** | 1.030 | 2.861(3) | 1.88 | 158 | x-1, y, z |
| **C6–H6···O1** | 1.080 | 3.473(3) | 2.49 | 150 | 2-x, ½ +y, ½ -z |
| **C7–H7···O2** | 1.080 | 3.573(3) | 2.50 | 170 | 2-x, ½ +y, ½ -z |
| **C13–H13···O2** | 1.080 | 3.430(3) | 2.48 | 146 | x, ½ -y, ½ +z |
| **C28–H28···O4** | 1.080 | 3.472(3) | 2.47 | 154 | x, ½ -y, ½ +z |
| **C22–H22···O4** | 1.080 | 3.467(3) | 2.40 | 168 | 1-x, ½ +y, ½ -z |
| **C27–H27···O3** | 1.080 | 3.520(3) | 2.59 | 143 | 1-x, 1-y, 1-z |

The experimental PXRD pattern of **2c-10** is found to match with the simulated PXRD pattern from the CIF of the single crystal structure solution indicating that the raw material and the recrystallized phases were same (Figure 2.3.9d).

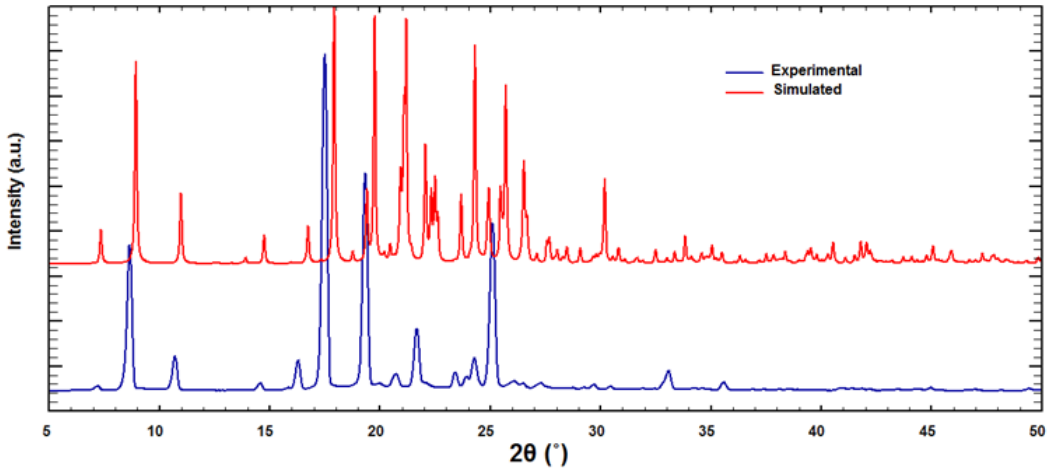


**Figure 2.3.9: (d)** Comparison of experimental and simulated PXRD patterns of **2c-10**.

## 2.4 Discussion

All the structures reported above indicate that strong N–H···O=C hydrogen bond generally governs the crystal structures of these amides in cooperation with weaker C–H···F–C hydrogen bonds and C–H···π($C_g$) interactions. It is well-known in the literature that the amide linkage can result into two types of hydrogen bonded synthons, namely dimer and chain (Scheme 2.4.1).

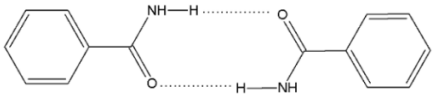


Amide Dimer

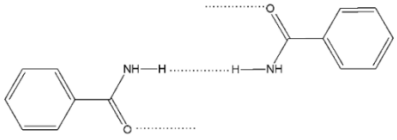


Amide Chain

**Scheme 2.4.1**

A recent search in the database (CSD, 2017) revels that among the structures reported in the latest version of CSD that there are 3742 hits having the dimer synthon and 7712 hits having the chain synthon. The dimers are mostly formed in cases where the amide is a part of a ring or having –CONHR moiety with R = H, $–CH_3$, $–C_2H_5$ groups. The formation of chain is preferred for molecules having two bulky groups attached to either side of the –CONH– group as is the condition in the structures reported herein. From the crystal data tables (Table 2.2.1 and Table 2.2.2), it is evident that the non-fluorinated analogue (**2c-10**) has the lowest density (1.295 g/cm$^3$) compared to the corresponding fluorinated analogues. The density of the difluorinated molecules are in the range between 1.459 g/cm$^3$ and 1.409 g/cm$^3$, while that for the two mono-fluorinated compounds are 1.385 g/cm$^3$ and 1.363 g/cm$^3$. This indicates that the incorporation of fluorine in the molecule produces better packing and hence higher density of the compounds. The interesting feature of this hydrogen bonded structure reported in this chapter is that the weaker C–H···F–C hydrogen bonds are forcing the molecules to pack differently [↑↑↑↑ directions of molecules compared to ↑↓↑↓↑↓ direction of the molecules] in the lattice. Because of such alteration, the unit cell parameters of these compounds are different though the space groups of all the structures (except one) were same ($P2_1/c$). It is interesting to observe that these compounds did not display polymorphism although there were possibilities of different molecular arrangements keeping the strong hydrogen bond unaltered. The molecular conformation of the compounds reported here are significantly different (Table 2.4.1). The orientations of the aromatic rings (C3-C8 and C10-C15) are significantly different in these 9 molecules thereby allowing the fluorine atoms to get involved in different C–H···F–C hydrogen bonds.

Supramolecular synthons involving 8 members (Scheme 2.4.1) forming a dimer through a pair of C–H···F–C hydrogen bonds have been a common feature in these structures. These dimers have been found to be interconnected to each other by

another C–H···F–C hydrogen bonds just like the known cases with strong hydrogen bonds involving carboxylic acid dimers. Therefore, it is evident that "organic fluorine" is also capable of acting as hydrogen bond acceptor and can behave in the same manner like other good hydrogen bond acceptors.

**Table 2.4.1: Torsion angle in (°) of the crystal structures**

| Compounds | Torsion Angle C4-C3-C2-C1 | Torsion Angle C3-C2-C1-O1 | Torsion Angle O1-C1-N1-C10 | Torsion Angle C11-C10-N1-C1 |
|---|---|---|---|---|
| **2c-1** | -70 | 1 | 5 | 137 |
| **2c-2** | -97 | -3 | 2 | 140 |
| **2c-3** | -74 | 32 | 6 | -157 |
| **2c-4** | -86 | -13 | -1 | 57 |
| **2c-5** | 104 | -69 | 0 | -28 |
| **2c-6** | -74 | 26 | 4 | 25 |
| **2c-7** | 98 | -20 | 2 | -125 |
| **2c-9** | -113 | 14 | -2 | -31 |
| **2c-10** | 103 | -25 | 3 | 33 |

## 2.5: Conclusions

The structural analysis of this series of fluorinated 2-(3-methoxyphenyl)-N-phenylacetamide derivatives invokes that although the structures of all these compounds are mostly controlled by strong hydrogen bonds, several weaker hydrogen bonds together are responsible for altering the molecular packing in the lattice. Different weak C–H···F–C hydrogen bonds and C–H···$\pi$($C_g$) interactions together immensely influence the crystal structures of these molecules. While strong hydrogen bonds are responsible for the formation of one dimensional molecular chain, the weaker hydrogen bonds involving "organic fluorine" are seen to form chains, dimers, tetramers *etc.* in the crystal lattice. It is also shown that the presence of several weaker interactions has resulted into different unit cell dimensions for these molecules though the unit cell volume remain similar. Therefore, it may be concluded that the influence of many weak hydrogen bonds involving "organic fluorine", which was earlier neglected by Dunitz,[43] Glusker[46] and Howard,[47] is highly significant in altering the crystalline architecture even in the presence of strong hydrogen bonds.

# Chapter 3

## Intermolecular Interactions Involving C–H···F Hydrogen Bond(s) and C–H···F–C Interactions in the Absence of Strong Hydrogen Bond in a Series of tetra-Fluorinated *N*-[2-(3-methoxyphenyl)ethyl]-*N*-phenylbenzamide Derivatives

# Chapter 3

## 3.1 Introduction

It has been demonstrated in the Chapter 2 that the fluorine mediated interactions can alter crystal packing in the case of compounds having the possibility of strong hydrogen bond involving a hydrogen bond acceptor carbonyl group (>C=O) and a strong hydrogen bond donor like –N–H group in the cases of the fluorinated phenylacetamides. In this Chapter we would focus on the structural aspects of 36 newly synthesized tetrafluorinated *N*-[2-(3-methoxyphenyl)ethyl]-*N*-phenylbenzamide derivatives and the corresponding non-fluorinated analogue. These compounds were synthesized from the amides (**2c-1** to **2c-10**) by a synthetic protocol reported in the experimental section 3.2. We have conducted a search in the CSD for compounds having Ph–CONR$^1$R$^2$ (R$^1$, R$^2$ = alkyl or aryl) functionality and a fluorophenyl ring. Among the compounds matching these criteria, we identified few acyclic amides which need to be addressed appropriately. Kato *et al*., in 2008 reported the evidences of polymorphism, pseudopolymorphism, and solid to solid structural transition in 1,2-bis-(N-4-fluorobenzoyl)-(N-methylamino)benzene where they observed total 11 pseudopolymorphs crystallized from different solvents.[76] They reported that the form III on heating lost solvent molecules near 60 $^{o}$C and then on further heating was converted to Form I, which on further heating was transformed to form II beyond 160 $^{o}$C. Similarly, the Form X was converted to Form I on heating beyond 60 $^{o}$C and on further hearing, Form II was observed beyond 150 $^{o}$C. Interestingly, the authors did not emphasise on the crystal packing and weak interactions that were present in these different forms (pseudopolymorphs and

polymorphs). We noted that the weak interactions involving the fluorine atom were mostly with the protons on the $–CH_3$ group present in the molecule or with the $sp^3$ protons present in the solvent molecules; rarely the C–H···F hydrogen bond involved aromatic protons in these structures. None of these structures indicated the existence of C–F···F interaction. All the structures of various pseudopolymorphs were found to be stabilized by C–H···O=C hydrogen bonds involving the aromatic C–H groups and in some cases the C–H groups from the solvent molecules. This report motivated us to investigate further on similar molecules with larger number of fluorine substitutions keeping the central functional group ($Ph–CONR^1R^2$) unchanged. Therefore, we synthesized a series of tetrafluorinated *N*-[2-(3-methoxyphenyl)ethyl]-*N*-phenylbenzamide derivatives and studied their structural features related to "organic fluorine"

### 3.2 Experimental

#### 3.2.1 Synthesis and Characterization

The synthesis of compound **4a** was carried out in two steps starting with **2a** as per the scheme 3.2.1. Synthesis of amine (3c) from the amide (2c) were done by Nagarajan *et al.,* by using $LiAlH_4$ as reducing agent in a mixture of dry ether and dioxane but the reaction was reported to continue overnight with maximum yield of 84% with fluorinated **2c**. The same procedure was tried for our substrates and we experienced poor yield and long-time (48-72 hrs) for reaction to reach maximum yield of 70-75%. Therefore, we adopted a different method for this reaction.[76(a)] In 100ml dry round bottom flask, substituted phenylacetamide (**2c**) (1.0 equiv) and $NaBH_4$ (2.3 equiv) were added. In another 50 ml round bottom flask, $I_2$ (1.0 equiv) was taken. In both the round bottom flask, 30 ml dry tetrahydrofuran (THF) was added. Then the $I_2$ solution in THF was taken out using syringe and added dropwise to the other round bottom flask having the substituted phenylacetamide and $NaBH_4$ in THF. The controlled addition was done at $0^oC$ for 2.5 h. After addition of each drop of $I_2$ solution, the reaction mixture showed slightly yellow colour but it disappeared immediately. After complete addition, the reaction mixture was refluxed at $80^oC$ for 10 hrs. After completion of the reaction, the reaction mixture was cooled to $0^oC$ and excess hydride was quenched by carefully addition of 3N HCl at $0^oC$ until effervescence stopped. Then the reaction mixture was refluxed for 1 hr at $80^oC$ to ensure the complete quenching of excess hydride. Then the reaction mixture was treated with 6N NaOH solution. The basic nature of the reaction mixture was checked using pH paper. Then

the workup was done with the ethyl acetate, brine solution and dried over sodium sulphate. The solvent was removed using rota-evaporator and the crude product was purified by column chromatography on basic alumina as the stationary phase and 2% ethyl acetate in hexane as the mobile phase. All the products (**3c**) were found to be dense liquid. All the amines (**3c**) were characterized by $^{1}H$, $^{13}C$ and $^{19}F$ NMR spectroscopy. Representative spectra are provided in the figures below and all the spectrum are enclosed in the ESI.

**Synthesis of 4a:** This step of synthesis was carried out following the method reported by Nagarajan *et al*., using the fluorinated benzoyl chloride as a reactant instead of the corresponding benzoic acid and 1,2-dichloroethane (DCE) instead of going through hazardous protocol using thionyl chloride and benzene solvent.[76(b)] In a 100ml dry round bottom flask, **3c** (1.0 equiv) was taken and 1,2-dichloroethane (DCE) solvent was added. The $N_2$ gas was purged to create inert atmosphere. In another 50 ml round bottom flask, difluorobenzoyl chloride (1.8 equiv) was taken under $N_2$ atmosphere and 20 ml of DCE solvent was added. Then the benzoyl chloride solution was added dropwise to the secondary amine solution using cannula at 0$^{o}$C. Then the reaction mixture was refluxed at 100 $^{o}$C for 4 hrs. After the completion of the reaction, work-up was done using DCM and brine solution and the crude products were dried over sodium sulphate. The crude product was purified by column chromatography using basic alumina as the stationary phase and 4-6% ethyl acetate in hexane as the stationary phase. All these amides (**4a**) were characterized by $^{1}H$, $^{13}C$ and $^{19}F$ NMR spectroscopy. Representative spectra are provided in the figures below and all the spectrum are enclosed in the ESI.

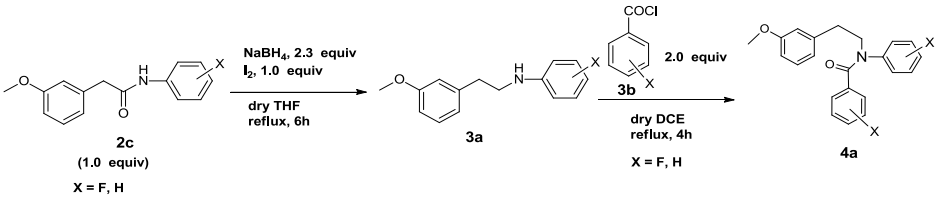
NaBH4, 2.3 equiv
I2, 1.0 equiv
dry THF
reflux, 6h
2c
(1.0 equiv)
X = F, H
3a
COCl
3b
2.0 equiv
dry DCE
reflux, 4h
X = F, H
4a

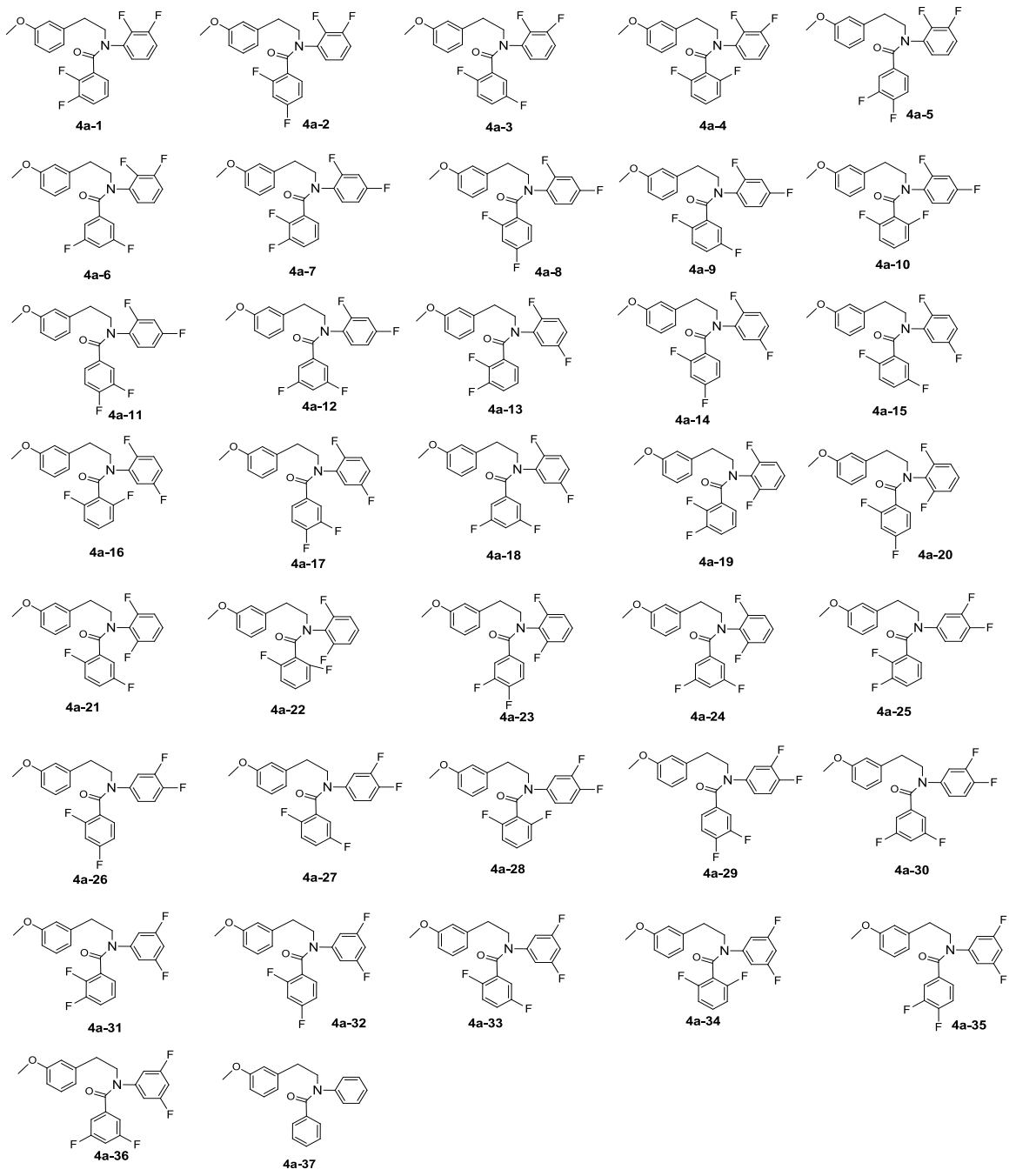
4a-1
4a-2
4a-3
4a-4
4a-5
4a-6
4a-7
4a-8
4a-9
4a-10
4a-11
4a-12
4a-13
4a-14
4a-15
4a-16
4a-17
4a-18
4a-19
4a-20
4a-21
4a-22
4a-23
4a-24
4a-25
4a-26
4a-27
4a-28
4a-29
4a-30
4a-31
4a-32
4a-33
4a-34
4a-35
4a-36
4a-37

**Scheme 3.2.1**

## NMR

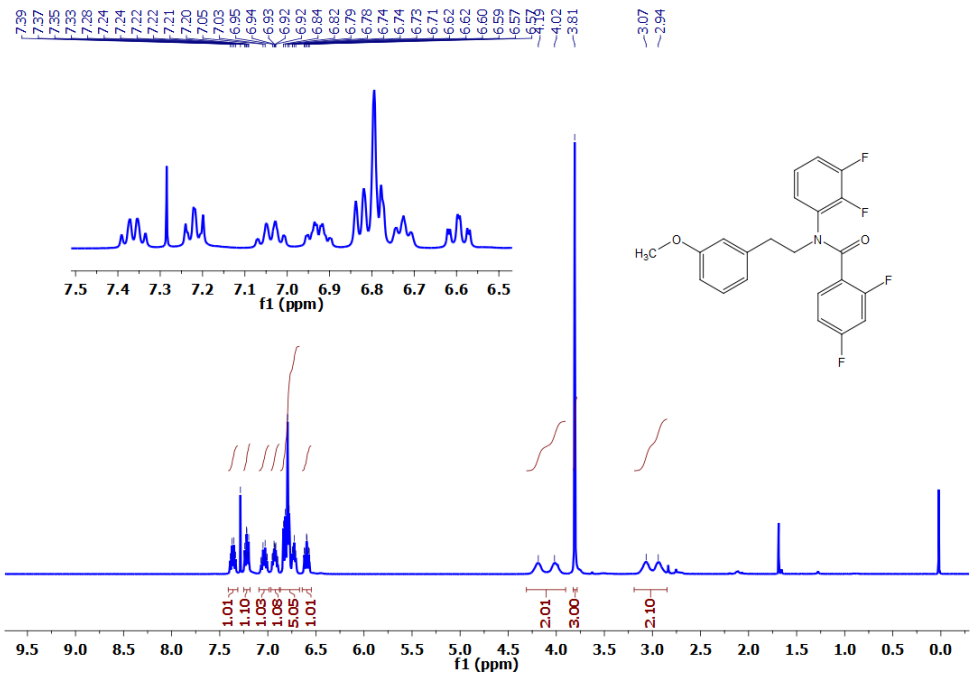

**$^{1}$H - NMR Spectra of 4a-2 (400 MHz, $CDCl_3$) : δ (ppm)** = 3.00 (d, 2H), 3.81 (s, 3H), 4.10 (d, 2H), 6.605 (dt, 1H), 6.71-6.84 (m, 5H), 6.92 (dt, 1H), 7.01-7.07 (m, 1H), 7.20-7.24 (m, 1H), 7.36 (q, 1H).

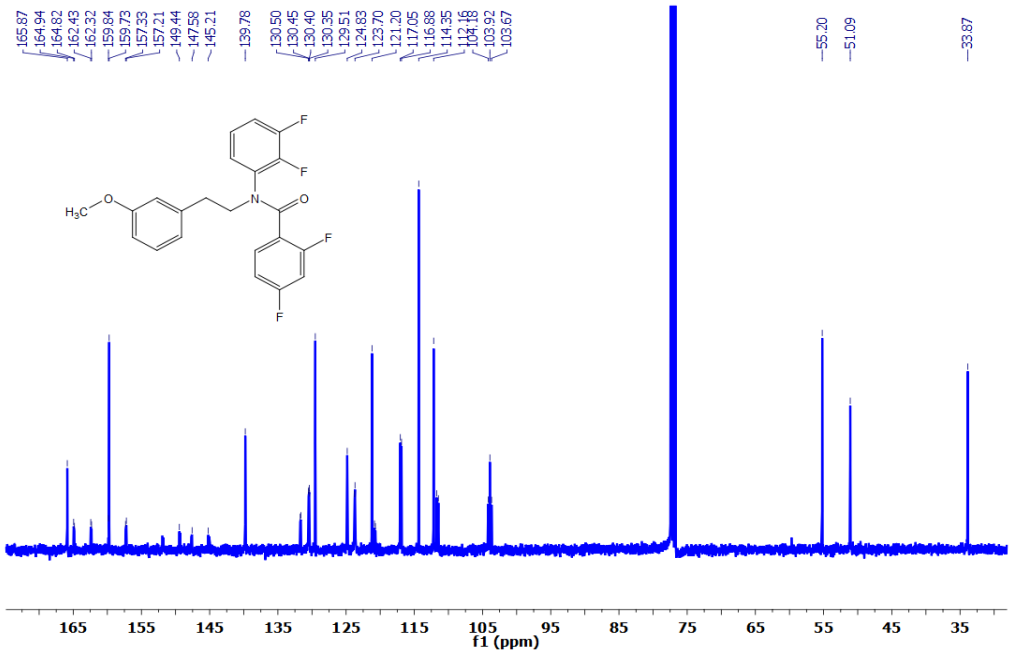

**$^{13}$C spectra of 4a-2, (125 MHz, $CDCl_3$): δ (ppm)** = 117.06, 116.89, 114.36, 112.17, 112.09, 111.73, 111.70, 111.51, 111.48, 104.19, 103.93, 103.68, 59.70, 55.27, 55.21, 51.10, 33.87

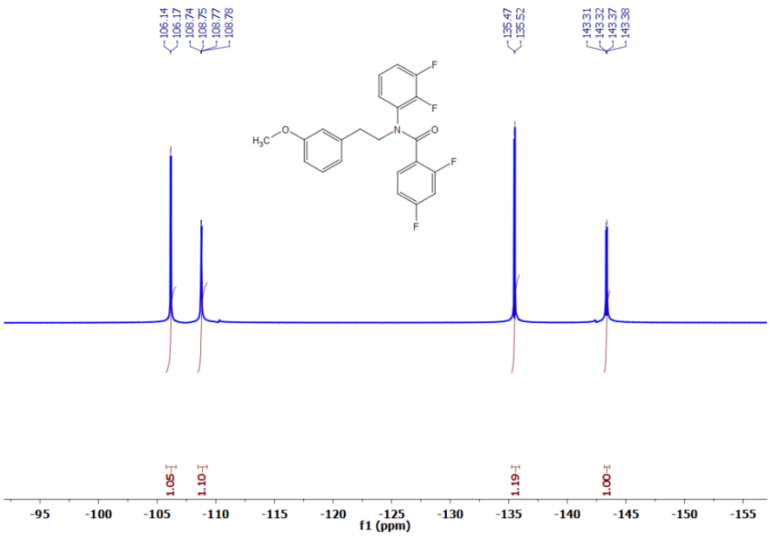


**$^{19}$F- NMR Spectra of 4a-2 (376 MHz, $CDCl_3$): δ (ppm)** = -143.34 (q, 1F), -135.49 (d, 1F), -108.76 (q, 1F), -106.15 (d, 1F)

**FT-IR**

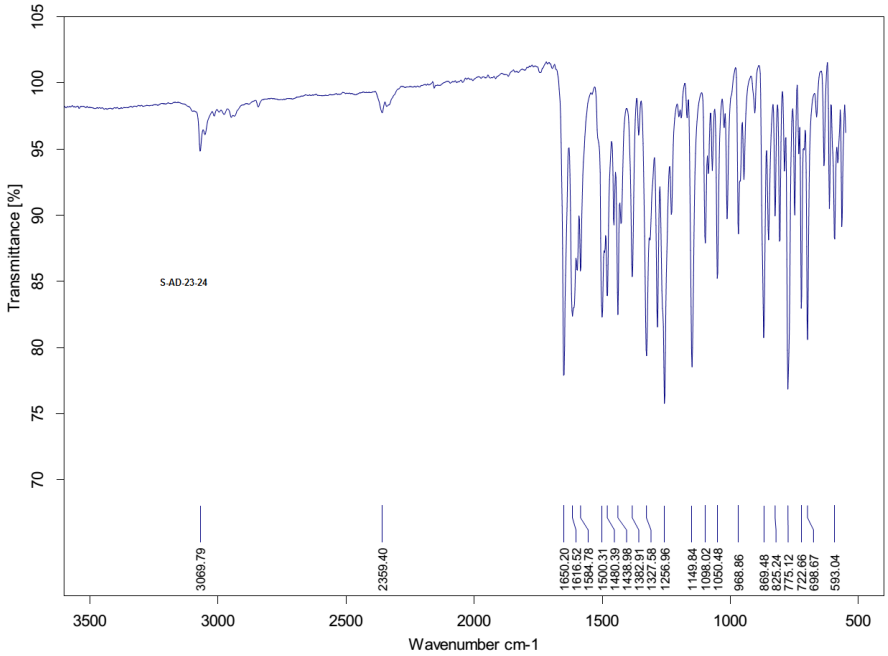


FT-IR of the compound **4a-2**

### 3.2.2 Structural Study:

All the crystal structures were determined using the same diffractometer and the same procedure reported in the Chapter 2. The compounds **4a-1**, **4a-2**, **4a-3**, **4a-6**, **4a-14**, **4a-21**, **4a-24**, **4a-26**, **4a-29** and **4a-32** could not be crystallized for structure determination. The structures of some of these compounds (**4a**) were found to have

disorder in the orientation of the fluorinated phenyl rings by the rotation of the fluorophenyl ring about the C–C or C–N bonds. This disorder was modelled using the methodology described below.

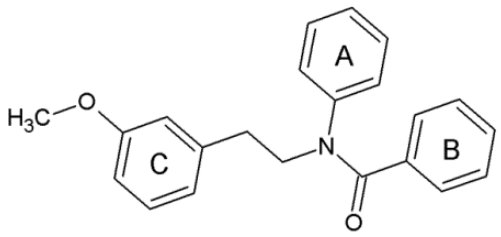


**Scheme 3.2.2**

**Crystallographic Modelling of Disorder**

All the data have collected at 100K. The compounds **4a-9**, **4a-10**, **4a-17**, **4a-25** and **4a-27** were found to be disordered structure. The positional disorder has been found due rotation of phenyl ring around C–C or C–N bonds in the molecule. These compounds were refined with 0.5 occupancy using PART command in SHELXL97. Thermal parameters of the atoms of the two parts, which belong to the same chemical environment, were constrained to be equal by EADP command in SHELXL 97. All the disordered structures have only one molecule in the asymmetric unit ($Z' = 1$). In case of the compounds **4a-9** (occupancy 0.87:0.13) and **4a-10** (occupancy 0.87:0.13) have the disorder in the phenyl ring **A** around C–N bond, while in the structure **4a-17** (occupancy 0.94:0.06) disorder have been found in the **B** phenyl ring around C–C bond. Both the phenyl rings **A** as well as **B** have observed the disordered structure at 100K data in the case of **4a-25** (occupancy 0.84:0.16 for both ring) and **4a-27** (occupancy 0.95:0.05 for both ring) (Scheme 3.2.1). Refinement of these compounds was done for two independent positions, namely **A** and **B** ('**A**' for higher occupancy and '**B**' for lower occupancy). For refinement, the positions of carbon atom in benzene ring for **A** and **B** were kept fixed using EXYZ command in SHELXL97. For the atoms at the same position, thermal parameters were also constrained to be equal using EADP command in SHELXL97. All hydrogen atoms were then positioned geometrically and refined using a riding model with $U_{iso}(H) = 1.2\ U_{eq}(C,N)$. Except fluorine all other atoms in the minor conformer were refined isotopically and the thermal parameter of all the carbon atoms was constrained to the same value using EADP command in SHELXL97.

## Table 3.2.2.1: Single crystal X-ray diffraction data of compounds 4a-4 to 4a-11

| **Identification code** | **4a-4** | **4a-5** | **4a-7** | **4a-8** | **4a-9** | **4a-11** |
|---|---|---|---|---|---|---|
| **CCDC No** | 1456822 | 1456823 | 1477818 | 1456811 | 1456814 | 1456813 |
| **Formula** | $C_{22}H_{17}F_4NO_2$ | $C_{22}H_{17}F_4NO_2$ | $C_{22}H_{17}F_4NO_2$ | $C_{22}H_{17}F_4NO_2$ | $C_{22}H_{17}F_4NO_2$ | $C_{22}H_{17}F_4NO_2$ |
| **Formula weight** | 403.36 | 403.36 | 403.36 | 403.36 | 403.36 | 403.36 |
| **Temperature (K)** | 100.0 | 100.0 | 100.0 | 100.0 | 100.0 | 100.0 |
| **Crystal system** | Triclinic | Orthorhombic | Monoclinic | Monoclinic | Orthorhombic | Monoclinic |
| **Space group** | $P\ \bar{1}$ | $P2_12_12_1$ | $P2_1/c$ | $P2_1$ | $Pbca$ | $P2_1$ |
| **a (Å)** | 7.0928(7) | 6.791(2) | 8.3192(14) | 11.2206(18) | 19.630(4) | 11.3092(16) |
| **b (Å)** | 11.30560(10) | 14.041(4) | 22.270(4) | 6.7281(8) | 12.640(3) | 6.6176(8) |
| **c (Å)** | 12.4136(10) | 19.036(4) | 20.451(3) | 12.6609(19) | 15.195(3) | 12.6738(18) |
| **α (°)** | 70.18(3) | 90 | 90 | 90 | 90 | 90 |
| **β (°)** | 84.28(4) | 90 | 97.292(8) | 100.742(8) | 90 | 100.290(7) |
| **γ (°)** | 75.44(4) | 90 | 90 | 90 | 90 | 90 |
| **V (Å$^3$)** | 906.29(12) | 1815.1(9) | 3758.2(11) | 939.1(2) | 3770.1(14) | 933.2(2) |
| **Z** | 2 | 4 | 8 | 2 | 8 | 2 |
| **Z′** | 1 | 2 | 2 | 1 | 1 | 1 |
| **$\rho_{calc}$ (g cm$^{-3}$)** | 1.478 | 1.476 | 1.426 | 1.427 | 1.421 | 1.435 |
| **μ/ mm$^{-1}$** | 0.122 | 0.122 | 0.118 | 0.118 | 0.118 | 0.119 |
| **F(000)** | 416 | 832 | 1664 | 416 | 1664 | 416 |
| **$2\theta_{min,max}$(°)** | 6.06-55.12 | 6.37-54.99 | 6.15-55.01 | 6.55-54.94 | 6.45-54.98 | 6.53-54.90 |
| **$h_{min,max}$; $k_{min,max}$; $l_{min,max}$** | -9, 9; -14, 14; -15, 16 | -8, 8; -18, 18; -24, 24 | -10, 10; -28, 28; -26, 18 | -14, 14; -8, 8; -16, 16 | -25, 25; -16, 16; -19, 19 | -14, 14; -8, 8; -16, 16 |
| **Total no. of reflections** | 9347 | 18705 | 23733 | 10161 | 33909 | 10071 |
| **$R_{int}$** | 0.0365 | 0.0437 | 0.0641 | 0.0559 | 0.0660 | 0.0255 |
| **No. of unique reflections** | 4137 | 4138 | 8571 | 4283 | 4309 | 4262 |
| **$R_1$ [I > 2σ(I)]** | 0.0398, | 0.0376 | 0.0573 | 0.0479 | 0.0631 | 0.0387 |
| **$wR_2$ (all data)** | 0.1089 | 0.0981 | 0.1604 | 0.1338 | 0.1775 | 0.1003 |
| **GooF** | 1.004 | 1.027 | 1.046 | 1.058 | 1.122 | 1.061 |
| **$\Delta\rho_{max,min}$/eÅ$^{-3}$** | 0.30/-0.25 | 0.24/-0.17 | 0.45/-0.29 | 0.39/-0.22 | 0.44/-0.29 | 0.33/-0.19 |

## Table 3.2.2.2: Single crystal X-ray diffraction data of compounds 4a-10 to 4a-16

| **Identification code** | **4a-10** | **4a-12** | **4a-13** | **4a-15** | **4a-16** |
|---|---|---|---|---|---|
| **CCDC No** | 1456812 | 1477817 | 1456815 | 1456804 | 1477815 |
| **Formula** | $C_{22}H_{17}F_4NO_2$ | $C_{22}H_{17}F_4NO_2$ | $C_{22}H_{17}F_4NO_2$ | $C_{22}H_{17}F_4NO_2$ | $C_{22}H_{17}F_4NO_2$ |
| **Formula weight** | 403.36 | 403.36 | 403.36 | 403.36 | 403.36 |
| **Temperature (K)** | 100.0 | 100.0 | 100.0 | 100.0 | 100.0 |
| **Crystal system** | Orthorhombic | Monoclinic | Triclinic | Triclinic | Triclinic |
| **Space group** | $P2_12_12_1$ | $P2_1/c$ | $P\ \bar{1}$ | $P\ \bar{1}$ | $P\ \bar{1}$ |
| **a (Å)** | 7.848(4) | 14.054(3) | 8.649(4) | 8.661(3) | 6.532(3) |
| **b (Å)** | 12.908(5) | 18.823(4) | 8.883(3) | 10.069(3) | 8.694(4) |
| **c (Å)** | 18.874(10) | 15.625(4) | 12.316(5) | 11.400(3) | 16.808(6) |
| **α (°)** | 90 | 90 | 91.08(2) | 93.191(12) | 94.99(2) |
| **β (°)** | 90 | 115.509(8) | 99.57(3) | 100.573(9) | 95.95(2) |
| **γ (°)** | 90 | 90 | 97.112(17) | 106.933(7) | 97.04(2) |
| **V (Å$^3$)** | 1912.1(15) | 3730.3(14) | 925.1(7) | 928.6(4) | 937.3(7) |
| **Z** | 4 | 8 | 2 | 2 | 2 |
| **Z′** | 1 | 2 | 1 | 1 | 1 |
| **$\rho_{calc}$ (g cm$^{-3}$)** | 1.401 | 1.436 | 1.448 | 1.443 | 1.429 |
| **μ/ mm$^{-1}$** | 0.116 | 0.119 | 0.120 | 0.119 | 0.118 |
| **F(000)** | 832 | 1664 | 416 | 416 | 416 |
| **$2\theta_{min,max}$(°)** | 6.08 - 55.03 | 6.17 - 54.99 | 6.23 - 54.92 | 6.29 - 55.00 | 6.33 - 55.06 |
| **$h_{min,max}$; $k_{min,max}$; $l_{min,max}$** | -10, 9; -16, 16; -23, 24 | -18, 17; -24, 24; -20, 20 | -11, 11; -11, 11; -15, 15 | -11,11; -13; 13, -14, 14 | -8, 8; -11, 11; -21, 21 |
| **Total no. of reflections** | 12786 | 33281 | 9945 | 10018 | 10231 |
| **$R_{int}$** | 0.0398 | 0.0697 | 0.0358 | 0.0297 | 0.0485 |
| **No. of unique reflections** | 4390 | 8508 | 4197 | 4253 | 4284 |
| **$R_1$ [I > 2σ(I)]** | 0.0431 | 0.0655 | 0.0409 | 0.0437 | 0.0528 |
| **w$R_2$ (all data)** | 0.1072 | 0.1665 | 0.1052 | 0.1241 | 0.1447 |
| **GooF** | 1.062 | 1.065 | 0.965 | 1.046 | 1.069 |
| **$\Delta\rho_{max,min}$/eÅ$^{-3}$** | 0.18/-0.18 | 0.55/-0.30 | 0.26/-0.29 | 0.32/-0.22 | 0.30/-0.23 |

## Table 3.2.2.3: Single crystal X-ray diffraction data of compounds 4a-17 to 4a-23

| **Identification code** | **4a-17** | **4a-18** | **4a-19** | **4a-20** | **4a-22** | **4a-23** |
|---|---|---|---|---|---|---|
| **CCDC No** | 1477814 | 1456807 | 1477816 | 1456805 | 1477813 | 1456798 |
| **Formula** | $C_{22}H_{17}F_4NO_2$ | $C_{22}H_{17}F_4NO_2$ | $C_{22}H_{17}F_4NO_2$ | $C_{22}H_{17}F_4NO_2$ | $C_{22}H_{17}F_4NO_2$ | $C_{22}H_{17}F_4NO_2$ |
| **Formula weight** | 403.36 | 403.36 | 403.36 | 403.36 | 403.36 | 403.36 |
| **Temperature (K)** | 100.0 | 100.0 | 100.0 | 100.0 | 100.0 | 100.0 |
| **Crystal system** | Monoclinic | Monoclinic | Monoclinic | Orthorhombic | Monoclinic | Orthorhombic |
| **Space group** | $P2_1/c$ | $P2_1/c$ | $P2_1/c$ | $Pbca$ | $P2_1/c$ | $Pbca$ |
| **a (Å)** | 7.699(8) | 7.686(3) | 10.3595(15) | 12.5050(16) | 9.550(3) | 12.646(2) |
| **b (Å)** | 14.711(14) | 14.586(4) | 12.9485(16) | 15.2686(19) | 8.6078(19) | 15.169(2) |
| **c (Å)** | 19.52(2) | 19.627(5) | 14.705(2) | 19.352(2) | 25.576(7) | 19.467(4) |
| **α (°)** | 90 | 90 | 90 | 90 | 90 | 90 |
| **β (°)** | 123.47(4) | 123.051(10) | 106.947(6) | 90 | 116.066(13) | 90 |
| **γ (°)** | 90 | 90 | 90 | 90 | 90 | 90 |
| **V (Å$^3$)** | 1844(3) | 1844.2(10) | 1886.9(5) | 3695.0(8) | 1888.6(8) | 3734.4(11) |
| **Z** | 4 | 4 | 4 | 8 | 4 | 8 |
| **Z′** | 1 | 1 | 1 | 1 | 1 | 1 |
| **$\rho_{calc}$ (g cm$^{-3}$)** | 1.453 | 1.453 | 1.420 | 1.450 | 1.419 | 1.435 |
| **μ/ mm$^{-1}$** | 0.120 | 0.120 | 0.117 | 0.120 | 0.117 | 0.119 |
| **F(000)** | 832 | 832 | 832 | 1664 | 832 | 1664 |
| **$2\theta_{min,max}$(°)** | 6.06 - 55.06 | 6.07 - 55.01 | 6.05 - 55.01 | 6.52 - 54.98 | 6.38 - 55.02 | 6.44 - 54.96 |
| **$h_{min,max}$; $k_{min,max}$; $l_{min,max}$** | -10, 10; -19, 19; -25, 25 | -9, 9; -18, 18; -25, 25 | -13, 13; -16, 16; -19, 19 | -6, 16; -17, 19; -25, 24 | -12, 12; -10, 11; -29, 29 | -12, 16; -19, 17; -25, 25 |
| **Total no. of reflections** | 19561 | 19614 | 19122 | 12628 | 17647 | 24357 |
| **$R_{int}$** | 0.0482 | 0.0459 | 0.0388 | 0.0814 | 0.0446 | 0.0451 |
| **No. of unique reflections** | 4214 | 4207 | 4313 | 4227 | 4320 | 4271 |
| **$R_1$ [I > 2σ(I)]** | 0.0502 | 0.0446 | 0.0484 | 0.0649 | 0.0491 | 0.0550 |
| **$wR_2$ (all data)** | 0.1515 | 0.1258 | 0.1346 | 0.1659 | 0.1257 | 0.1461 |
| **GooF** | 1.081 | 1.051 | 1.073 | 1.073 | 1.067 | 1.104 |
| **$\Delta\rho_{max,min}$/eÅ$^{-3}$** | 0.86/-0.28 | 0.36/-0.27 | 0.32/-0.23 | 0.28/-0.28 | 0.28/-0.23 | 0.56/-0.26 |

**Table 3.2.2.4: Single crystal X-ray diffraction data of compounds 4a-25 to 4a-33**

| **Identification code** | **4a-25** | **4a-27** | **4a-28** | **4a-30** | **4a-31** | **4a-33** |
|---|---|---|---|---|---|---|
| **CCDC No** | 1456799 | 1456800 | 1456801 | 1456802 | 1456792 | 1456793 |
| **Formula** | $C_{22}H_{17}F_4NO_2$ | $C_{22}H_{17}F_4NO_2$ | $C_{22}H_{17}F_4NO_2$ | $C_{22}H_{17}F_4NO_2$ | $C_{22}H_{17}F_4NO_2$ | $C_{22}H_{17}F_4NO_2$ |
| **Formula weight** | 403.36 | 403.36 | 403.36 | 403.36 | 403.36 | 403.36 |
| **Temperature (K)** | 100.0 | 100.0 | 100.0 | 100.0 | 100.0 | 100.0 |
| **Crystal system** | Monoclinic | Monoclinic | Orthorhombic | Triclinic | Triclinic | Monoclinic |
| **Space group** | $P2_1/c$ | $P2_1/c$ | $P2_12_12_1$ | $P\bar{1}$ | $P\bar{1}$ | $P2_1/c$ |
| **a (Å)** | 12.511(4) | 12.9586(15) | 8.1631(14) | 8.062(4) | 7.1119(11) | 14.7833(15) |
| **b (Å)** | 8.430(3) | 7.8587(7) | 12.524(2) | 9.592(5) | 9.5666(9) | 8.5522(7) |
| **c (Å)** | 18.189(5) | 19.129(2) | 18.705(3) | 13.231(6) | 14.8367(18) | 24.482(2) |
| **α (°)** | 90 | 90 | 90 | 103.535(19) | 83.93(3) | 90 |
| **β (°)** | 102.301(12) | 105.267(4) | 90 | 91.312(6) | 76.68(3) | 143.319(4) |
| **γ (°)** | 90 | 90 | 90 | 108.621(17) | 73.34(3) | 90 |
| **V (Å$^3$)** | 1874.2(11) | 1879.3(4) | 1912.3(6) | 937.4(8) | 940.2(3) | 1849.0(3) |
| **Z** | 4 | 4 | 4 | 2 | 2 | 4 |
| **Z′** | 1 | 1 | 1 | 1 | 1 | 1 |
| **$\rho_{calc}$ (g cm$^{-3}$)** | 1.430 | 1.426 | 1.401 | 1.429 | 1.425 | 1.449 |
| **μ/ mm$^{-1}$** | 0.118 | 0.118 | 0.116 | 0.118 | 0.118 | 0.120 |
| **F(000)** | 832 | 832 | 832 | 416 | 416 | 832 |
| **$2\theta_{min,max}$(°)** | 6.04 - 50.05 | 6.124 - 50.03 | 6.344 - 54.972 | 6.258 - 55.12 | 6.12 - 55.03 | 6.63 - 55.06 |
| **$h_{min,max}$; $k_{min,max}$; $l_{min,max}$** | -14,14; -10, 10; -21, 21 | -10, 10; -19, 19; -21, 21 | -10, 16; -16, 18; -24, 24 | -10, 10; -12, 12; -17, 17 | -9, 9; -12, 12; -19, 19 | -19, 19; -11, 10; -31,31 |
| **Total no. of reflections** | 9821 | 9776 | 19334 | 10119 | 9627 | 12159 |
| **$R_{int}$** | 0.0502 | 0.0285 | 0.0629 | 0.0290 | 0.0389 | 0.0494 |
| **No. of unique reflections** | 3289 | 3301 | 4232 | 4302 | 4290 | 4223 |
| **$R_1$ [I > 2σ(I)]** | 0.0507 | 0.0414 | 0.0941 | 0.0391 | 0.0445 | 0.0391 |
| **w$R_2$ (all data)** | 0.1431 | 0.1161 | 0.2645 | 0.1117 | 0.1301 | 0.1087 |
| **GooF** | 1.052 | 1.072 | 1.155 | 1.070 | 1.077 | 1.062 |
| **$\Delta\rho_{max,min}$/eÅ$^{-3}$** | 0.30/-0.31 | 0.23/-0.24 | 0.89/-0.33 | 0.30/-0.24 | 0.37/-0.27 | 0.36/-0.27 |

**Table 3.2.2.5: Single crystal X-ray diffraction data of compounds 4a-34 to 4a-37**

| **Identification code** | **4a-34** | **4a-35** | **4a-36** | **4a-37** |
|---|---|---|---|---|
| **CCDC No** | 1456794 | 1477819 | 1456796 | 1456795 |
| **Formula** | $C_{22}H_{17}F_4NO_2$ | $C_{22}H_{17}F_4NO_2$ | $C_{22}H_{17}F_4NO_2$ | $C_{22}H_{21}NO_2$ |
| **Formula weight** | 403.36 | 403.36 | 403.36 | 331.40 |
| **Temperature (K)** | 100.0 | 100.0 | 100.0 | 100.0 |
| **Crystal system** | Monoclinic | Triclinic | Monoclinic | Monoclinic |
| **Space group** | $P2_1/c$ | $P\bar{1}$ | $P2_1/c$ | $C2/c$ |
| **a (Å)** | 15.170(5) | 9.21160(10) | 13.4004(19) | 17.640(4) |
| **b (Å)** | 8.022(2) | 9.7778(15) | 8.4135(10) | 9.1027(14) |
| **c (Å)** | 15.485(5) | 12.026(2) | 26.011(3) | 22.797(4) |
| **α (°)** | 90 | 89.67(5) | 90 | 90 |
| **β (°)** | 90.823(16) | 78.40(5) | 138.825(4) | 103.211(6) |
| **γ (°)** | 90 | 62.05(3) | 90 | 90 |
| **V (Å$^3$)** | 1884.2(10) | 932.3(3) | 1930.7(4) | 3563.6(11) |
| **Z** | 4 | 2 | 4 | 8 |
| **Z′** | 1 | 1 | 1 | 1 |
| **$\rho_{calc}$ (g cm$^{-3}$)** | 1.422 | 1.437 | 1.388 | 1.235 |
| **μ/ mm$^{-1}$** | 0.118 | 0.119 | 0.115 | 0.079 |
| **F(000)** | 832 | 416 | 832 | 1408 |
| **$2\theta_{min,max}$(°)** | 6.304 - 55.144 | 6.51 - 50.03 | 6.46 - 54.96 | 6.56 - 55 |
| **$h_{min,max}$; $k_{min,max}$;$l_{min,max}$** | -14 ,14; -10, 10; -21, 21 | -19, 19; -11, 10; -31, 31 | -17, 17; -10, 10; -32, 33 | -22, 22; -11, 11; -29, 29 |
| **Total no. of reflections** | 19677 | 8176 | 12686 | 17533 |
| **$R_{int}$** | 0.1278 | 0.0896 | 0.0421 | 0.0565 |
| **No. of unique reflections** | 4304 | 3286 | 4387 | 4065 |
| **$R_1$ [I > 2σ(I)]** | 0.0821 | 0.0505 | 0.0418 | 0.0404 |
| **w$R_2$ (all data)** | 0.2140 | 0.1396 | 0.1207 | 0.1084 |
| **GooF** | 1.069 | 0.922 | 1.065 | 1.068 |
| **$\Delta\rho_{max,min}$/eÅ$^{-3}$** | 0.31/-0.27 | 0.46/-0.29 | 0.29/-0.25 | 0.24/-0.20 |

### 3.3 Results

**N-(2,3-difluorophenyl)-2,6-difluoro-N-[2-(3-methoxyphenyl)ethyl]benzamide (4a-4):** The compound **4a-4** adopted triclinic centrosymmetric $P\bar{1}$ space group with Z = 2 and Z' =1 (Figure 3.3.1a). As these compounds, do not have any N–H bond like the molecules reported in the chapter 2, there is no possibility of formation of strong hydrogen bonds in the crystal lattice. Only weak hydrogen bonds like C–H···F, C–H···O, and C–H···π interactions are observed in crystal packing. Out of the four fluorine substitutions, two fluorine atoms (F1 and F2) on the B ring, are simultaneously involved in weak C19–H19···F1 and C1–H1A···F2 hydrogen bonds (Table 3.3.1). These C–H···F hydrogen bonds are found to make one dimensional infinite catameric chain along the crystallographic *a* direction through the translational lattice symmetry (Figure 3.3.1b). It is noteworthy that one of these hydrogen bonds involves hydrogen atom attached to a $sp^3$ hybridized carbon.

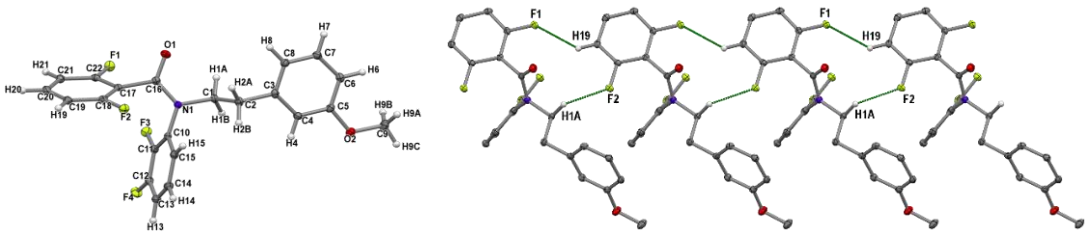


**(a)** **(b)**

**Figure 3.3.1: (a)** ORTEP of **4a-4** drawn with 50% probability ellipsoid, **(b)** Formation of one dimensional infinite catameric chain along the crystallographic *a* direction through C–H···F hydrogen bonds.

In addition, *m*- hydrogen (H21) of the B ring and *o*- hydrogen (H15) of the A ring are simultaneously involved in a weak C–H···π interaction with the common centroid of the C ring and thus generates an infinite chain (Figure 3.3.1c). Further the *p*-hydrogen (H13) of the A ring and the centroid of the B ring also forms weak C13–H13···π interaction across the inversion centre and produces a dimer in the crystal lattice (Figure 3.3.1d). In this series of the compounds, all the molecules have a carbonyl functional group and this carbonyl group can offer weak C–H···O=C hydrogen bonds. In this molecule, this hydrogen bond is propagating as 1D chain in the *x*- direction and this one-dimensional chain is also supported by C19–H19···F1 hydrogen bonds (Figure 3.3.1e). In this crystal structure F···F contact have also been

observed. This F···F contact simultaneously exist in type-1(θ1= θ2=89 º) and quasi type-I/type-II (θ1=89 º and θ2=116 º) *via* inversion centre (Figure 3.3.1f). The experimental PXRD pattern of **4a-4** matches with the corresponding simulated PXRD pattern.

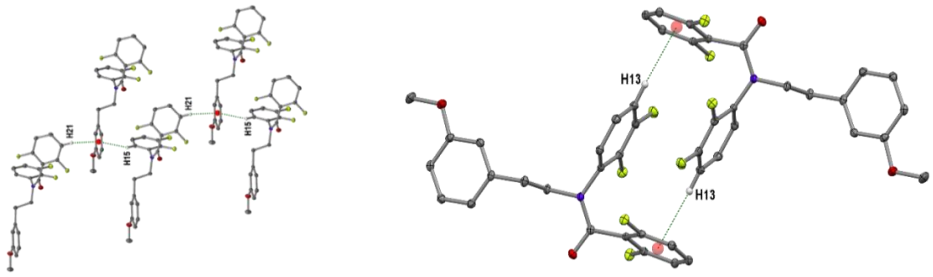


**(c)** **(d)**

**Figure 3.3.1: (c)** Molecular chain *via* C–H···π interaction up to infinite chain length **(d)** Formation of a centrosymmetric dimer by C13–H13···π interaction.

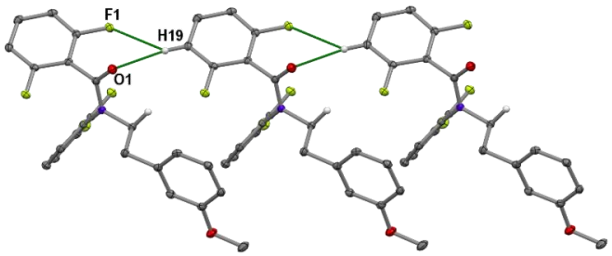


**(e)**

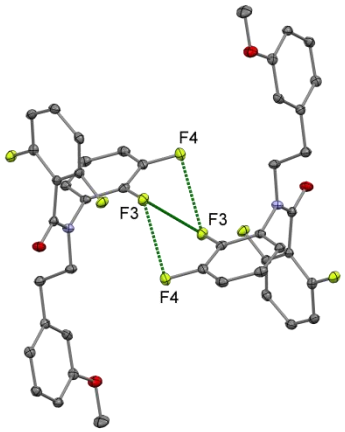


**(f)**

**Figure 3.3.1: (e)** Weak C–H···O and C–H···F hydrogen bonds both are propagating in the same direction along *x*- axis. **(f)** F3 and F4 are simultaneously forming Type -I (θ1 = θ2 = 89º) and quasi type-I/type-II (θ1 = 89 º and θ2 = 116 º) *via* C–F···F–C interaction across the inversion centre.

**Table 3.3.1: Intermolecular interactions in 4a-4**

| D–B···A | D–B/Å | *D*(D···A )/ Å | *d*(B···A )/Å | ∠D–B···A/º | SYMMETRY |
|---|---|---|---|---|---|
| **C1–H1A···F2** | 1.080 | 3.266(2) | 2.32 | 146 | x + 1, y, z |
| **C19–H19···F1** | 1.080 | 3.370(2) | 2.60 | 127 | x - 1, y, z |
| **C19–H19···O1** | 1.080 | 3.456(2) | 2.43 | 158 | x - 1, y, z |
| **C13–H13···π ($C_{gB}$)** | 1.080 | 3.680(2) | 2.81 | 152 | 3 - x, - y,1 - z |
| **C15–H15···π ($C_{gB}$)** | 1.080 | 3.660(2) | 2.81 | 150 | 1 + x, y, z |
| **C21–H21···π ($C_{gC}$)** | 1.080 | 3.472(2) | 2.57 | 158 | 1 + x, y - 1, z |
| **C11–F3···F3–C11** | 1.349(1), 1.349(1) | 3.917(2) | 2.897(1) | 89, 89 | 2 - x, - y, 1 - z |
| **C11–F3···F4–C12** | 1.349(1), 1.355(1) | 4.135(2) | 2.839(1) | 116, 90 | 2 - x, - y, 1 - z |

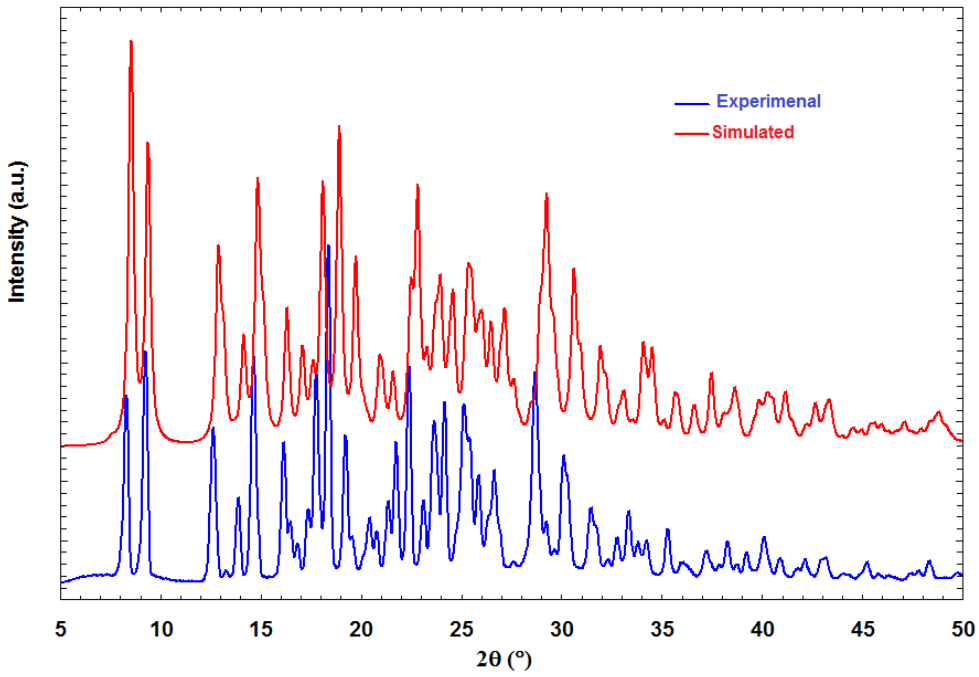


**Figure 3.3.1: (g)** Comparison of experimental and simulated PXRD patterns of **4a-4**

**N-(2,3-difluorophenyl)-34-difluoro-N-[2-(3-methoxyphenyl)ethyl]benzamide (4a-5):** The compound **4a-5** (Figure 3.3.2a) crystallized in chiral $P2_12_12_1$ space group with Z = 4. Three out of four fluorine atoms of this molecules are involved in C–H···F hydrogen bonds in the crystal lattice. One of the two F atoms of the A ring (F1) and one F atom of the B ring (F4) are found to form two different bifurcated C–H···F–C hydrogen bonds (Table 3.3.2**)**. The molecules form a helical chain through $2_1$ screw

operation along the *b*-axis involving bifurcated C–H···F–C hydrogen bonds (C2–H2A···F1 and C4–H4···F1) (Figure 3.3.2b). Similarly, another chain of molecule is formed through bifurcated C–H···F–C hydrogen bonds involving F4 (C6–H6···F4 and C7–H7···F4) through $2_1$ screw along the *c*- axis (Figure 3.3.2c). Further, the third fluorine (F2) also forms molecular chain involving C14–H14···F2 hydrogen bonds through $2_1$ screw along the *b*- direction (Figure 3.3.2.d). In addition, catameric chain of dimers through weak C–H···π [C1–H1B···π($C_{gB}$) and C15–H15···π($C_{gB}$)] interaction is also observed (Figure 3.3.2e). The experimental PXRD pattern of **4a-5** matches with the corresponding simulated PXRD pattern (Figure 3.3.2f).

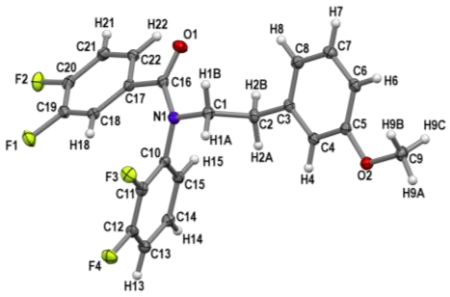


**(a)**

**Figure 3.3.2: (a)** ORTEP of **4a-5** drawn with 50% ellipsoidal probability.

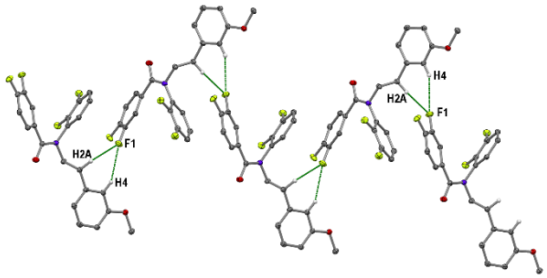


**(b)**

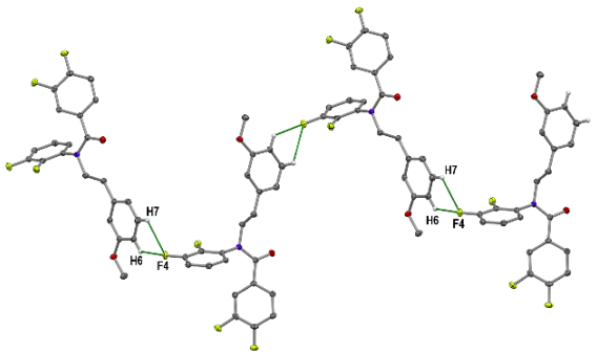


**(c)**

**Figure 3.3.2: (b)** (F1) interacts with the bifurcated way with H4 and H2A and generate a long one dimensional infinite chain along b-axis. **(c)** $2_1$ screw related one dimensional wave like pattern propagating along c- axis through the bifurcated C–H···F hydrogen bonds.

**Table 3.3.2: Intermolecular interactions in 4a-5**

| D–B···A | D–B/Å | *D*(D···A )/Å | *d*(B···A )/Å | ∠D–B···A/º | SYMMETRY |
|---|---|---|---|---|---|
| **C2–H2A···F1** | 1.080 | 3.390(3) | 2.39 | 153 | -x, ½ + y, ½ - z |
| **C4–H4···F1** | 1.080 | 3.516(3) | 2.56 | 147 | -x, ½ + y, ½ - z |
| **C6–H6···F4** | 1.080 | 3.202(3) | 2.49 | 122 | $^{3}/_{2}$ - x, 1 - y, ½ + z |
| **C7–H7···F4** | 1.080 | 3.246(3) | 2.66 | 122 | $^{3}/_{2}$ -x, 1-y, ½+z |
| **C14–H14···F2** | 1.080 | 3.175(3) | 2.42 | 126 | -x - 1, y + ½, ½ - z |
| **C1–H1B···π ($C_{gB}$)** | 1.080 | 3.728(3) | 2.88 | 147 | 1 + x, y, z |
| **C15–H15···π ($C_{gB}$)** | 1.080 | 3.583(3) | 2.73 | 153 | x - 1, y, z |

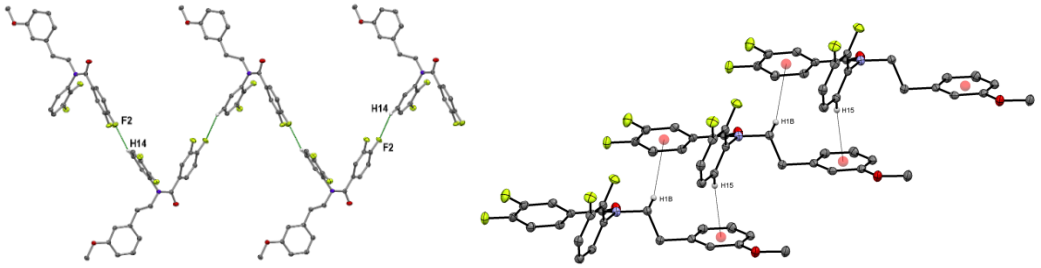


**(d)** **(e)**

**Figure 3.3.2: (d)** screw ($2_1$) related C14–H14···F2 hydrogen bond creates a 1D zig-zag pattern along crystallographic b-axis. **(e)** A dimer formation by weak C1–H1B···π and C15–H15···π interactions.

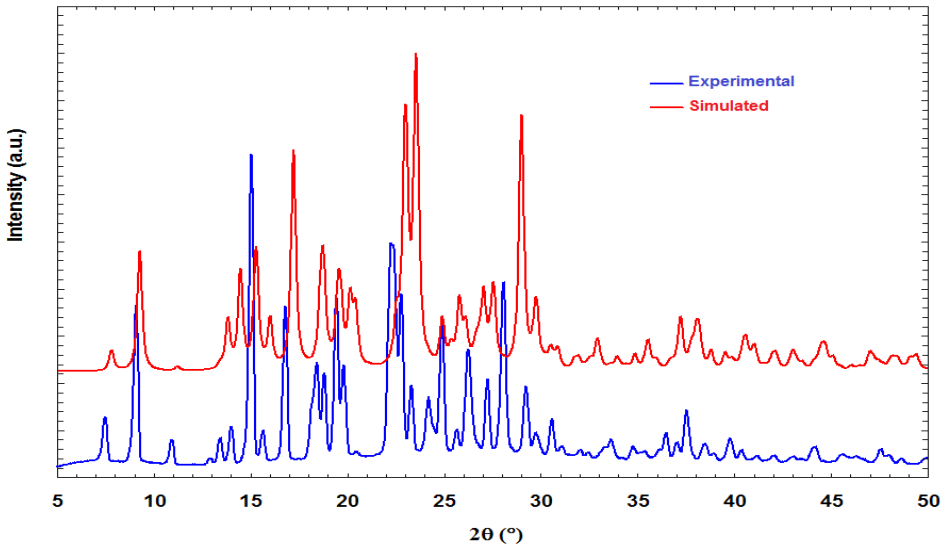


**Figure 3.3.2: (f)** Comparison of experimental and simulated PXRD patterns of **4a-5**

**N-(2,4-difluorophenyl)-2,3-difluoro-N-[2-(3-methoxyphenyl)ethyl]benzamide (4a-7):**This molecule **4a-7** was found to crystallize in $P2_1/c$ space group and the asymmetric unit contained two molecules (Z = 4, Z' = 2), namely molecule A and molecule B (Figure 3.3.3a). These two molecules which are symmetry independent are itself connected by C20–H20A···F4B and C20A–H20A···O1A hydrogen bonds (Figure 3.3.3b) and this asymmetric dimer interacts with another asymmetric dimer *via* C14B–H14B···F1B and C14A–H14A···O2B hydrogen bonds and thereby creates a tetrameric unit (Table 3.3.3**)**. This tetramer unit is further translating by C7B–H7B···O2A hydrogen bond along the crystallographic *b*- direction and creates a 3D structure (Figure 3.3.3c).

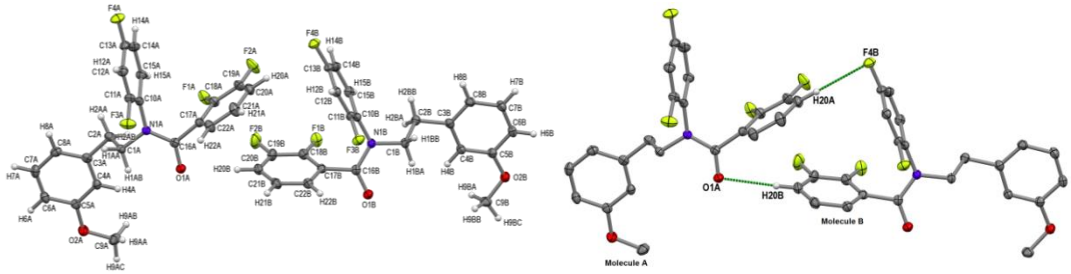

**(a)** **(b)**

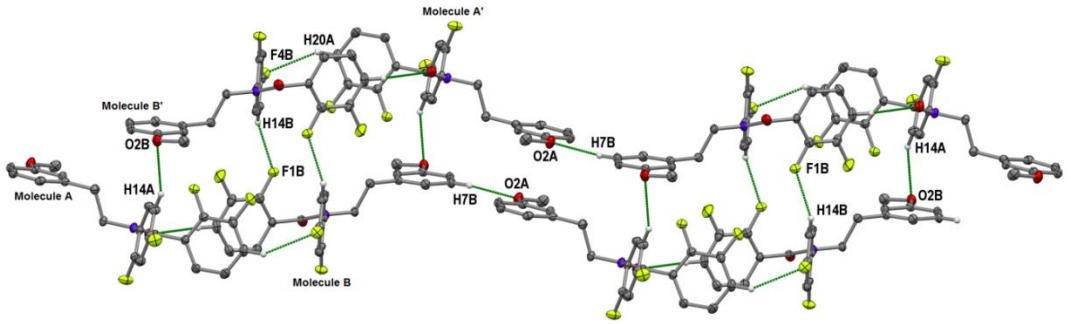


**(c)**

**Figure 3.3.3: (a)** ORTEP of **4a-7** drawn with 50% ellipsoidal probability. There are two molecules in the asymmetric unit **(b)** Two molecules which are symmetry independent are itself connected by C20–H20A···F4B and C20–H20A···O1A hydrogen bonds **(c)** Two tetramer units, formed by two dimers of symmetry independent molecules by C14B–H14B···F1B and C14A–H14A···O2B hydrogen bonds are connected to form molecular network through C7B–H7B···O2A hydrogen bond.

**Table 3.3.3: Intermolecular interactions in 4a-7**

| D–B···A | D–B/Å | *D*(D···A )/ Å | *d*(B···A )/Å | ∠D–B···A/º | SYMMETRY |
|---|---|---|---|---|---|
| **C1B–H1BA···F3A** | 1.080 | 3.557(2) | 2.56 | 152 | 1 - x, ½ + y, $^3/_2$ - z |
| **C20A–H20A···F4B** | 1.080 | 3.351(2) | 2.45 | 140 | 1 + x, y, z |
| **C2A–H2AB···F4A** | 1.080 | 3.603(2) | 2.58 | 159 | 1 + x, y, z |
| **C14B–H14B···F1B** | 1.080 | 3.221(2) | 2.29 | 143 | 1 - x, 1 - y, 1 - z |
| **C20B–H20B···O1A** | 1.080 | 3.423(2) | 2.35 | 175 | x, y, z |
| **C7B–H7B···O2A** | 1.080 | 3.320(2) | 2.26 | 167 | x, y + 1, z |
| **C14A–H14A···O2B** | 1.080 | 3.471(3) | 2.48 | 152 | 1 - x, 1 - y, 1 – z |
| **C15A–H15A···π ($C_{gC}$)** | 1.080 | 3.603(2) | 2.8 | 143 | x, ½ - y, z - ½ |
| **C22A–H22A···π ($C_{gC'}$)** | 1.080 | 3.590(2) | 2.7 | 154 | x, y, z |
| **C22B–H22B···π ($C_{gC}$)** | 1.080 | 3.627(2) | 2.77 | 154 | x, y, z |

Individual molecule of the asymmetric unit also forms C15A–H15A···π($C_{gC}$) and C22A–H22A···π($C_{gC'}$) interactions, which offers additional stabilisation of the crystal structure (Figure 3.3.3e and 3.3.3f). The experimental PXRD pattern of **4a-7** matches with the corresponding simulated PXRD pattern (Figure 3.1.2g).

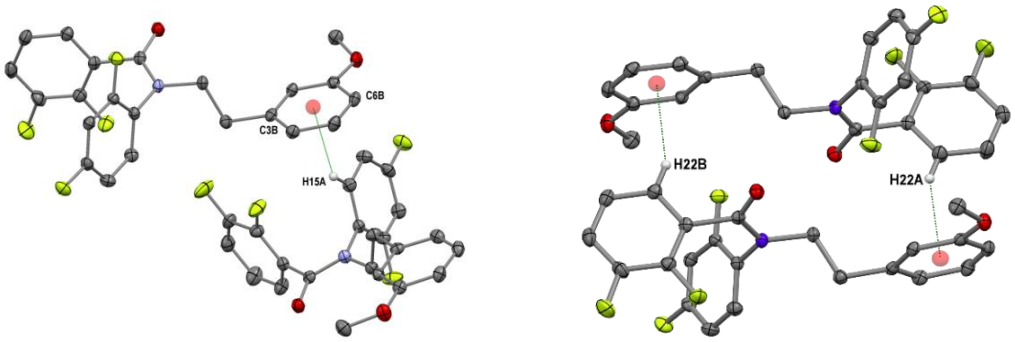


**(e)** **(f)**

**Figure 3.3.3: (e)** A dimer form by C–H···π interaction of one of the molecules of asymmetric unit **(f)** Inversion centre related dimer synthon by C–H···π interaction of another molecules of asymmetric unit.

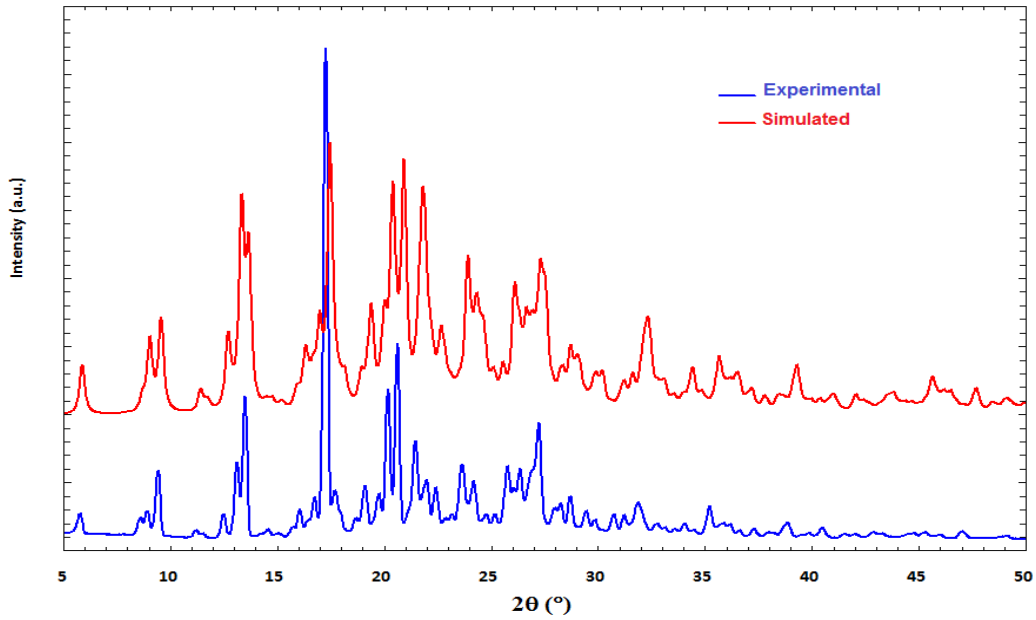


**Figure 3.3.3: (g)** Comparison of experimental and simulated PXRD patterns of **4a-7 N-(2,4-difluorophenyl)-2,4-difluoro-N-[2-(3-methoxyphenyl)ethyl]benzamide(4a-8) and N-(2,4-difluorophenyl)-3,4-difluoro-N-[2-(3-methoxyphenyl)ethyl]benzamide (4a-11):** The compounds **4a-8** (Figure 3.3.4a) and **4a-11** (Figure 3.3.5a) are found to be isostructural and were crystallised in monoclinic chiral $P2_1$ space group. Their unit cell similarity index ($\pi$ = 0.0007) indicates that the crystals structures truly isostructural. In the both compounds, the *p*-F of the A ring and *o*-F of the B ring are found to generate identical type of interactions in the crystal lattice. While the *p*-F of the A ring is involved in the formation of C4–H4···F4 hydrogen bond, the methoxy group present in the C ring is also involved in the formation of C12–H12···O2 hydrogen bond thereby resulting in the formation of dimer in both the crystal structures (Figure 3.3.4b and Figure 3.3.5b) (Table 3.3.4 and Table 3.3.5).

**Table 3.3.4: Intermolecular interactions in 4a-8**

| **D–B···A/** | **D–B/Å** | ***D*(D···A )/Å** | ***d*(B···A )/Å** | **∠D–B···A/º** | **SYMMETRY** |
|---|---|---|---|---|---|
| **C4–H4···F4** | 1.080 | 3.496(3) | 2.49 | 154 | 1 - x, ½ + y, 1 - z |
| **C19–H19···F3** | 1.080 | 3.353(4) | 2.59 | 127 | - x, y- ½, 1 - z |
| **C19–H19···F1** | 1.080 | 3.403(4) | 2.38 | 157 | - x, y - ½, 1 - z |
| **C12–H12···O2** | 1.080 | 3.356(3) | 2.41 | 174 | 1 - x, y - ½, 1 - y |
| **C15–H15···π($C_{gC}$)** | 1.080 | 3.520(3) | 2.72 | 142 | x, y - 1, z |

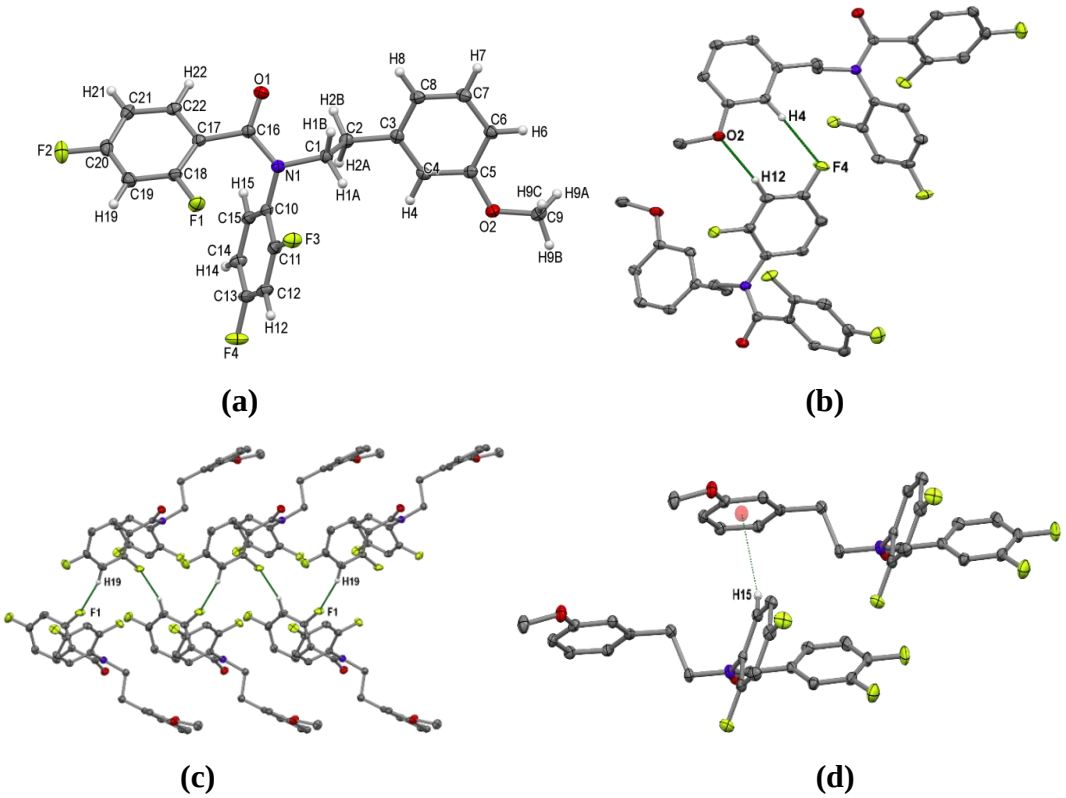


**Figure 3.3.4: (a)** ORTEP of **4a-8** drawn with 50% ellipsoidal probability. **(b)** Molecular dimer through C–H···F and C–H···O hydrogen bond through the $2_1$ symmetry in **4a-8. (c)** zig-zag pattern by C19–H19···F1 hydrogen bond in **4a-8. (d)** Formation of C15–H15···π interaction in **4a-8.**

**Table 3.3.5: Intermolecular interactions in 4a-11**

| **D–B···A/** | **D–B/Å** | ***D*(D···A )/Å** | ***d*(B···A )/Å** | **∠D–B···A/º** | **SYMMETRY** |
|---|---|---|---|---|---|
| **C4–H4···F4** | 1.080 | 3.463(3) | 2.47 | 152 | 1 - x, ½ + y, 1 - z |
| **C18–H18···F1** | 1.080 | 3.330(3) | 2.37 | 147 | 2 - x, ½ + y, 1 - z |
| **C12–H12···O2** | 1.080 | 3.345(3) | 2.42 | 175 | 1 - x, y + ½, 1 - z |
| **C15–H15···π ($C_{gC}$)** | 1.080 | 3.497(2) | 2.69 | 146 | x, y - 1, z |
| **C19–F1···F3–C11** | 1.344(3)<br>1.341(3) | 4.004(4) | 2.864(2) | 110<br>88 | - x, y - ½, 1 - z |

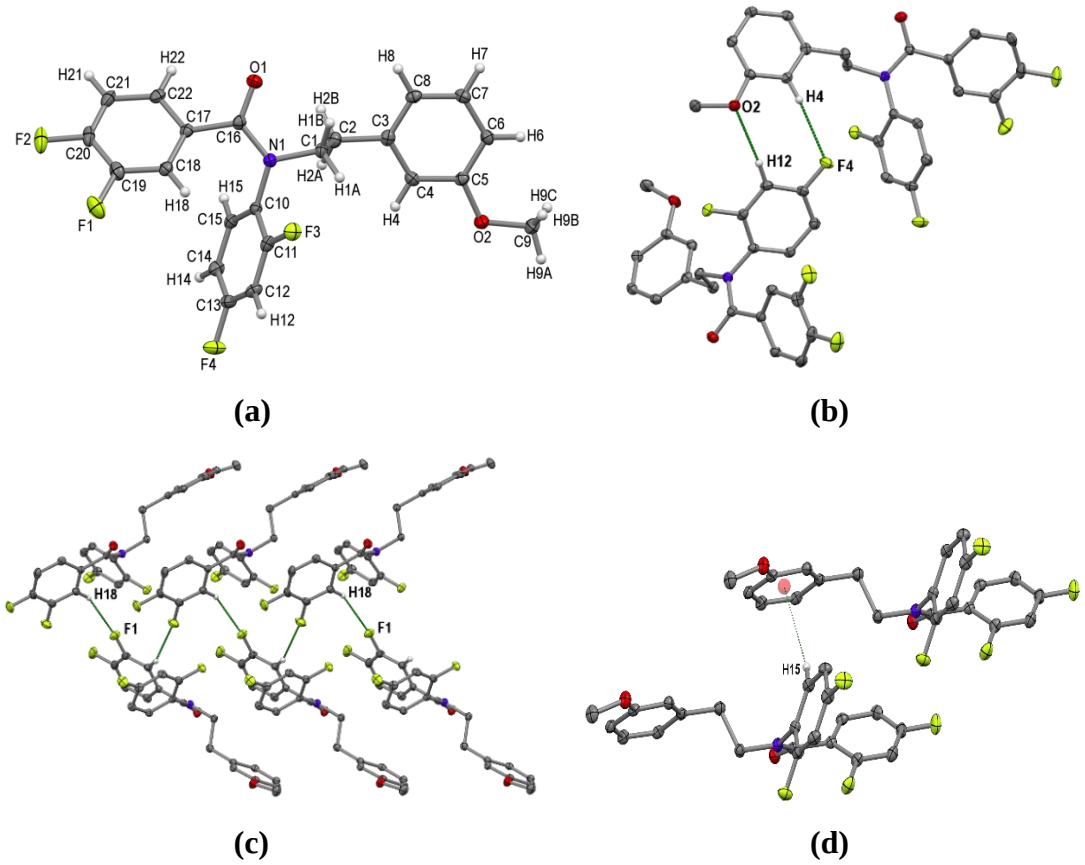


**Figure 3.3.5: (a)** ORTEP of **4a-11** drawn with 50% ellipsoidal probability. **(b)** Molecular dimer through C–H···F and C–H···O hydrogen bond through the $2_1$ symmetry in **4a-11. (c)** zig-zag pattern by C18–H18···F1 hydrogen bond in **4a-11** respectively. **(d)** Formation of C15–H15···π($C_{gC}$) interaction in **4a-11.**

Similarly, *o*-F of the B ring participates in C–H···F hydrogen bond (C19–H19···F1 and C18–H18···F1) *via* $2_1$ screw symmetry thereby making one dimensional tape like structure in the direction of *b*- direction (Figure 3.1.4a and Figure 3.3.5c). Along with these C–H···F hydrogen bonds, C15–H15···π interaction is also observed in the both the crystal structures involving the π cloud of the C ring (Figure 3.3.4d and 3.3.5d). It is noteworthy that the C19–H19···F3 hydrogen bond observed in **4a-8** is absent in **4a-11** as the position of H19 (in **4a-8**) is occupied by F1 (in **4a-11**). Therefore, a new weak C19–F1···F3–C11 contact is generated between F3 and F1 atoms, but this difference did not result in any major difference in the crystal packing. The experimental PXRD pattern of **4a-5** and **4a-11** is matching with the corresponding simulated PXRD pattern (Figure 3.3.4e and Figure 3.3.5e).

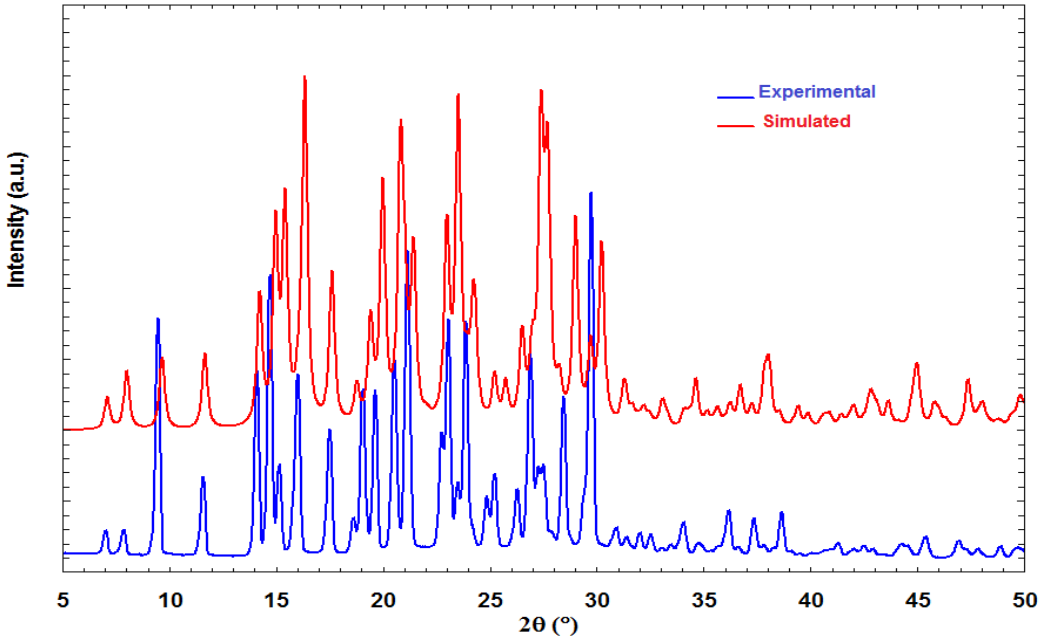


**Figure 3.3.4:** (e) Comparison of experimental and simulated PXRD patterns of **4a-8**

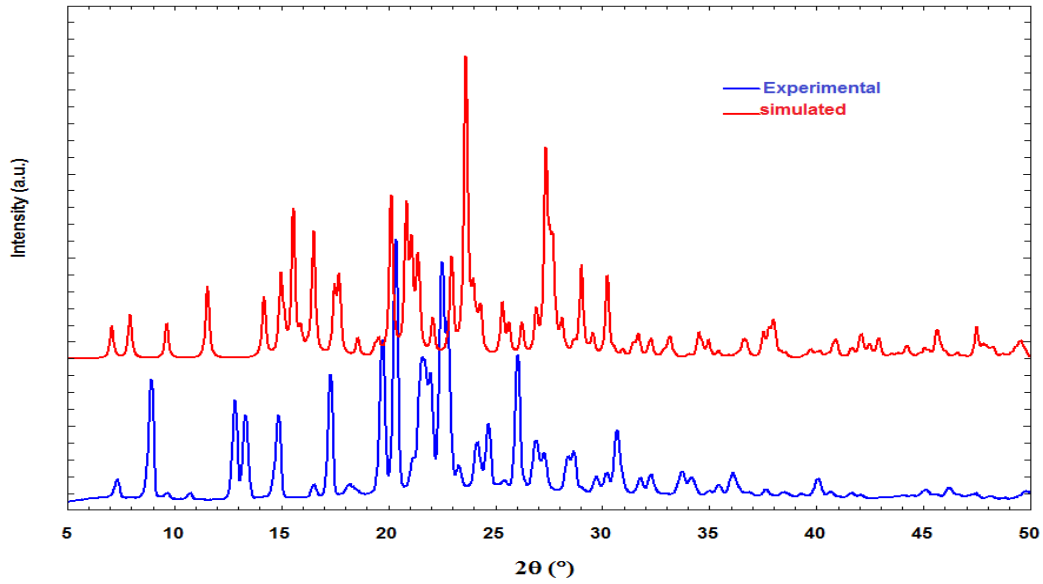


**Figure 3.3.5:** (e) Comparison of experimental and simulated PXRD patterns of **4a-11**

**N-(2,4-difluorophenyl)-2,5-difluoro-N-[2-(3-methoxyphenyl)ethyl]benzamide (4a-9):** The compound **4a-9** was found to crystallize in orthorhombic centrosymmetric *Pbca* space group with $Z = 8$ and $Z' = 1$ (Figure 3.3.6a). The A ring of this compound is disordered about the N1–C10 bond leading to the positioning of the *o*-F on either side at X : Y ratio thereby, although this disorder is not resulting into different interactions offered by the *o*-F atom on the A ring. The *p*-F on the A ring contributes in the formation of C20–H20···F4 hydrogen bond and generates a zig-zag catameric

chain like structure along the crystallographic *c*- direction (Table 3.3.6**)**. In addition to the C–H···F hydrogen bond, the oxygen of the carbonyl group also participates in C6–H6···O1 hydrogen bond formation and hence the combination of both C–H···F and C–H···O hydrogen bonds generates two-dimensional sheet like structure (Figure 3.3.6b). Similarly, the *m*-F of the B ring offers C8–H8···F2 hydrogen bond to form a chain along the *c*- direction (Figure 3.3.6c). Additionally, weak C14A–H14A···π($C_{gC}$) interactions have also been identified in this structure (Figure 3.3.6d). The experimental PXRD pattern of **4a-9** matches with the corresponding simulated PXRD pattern (Figure 3.3.6e).

**Table 3.3.6: Intermolecular interactions in 4a-9**

| **D–B···A/** | **D–B/Å** | ***D*(D···A )/Å** | ***d*(B···A )/Å** | **∠D–B···A/º** | **SYMMETRY** |
|---|---|---|---|---|---|
| **C1–H1B···F4** | 1.080 | 3.633(2) | 2.60 | 160 | ½ - x, ½ + y, z |
| **C8–H8···F2** | 1.080 | 3.326(2) | 2.33 | 153 | x, ½ - y, z - ½ |
| **C2–H2B···F2** | 1.080 | 3.530(2) | 2.65 | 139 | x, ½ - y, z - ½ |
| **C20–H20···F4** | 1.080 | 3.313(2) | 2.39 | 143 | ½ - x, - y, ½ + z |
| **C14A–H14A···π($C_{gC}$)** | 1.080 | 3.500(2) | 2.67 | 149 | ½ - x, y - ½, z |
| **C14B–H14B···π($C_{gC}$)** | 1.080 | 3.500(2) | 2.67 | 149 | ½ - x, y -½, z |
| **C22–H22···π($C_{gC}$)** | 1.080 | 3.597(2) | 2.74 | 153 | 1 - x, 1 - y, 1 - z |

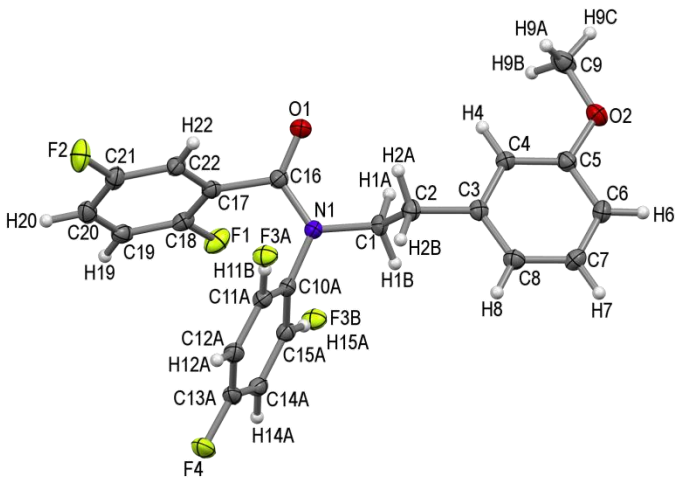


**(a)**

**Figure 3.3.6: (a)** ORTEP of **4a-9** drawn with 50% ellipsoidal probability.

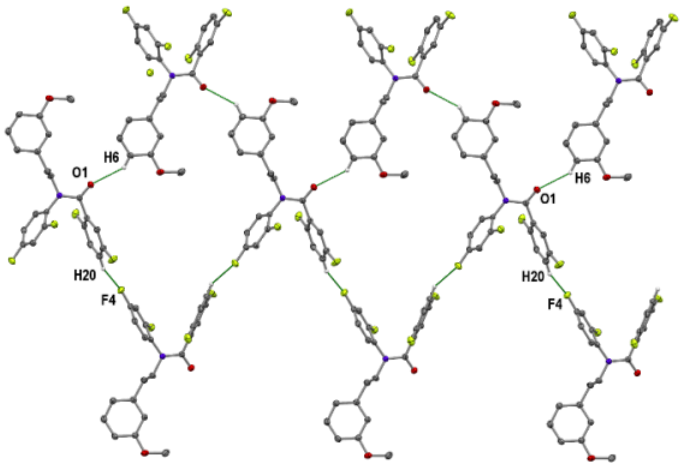


**(b)**

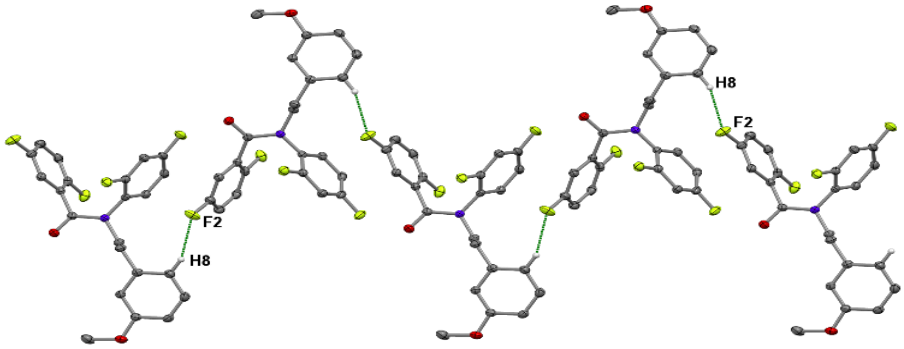


**(c)**

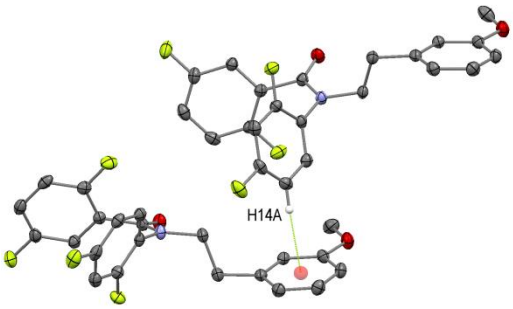


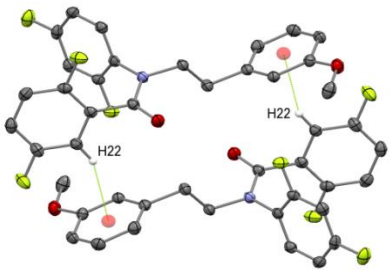


**(d)** **(e)**

**Figure 3.3.6: (b)** combination of both C–H···F and C–H···O hydrogen bond generating two-dimensional sheet like structure. **(c)** C8–H8···F2 hydrogen bond creates a 1D chain like structure. **(d)** A dimer formation by C14–H14A···π ($C_{gC}$) interaction. **(e)** A dimer formation by C14–H14A···π interaction. **(f)** A dimer formation by C22–H22···π ($C_{gC}$) interaction.

**N-(2,4-difluorophenyl)-2,6-difluoro-N-[2-(3-methoxyphenyl)ethyl]benzamide (4a-10):** The compound **4a-10** is found to crystallize in orthorhombic chiral $P2_12_12_1$ space group with Z = 4 (Figure 3.3.7a). One *o*-F (F1) of the B ring acts as a bifurcated acceptor to form C8–H8···F1 and C20–H20···F1 hydrogen bonds (Figure 3.3.7b) (Table 3.3.1**)**. Additionally, the weak C20–H20···F hydrogen bond also results in the formation of a dimer (Figure 3.3.7b). It is noteworthy that the C20–H20 acts as bifurcated donor forming C20–H20···F1 and C20–H20···F4 hydrogen bonds simultaneously propagating in crystallographic *a*- direction *via* $2_1$ symmetry thereby making a ribbon like structure. This chain is further supported by the weak C12A–H12A···O1 hydrogen bonds involving the carbonyl group (Figure 3.3.7c). The disordered *o*-F of the A ring interacts further with through C14A–H14A···F3A hydrogen bond (Figure 3.3.7d). The experimental PXRD pattern of **4a-10** matches with the corresponding simulated PXRD pattern (Figure 3.3.7e).

**Table 3.3.7: Intermolecular interactions in 4a-10**

| **D–B···A/** | **D–B/Å** | ***D*(D···A )/Å** | ***d*(B···A )/Å** | **∠D–B···A/º** | **SYMMETRY** |
|---|---|---|---|---|---|
| **C2–H2B···F3B** | 1.080 | 3.614(1) | 2.57 | 162 | 1 - x, y - ½, ½ - z |
| **C8–H8···F1** | 1.080 | 3.343(3) | 2.56 | 129 | 1 - x, y - ½, ½ - z |
| **C14A–H14A···F3A** | 1.080 | 3.306(4) | 2.60 | 123 | - x, ½ + y, ½ - z |
| **C20–H20···F4** | 1.080 | 3.484(4) | 2.52 | 148 | ½ + x, $^3/_2$ - y, - z |

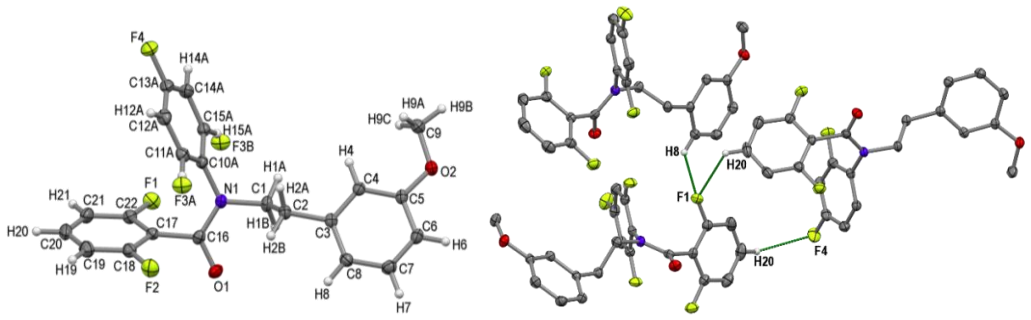


**(a)** **(b)**

**Figure 3.3.7: (a)** ORTEP of **4a-10** drawn with 50% ellipsoidal probability **(b)** C–F group act as a bifurcated acceptor with H8 and H20 hydrogen.

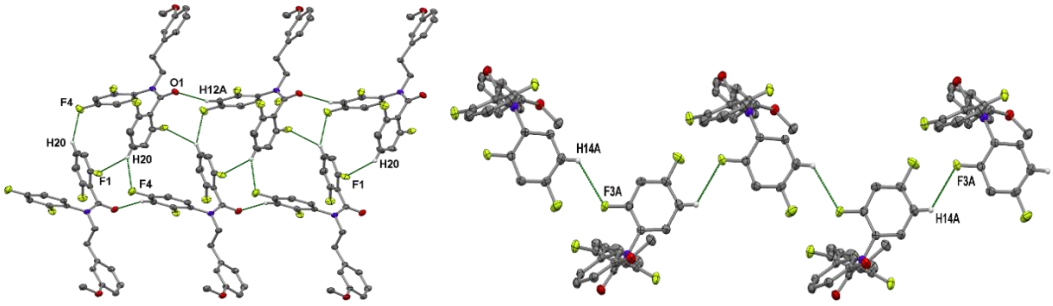


**(c)** **(d)**

**Figure 3.3.7: (c)** Formation of one dimensional ribbon like structure through the C–H···F hydrogen bond. **(d)** One dimensional zig-zag chain up to infinite length along y-axis.

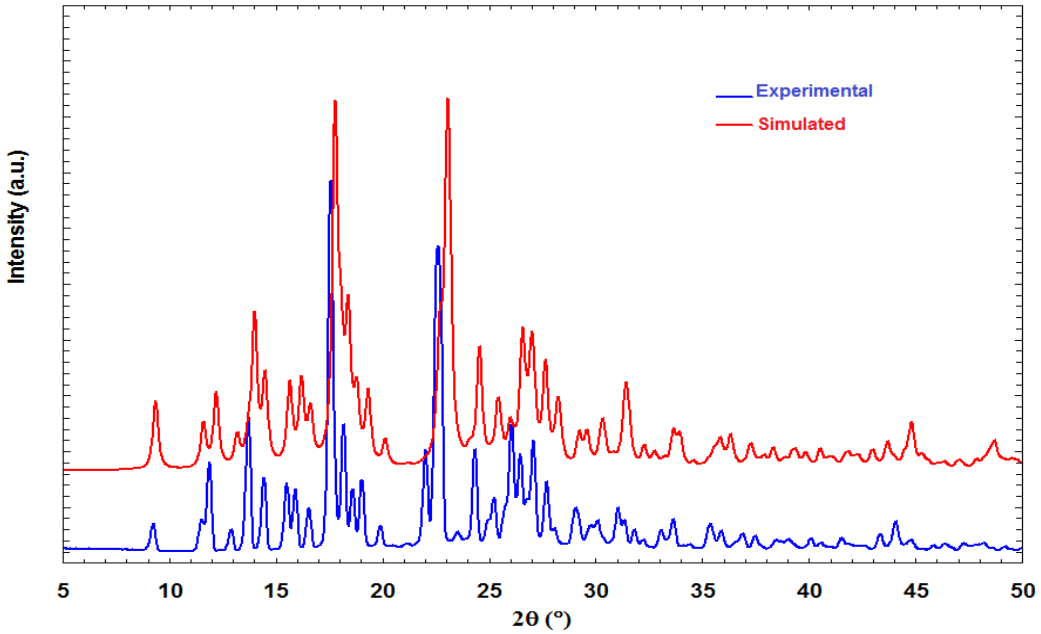


**Figure 3.3.7: (e)** Comparison of experimental and simulated PXRD patterns of **4a-10**

**N-(2,4-difluorophenyl)-3,5-difluoro-N-[2-(3-methoxyphenyl)ethyl]benzamide (4a-12):** This molecule was found to crystallize in $P2_1/c$ space group and the asymmetric unit contained two molecules (molecule A and molecule B) with different molecular conformations (Figure 3.3.8a). These two molecules are connected by C–F···F–C contact (Figure 3.3.8b). The *o*-F of the A ring of the molecule A of asymmetric unit and *m*-F of the B ring of a symmetry related molecule A are simultaneously involved in C–H···F hydrogen bond utilizing C4B–H4B donor of another symmetry related molecule B (Figure 3.3.8c) (Table 3.3.8**)**. Further, another short type II F···F contact has also observed between the *p*-F of

the A with *m*-F of the B ring generating a homo dimer (between two symmetry related molecule A) through the inversion centre (Figure 3.3.8d).

The molecule B utilises the *p*-fluorine of A ring to form centrosymmetric C14B–H14B···F4B hydrogen bonded dimer with a symmetry related molecule B. These dimers are interconnected by utilizing C12–H12B···O1B hydrogen bond involving the C=O group (Figure 3.3.8e). The experimental PXRD pattern of **4a-12** matches with the corresponding simulated PXRD pattern (Figure 3.3.8f).

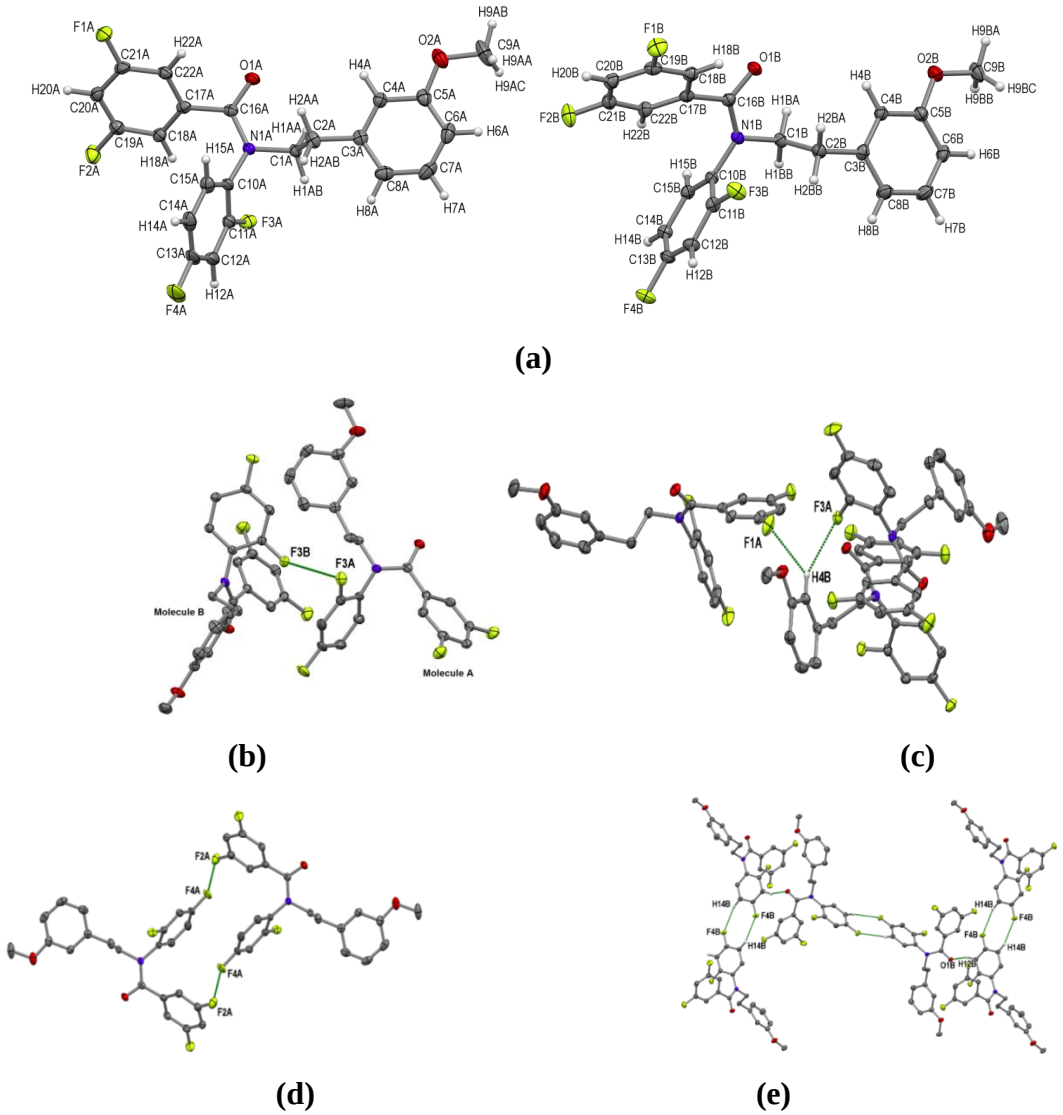


**Figure 3.3.8: (a)** ORTEP of **4a-12** drawn with 50% ellipsoidal probability. There are two molecules in one asymmetric unit. **(b)** A symmetry independent F···F contact between two molecules (A and B) within the asymmetric unit. **(c)** Bifurcated C–H···F hydrogen bonds involving three symmetry related molecules **(d)** A type II F···F short contact generating a homo dimer across the inversion centre. (e) C–H···F

hydrogen bonded dimers of molecule B are connected to each other through weak C–H···O hydrogen bonds involving C=O group.

**Table 3.3.8: Intermolecular interactions in 4a-12**

| D–B···A/ | D–B/Å | *D*(D···A )/Å | *d*(B···A )/Å | ∠D–B···A/º | SYMMETRY |
|---|---|---|---|---|---|
| **C4A–H4A···F1B** | 1.080 | 3.668(3) | 2.63 | 162 | 1 - x, 1 - y, 1 - z |
| **C22A–H22A···F2B** | 1.080 | 3.525(4) | 2.66 | 137 | 1 - x, 1 - y, 1 - z |
| **C20A–H20A···F3A** | 1.080 | 3.573(3) | 2.68 | 140 | 2 - x, ½ + y, $^{3}/_{2}$ - z |
| **C4B–H4B···F1A** | 1.080 | 3.250(4) | 2.48 | 128 | 2 - x, 1 - y, 1 - z |
| **C4B–H4B···F3A** | 1.080 | 3.347(3) | 2.45 | 140 | x, ½ - y, - ½ + z |
| **C1B–H1BA···F3A** | 1.080 | 3.576(4) | 2.51 | 168 | x, ½ - y, - ½ + z |
| **C14B–H14B···F4B** | 1.080 | 3.519(3) | 2.57 | 146 | 1 - x, - y, 1 - z |
| **C14B–H14B···F1B** | 1.080 | 3.406(3) | 2.62 | 129 | 1 - x, - ½ + y, ½ - z |

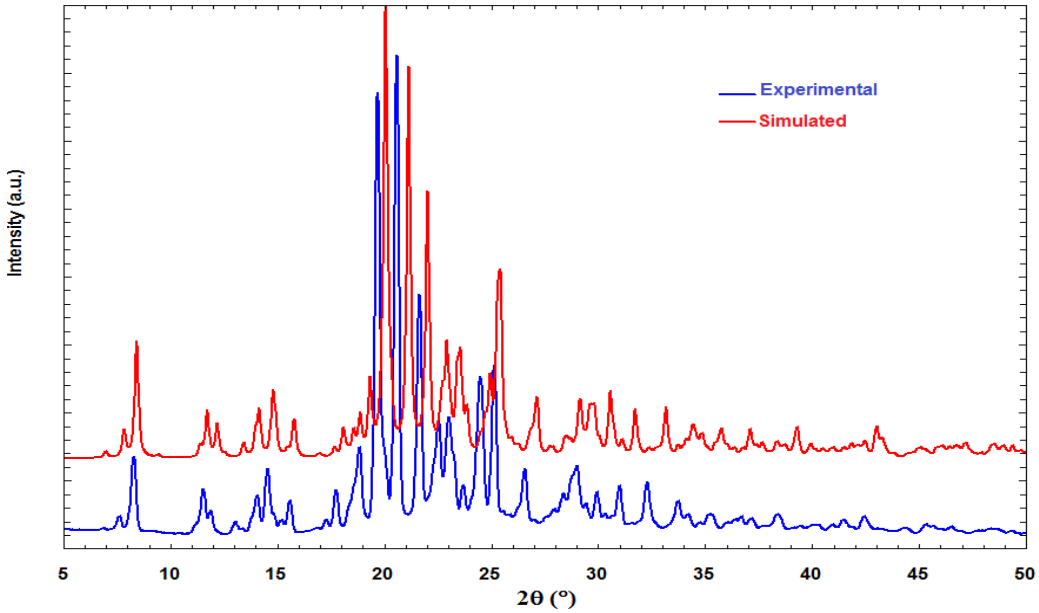


**Figure3.3.8:(f)** Comparison of experimental and simulated PXRD patterns of **4a-12**

**N-(2,5-difluorophenyl)-2,3-difluoro-N-[2-(3-methoxyphenyl)ethyl]benzamide (4a-13):** This compound crystallizes in the triclinic $P\bar{1}$ space group (Figure 3.3.9a). Out of four F atoms, only F4 participated in the formation of a dimer involving C4–H4···F4 hydrogen bonds (Table 3.3.9**)**. These dimers are interconnected by C6–H6···O2 hydrogen bonds (Figure 3.3.9b). Additionally, C–H···O hydrogen bonds involving the C=O group is found to generate a chain of molecules along the

crystallographic *a*-direction (Figure 3.3.9c). The experimental PXRD pattern of **4a-13** is matching with the corresponding simulated PXRD pattern (Figure 3.3.9d).

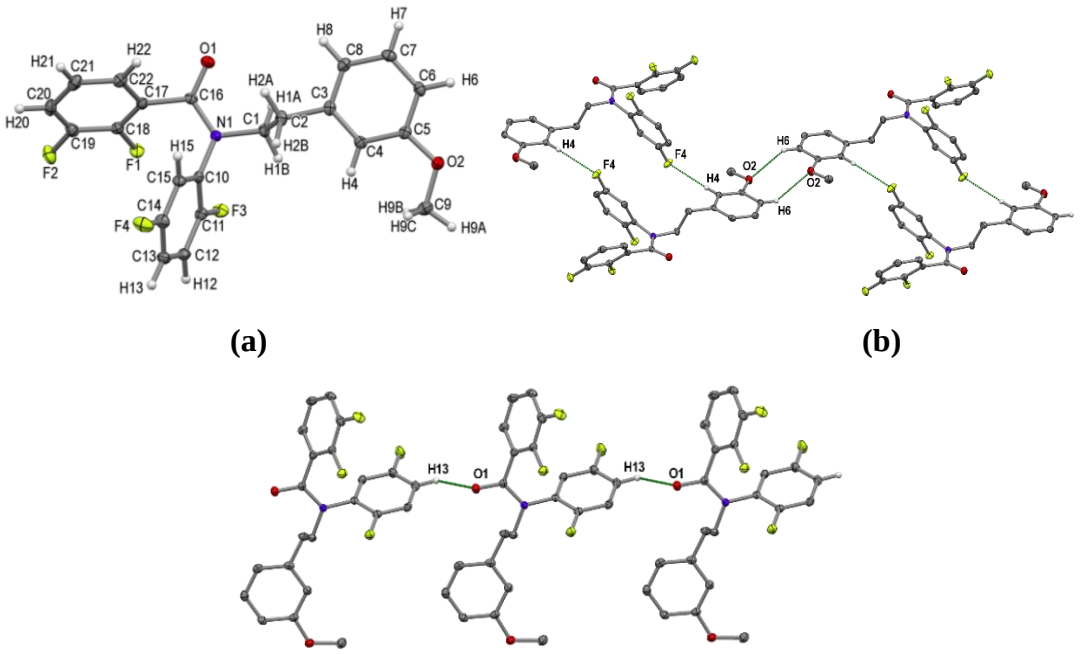


**Figure 3.3.9: (a)** ORTEP of **4a-13** drawn with 50% ellipsoidal probability. **(b)** Formation of molecular network through by dimers (through C4–H4···F4) connected by C6–H6···O2 hydrogen bonds. **(c)** A one dimensional molecular chain *via* C13–H13···O1 hydrogen bonds.

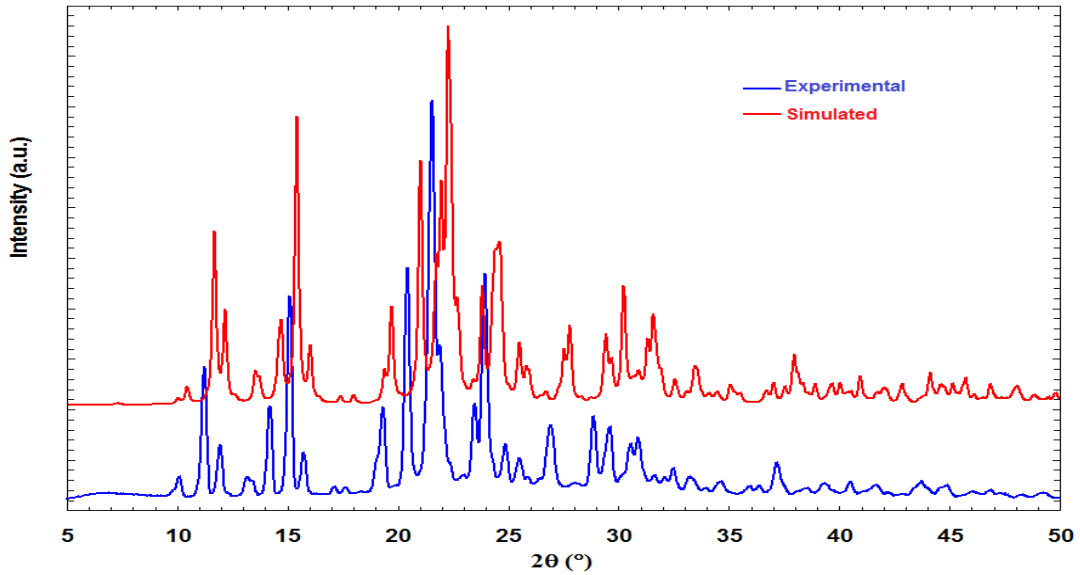


**(d)**

**Figure 3.3.9: (d)** Comparison of experimental and simulated PXRD patterns of **4a-13**

**Table 3.3.: Intermolecular interactions in 4a-13**

| D–B···A | D–B/Å | *D*(D···A )/Å | *d*(B···A )/Å | ∠D–B···A/º | SYMMETRY |
|---|---|---|---|---|---|
| **C4–H4···F4** | 1.080 | 3.430(2) | 2.48 | 146 | 1 - x, - y, 1 - z |
| **C13–H13···O1** | 1.080 | 3.073(2) | 2.38 | 120 | x, y - 1, z |

**N-(2,5-difluorophenyl)-2,5-difluoro-N-[2-(3-methoxyphenyl)ethyl]benzamide (4a-15):** The compound **4a-15** adopted triclinic centrosymmetric $P\bar{1}$ space group with Z = 2 and Z' =1 (Figure 3.3.10a). Like in S-AD-2-23, in this molecule also only *o*-F (F3) of the A ring offered C12–H12···F3 hydrogen bonds, which generated homo dimer synthon across the inversion centre (Figure 3.3.10b) (Table 3.3.10**)**. These dimers are interconnected along the crystallographic *a*- direction by the utilisation of C12–H12···O1 hydrogen bond involving the carbonyl group (Figure 3.3.10c). Along with these C–H···F hydrogen bonds, the π cloud of C ring interacts with the H2A hydrogen leading to the C2–H2A···π($C_{gC}$) interaction in the crystal structure (Figure 3.3.10d).

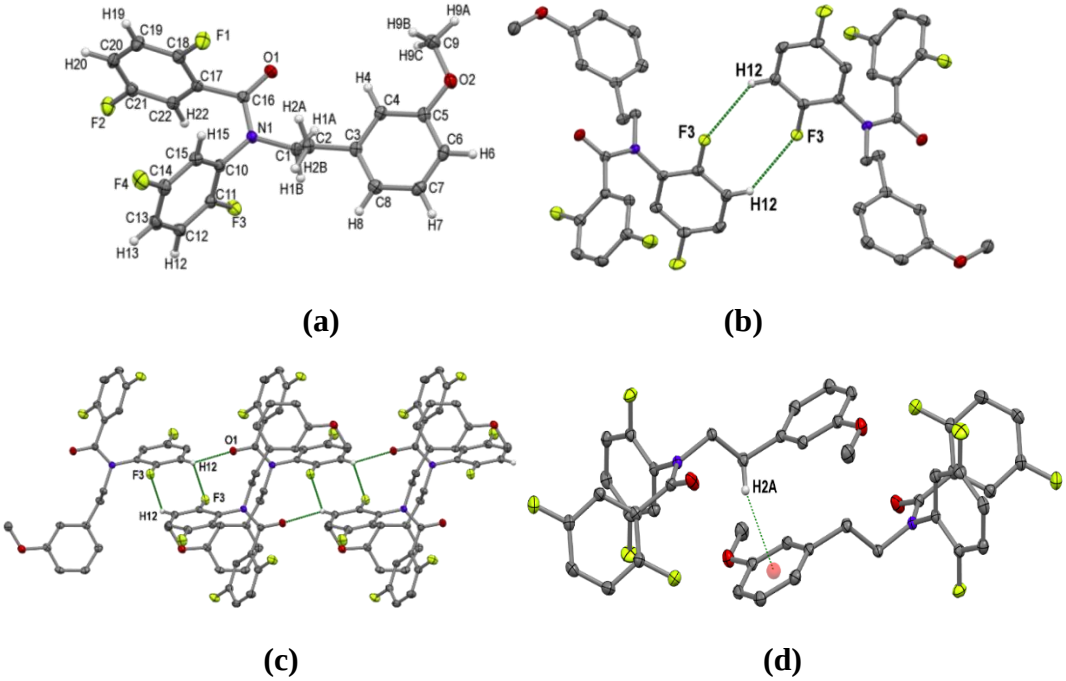


**Figure 3.2.4: (a)** ORTEP of **4a-15** drawn with 50% ellipsoidal probability. **(b)** C–H···F hydrogen bonded dimer across center of symmetry. **(c)** C–H···F hydrogen bonded dimers are interconnected by C–H···O hydrogen bonds **(d)** Weak C–H···π ($C_{gC}$) interaction in the crystal structure

**Table 3.3.10: Intermolecular interactions in 4a-15**

| D–B···A | D–B/Å | *D*(D···A )/Å | *d*(B···A )/Å | ∠D–B···A/º | SYMMETRY |
|---|---|---|---|---|---|
| **C12–H12···F3** | 1.080 | 3.418(2) | 2.56 | 136 | 2 - x, 1 - y, 1 - z |
| **C2–H2A···π** ($C_{gC}$) | 1.080 | 3.520(1) | 2.79 | 132 | 1 - x, - y, 1 - z |
| **C12–H12···O1** | 1.080 | 3.076(2) | 2.20 | 137 | x+1, y, z |

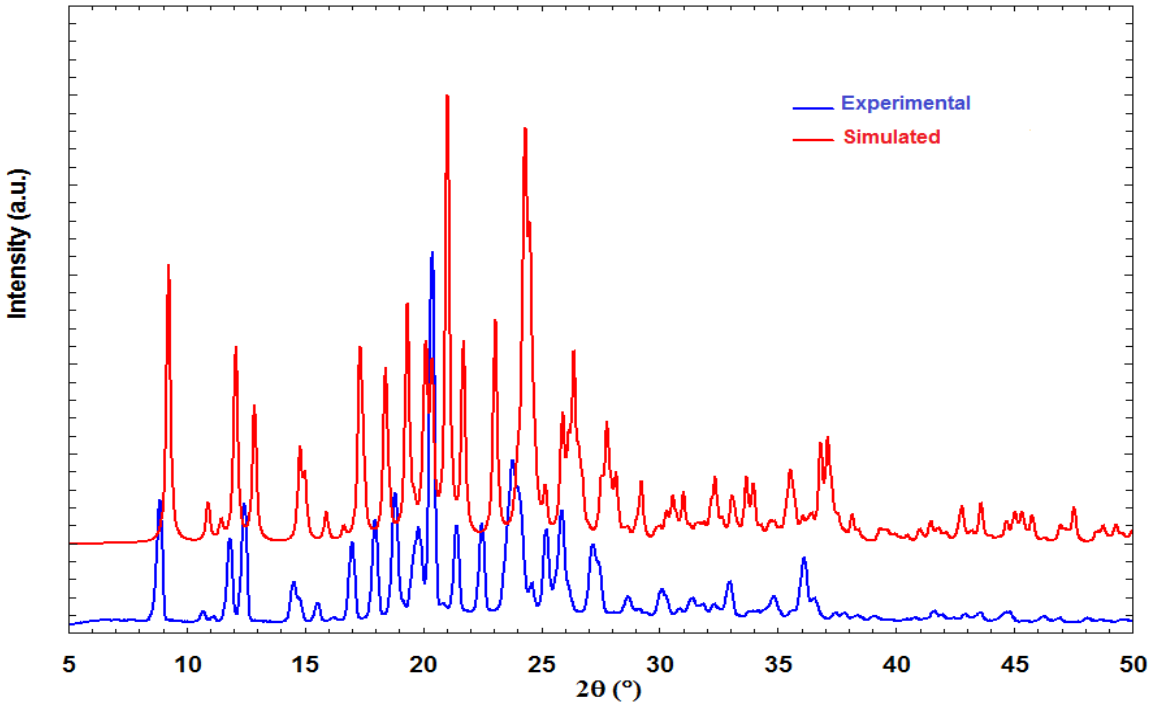


**Figure 3.3.10: (e)** The experimental and simulated PXRD patterns of **4a-15**.

**N-(2,5-difluorophenyl)-2,6-difluoro-N-[2-(3-methoxyphenyl)ethyl]benzamide (4a-16):** The compound **4a-16** adopted triclinic centrosymmetric *P* $\bar{1}$ *space* group with Z = 2 and Z' =1 (Figure 3.3.11a). The carbonyl oxygen acts as a bifurcated acceptor and forms C12–H12···O1 and C19–H19···O1 hydrogen bonds (Figure 3.3.11b) (Table 3.3.11**)**. Among the four fluorine atoms, only one fluorine (F1) participated in the formation of a dimer by the utilisation of C21–H21···F1 hydrogen bond through the inversion centre. These dimmers have been found to be interconnected by another symmetrical dimer through C–H···O hydrogen bonds involving H4 and O2 through another inversion centre (Figure 3.3.11c). The experimental PXRD pattern of **4a-16** is matching with the corresponding simulated PXRD pattern (Figure 3.3.11d).

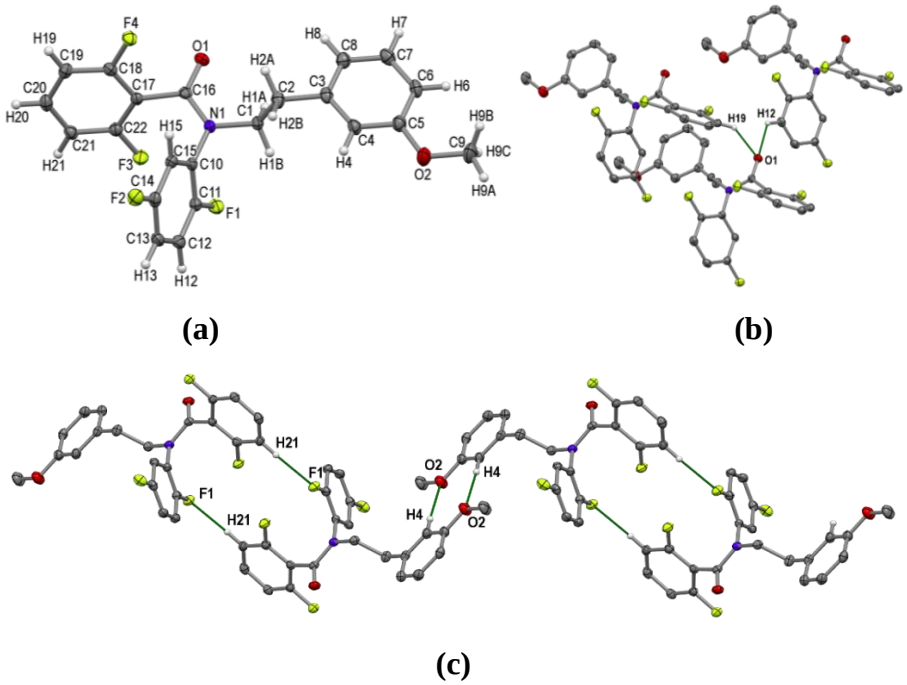


**Figure 3.3.11: (a)** ORTEP of **4a-16** drawn with 50% ellipsoidal probability. **(b)** Carbonyl oxygen acting as a bifurcated acceptor **(c)** A molecular network by interlinked C12–H12···F1 and C4–H4···O2 hydrogen bonded dimers.

**Table 3.3.11: Intermolecular interactions in 4a-16**

| D–H···A/(Å) | (D···H) | *D*(D···A ) | *d*(H···A ) | ∠D–H···A/º | SYMMETRY |
|---|---|---|---|---|---|
| **C21–H21···F1** | 1.080 | 3.381(3) | 2.47 | 142 | 1-x, 1-y, 2-z |
| **C4–H4···O2** | 1.080 | 3.612(3) | 2.54 | 174 | -x, 1-y, 1- z |
| **C19–H19···O1** | 1.080 | 3.286(3) | 2.40 | 139 | x+1, y, z |
| **C12–H12···O1** | 1.080 | 3.019(3) | 2.29 | 123 | x, y-1, z |

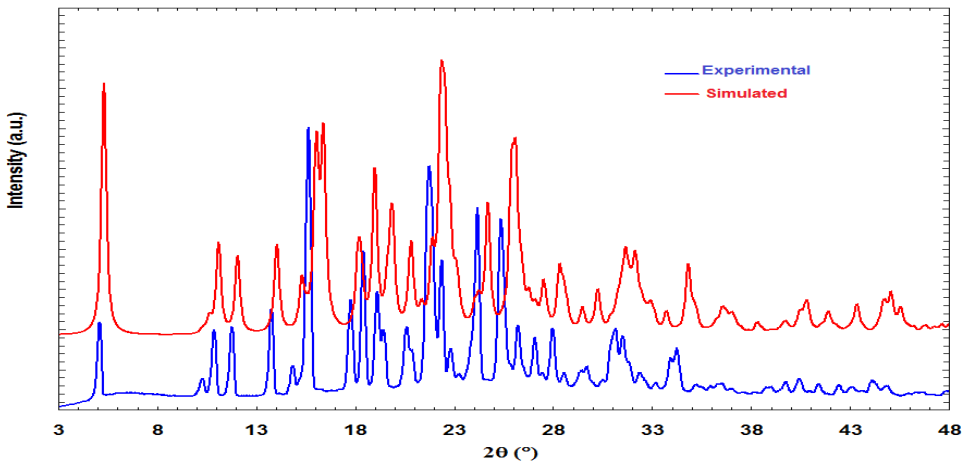


**Figure 3.3.11: (d)** Comparison of experimental and simulated PXRD patterns of **4a-16**

**N-(2,5-difluorophenyl)-3,4-difluoro-N-[2-(3-methoxyphenyl)ethyl]benzamide – (4a-17) and N-(2,5-difluorophenyl)-3,5-difluoro-N-[2-(3-methoxyphenyl)ethyl]benzamide (4a-18):** The crystal structure of **4a-17** and **4a-18** are found to be isostructural. Their unit cell similarity index ($\pi$) is 0.001. Both the molecules are crystallised in centrosymmetric monoclinic $P2_1/c$ space group with Z = 4 and Z' = 1 (Figure 3.3.12a and 3.3.13a). In both the compounds, C=O group acts as a bifurcated acceptor with *p*-H of the A ring through *c*- glide and *o*-H of the C ring by $2_1$ screw symmetry to form C–H···O hydrogen bonds (Table 3.3.12 and Table 3.3.13**)**. Two donor molecules and two acceptor molecules thereby formed a cyclic tetramer unit (Figure 3.3.12b and 3.3.13b). Similarly, C–H···F hydrogen bonds are found to form dimers involving H21 and F2 in both the compounds. These dimers are further linked to another dimer involving a pair of C–H···F hydrogen bonds involving H8 and F4 in both the compounds (Figure 3.3.12c and 3.3.13c). Three fluorine atoms of **4a-17** were involved in the formation of F···F contacts, where F3 interacts with both F1 and F2 of the B ring and creates a cyclic dimer synthon *via* inversion centre (Figure 3.3.12d). Whereas, in the crystal structure of **4a-18**, only two fluorine atoms i.e. F1 and F3 participated in the formation of F···F contacts through the inversion centre and generated a dimer synthon (Figure 3.3.13d). These dimers are again interconnected by another dimer, formed by the combination of C–H···F and C–H···O hydrogen bonds. Along with these hydrogen bonds and F···F contacts, C–H···$\pi$ interactions are also identified in these two structures (Figure 3.3.12e and 3.3.13e). The experimental PXRD pattern of **4a-18** matches with the corresponding simulated PXRD pattern (Figure 3.3.13f).

**Table 3.3.12: Intermolecular interactions in 4a-17**

| **D–B···A** | **D–B/Å** | ***D*(D···A )/Å** | ***d*(B···A )/Å** | **∠D–B···A/º** | **SYMMETRY** |
|---|---|---|---|---|---|
| **C8–H8···F4** | 1.080 | 3.386(3) | 2.39 | 153 | - x, 2 - y, 1 - z |
| **C21A–H21A···F2** | 1.080 | 3.401(3) | 2.56 | 134 | - x - 1, 1 - y, 1 - z |
| **C21B–H21A···F2** | 1.080 | 3.401(3) | 2.56 | 134 | - x - 1, 1 - y, 1 - z |
| **C19–F1···F3–C11** | 1.349(2)<br>1.348(2) | 4.403(4) | 2.884(4) | 121<br>92 | 2 - x, 1 - y, 1 - z |
| **C20–F2···F3–C11** | 1.339(2)<br>1.348(2) | 4.733(5) | 2.828(4) | 124<br>148 | 2 - x, 1 - y, 1 - z |
| **C15–H15···π ($C_g$c)** | 1.080 | 3.407(4) | 2.53 | 158 | 1 + x, y, z |

**Table 3.3.13: Intermolecular interactions in 4a-18**

| D–B···A | D–B/Å | *D*(D···A )/Å | *d*(B···A )/Å | ∠D–B···A/º | SYMMETRY |
|---|---|---|---|---|---|
| **C8–H8···F4** | 1.080 | 3.396(2) | 2.39 | 154 | 2 - x, 2 - y, 1 - z |
| **C15–H15···π ($C_{gC}$)** | 1.080 | 3.423(2) | 2.54 | 158 | x - 1, y, z |
| **C19–F1···F3–C11** | 1.3529(16)<br>1.3508(16) | 4.270(2) | 2.819(2) | 117<br>90 | 1 + x, y, z |

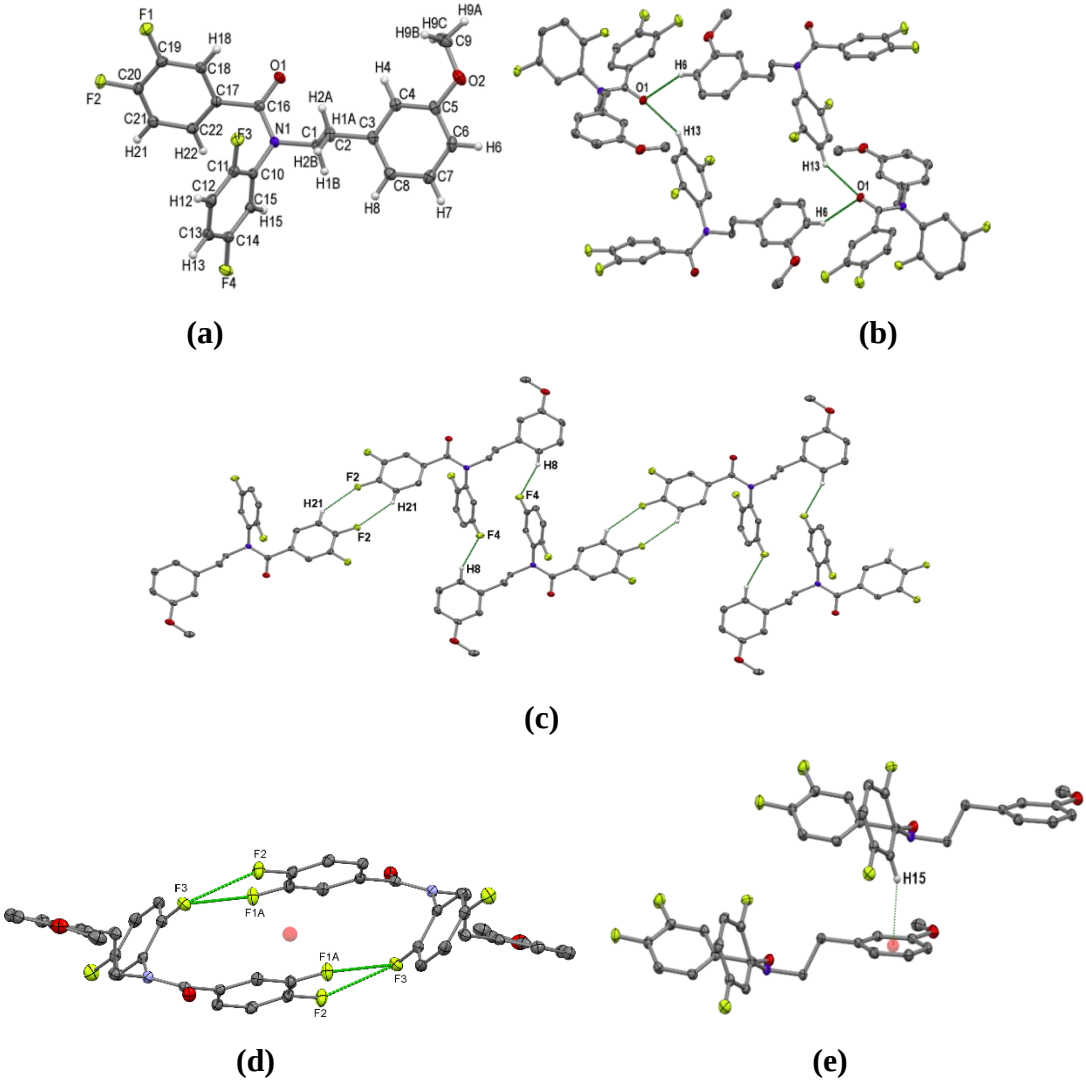


**Figure 3.3.12: (a)** ORTEP of **4a-17** drawn with 50% ellipsoidal probability. **(b)** Two donor molecules and two acceptor molecules making an inversion centre related cyclic tetramer unit by C–H···O hydrogen bonds. **(c)** C–H···F hydrogen bonded dimers are interconnected by pairs of C–H···F hydrogen bonds forming 3D molecular network. **(d)** A pair of bifurcated F···F contacts forming dimer. **(e)** C15–H15···π($C_{gC}$) interaction holding the molecules in a chain.

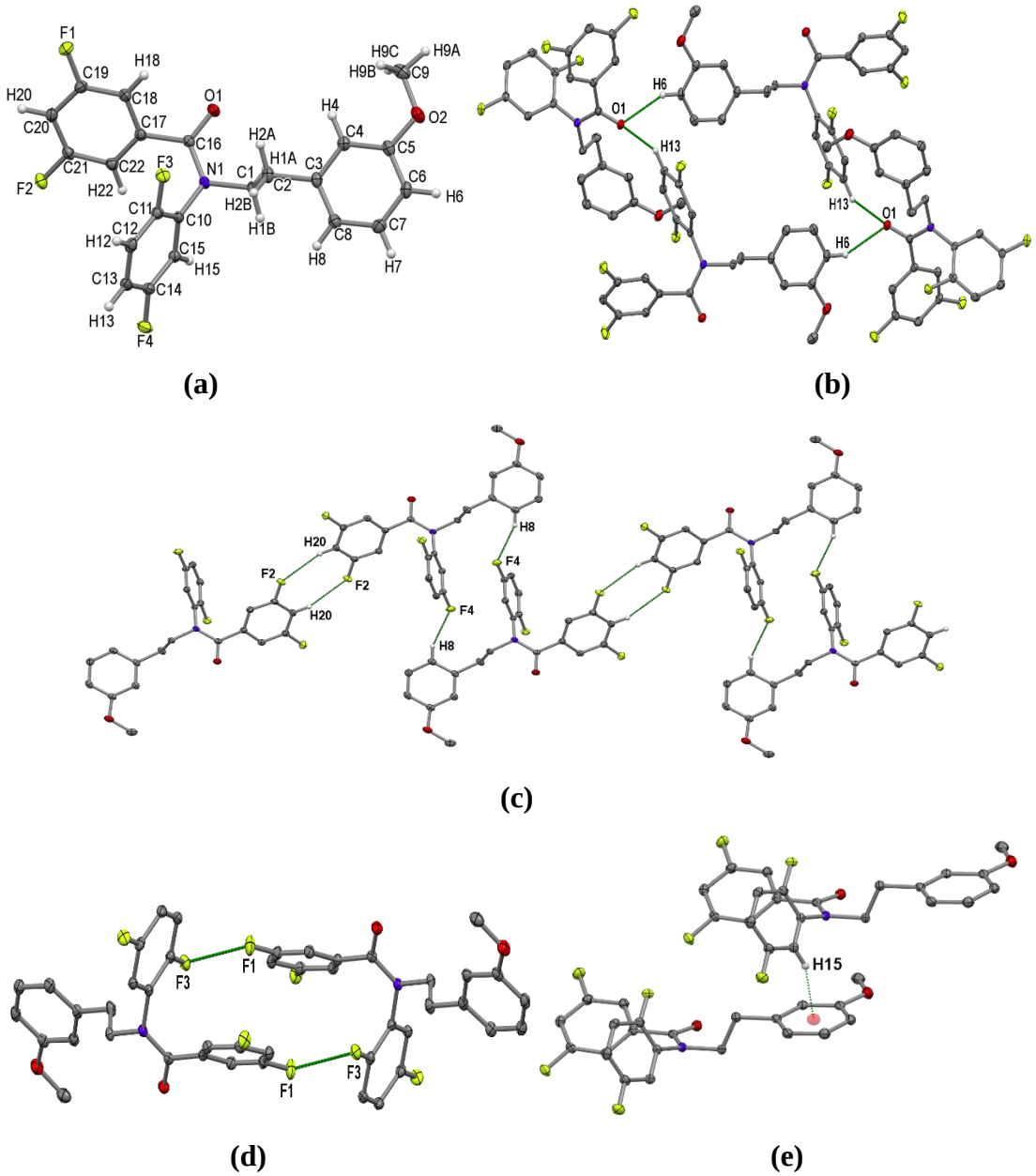


**Figure: 3.3.13: (a)** ORTEP of **4a-18** drawn with 50% ellipsoidal probability. **(b)** Two donor molecules and two acceptor molecules making an inversion centre related cyclic tetramer unit by C–H···O hydrogen bonds. **(c)** C–H···F hydrogen bonded dimers are interconnected by pairs of C–H···F hydrogen bonds forming 3D molecular network. **(d)** A pair of F···F contacts forming dimer. **(e)** C15–H15···π ($C_{gC}$) interaction holding the molecules in a chain.

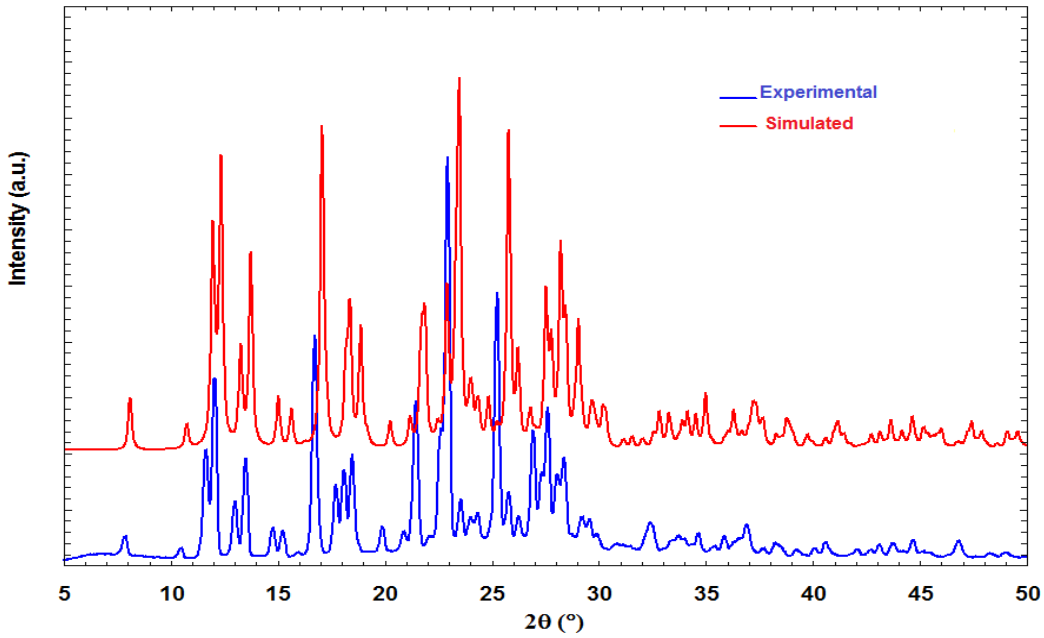


**Figure: 3.3.13: (f)** Comparison of experimental and simulated PXRD patterns of **4a-18**

**N-(2,6-difluorophenyl)-2,3-difluoro-N-[2-(3-methoxyphenyl)ethyl]benzamide (4a-19):** This compound crystallizes in the centrosymmetric monoclinic $P2_1/c$ space group with Z = 4 and Z' = 1 (Figure 3.3.14a). In this crystal structure, only one fluorine i.e. o-F of the B ring participates in C–H···F hydrogen bond and forms one dimension chains in the crystal lattice of by the utilization of *c*-glide (Figure 3.3.14b) (Table 3.3.14**)**.

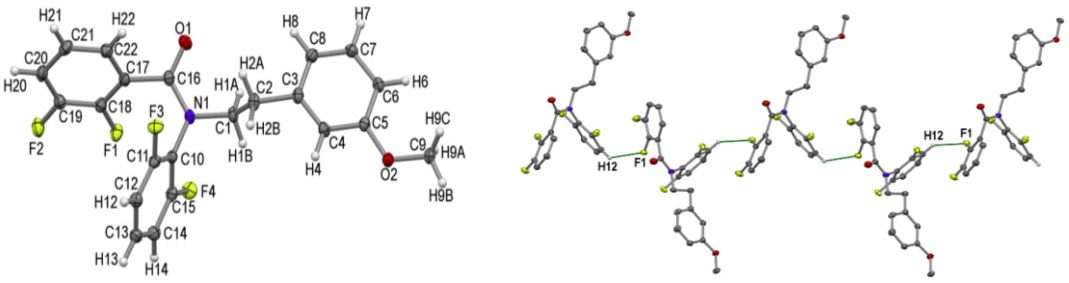


**(a)** **(b)**

**Figure 3.3.14: (a)** ORTEP of **4a-19** drawn with 50% ellipsoidal probability. **(b)** A zig-zag one dimension chains have been found through C12–H12···F1 hydrogen bonds in the crystal lattice of by the utilization of c glide.

**Table 3.3.14: Intermolecular interactions in 4a-19**

| D–B···A | D–B/Å | *D*(D···A )/Å | *d*(B···A )/Å | ∠D–B···A/º | SYMMETRY |
|---|---|---|---|---|---|
| **C12–H12···F1** | 1.080 | 3.362(2) | 2.57 | 129 | 1 - x, y - ½, ½ - z |
| **C14–H14··· π ($C_{gC}$)** | 1.080 | 3.385(2) | 2.69 | 132 | 1 - x, ½ + y, ½ - z |

Like the previous structure, the π cloud of the C ring interacts with the H14 hydrogen leading to the C14–H14···π($C_{gC}$) interaction in the lattice which further stabilises the crystal structure.

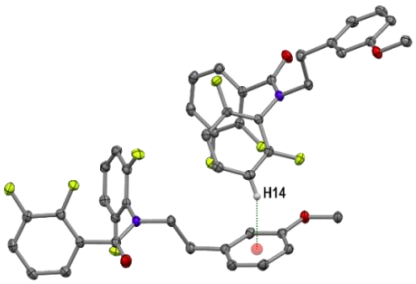


**(c)**

**Figure 3.3.14: (c)** π cloud of methoxy phenyl ring involved in C–H···π($C_{gC}$) interaction.

**N-(2,6-difluorophenyl)-2,4-difluoro-N-[2-(3-methoxyphenyl)ethyl]benzamide (4a-20) and N-(2,6-difluorophenyl)-3,4-difluoro-N-[2-(3-methoxyphenyl)ethyl]benzamide (4a-23): 4a-20** and **4a-23** are found to be isostructural with unit cell similarity index 0.003 crystallized in orthorhombic *Pbca* space group with Z = 8 (Figure 3.3.15a and 3.3.16a). In both the compounds, *p*-F (F2) of the B ring and *p*-H (H13) of the A ring form C13–H13···F2 hydrogen bond by the utilization of two consecutive glide planes thereby generating a $2_1$ symmetry parallel to *b*-axis (Figure 3.3.15b and 3.3.16b) (Table 3.3.15 and Table 3.3.16**)**. The F atoms on the A ring do not offer any interactions in both the compounds.

In addition to similar C–H···F hydrogen bonds, both the O atoms of both the molecules were also found to play a role in forming weak C19–H19···O1 and C14–H14···O2 hydrogen bonds. These C–H···O hydrogen bonds generates a tetrameric unit, which is further extended involving the same hydrogen bonds to form a molecular stacking along crystallographic *a*- direction (Figure 3.3.15b and 3.3.16b).

Additionally, C–H···π interactions have also been identified in these two structures which provides additional stability to the crystal lattice (Figure 3.3.15a and 3.3.16c). Both the fluorine atoms of the B ring of 4a-23 were involved in C–H···F hydrogen bonds while in 4a-20, only one fluorine was involved in C–H···F hydrogen bond. This is due to the change in the position of fluorine substituent in 4a-23. The m-F of the B ring of 4a-23 interacts with the H8 through *b*-glide to make a zig-zag catameric chain pattern along the *b*-axis (Figure 3.3.15d). The experimental PXRD pattern of **4a-20** and **4a-23** match with the corresponding simulated PXRD pattern (Figure 3.3.15f and Figure 3.3.16e).

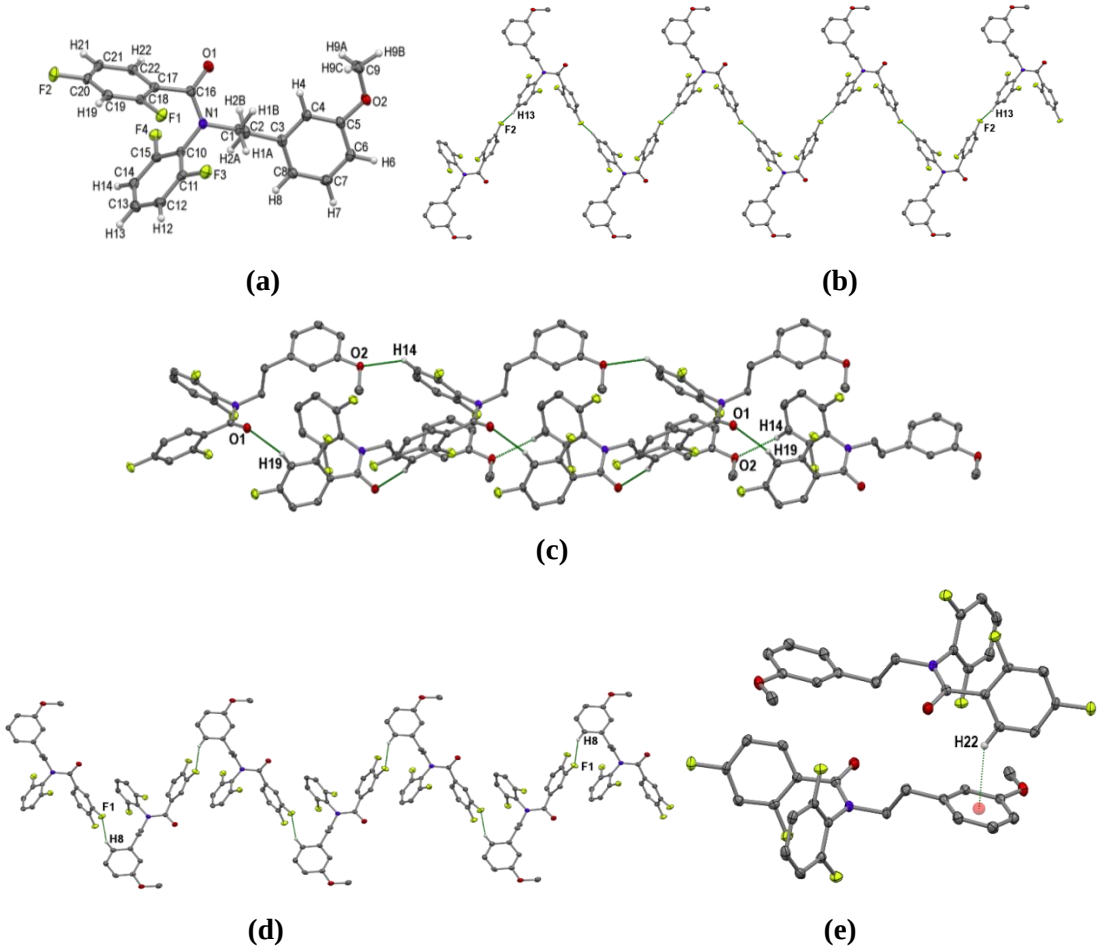


**Figure 3.3.15: (a)** ORTEP of **4a-20** drawn with 50% ellipsoidal probability. **(b)** C13-H13···F2 hydrogen bond generating a zig-zag catameric chain like structure along the crystallographic *b*-axis. (c) C19–H19···O1 and C14–H14···O2 hydrogen bonds generating a molecular stacking through tetramer formation. **(d)** A zig-zag pattern has been found only in **4a-20**. **(e)** C–H···π ($C_g$c) interactions in **4a-20**.

**Table 3.3.15: Intermolecular interactions in 4a-20**

| D–B···A | D–B/Å | *D*(D···A )/Å | *d*(B···A )/Å | ∠D–B···A/º | SYMMETRY |
|---|---|---|---|---|---|
| **C13–H13···F2** | 1.080 | 3.306(4) | 2.46 | 134 | 1 - x, ½ + y, ½ - z |
| **C22–H22···π ($C_{gC}$)** | 1.080 | 3.470(3) | 2.64 | 147 | 1 - x, 1 - y, 1 - z |

**Table 3.3.16: Intermolecular interactions in 4a-23**

| D–B···A | D–B/Å | *D*(D···A )/Å | *d*(B···A )/Å | ∠D–B···A/º | SYMMETRY |
|---|---|---|---|---|---|
| **C8–H8···F1** | 1.080 | 3.324(2) | 2.36 | 148 | ½ - x, ½ + y, z |
| **C13–H13···F2** | 1.080 | 3.359(2) | 2.44 | 142 | 1 - x, ½ + y, ½ - z |
| **C18–H18···π ($C_{gC}$)** | 1.080 | 3.584(2) | 2.74 | 151 | 1 - x, - y, - z |

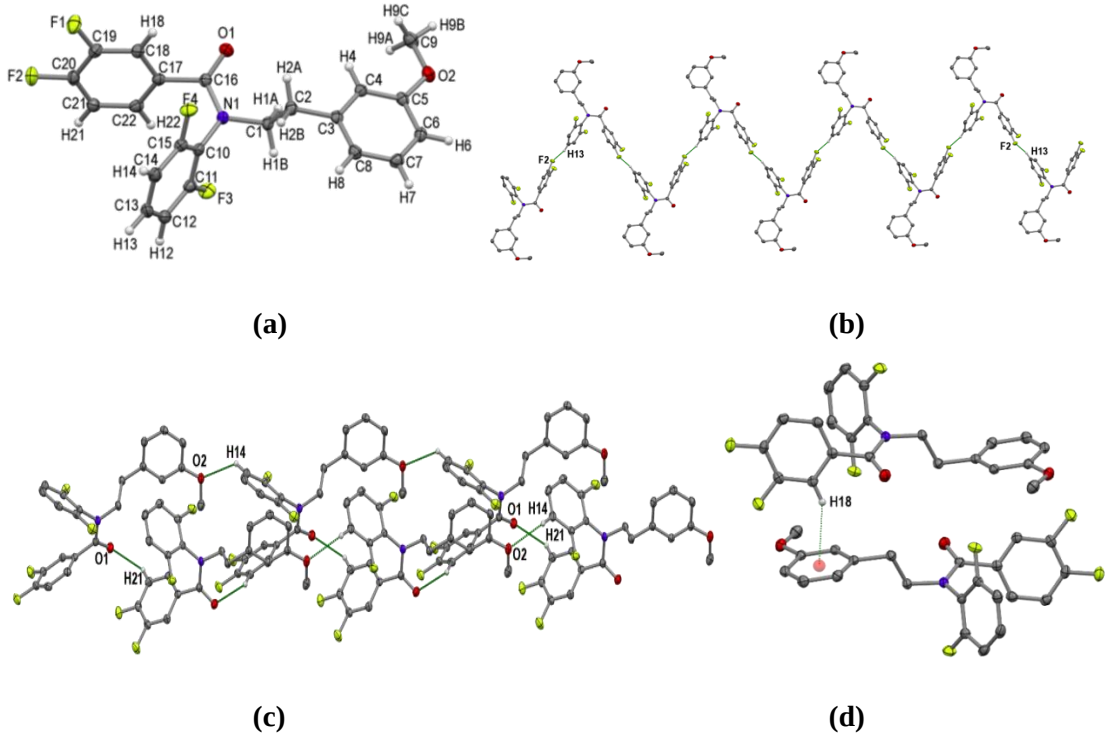


**Figure 3.3.5: (a)** ORTEP of **4a-23** drawn with 50% ellipsoidal probability. **(b)** C13-H13···F2 hydrogen bond generating a zig-zag catameric chain like structure along the crystallographic *b*-axis. (c) C19–H19···O1 and C14–H14···O2 hydrogen bonds generating a molecular stacking through tetramer formation. **(d)** C–H···π ($C_{gC}$) interactions in **4a-23**.

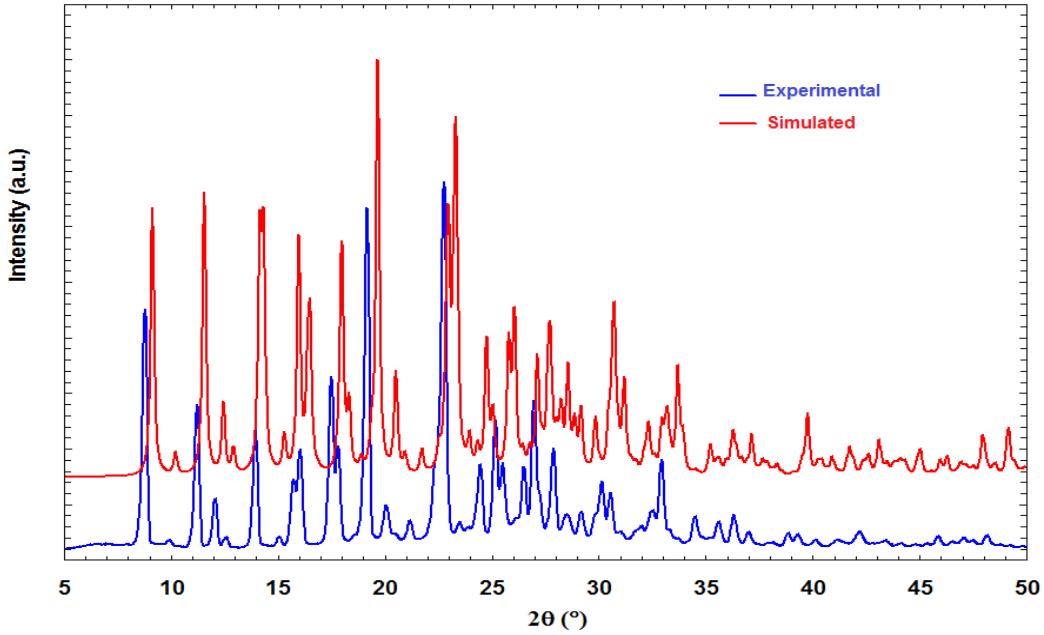


**Figure 3.3.15: (f)** Comparison of experimental and simulated PXRD patterns of **4a-20**

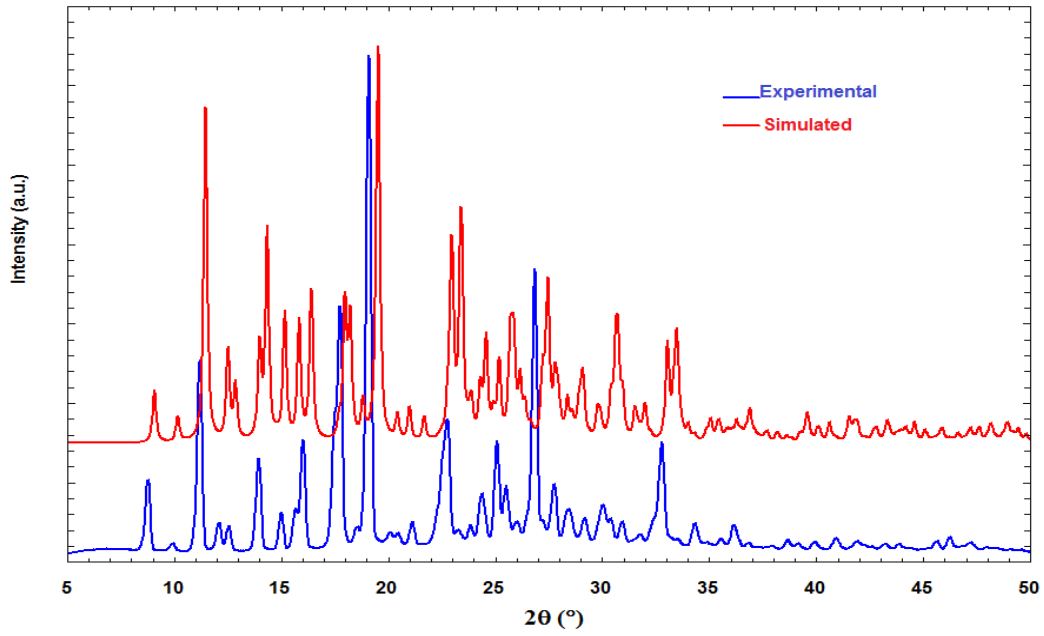


**Figure 3.3.16: (e)** Comparison of experimental and simulated PXRD pattern of **4a-23**

**N-(2,6-difluorophenyl)-2,6-difluoro-N-[2-(3-methoxyphenyl)ethyl]benzamide (4a-22):** This compound (Figure 3.3.17a) crystallizes in monoclinic $P2_1/c$ space group. Only one fluorine is involved in the C–H···F hydrogen bond formation by the utilization of translational symmetry. Molecular ribbons have been found to form through cooperative involvement C13–H13···F1 and C14–H14···O1 hydrogen

bonds along the *b*-direction (Figure 3.3.17b) (Table 3.3.17**)**. Further, translational related C12–H12···O2 hydrogen bond through the oxygen of the methoxy group is responsible for producing one dimensional molecular chain in the lattice (Figure 3.3.17c).

**Table 3.3.17: Intermolecular interactions in 4a-22**

| D–B···A | D–B/Å | *D*(D···A )/ Å | *d*(B···A )/Å | ∠D–B···A/º | SYMMETRY |
|---|---|---|---|---|---|
| **C13–H13···F1** | 1.080 | 3.562(2) | 2.58 | 150 | x, 1 + y, z |
| **C14–H14···O2** | 1.080 | 3.282(2) | 2.39 | 139 | x - 1, y + 1, z |
| **C12–H12···O1** | 1.080 | 3.167(2) | 2.39 | 128 | x, y + 1, z |

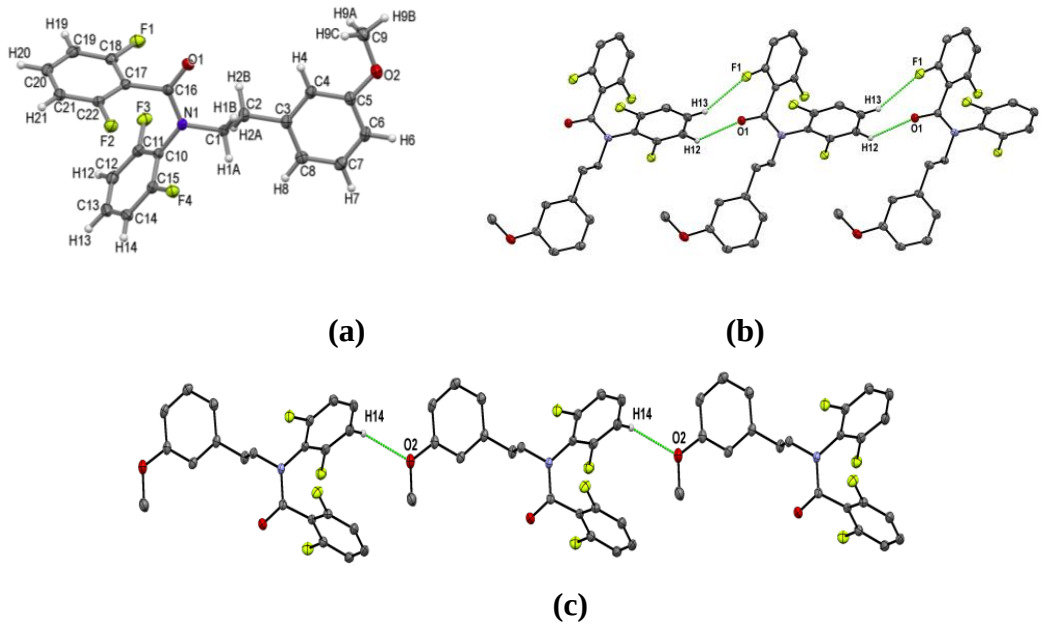


**Figure 3.3.17: (a)** ORTEP of **4a-22** drawn with 50% ellipsoidal probability. **(b)** C13–H13···F1 and C14–H14···O1 hydrogen bonds together forms molecular ribbon in the crystallographic *b*-direction. **(c)** C12–H12···O2 hydrogen bonded chain involving the oxygen of the methoxy group.

**N-(3,4-difluorophenyl)-2,3-difluoro-N-[2-(3-methoxyphenyl)ethyl]benzamide (4a-25):** This compound crystallizes in the centrosymmetric monoclinic $P2_1/c$ space group with Z = 4 and Z' = 1. Both A ring and B ring of this compound have static disorder about the C10(A/B)–N1 and C16–C17(A/B) bonds respectively (Figure 3.3.18a) (Table 3.3.18**)**. Therefore, the fluorine atoms at the *o*- position and the *m*-position found to be on both the sides of the aromatic ring while the *p*-F remaining at the same position. Out of four fluorine atoms (including disorder), only one fluorine

(*m*-F) of the B ring is involved in C–H···F hydrogen bond generating a zig-zag catameric chain like structure along the crystallographic *b*-direction by the utilization of $2_1$ symmetry (Figure 3.3.18b).

**Table 3.3.18: Intermolecular interactions in 4a-25**

| D–B···A | D–B/Å | *D*(D···A )/Å | *d*(B···A )/Å | ∠D–B···A/º | SYMMETRY |
|---|---|---|---|---|---|
| **C14A–H14A···F2A** | 1.080 | 3.349(3) | 2.54 | 131 | - x, y - ½, ½ - z |
| **C11A–H11A···O1** | 1.080 | 3.204(3) | 2.22 | 151 | 1 - x, y - ½, ½ - z |
| **C18A–F1A···F3A–C12A** | 1.293(3)<br>1.331(2) | 4.965(3) | 2.632(2) | 138<br>152 | x, y - 1, z |

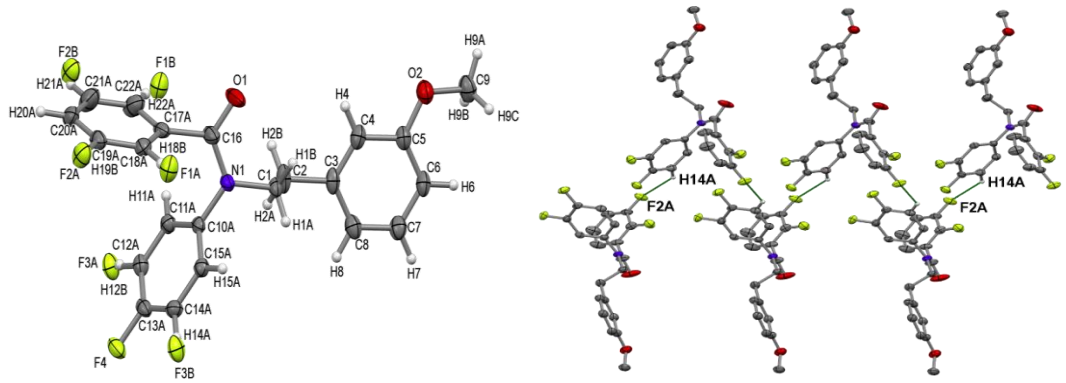


**(a)** **(b)**

**Figure: 3.3.18: (a)** ORTEP of **4a-25** drawn with 50% ellipsoidal probability. **(b)** Generation of a molecular chain along the *b*-direction involving C–H···F hydrogen bond.

The *m*-F (F3A) of the A ring and the *o*-F (F1A) of the B ring are found to share a short quasi Type I / Type II C–F···F–C contact forming a chain along the *b*-direction (Figure 3.3.18c). In addition to the C–H···F hydrogen bond and F···F contact, the oxygen of the carbonyl group also participates through C11A–H11A···O1 hydrogen bond generating molecular chain *via* $2_1$ symmetry along the *b*-direction (Figure 3.3.18d). The experimental PXRD pattern of **4a-25** is matching with the corresponding simulated PXRD pattern (Figure 3.3.18e).

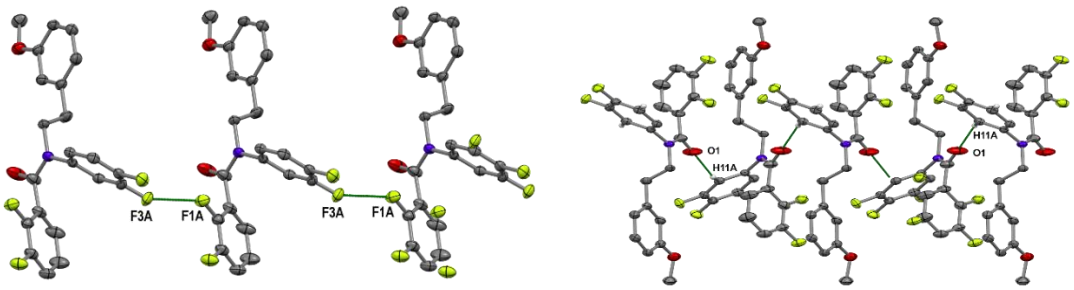


**(c)** **(d)**

**Figure 3.3.18: (c)** Quasi Type I / Type II C–F···F–C contact leading to the formation of one dimensional catameric chain along *b*-axis. **(d)** C11A–H11A···O1 hydrogen bond producing a molecular chain along the *b*-axis.

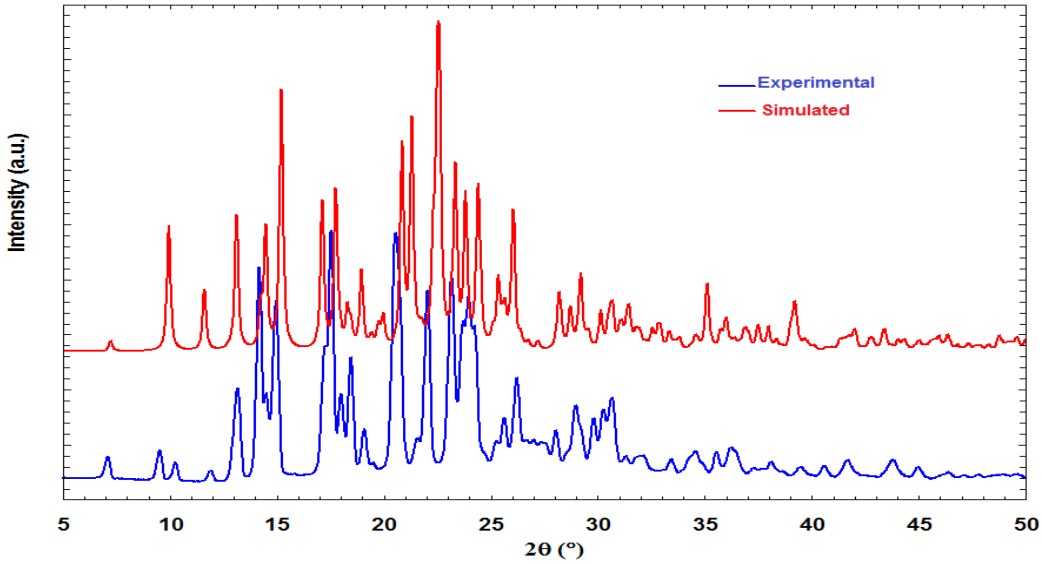


**Figure: 3.3.18: (e)** Comparison of experimental and simulated PXRD patterns of **4a-25**

**N-(3,4-difluorophenyl)-2,5-difluoro-N-[2-(3-methoxyphenyl)ethyl]benzamide (4a-27):** This compound crystallizes in the monoclinic centrosymmetric $P2_1/c$ space group with Z = 4 and Z' = 1. Both A ring and B ring of this compound have static disorder about the C10(A/B)–N1 and C16–C17(A/B) bonds respectively (Figure 3.3.19a) as in the earlier case. Out of four fluorine atoms, three fluorine atoms appear in two positions each in the asymmetric unit due to this disorder while *p*-F of the A ring remained at the same position. C14A–H14A···F1A hydrogen bond *via* translation symmetry along *b*-axis creates one dimensional chain involving *o*-F (F1A) of the B ring (Figure 3.3.19b) (Table 3.3.19**)**.

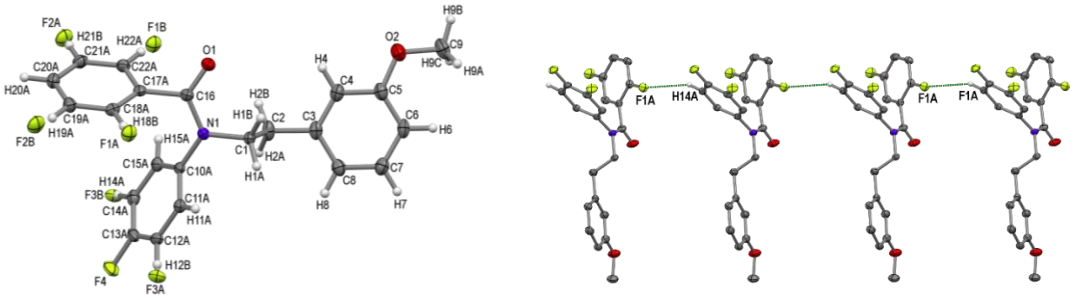


**(a)** **(b)**

**Figure 3.3.19: (a)** ORTEP of **4a-27** drawn with 50% ellipsoidal probability. **(b)** C14A–H14A···F1A hydrogen bonded molecular chain through translational symmetry along the *b*-axis.

The fluorine atom F3A present at the *m*-position of the A ring, acts as a bifurcated acceptor with the H19A and H20A to form weak C–H···F hydrogen bonds thereby resulting into the formation of a cyclic tetramer unit by utilisation of screw ($2_1$) symmetry (Figure 3.3.19c). This tetramer unit further interconnected by another tetramer unit through C–H···F and C–H···O hydrogen bonds. The experimental PXRD pattern of **4a-27** matches with the corresponding simulated PXRD pattern (Figure 3.3.19d).

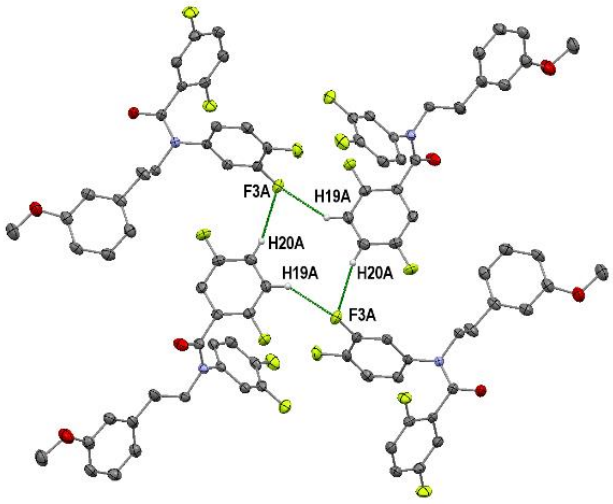


**(c)**

**Figure 3.3.19: (c)** One tetramer unit through bifurcated acceptor units involving C–H···F hydrogen bonds.

**Table 3.3.19: Intermolecular interactions in 4a-27**

| D–B···A | D–B/Å | *D*(D···A)/Å | *d*(B···A )/Å | ∠D–B···A/º | SYMMETRY |
|---|---|---|---|---|---|
| **C14A–H14A···F1A** | 1.080 | 3.332(2) | 2.47 | 136 | x, y - 1, z |
| **C19A–H19A···F3A** | 1.080 | 3.326(2) | 2.38 | 145 | 2 - x, ½ + y, $^{3}/_{2}$ - z |
| **C20A–H20A···F3A** | 1.080 | 3.537(2) | 2.49 | 162 | x, ½ - y, ½ + z |

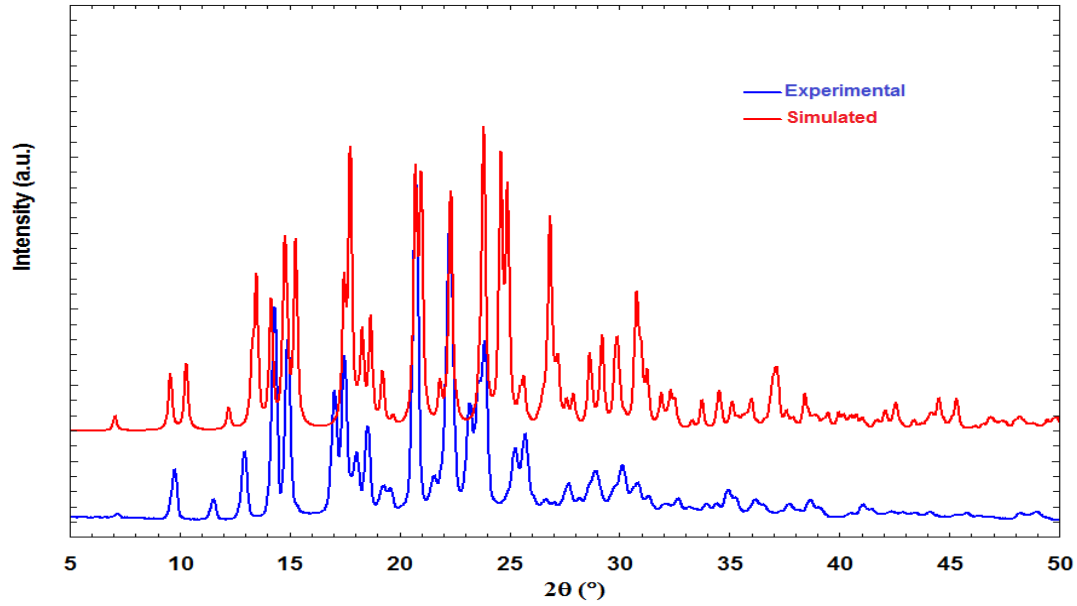


**Figure 3.3.19: (d)** Comparison of experimental and simulated PXRD patterns of **4a-27**

**N-(3,4-difluorophenyl)-2,6-difluoro-N-[2-(3-methoxyphenyl)ethyl]benzamide (4a-28):** This compound **4a-28** crystallizes in the orthorhombic non-centrosymmetric $P2_12_12_1$ space group with Z = 4 and Z' = 1 (Figure 3.3.20a). In this compound, one *o*-F of the B ring and carbonyl oxygen have been found to form head-to-tail dimer through simultaneously C8–H8···F2 and C11–H11···O1 hydrogen bonds respectively (Figure 3.3.20b) (Table 3.3.20**)**. The molecules which are involved in such kind of anti-periplanar dimers are related to each other $2_1$ screw along *b*-axis and are propagating as one dimensional ribbon type structure along the *b*-direction.

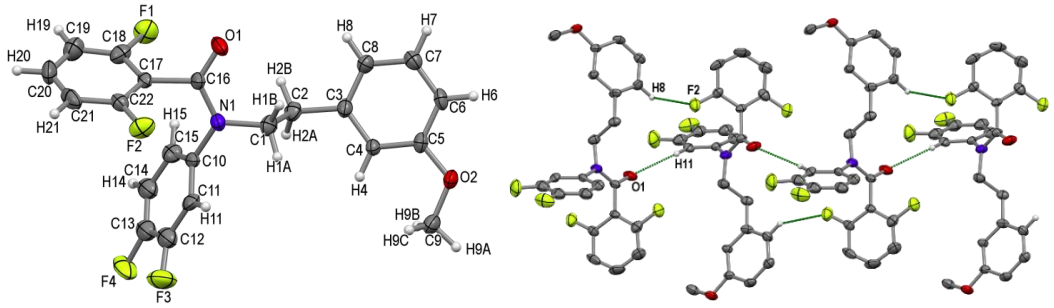


**(a)** **(b)**

**Figure 3.3.20: (a)** ORTEP of **4a-28** drawn with 50% ellipsoidal probability. **(b)** Anti-parallel molecular dimers are related to each other by $2_1$ screw along *b*-axis and propagating in one dimensional ribbon type structure.

Additionally, the *p*-F (F4) of the A ring with the *p*-H (H20) of the B ring are also involved in the formation of C–H···F hydrogen bond while the carbonyl oxygen atom is involved in C–H···O hydrogen bond with H14. This combination of two weak hydrogen bonding interaction is responsible for the formation of a ladder type structure along *a*-axis (Figure 3.3.20c). The experimental PXRD pattern of **4a-28** is in agreement with the corresponding simulated PXRD pattern (Figure 3.3.20d).

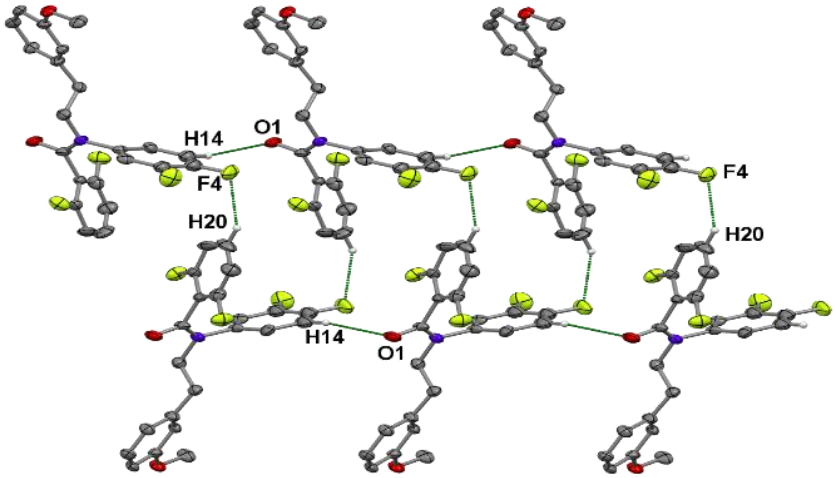


**(c)**

**Figure 3.3.20: (c)** Combination of C14–H14···O1 and C20–H20···F4 hydrogen bonds generating a ladder type structure along the *x*-axis.

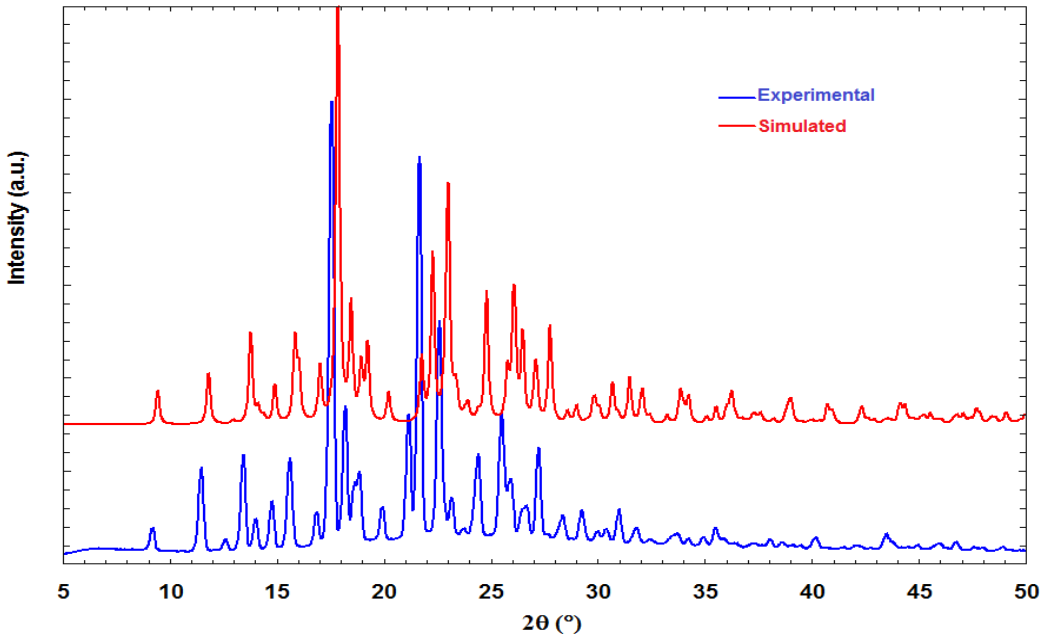


**Figure 3.3.20: (d)** Comparison of experimental and simulated PXRD patterns of **4a-28**

**Table 3.3.20: Intermolecular interactions in 4a-28**

| D–B···A | D–B/Å | *D*(D···A )/Å | *d*(B···A )/Å | ∠D–B···A/º | SYMMETRY |
|---|---|---|---|---|---|
| **C8–H8···F2** | 1.080 | 3.263(7) | 2.58 | 120 | 1 - x, y - ½, $^{3}/_{2}$ – z |
| **C20–H20···F4** | 1.080 | 3.436(9) | 2.49 | 146 | x - ½, $^{3}/_{2}$ - y, 2 - z |
| **C11–H11···O1** | 1.080 | 3.235(8) | 2.40 | 133 | 1 - x, ½ + y, $^{3}/_{2}$ - z |

**N-(3,4-difluorophenyl)-3,5-difluoro-N-[2-(3-methoxyphenyl)ethyl]benzamide (4a-30):** This compound crystallizes in the triclinic $P\ \bar{1}$ space group (Figure 3.3.21a). Two fluorine atoms (F2 and F3) located at the *m*-positions participate in C–H···F hydrogen bonds formation. A pair of C4–H4···F3 hydrogen bonds are involved in the formation of a cyclic head-to-tail dimer through the inversion centre (Figure 3.3.21b) (Table 3.3.21**)**. These dimers are further interconnected by C6–H6···F2 hydrogen bonds (Figure 3.3.21b). Carbonyl oxygen is also contributed in the packing through C14–H14···O1 hydrogen bonds by forming a molecular chain in the lattice (Figure 3.3.21c). The experimental PXRD pattern of **4a-30** matches with the corresponding simulated PXRD pattern (Figure 3.3.21d).

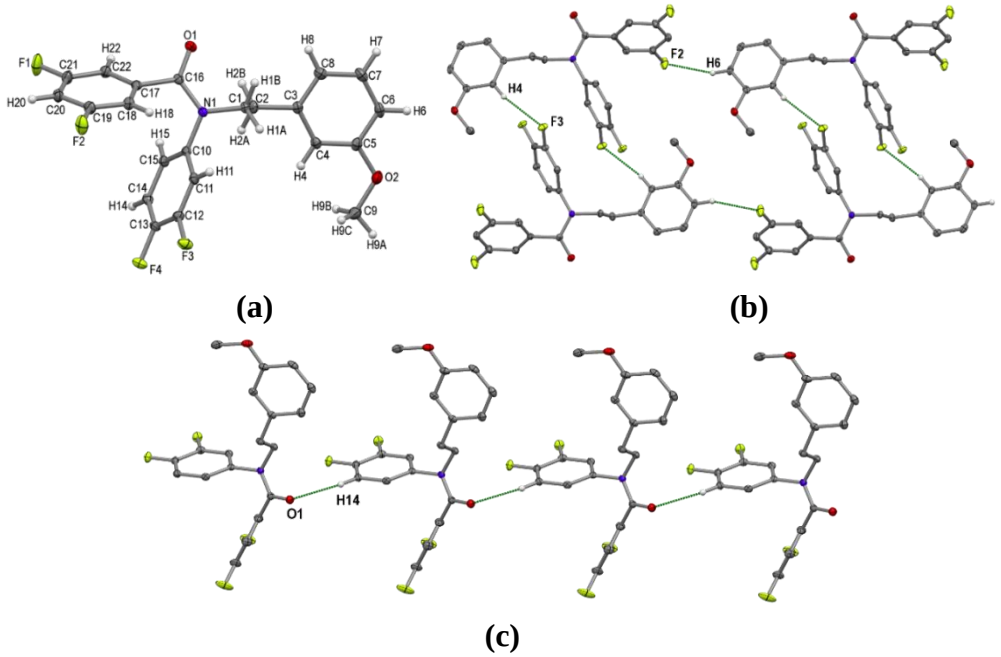


**Figure 3.3.21: (a)** ORTEP of **4a-30** drawn with 50% ellipsoidal probability. **(b)** Molecular ribbon involving chains of dimers through C–H···F hydrogen bonds. **(c)** C–H···O hydrogen bond in polymeric chain type structure.

**Table 3.3.21: Intermolecular interactions in 4a-30**

| D–B···A | D–B/Å | *D*(D···A )/Å | *d*(B···A )/Å | ∠D–B···A/º | SYMMETRY |
|---|---|---|---|---|---|
| **C4–H4···F3** | 1.080 | 3.477(2) | 2.45 | 159 | 2 - x, 1 - y, 1 - z |
| **C6–H6···F2** | 1.080 | 3.465(2) | 2.44 | 158 | x - 1, y - 1, z - 1 |
| **C14–H14···O1** | 1.080 | 3.289(2) | 2.257 | 159 | x+1, y, z |

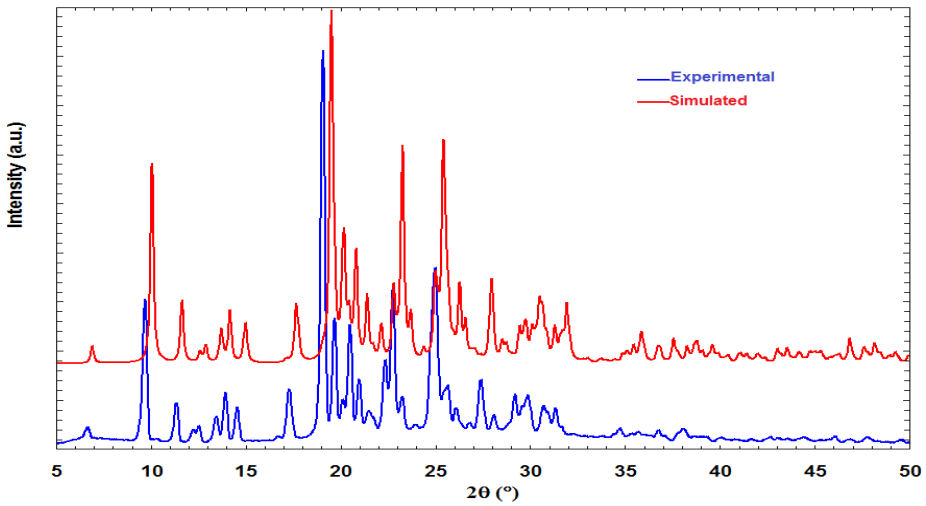


**Figure 3.3.21: (d)** Comparison of experimental and simulated PXRD patterns of **4a-30**

**N-(3,5-difluorophenyl)-2,3-difluoro-N-[2-(3-methoxyphenyl)ethyl]benzamide (4a-31):** This compound crystallizes in the triclinic centrosymmetric $P\bar{1}$ space group with Z = 2 (Figure 3.3.22a). Two fluorine atoms (F4 and F2) are involved in C–H···F hydrogen bonds. C22–H22···F4 hydrogen bond formed by the *m*-F of the A ring and *o*-H of the B ring propagates in the linear fashion by the translation symmetry in the crystallographic *b*-direction (Figure 3.3.22b) (Table 3.3.22**)**. A head-to-tail dimer is formed by the involvement of C11–H11···F2 hydrogen bonds across the inversion centre (Figure 3.3.22c). These dimers are interconnected by another pair of C22–H22···F4 hydrogen bonds leading to the formation of ladder type structure (Figure 3.3.22d).

**Table 3.3.22: Intermolecular interactions in 4a-31**

| D–B···A | D–B/Å | *D*(D···A )/Å | *d*(B···A )/Å | ∠D–B···A/º | SYMMETRY |
|---|---|---|---|---|---|
| **C22–H22···F4** | 1.080 | 3.161(2) | 2.42 | 125 | x - 1, 1 + y, z |
| **C11–H11···F2** | 1.080 | 3.376(2) | 2.38 | 152 | 1 - x, 1 - y, - z |

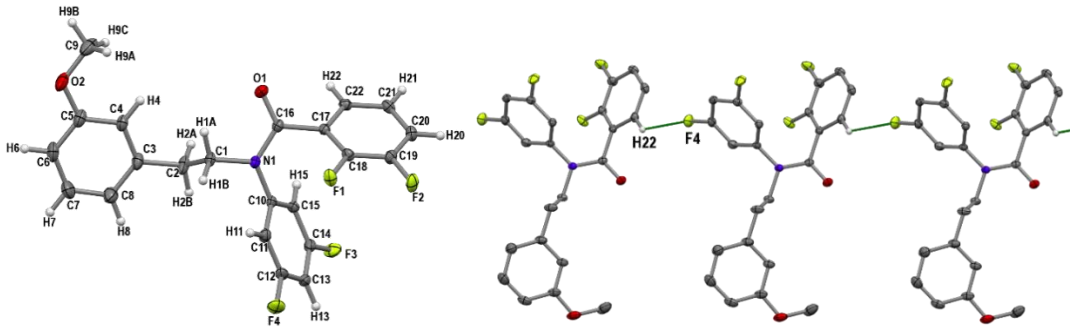


**(a)** **(b)**

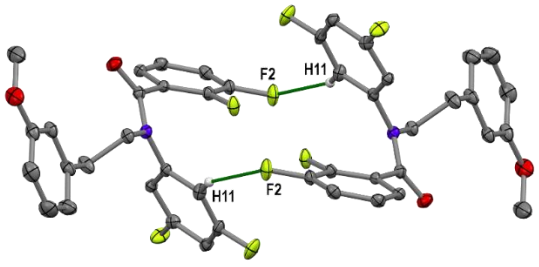


**(c)**

**Figure 3.3.22: (a)** ORTEP of **4a-31** drawn with 50% ellipsoidal probability. **(b)** A linear chain type structure by the using of C22–H22···F4 hydrogen bond up to infinite length. **(c)** An inversion centre related dimer through the C11–H11···F2 hydrogen bonds.

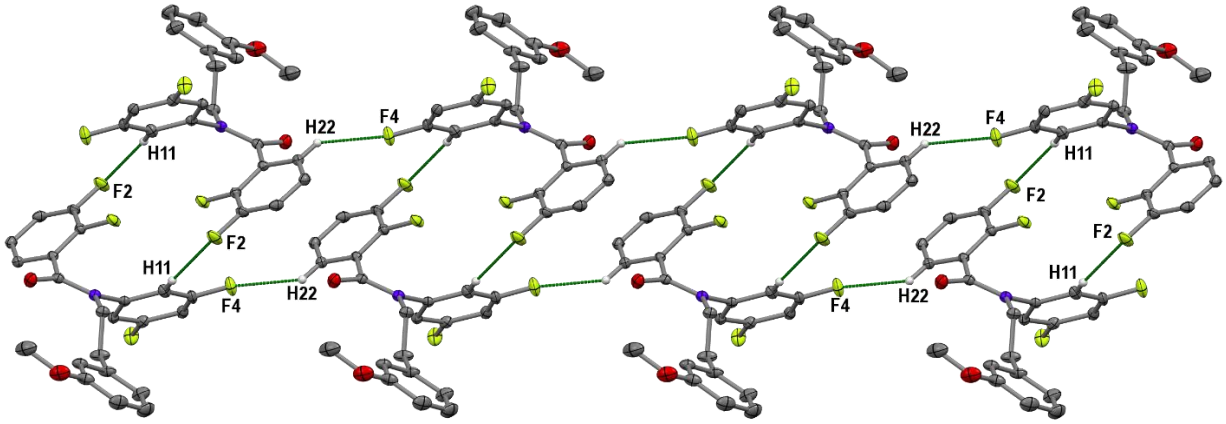


**(d)**

**Figure 3.3.22: (d)** A ladder type structure involving both C22–H22···F4 and C11–H11···F2 hydrogen bonds.

In addition to C–H···F hydrogen bonds, carbonyl oxygen is also involved in weak C–H···O hydrogen bonds with the acidic *p*-H of the A ring to form one dimensional chain along the *b*-axis (Figure 3.3.22e). The experimental PXRD pattern of **4a-31** is matching with the corresponding simulated PXRD pattern (Figure 3.3.22f).

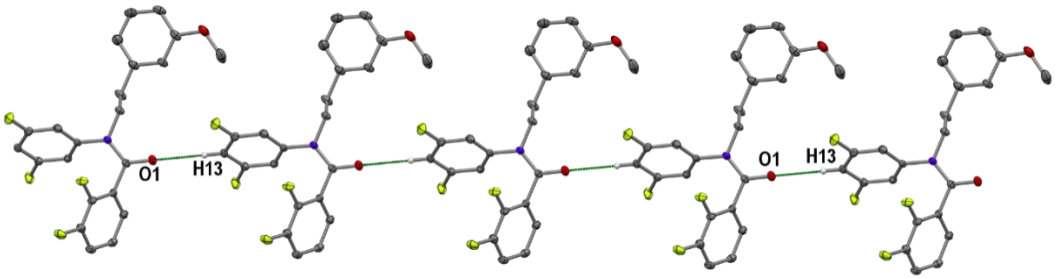


**(e)**

**Figure 3.3.22: (e)** A one dimensional linear chain through C13–H13···O1 hydrogen bonds.

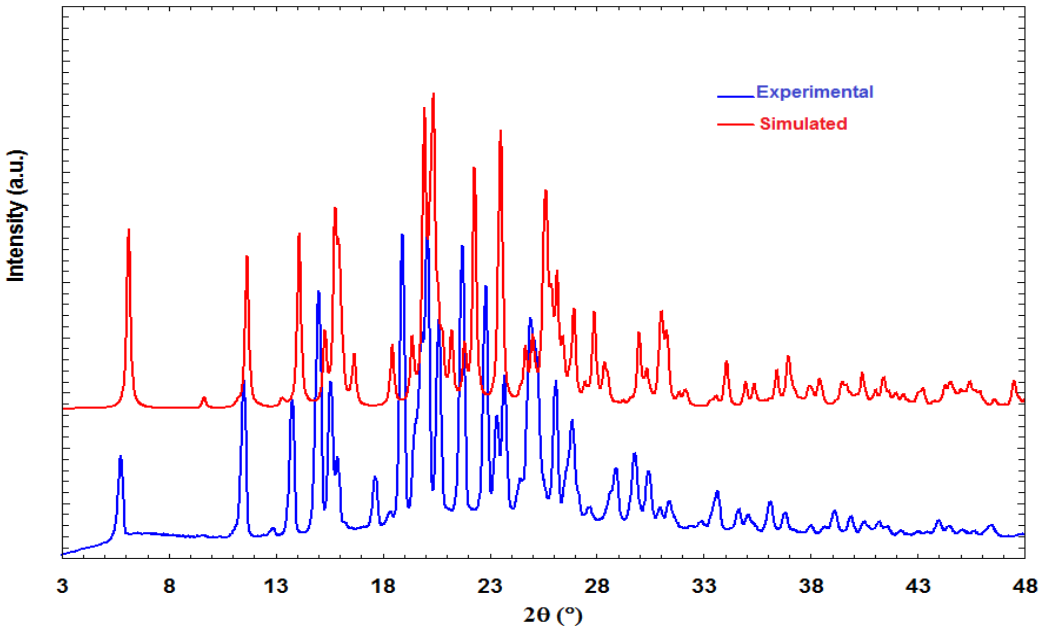


**Figure 3.3.22: (f)** Comparison of experimental and simulated PXRD patterns of **4a-31**

**N-(3,5-difluorophenyl)-2,5-difluoro-N-[2-(3-methoxyphenyl)ethyl]benzamide (4a-33):** This compound **4a-33** crystallizes in the monoclinic centrosymmetric $P2_1/c$ space group with Z = 4 and Z' = 1(Figure 3.3.23a). In this crystal structure the packing is only involving fluorine atoms available in the B ring. C13–H13···F3 hydrogen bonds generated head-to-tail dimer through the inversion centre (Table 3.3.23**)**. These dimers are further interconnected to another dimer by C20–H20···O2 hydrogen bonds creating a ladder type structure (Figure 3.3.23b). Further the *o*-F (F1) of the B ring forms hydrogen bond using $2_1$ symmetry with the *o*-H of another molecule to form a dimer (Figure 3.3.23c). The experimental PXRD pattern of **4a-33** matches with the corresponding simulated PXRD pattern (Figure 3.3.23d).

**Table 3.4.23: Intermolecular interactions in 4a-33**

| D–B···A | D–B/Å | *D*(D···A )/Å | *d*(B···A )/Å | ∠D–B···A/º | SYMMETRY |
|---|---|---|---|---|---|
| **C13–H13···F2** | 1.080 | 3.416(1) | 2.55 | 137 | - x, - y, - z |
| **C22–H22···F1** | 1.080 | 3.551(1) | 2.58 | 150 | 1 - x, y - ½, ½ - z |
| **C15–H15···O1** | 1.080 | 3.370(2) | 2.45 | 142 | 1 - x, y - ½, ½ - z |
| **C20–H20···O2** | 1.080 | 3.362(3) | 2.31 | 165 | x - 1, y, z |

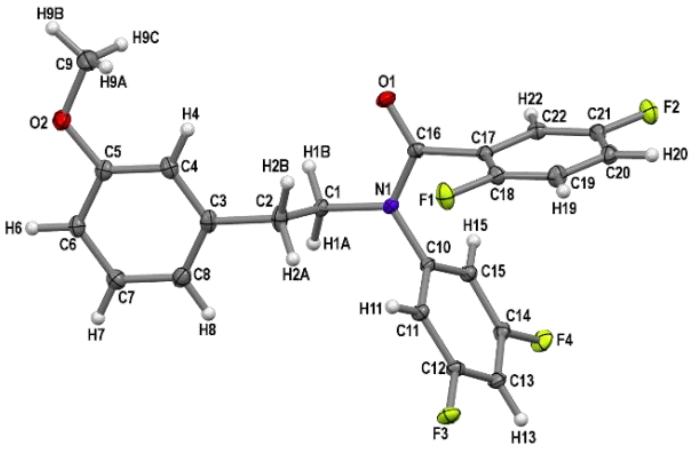


**(a)**

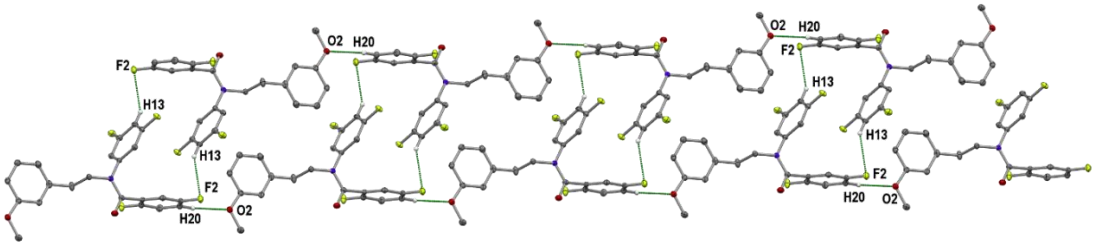


**(b)**

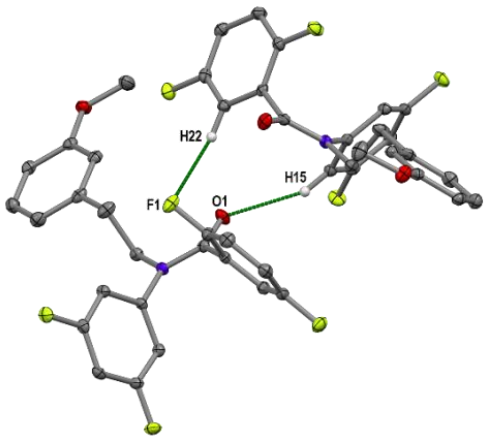


**(c)**

**Figure 3.3.23: (a)** ORTEP of **33** drawn with 50% ellipsoidal probability. **(b)** A ladder type molecular arrangement by utilization of C13–H13···F2 and C20–H20···O2 hydrogen bonds which are perpendicular to each other. **(c)** A screw ($2_1$) related dimer via C22–H22···F1 and C15–H15···O1 hydrogen bonds.

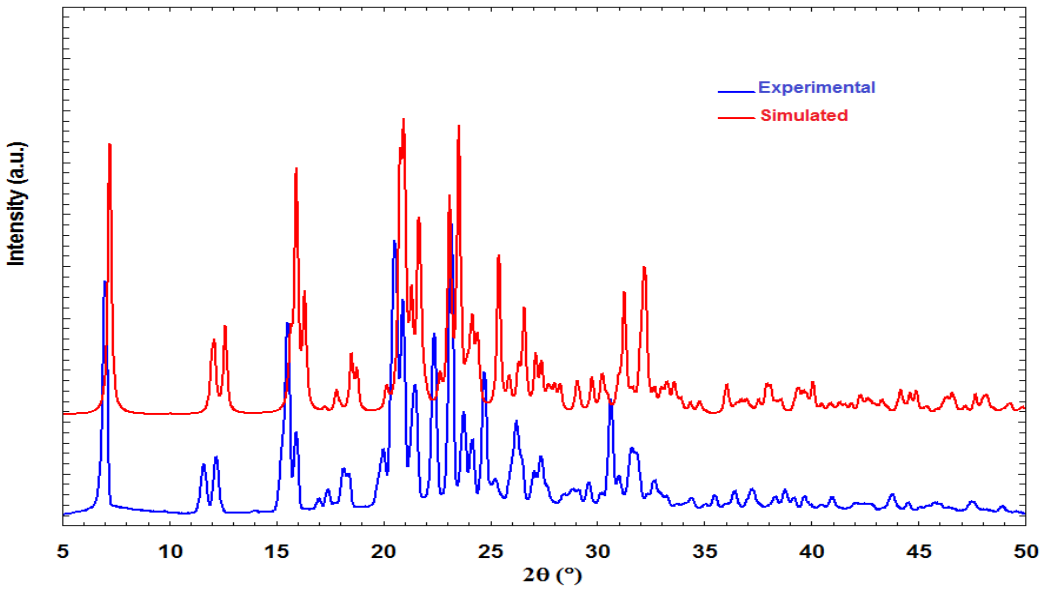


**Figure 3.3.23: (d)** Comparison of experimental and simulated PXRD patterns of **4a-33**

**N-(3,5-difluorophenyl)-2,6-difluoro-N-[2-(3-methoxyphenyl)ethyl]benzamide (4a-34):** This compound crystallizes in the monoclinic centrosymmetric $P2_1/c$ space group with Z = 4 and Z' = 1(Figure 3.3.24a). Out of four fluorine atoms, only *m*-F (F3) of the A ring and *p*-H (H6) of the C ring are involved in the formation of C6–H6···F3 hydrogen bond through $2_1$ symmetry (Figure 3.3.24b) (Table 3.3.24**)**. The carbonyl oxygen is also involved in weak C20–H20···O1 hydrogen bond, which runs in a direction perpendicular to the C–H···F hydrogen bond, and hence the combination of these two bonds generated a ladder type structure in the lattice (Figure 3.3.24b).

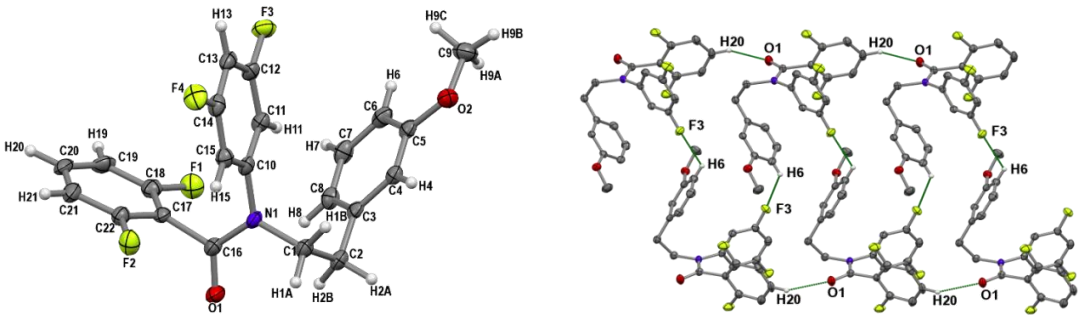


**(a)** **(b)**

**Figure 3.3.24: (a)** ORTEP of **4a-34** drawn with 50% ellipsoidal probability. **(b)** C6–H6···F3 and C20–H20···O1 hydrogen bonds, which are perpendicular to each other, leading to the formation a ladder type molecular arrangement.

**Table 3.3.24: Intermolecular interactions in 4a-34**

| D–B···A | D–B/Å | *D*(D···A )/Å | *d*(B···A )/Å | ∠D–B···A/º | SYMMETRY |
|---|---|---|---|---|---|
| **C6–H6···F3** | 1.080 | 3.334(4) | 2.63 | 122 | 1 - x, ½ + y, $^{3}/_{2}$ - z |
| **C20–H20···O1** | 1.080 | 3.172(4) | 2.34 | 133 | x, y - 1, z |

**N-(3,5-difluorophenyl)-3,4-difluoro-N-[2-(3-methoxyphenyl)ethyl]benzamide (4a-35):** This compound **4a-35** crystallizes in the triclinic centrosymmetric $P\bar{1}$ space group with Z = 2 (Figure 3.3.25a). Fluorine mediated C4–H4···F1 hydrogen bonds and carbonyl oxygen mediated C18–H18···O1 hydrogen bonds generate a centrosymmetric dimer (Figure 3.3.25b) (Table 3.3.25**)**. Further, the carbonyl oxygen participates in another hydrogen bond (C7–H7···O1), which propagates in the linear fashion by the translation symmetry forming an infinite chain (Figure 3.3.25c).

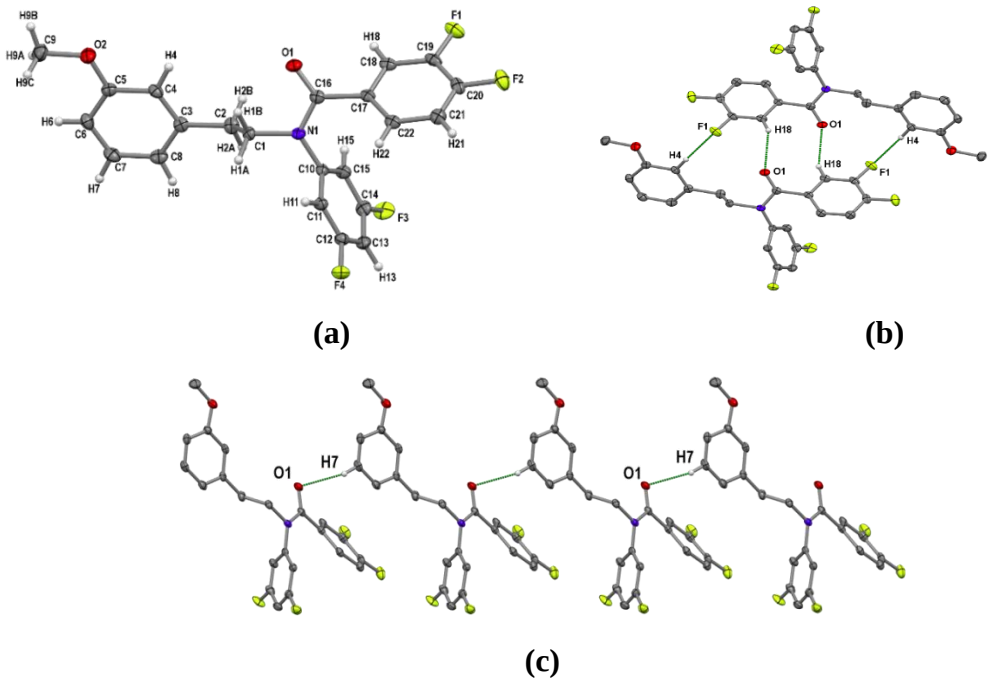


**Figure 3.3.25: (a)** ORTEP of **4a-35** drawn with 50% ellipsoidal probability. **(b)** A centrosymmetric dimer synthon by C4–H4···F1 and C18–H18···O1 hydrogen bonds. **(c)** A linear chain generated by carbonyl oxygen as a C7–H7···O1 hydrogen bonds.

Interestingly F1 of the B ring and F4 of the A ring are found to form C4–F1···F4–C type I contact where $\theta 1$ = 105 º and $\theta 2$ = 108 º, which propagates along the crystallographic *a*- direction *via* translational symmetry (Figure 3.3.25d).

In addition to these weak interactions, C–H···π mediated dimers also contribute in the stabilization of the crystal packing (Figure 3.3.25e). The experimental PXRD pattern of **4a-35** matches with the corresponding simulated PXRD pattern (Figure 3.3.25f).

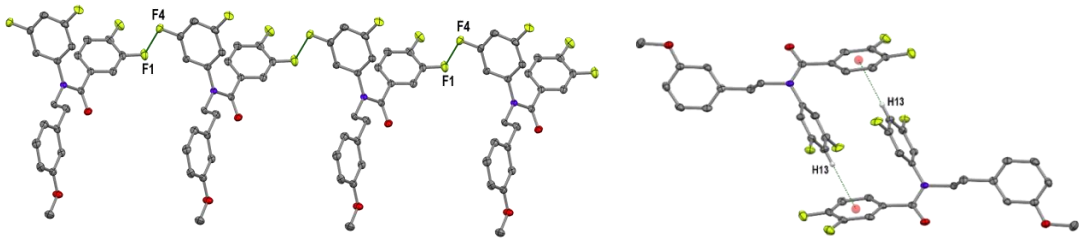


**(d)** **(e)**

**Figure 3.3.25: (d)** A linear chain of one dimensional halogen-halogen F1···F4 contact type-I via the translational symmetry. **(e)** A centrosymmetric dimer formation by C13–H13···π ($C_{gB}$) interaction.

**Table 3.3.25: Intermolecular interactions in 4a-35**

| **D–B···A** | **D–B/Å** | ***D*(D···A)/Å** | ***d*(B···A )/Å** | **∠D–B···A/º** | **SYMMETRY** |
|---|---|---|---|---|---|
| **C4–H4···F1** | 1.080 | 3.274(3) | 2.21 | 167 | - x, 1 - y, 1 - z |
| **C18–H18···O1** | 1.080 | 3.346(4) | 2.45 | 140 | - x, 1 - y, 1 - z |
| **C7–H7···O1** | 1.080 | 3.241(3) | 2.26 | 151 | 1 + x, y - 1, z |
| **C13–H13···π ($C_{gB}$)** | 1.080 | 3.678(3) | 2.78 | 163 | 1 - x,1 - y, - z |
| **C19–F1···F4–C12** | 1.348(3)<br>1.376(3) | 4.335(5) | 2.743(2) | 105<br>108 | x - 1, y, z |

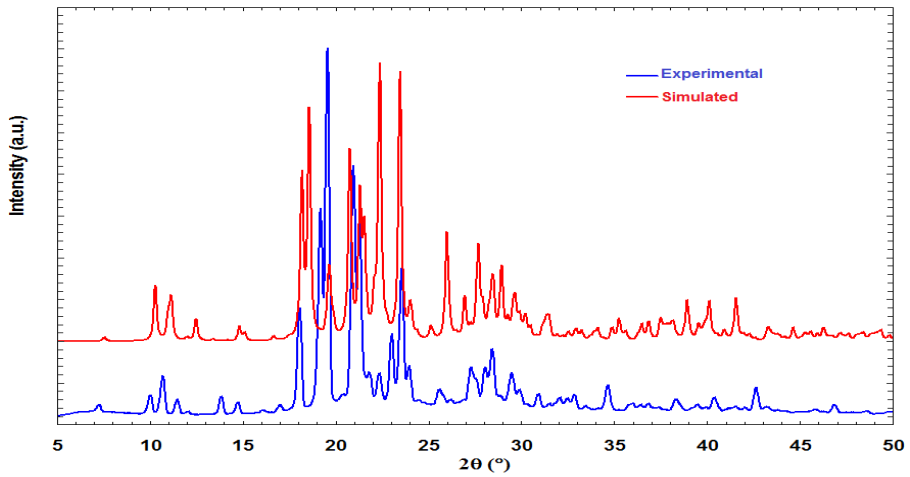


**Figure 3.3.25: (f)** Comparison of experimental and simulated PXRD patterns of **4a-35**

**N-(3,5-difluorophenyl)-3,5-difluoro-N-[2-(3-methoxyphenyl)ethyl]benzamide (4a-36):** This compound **4a-36** crystallizes in the monoclinic centrosymmetric $P2_1/c$ space group with Z = 4 and Z' = 1 (Figure 3.3.26a). Two fluorine atoms (F1 and F4) are involved in weak interaction. The F1 of the B ring and *o*-H of the C ring are interconnected by C8–H8···F1 hydrogen bonds through the *c*-glide symmetry along the *a*-direction and generates one dimensional ribbon like structure (Figure 3.3.26b) (Table 3.3.26**)**. Similarly, F4 of the A ring forms weak C13–H13···F4 hydrogen bond through the screw $2_1$ symmetry and creates a zig-zag chain like structure along the *b*-direction (Figure 3.3.26c). When these two hydrogen-bonded atoms are plotted, it generates a tetramer unit across the inversion centre in the crystal structure (Figure 3.3.26d). Additionally, type-I F···F contact have also been observed to form a dimer across a centre of symmetry (Figure 3.3.26e). The experimental PXRD pattern of **4a-36** is matching with the corresponding simulated PXRD pattern (Figure 3.3.26f).

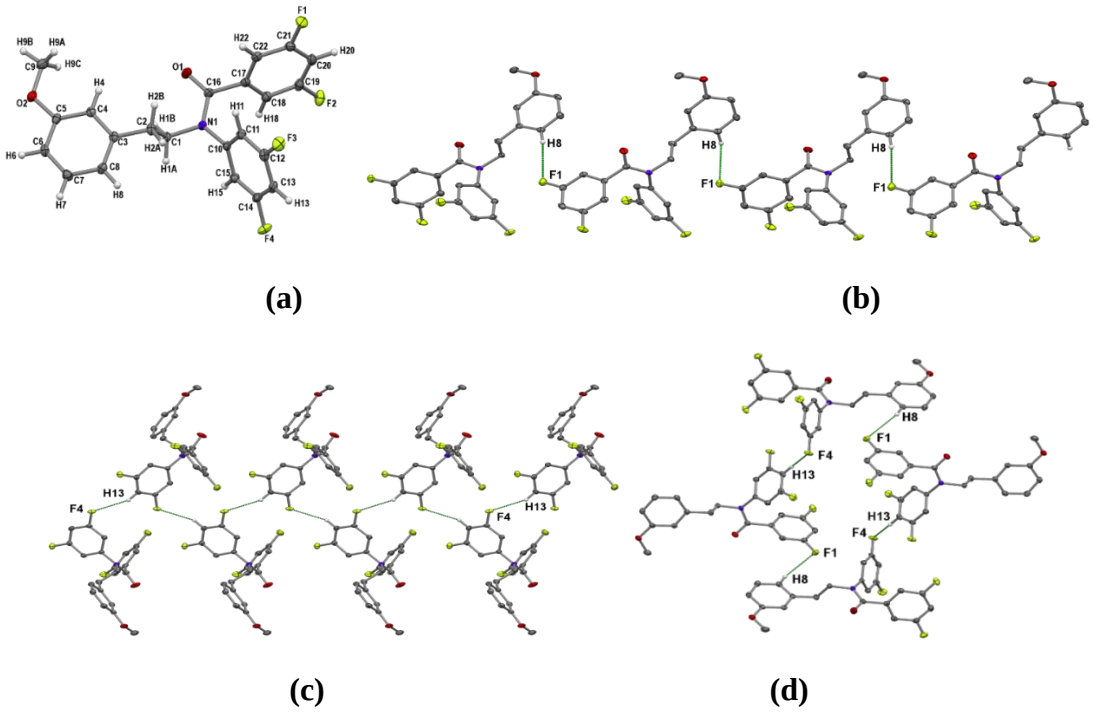


**Figure 3.3.26: (a)** ORTEP of **4a-36** drawn with 50% ellipsoidal probability. **(b)** *c*-glide related one dimensional ribbon like structure by C8–H8···F1 hydrogen bond. **(c)** Molecular chain generated by C13–H13···F4 hydrogen bonds along the *b*-direction through screw $2_1$ operation. **(d)** A tetrameric unit around the inversion centre, formed because of the combination of C8–H8···F1(*c*-glide) and C13–H13···F4 (screw) hydrogen bonds.

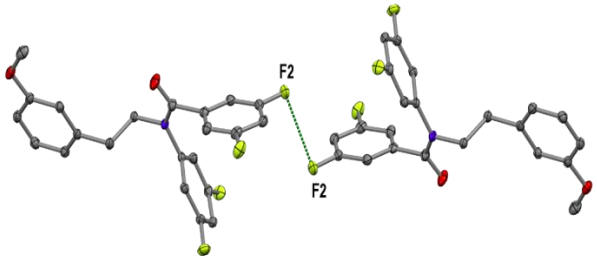


**(e)**

**Figure 3.3.26: (e)** A dimer form of halogen-halogen bond type-I F2···F2 contact.

**Table 3.3.26: Intermolecular interactions in 4a-36**

| D–B···A | D–B/Å | *D*(D···A)/Å | *d*(B···A )/Å | ∠D–B···A/º | SYMMETRY |
|---|---|---|---|---|---|
| **C8–H8···F1** | 1.080 | 3.450(3) | 2.57 | 138 | x + 1, $^{3}/_{2}$ - y, ½ + z |
| **C13–H13···F4** | 1.080 | 3.414(2) | 2.42 | 153 | 2 - x, ½ + y, ½ - z |
| **C19–F2···F2–C19** | 1.357(1) | 4.016(3) | 2.938(1) | 90 | 1 - x, - y, 1 - z |

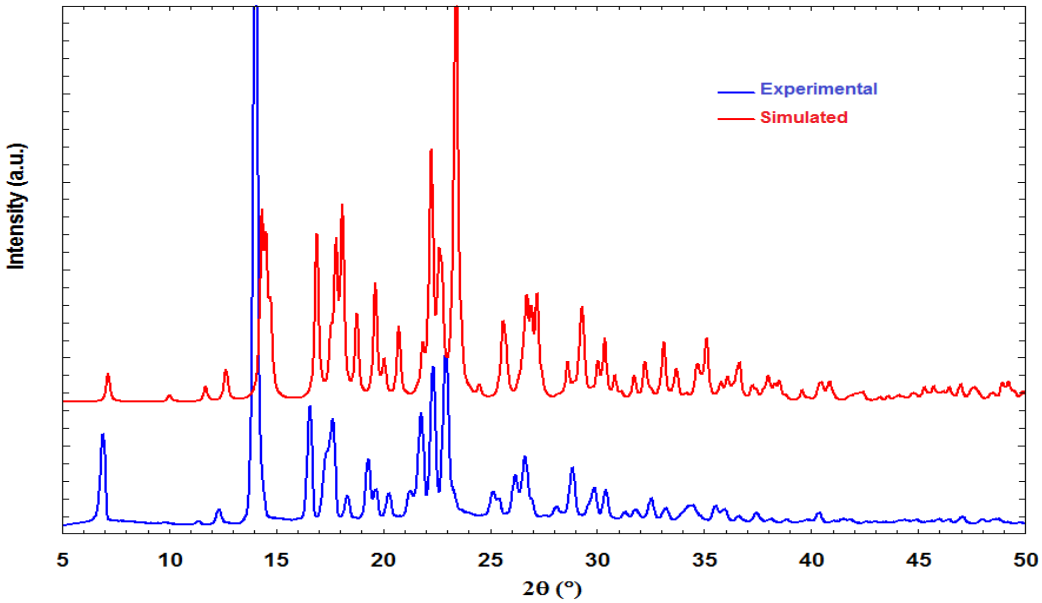


**Figure 3.5.3: (f)** Comparison of experimental and simulated PXRD patterns of **4a-36**

***N*-[2-(3-methoxyphenyl)ethyl]-*N*-phenylbenzamide (4a-37):** This compound **4a-37** crystallized in monoclinic centrosymmetric *C*2/*c* space group with Z = 8 and Z′ = 1 (Figure 3.3.27a). This non-fluorinated analogue doesn't have possibility of formation of C–H···F hydrogen bonds in the crystal structure. Therefore, the molecules are packed by C–H···O=C hydrogen bonds. The carbonyl Oxygen behave as a bifurcated acceptor for C7–H7···O1 and C18–H18··· O1 hydrogen bonds. One of the C18–H18···O1 hydrogen bond involve in the formation of dimer synthon by the utilization

of inversion centre symmetry (Figure 3.3.27b). Another one C7–H7···O1 hydrogen bond works as a linker between above two dimers and hence creates a tetramer unit in the entire crystal structure (Figure 3.3.27c). Methoxy group takes part in the C12–H12···O2 hydrogen bonds which leads to the formation of dimer motif *via* inversion centre (Figure 3.3.27d). No C–H···π interaction have been observed.

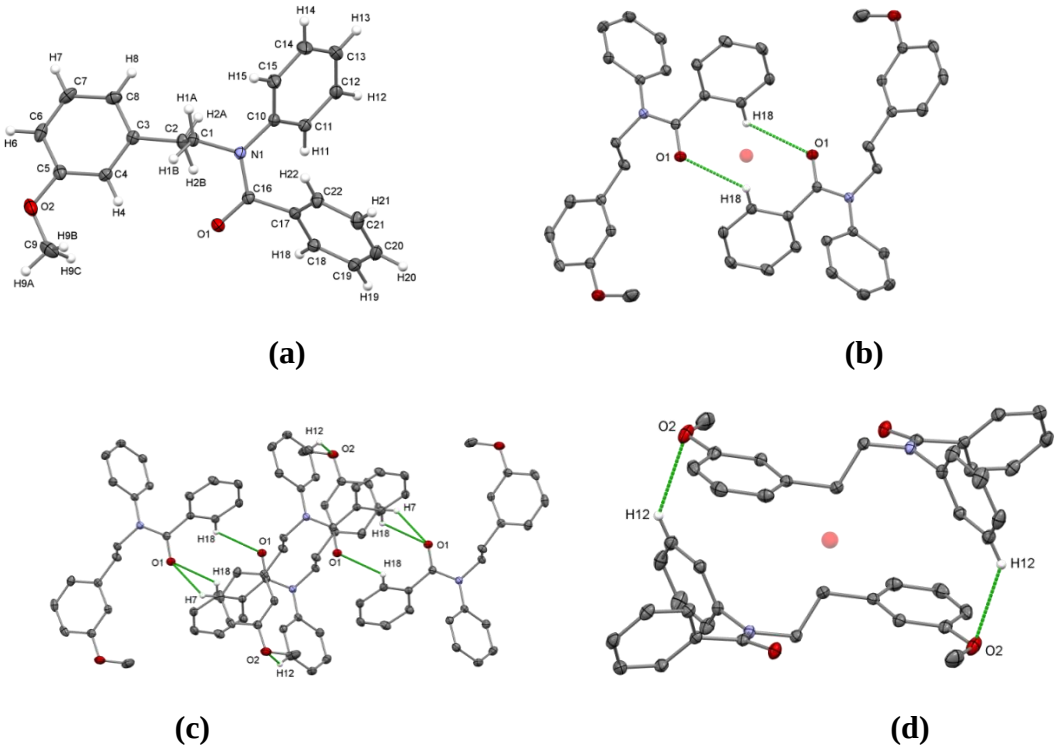


**Figure 3.3.27: (a)** ORTEP of **4a-37** drawn with 50% ellipsoidal probability. **(b)** An inversion centre related dimer synthon through the C18–H18···O1 hydrogen bonds. **(c)** A tetramer unit by the combination of two dimer motif *via* C7–H7···O1 hydrogen bond. **(d)** A centrosymmetric dimer motif by C12–H12···O2 hydrogen bonds.

**Table 3.3.27: Intermolecular interactions in 4a-37**

| D–B···A | D–B/Å | *D*(D···A )/Å | *d*(B···A )/Å | ∠D–B···A/º | SYMMETRY |
|---|---|---|---|---|---|
| **C7–H7···O1** | 1.080 | 3.377(1) | 2.48 | 139 | x, 1 + y, z |
| **C18–H18··· O1** | 1.080 | 3.331(2) | 2.59 | 125 | $^{1}/_{2}$ - x, $^{3}/_{2}$ - y, 1 - z |
| **C12–H12··· O2** | 1.080 | 3.441(2) | 2.58 | 137 | $^{1}/_{2}$ - x, $^{5}/_{2}$ - y, 1 - z |

The experimental PXRD pattern of **4a-37** is matching with the corresponding simulated PXRD pattern (Figure 3.3.27e).

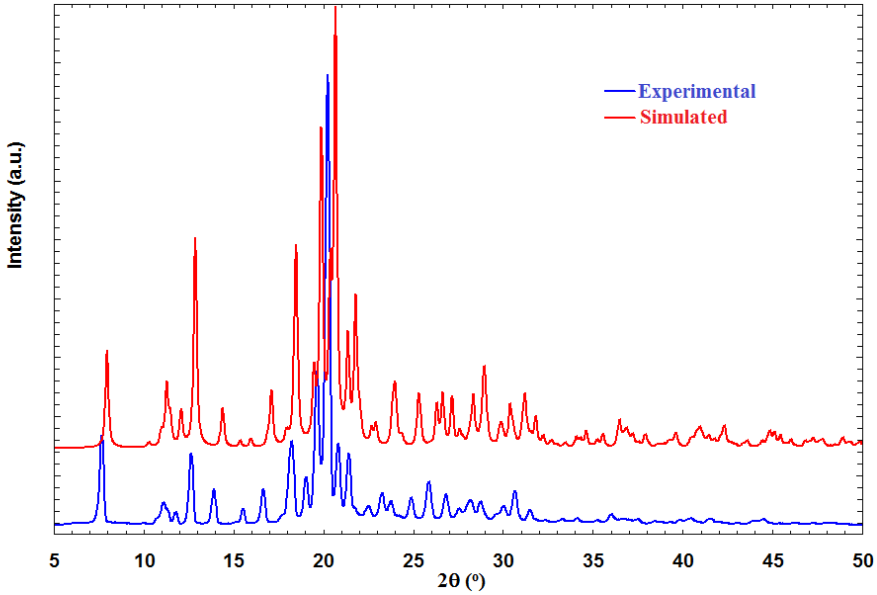


**Figure 3.3.27: (e)** Comparison of experimental and simulated PXRD patterns of **4a-37**

### 3.4 Discussion

The structural descriptions of these compound revel that the molecules are generally packed through C–H···F–C and C–H···O=C hydrogen bonds and weak C–H···π($C_g$) interactions involving different supramolecular synthons. From the crystal data tables (Table 3.2.2.1 to Table 3.2.2.5), we noted that the non-fluorinated analogue (**4a-37**) has the lowest density (1.235 g/cm$^3$) compared to the corresponding fluorinated analogues. Interestingly, this molecule has density lower than **2c-10**, which is the non-fluorinated analogue reported in the Chapter 2. The densities of the tetrafluorinated molecules reported in this chapter are in the range between 1.478 g/cm$^3$ and 1.388 g/cm$^3$. This once again clearly indicates that the incorporation of fluorine in the molecule produces better packing and hence higher density of the compounds. The important feature of these structures is that the correspondence of the experimental PXRD pattern with the simulated PXRD patterns of all compound thereby eliminating the probability of polymorphism in these molecules. Several crystallization experiments (both at RT and at 4$^o$C) using various solvents (both polar (chloroform, dichloromethane, acetonitrile) and non-polar (carbon tetrachloride, toluene), protic (methanol, ethanol) and aprotic (dicholoromethane, chloroform, acetonitrile, ethyl acetate)) and solvent mixtures (dichloromethane and hexane, ethyle acetate and hexane) for crystal growth resulted into only one form for each compound. These observations infer that these compounds (solutes) do not interact

with the solvent molecules using strong intermolecular forces and hence they crystallize without any the incorporation of solvent of crystallization to a particular crystalline form for each of the compounds based on the intermolecular interactions viable between the solute molecules.

The crystal structures are generally stabilized by several weak C–H···F–C hydrogen bonds. A statistical summary of these hydrogen bonds (Table 3.4.1) indicates that the molecules are packed in the lattice through many C–H···F–C hydrogen bonds, which are centred around the H···F distance ranging between 2.4 and 2.6Å and the ∠C–H···F centred between 130$^{o}$ and 160$^{o}$. Similar trends were observed by computational analyses of these weak hydrogen bonds involving simpler model systems of ethylene, fluoroethylene and difluoroethylene based systems recently.[12n] It is also evident from the Table 3.4.1 that the frequency of occurrence of C–H···F–C hydrogen bonds in these molecules is much larger than that for C–H···O=C hydrogen bonds, indicating that the four different C–F groups present in each molecule provided favourable platform for the formation of various supramolecular synthons involving C–H···F–C hydrogen bonds rather than formation of C–H···O=C hydrogen bonds in the lattice.

**Table 3.4.1: Statistical Summary of C–H···F and C–H···O hydrogen bonds**

| **H···F Distance Range** | **Number of C–H···F hydrogen bonds** | **Angle Range ∠C–H···F** | **Number of C–H···F hydrogen bonds** |
|---|---|---|---|
| **2.2≥d>2.0Å** | 0 | **130≥θ>120.0** | 12 |
| **2.3≥d>2.2Å** | 2 | **140≥θ>130.0** | 13 |
| **2.4≥d>2.3Å** | 11 | **150≥θ>140.0** | 14 |
| **2.5≥d>2.4Å** | 17 | **160≥θ>150.0** | 14 |
| **2.6≥d>2.5Å** | 22 | **170≥θ>160.0** | 5 |
| **2.7≥d>2.6Å** | 7 | **180≥θ>170.0** | 0 |
| **H···O Distance Range** | **Number of C–H···O hydrogen bonds** | **Angle Range ∠C–H···O** | **Number of C–H···O hydrogen bonds** |
| **2.2≥d>2.0Å** | 0 | **130≥θ>120.0** | 1 |
| **2.3≥d>2.2Å** | 3 | **140≥θ>130.0** | 4 |
| **2.4≥d>2.3Å** | 7 | **150≥θ>140.0** | 1 |
| **2.5≥d>2.4Å** | 6 | **160≥θ>150.0** | 4 |
| **2.6≥d>2.5Å** | 0 | **170≥θ>160.0** | 2 |
| **2.7≥d>2.6Å** | 0 | **180≥θ>170.0** | 3 |

Several structures displayed various types (namely Type I, Type II and quasi Type-I/Type-II) of intermolecular C–F···F–C contacts as well. It has always been debated that the C–F···F–C contacts generally symmetry driven (generally across an

inversion centre), unfavourable and hence destabilizing in nature. But, in our study, we have encountered symmetry independent type II C–F···F–C contact in the asymmetric unit of **4a-12**, where two molecules of the asymmetric unit were connected by weak C–F···F–C contact. We have observed that the weak C–F···F–C contacts were responsible for the formation of molecular dimer across the inversion point through bifurcated C–F···F–C contacts in **4a-17** (Figure 3.3.12d). It is noteworthy that the F3···F1A contact is between an ordered and disordered fluorophenyl ring, with the preferential orientation (higher occupancy, 96:6) of the disordered fluorophenyl ring (containing F1A) towards the formation of F3···F1A contact in lieu of F3···H19A hydrogen bonding. The isostructural **4a-18** also displays the same features through the formation of C–F···F–C contact between the same pair of phenyl rings; which are not disordered in this case and unequivocally accept the C–F···F–C contact. A detailed analysis of these molecules through experimental charge density measurements would elucidate the strength and nature of these weak interactions, characterized here through the distance and angle criteria.

### 3.5 Conclusion

From the above structural analysis, it may be concluded that the weak C–H···F–C hydrogen bonds in association with C–F···F–C contacts and weak C–H···O=C hydrogen bonds and other weaker interactions involving the π systems are efficient to generate various supramleccular assemblies, just like the strong hydrogen bonds, and are proficient to pack large, flexible and unsymmetrical organic molecules in a dense crystal lattice. C–H···F–C hydrogen bonds, just like strong hydrogen bonds, can form various supramolecular synthons and maintain the same synthon in different organic molecules. Therefore, the contribution of "organic fluorine" in directing and building crystalline architecture cannot be ignored.

# Chapter 4

## Intermolecular Interactions Involving C–H···F Hydrogen Bond(s) and C–H···F–C Interactions in a Series of Tetra-Fluorinated Diphenyl Tetrahydroisoquinoline Derivatives

# Chapter 4

## 4.1 Introduction

In this chapter, would discuss the structural features observed in a series of fluorinated diphenyl-tetrahydroisoquinoline derivatives based on our findings reported in the earlier chapters. Diphenyl-tetrahydroisoquinoline derivatives are known since long for their antiimplantation activity in rats reported by Nagarajan *et al*.[65] A series of compounds were synthesized, spectroscopically characterized and biological property was evaluated by Nagarajan *et al.* Based on their observation it was clear that the fluorinated molecules among all others with various substitutions showed remarkable antiimplantation activity in rats. Later, Choudhury *et al.*,[50(a)] reported the structural analysis of some of the compounds synthesized by Nagarajan *et al.* Their initial reports indicated that the fluorine mediated weak intermolecular interactions were responsible for their crystal packing and they emphasized that the interaction involving fluorine might be responsible for the biological activity of the folurinated diphenyl tetrahydroisoquinoline. Later Choudhury and Guru Row reported structural analysis of few more novel molecules belonging to the same molecular skeleton with two fluorine substitutions on two different phenyl rings and showed that the incorporation of second fluorine atom in the molecule resulted into a wider range of structural variations and several fluorine mediated supramolecular synthons were evident.[50(b,d)] A competition between C–H···F hydrogen bond and weak C–F···F–C interactions resulted into the static disorder in two compounds among fifteen mono/difluorinated diphenyl tetrahydroisoquinolines reported by Choudhury and Guru Row.[50(b,d)] These observations led us to investigate the structural features, that may result due to a variety of fluorine mediated interactions, of a series of tetrafluorinated diphenyl tetrahydroisoquinoline derivatives (Compounds 6c, Scheme 4.1), where we intend to incorporate two fluorine atoms in each of the two phenyl rings of the mother compound.

## 4.2 Experimental

### 4.2.1 Synthesis and Characterization:

The synthesis of compound **6c** was carried out in two steps starting with **4a** following the reaction scheme 4.1.

**Synthesis of 5b:** In 100 ml dry round bottom flask, substituted secondary amide (**4a**) (1.0 equiv), 0.1 ml conc. HCl and $POCl_3$ were added and the reaction mixture was refluxed for 4 hrs by using of anhydrous calcium chloride as a guard tube fitted in the condenser. After the completion of the reaction, excess $POCl_3$ was removed completely by high vacuum fitted with liquid nitrogen trap. The solid crude product was a chloride salt (**5b**) which was dark brown in colour. Then this solid salt was directly used for the next step, without any further purification.

**Synthesis of 6c:** Dry methanol and $NaBH_4$ (2.2 equiv) were added the flask containing the chloride salt **5c**. Then reaction mixture was refluxed for 2 hrs. Then the reaction mixture was cooled to 0 $^oC$ and water was added to decompose the excess $NaBH_4$. The product (**6c**) was precipitated, filtered and dried. The crude product was purified by column chromatography using basic alumina as the stationary phase and 2-3% ethyl acetate in hexane as the mobile phase. Most of the products were found to be solid upon purification, but some of them were dense liquid at the room temperature. All the products (**6c**) were characterized by $^1H$, $^{13}C$ and $^{19}F$ NMR, differential scanning calorimetry (DSC), PXRD and FTIR spectroscopy. Representative spectra are provided in the figures below and all the spectrum are enclosed in the ESI.

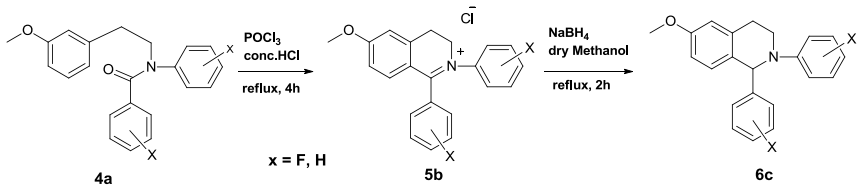


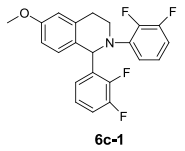
6c-1

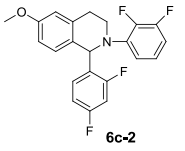
6c-2

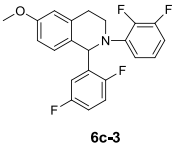
6c-3

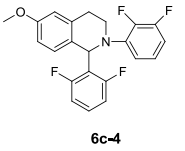
6c-4

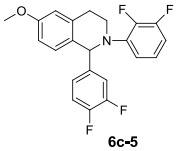
6c-5

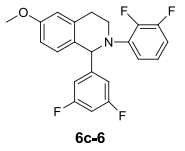
6c-6

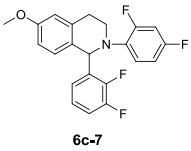
6c-7

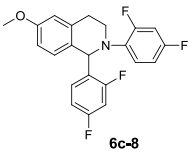
6c-8

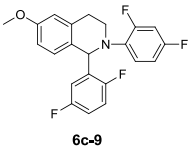
6c-9

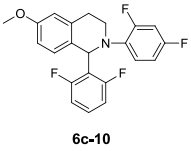
6c-10

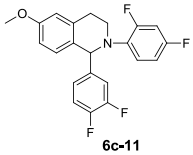
6c-11

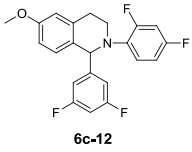
6c-12

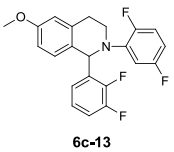
6c-13

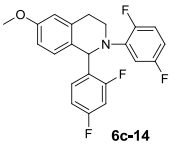
6c-14

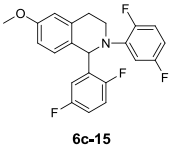
6c-15

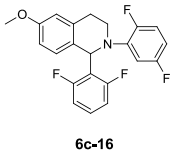
6c-16

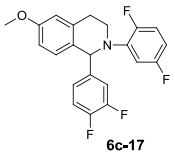
6c-17

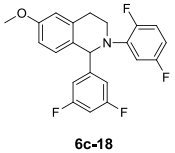
6c-18

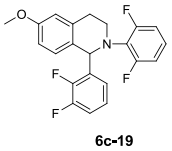
6c-19

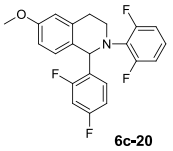
6c-20

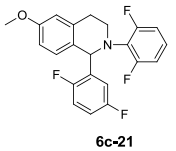
6c-21

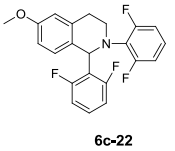
6c-22

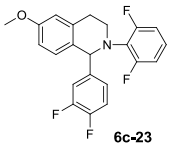
6c-23

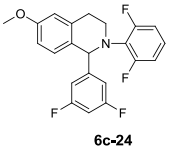
6c-24

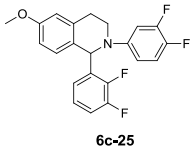
6c-25

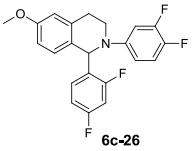
6c-26

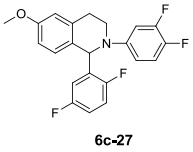
6c-27

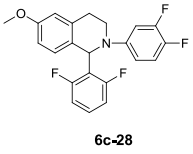
6c-28

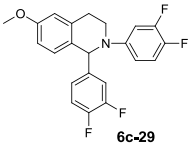
6c-29

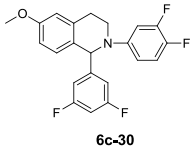
6c-30

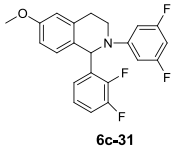
6c-31

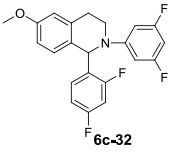
6c-32

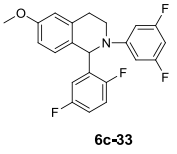
6c-33

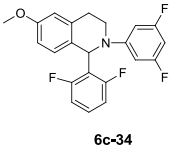
6c-34

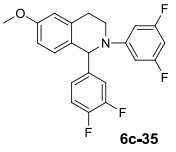
6c-35

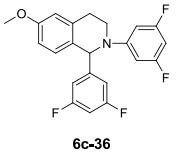
6c-36

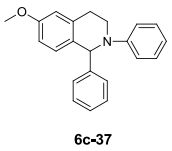
6c-37

**Scheme 4.1**

## NMR

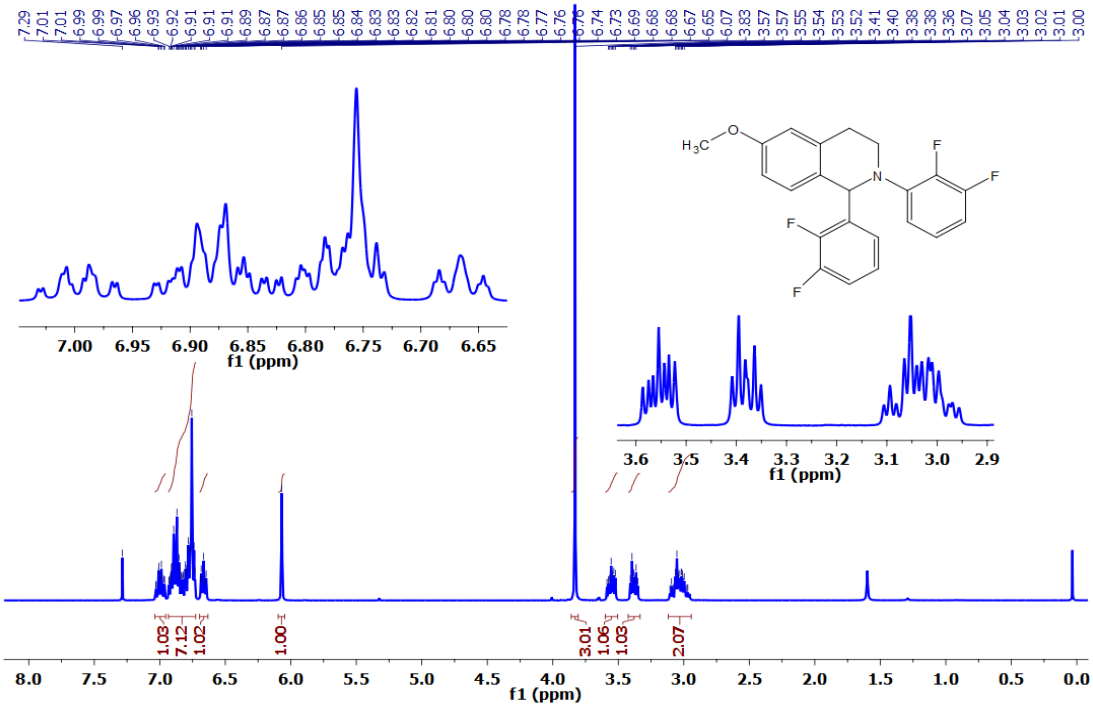

**$^{1}$H - NMR Spectra of 6c-1, (400 MHz, $CDCl_3$) : δ (ppm)** = 2.97 – 3.11 (m, 2H), 3.35 – 3.41 (m, 1H), 3.52-3.59 (m, 1H), 3.01 (s, 3H), 6.07 (d, 1H), 6.65-6.69 (m, 1H), 6.73-6.93 (m, 7H), 6.96-7.03 (m, 1H).

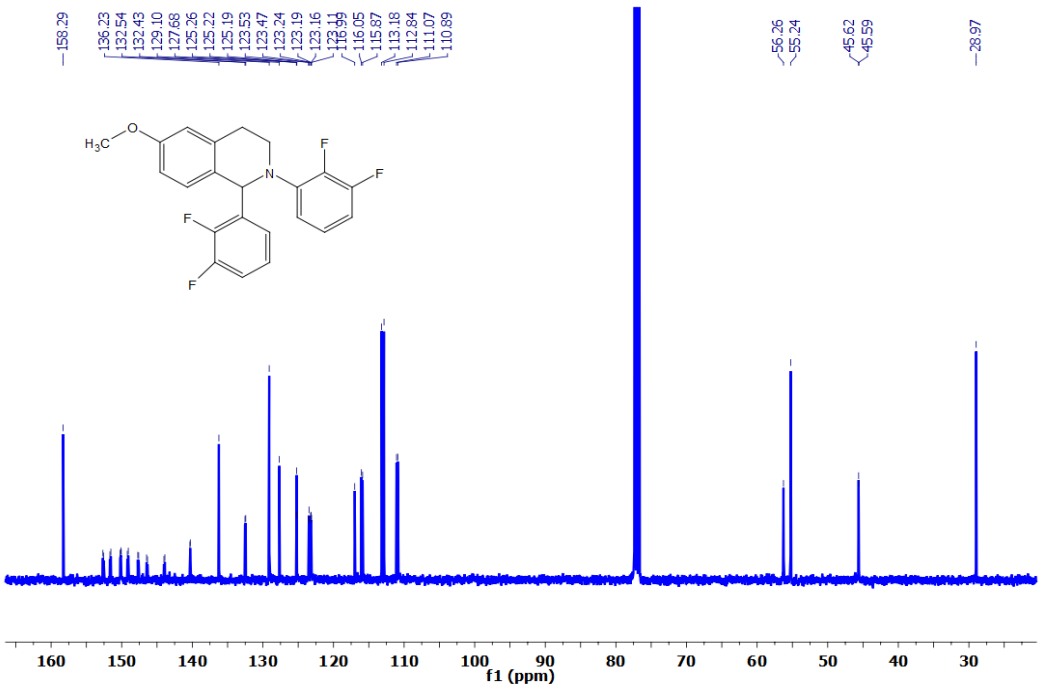

**$^{13}$C spectra of 6c-1, (125 MHz, $CDCl_3$): δ (ppm)** = 140.35, 140.30, 140.28, 136.23, 132.55, 132.44, 129.12, 127.69, 125.27, 125.24, 125.21, 123.55, 123.50, 123.48, 123.44, 123.25, 123.20, 123.17, 123.12, 117.00, 116.06, 115.89, 113.19, 112.86, 111.08, 110.90, 56.27, 55.24, 45.62, 45.59, 28.978

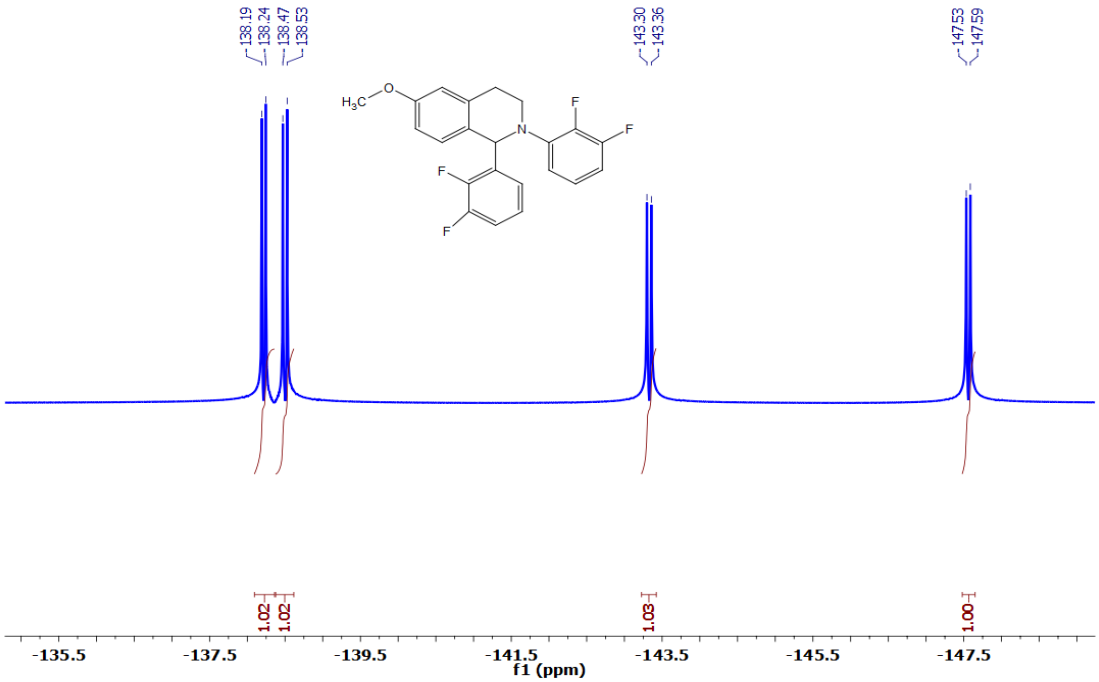


**$^{19}$F- NMR Spectra of 6c-1, (376 MHz, $CDCl_3$): δ (ppm)** = -147.56 (d,1F), -143.33 (d, 1F), -138.50 (d, 1F), -138.22 (d, 1F).

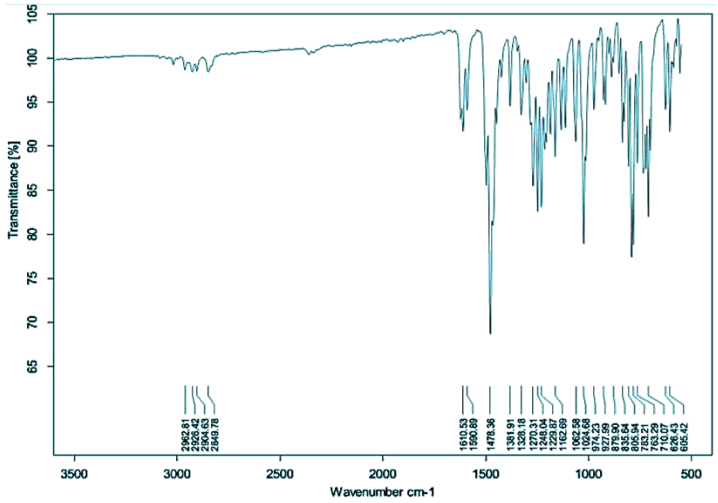


FT-IR spectra of **6c-1**

### 4.2.2 Structural Study:

All the crystal structures were determined using the same diffractometer and the same procedure reported in the Chapter 2 and Chapter 3. Only one crystal structure was found to have disorder in the orientation of the fluorinated phenyl rings by the rotation of the fluorophenyl ring about the C–C bond. This disorder was modelled using the methodology described below. The crystallographic data including the details of data collection, structure solution and refinement are listed in the Table 4.1-4.4. The phenyl ring attached to the N atoms is termed as the "A ring", the phenyl

ring connected to the C=O group is termed as the “B ring” and the 3rd phenyl ring containing the –OMe groups is termed as the “C ring” in the structural descriptions in this chapter (Scheme 4.2).

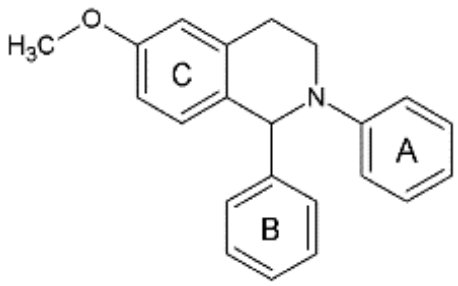


**Scheme 4.2**

**Crystallographic Modelling of Disorder**

All the data sets were recorded at 100K. Only one compound (**6c-23**) was found to be disordered. The positional disorder has been found due 180° rotation of phenyl ring (B ring) around C–C bonds in the molecule. The ratio of the occupancy of fluorophenyl ring B is 0.6557**:** 0.3443. This disorder was modelled using the same methodology which is already described in the previous chapter 3.

**Table 4.2.2.1: Single crystal X-ray diffraction data of 6c-1 to 6c-6**

| Identification code | 6c-1 | 6c-2 | 6c-3 | 6c-4 | 6c-5 | 6c-6 |
|---|---|---|---|---|---|---|
| CCDC No | 1540717 | 1540721 | 1540725 | 1540731 | 1540732 | 1540733 |
| Formula | $C_{22}H_{17}F_4NO$ | $C_{22}H_{17}F_4NO$ | $C_{22}H_{17}F_4NO$ | $C_{22}H_{17}F_4NO$ | $C_{22}H_{17}F_4NO$ | $C_{22}H_{17}F_4NO$ |
| Formula weight | 387.37 | 387.37 | 387.37 | 387.37 | 387.37 | 387.37 |
| Temperature (K) | 100.0 | 100.0 | 100.0 | 100.0 | 100.0 | 100.0 |
| Crystal system | Monoclinic | Monoclinic | Monoclinic | Monoclinic | Monoclinic | Monoclinic |
| Space group | $P2_1$ | $P2_1/c$ | $P2_1/c$ | $P2_1$ | $P2_1/c$ | $C2/c$ |
| a (Å) | 8.210(4) | 9.705(3) | 9.642(2) | 8.317(3) | 13.3660(13) | 22.323(8) |
| b (Å) | 6.330(2) | 13.476(3) | 13.292(2) | 6.0774(19) | 11.6008(10) | 13.499(5) |
| c (Å) | 17.277(9) | 13.843(4) | 13.931(3) | 17.513(6) | 30.052(3) | 11.828(5) |
| α (°) | 90 | 90 | 90 | 90 | 90 | 90 |
| β (°) | 102.410(19) | 101.162(11) | 99.890(9) | 103.095(13) | 130.787(3) | 98.459(17) |
| γ (°) | 90 | 90 | 90 | 90 | 90 | 90 |
| V (Å$^3$) | 876.9(7) | 1776.3(8) | 1758.9(6) | 862.2(5) | 3528.1(6) | 3526(2) |
| Z | 2 | 4 | 4 | 2 | 8 | 8 |
| Z' | 1 | 1 | 1 | 1 | 2 | 1 |
| $\rho_{calc}$ (g cm$^{-3}$) | 1.467 | 1.449 | 1.463 | 1.492 | 1.459 | 1.460 |
| μ/ mm$^{-1}$ | 0.119 | 0.117 | 0.119 | 0.121 | 0.118 | 0.118 |
| 2$\theta$ (°) ranges for data collection | 6.08 - 55.01 | 6.00 - 55.00 | 6.14 - 50.04 | 6.10 - 55.02 | 6.32 - 50.05 | 6.04 - 54.94 |
| F(000) | 400 | 800 | 800 | 400 | 1600 | 1600 |
| Index ranges | -10, 10; -8, 8; -22, 22 | -12, 12; -17, 17; -16, 17 | -11, 11; -15, 15; -16, 16 | -10, 10; -7, 7; -22 ,22 | -15, 15; -13, 12; -35, 35 | -28, 28; -17, 17; -15, 13 |
| No. of reflections collected | 9368 | 11924 | 14416 | 8616 | 18749 | 10335 |
| $R_{int}$ | 0.0433 | 0.0575 | 0.0290 | 0.0828 | 0.0396 | 0.0774 |
| No. of unique reflections | 4001 | 4040 | 3089 | 3898 | 6207 | 4010 |
| $R_1$ [I > 2σ(I)] | 0.0513 | 0.0485 | 0.0372 | 0.0449 | 0.406 | 0.0572 |
| $wR_2$ (all data) | 0.1440 | 0.1280 | 0.1063 | 0.1220 | 0.1052 | 0.1392 |
| GooF | 1.125 | 1.066 | 1.110 | 1.052 | 1.051 | 0.955 |
| Largest diff. Peak/Hole/e Å$^{-3}$ | 0.40, -0.27 | 0.30, -0.22 | 0.27, -0.24 | 0.41, -0.29 | 0.22, -0.22 | 0.28, -0.31 |

**Table: 4.2.2.2: Single crystal X-ray diffraction data of 6c-7 to 6c-16**

| Identification code | 6c-7 | 6c-8 | 6c-9 | 6c-13 | 6c-16 |
|---|---|---|---|---|---|
| CCDC No | 1540734 | 1540735 | 1540736 | 1540718 | 1540719 |
| Formula | $C_{22}H_{17}F_4NO$ | $C_{22}H_{17}F_4NO$ | $C_{22}H_{17}F_4NO$ | $C_{22}H_{17}F_4NO$ | $C_{22}H_{17}F_4NO$ |
| Formula weight | 387.37 | 387.37 | 387.37 | 387.37 | 387.37 |
| Temperature (K) | 100.0 | 100.0 | 100.0 | 100.0 | 100.0 |
| Crystal system | Monoclinic | Orthorhombic | Monoclinic | Monoclinic | Monoclinic |
| Space group | *C*2/*c* | *Pca*2$_1$ | *P*2$_1$/*c* | *C*2/*c* | *Pc* |
| a (Å) | 36.448(11) | 16.559(2) | 9.445(6) | 36.079(4) | 17.468(3) |
| b (Å) | 6.1171(18) | 17.595(2) | 21.293(11) | 6.2372(6) | 6.2025(10) |
| c (Å) | 16.087(4) | 6.1048(9) | 9.590(6) | 16.051(2) | 16.338(3) |
| α (°) | 90 | 90 | 90 | 90 | 90 |
| β (°) | 102.193(7) | 90 | 112.96(2) | 104.627(6) | 92.208(9) |
| γ (°) | 90 | 90 | 90 | 90 | 90 |
| V (Å$^3$) | 3505.8(17) | 1778.7(4) | 1775.9(18) | 3495.0(7) | 1768.9(5) |
| Z | 8 | 4 | 4 | 8 | 4 |
| Z' | 1 | 1 | 1 | 1 | 2 |
| $\rho_{calc}$ (g cm$^{-3}$) | 1.468 | 1.446 | 1.449 | 1.472 | 1.455 |
| μ/ mm$^{-1}$ | 0.119 | 0.117 | 0.118 | 0.119 | 0.118 |
| F(000) | 1600 | 800 | 800 | 1600 | 800 |
| 2$\theta$ (°) ranges for data collection | 6.09 - 54.91 | 6.76 - 54.97 | 6.05 - 50.05 | 6.08 - 54.99 | 6.57 - 50.05 |
| Index ranges | -46, 46; -7, 7; -20, 20 | -21, 20; -22, 22; -7, 7 | -11, 11; -25, 25; -11, 10 | -45, 46; -8, 8; -20, 20 | -20, 20; -7, 7; -15, 19 |
| Total reflections | 11505 | 15664 | 9543 | 11954 | 9932 |
| $R_{int}$ | 0.0596 | 0.0411 | 0.0617 | 0.0765 | 0.0468 |
| No. of unique reflections | 3977 | 4061 | 3113 | 3975 | 5388 |
| $R_1$ [I > 2σ(I)] | 0.0524 | 0.0438 | 0.0717 | 0.0431 | 0.1040 |
| $wR_2$ (all data) | 0.1454 | 0.1058 | 0.2162 | 0.1145 | 0.2353 |
| GooF | 1.048 | 1.073 | 1.080 | 1.045 | 1.042 |
| Largest diff. Peak/Hole/e Å$^{-3}$ | 0.34, -0.24 | 0.27, -0.22 | 0.60, -0.36 | 0.25, -0.27 | 1.08, -0.34 |

**Table: 4.2.2.3: Single crystal X-ray diffraction data of 6c-19 to 6c-30**

| Identification code | 6c-19 | 6c-21 | 6c-23 | 6c-25 | 6c-30 |
|---|---|---|---|---|---|
| CCDC No | 1540720 | 1540722 | 1540723 | 1540724 | 1540726 |
| Formula | $C_{22}H_{17}F_4NO$ | $C_{22}H_{17}F_4NO$ | $C_{22}H_{17}F_4NO$ | $C_{22}H_{17}F_4NO$ | $C_{22}H_{17}F_4NO$ |
| Formula weight | 387.37 | 387.37 | 387.37 | 387.37 | 387.36 |
| Temperature (K) | 100.0 | 100.0 | 100.0 | 100.0 | 100.0 |
| Crystal system | Monoclinic | Monoclinic | Orthorhombic | Monoclinic | Monoclinic |
| Space group | $P2_1/c$ | $Pn$ | $Pbca$ | $P2_1/c$ | $P2_1/c$ |
| a (Å) | 18.194(6) | 7.6714(11) | 16.643(3) | 12.287(2) | 12.947(3) |
| b (Å) | 6.147(2) | 7.1287(9) | 6.1042(10) | 11.3169(16) | 10.4113(18) |
| c (Å) | 16.182(5) | 16.428(2) | 35.217(7) | 22.191(4) | 22.590(5) |
| α (°) | 90 | 90 | 90 | 90 | 90 |
| β (°) | 104.903(11) | 100.298(6) | 90 | 145.954(6) | 145.306(10) |
| γ (°) | 90 | 90 | 90 | 90 | 90 |
| V (Å$^3$) | 1749.0(10) | 883.9(2) | 3577.8(11) | 1727.5(5) | 1733.2(7) |
| Z | 4 | 2 | 8 | 4 | 4 |
| Z' | 1 | 1 | 1 | 1 | 1 |
| $\rho_{calc}$ (g cm$^{-3}$) | 1.471 | 1.455 | 1.438 | 1.489 | 1.484 |
| μ/ mm$^{-1}$ | 0.119 | 0.118 | 0.117 | 0.121 | 0.120 |
| F(000) | 800 | 400 | 1600 | 800 | 800 |
| 2$\theta$ (°) ranges for data collection | 6.22 - 55.05 | 6.25 - 50.05 | 6.74 - 55.00 | 6.56 - 50.04 | 6.34 - 54.97 |
| Index ranges | -23, 23; -6, 7; -20, 21 | -9, 9; -8; 8; -19; 19 | -19, 21; -7, 7; -45, 45 | -12, 14; -13, 13; -26, 26 | -16, 16; -13, 13; -29, 29 |
| Total reflections | 11916 | 4823 | 22278 | 9203 | 18101 |
| $R_{int}$ | 0.0662 | 0.0340 | 0.1343 | 0.0293 | 0.0272 |
| No. of unique reflections | 3963 | 2621 | 4056 | 3048 | 3967 |
| $R_1$ [I > 2σ(I)] | 0.0658 | 0.0386 | 0.0935 | 0.0402 | 0.0404 |
| $wR_2$(all data) | 0.1916 | 0.0949 | 0.2660 | 0.1060 | 0.1141 |
| GooF | 1.072 | 1.098 | 1.140 | 1.048 | 1.053 |
| Largest diff. Peak/Hole/e Å$^{-3}$ | 0.38, -0.38 | 0.19, -0.18 | 0.52/-0.30 | 0.25, -0.26 | 0.31, -0.24 |

**Table 4.2.2.4: Single crystal X-ray diffraction data of 6c-31 to 6c-37**

| Identification code | 6c-31 | 6c-33 | 6c-34 | 6c-37 |
|---|---|---|---|---|
| CCDC No | 1540727 | 1540728 | 1540729 | 1540730 |
| Formula | $C_{22}H_{17}F_4NO$ | $C_{22}H_{17}F_4NO$ | $C_{22}H_{17}F_4NO$ | $C_{22}H_{21}NO$ |
| Formula weight | 387.38 | 387.38 | 387.38 | 315.40 |
| Temperature (K) | 100.0 | 100.0 | 100.0 | 100.0 |
| Crystal system | Triclinic | Triclinic | Monoclinic | Monoclinic |
| Space group | $P\ \bar{1}$ | $P\ \bar{1}$ | $P2_1/c$ | *Pbca* |
| a (Å) | 11.13700(10) | 10.6975(7) | 11.322(2) | 10.3744(14) |
| b (Å) | 11.8983(2) | 13.2186(4) | 12.437(2) | 16.379(2) |
| c (Å) | 15.127 | 13.6339(2) | 20.012(3) | 19.851(3) |
| α (°) | 73.675(12) | 68.667(14) | 90 | 90 |
| β (°) | 71.730(13) | 80.428(18) | 140.922(8) | 90 |
| γ (°) | 72.936(11) | 81.09(2) | 90 | 90 |
| V (Å$^3$) | 1779.8(2) | 1761.4(2) | 1776.3(5) | 3373.2(8) |
| Z | 4 | 4 | 4 | 8 |
| Z' | 2 | 2 | 1 | 1 |
| $\rho_{calc}$ (g cm$^{-3}$) | 1.446 | 1.461 | 1.448 | 1.242 |
| μ/ mm$^{-1}$ | 0.117 | 0.118 | 0.117 | 0.075 |
| F(000) | 800 | 800 | 800 | 1344 |
| 2$\theta$ (°) ranges for data collection | 6.14 - 54.99 | 6.16 - 55.01 | 6.46 - 55.04 | 4.10 - 50.36 |
| Index ranges | -14, 14; -15, 15; -19, 19 | -13, 13; -17, 17; -17, 17 | -14, 14; -16, 16; -25, 25 | -11, 12; -19, 19; -23, 23 |
| Total reflections | 18292 | 18147 | 17876 | 16968 |
| $R_{int}$ | 0.0264 | 0.0276 | 0.0480 | 0.0415 |
| No. of unique reflections | 8136 | 8043 | 4065 | 3014 |
| $R_1$ [I > 2σ(I)] | 0.0427 | 0.0407 | 0.0549 | 0.0359 |
| $wR_2$(all data) | 0.1186 | 0.1070 | 0.1459 | 0.0891 |
| GooF | 1.047 | 1.045 | 1.076 | 1.017 |
| Largest diff. Peak/Hole/e Å$^{-3}$ | 0.29, -0.23 | 0.29, -0.23 | 0.44, -0.27 | 0.18, -0.19 |

### 4.3: Results:

### *N*-(2,3-difluorophenyl)-1-(2,3-difluorophenyl)-6-methoxy-1,2,3,4-tetrahydroisoquinoline(6c-1) and *N*-(2,3-difluorophenyl)-1-(2,6-difluorophenyl)-6-methoxy-1,2,3,4-tetrahydroisoquinoline(6c-4):

The compounds **6c-1** (Figure 4.3.1a) and **6c-4** (Figure 4.3.2a) are found to be isostructural with the unit cell similarity index $\pi$ = 0.0028 and were crystallised in monoclinic chiral $P2_1$ space group with Z = 2 and Z' =1. None of the compounds in this series have any N–H bond like the molecules reported in chapter 2. Therefore, there is no possibility of formation of strong hydrogen bonds in the crystal lattice. Only weak hydrogen bonds like C–H···F, C–H···O, and C–H···π interactions are possible in crystal packing of these molecules. In both the compounds **6c-1** and **6c-4**, the *o*-F (F1) of the A ring participates in the C2–H2A···F1 hydrogen bond by the utilization of translational symmetry and generates a long one-dimensional chain parallel to the *b*-axis (Figure 4.3.1b and 4.3.2b) (Table 4.3.1 and 4.3.2). The F2 atoms on the A ring do not offer any interactions in both the compounds. In both the compounds, the Fluorine F3 on the B ring and F1, are simultaneously involved in weak C14–H14···F3 and C2–H2A···F1 hydrogen bonds and creates tetramer and trimer unit by $2_1$ symmetry operation (Figure 4.3.1c and 4.3.2c). Screw ($2_1$) symmetry related methoxy oxygens are also involved in weak C7–H7···O1 hydrogen bond with the support of C2–H2A···F1 hydrogen bonds (Figure 4.3.1d and 4.3.2d). In this isostructural compounds, *p*-hydrogen (H20) of the B ring makes C20–H20···π($C_{gA}$) interaction, which further stabilizes the crystal packing (Figure 4.3.1e and 4.3.2e). It is noteworthy that one of these hydrogen bonds (C2–H2A···F1) involves hydrogen atom attached to a $sp^3$ hybridized carbon. The experimental PXRD patterns of **6c-1** and **6c-4** are matching with the corresponding simulated PXRD patterns (Figure 4.3.1f and 4.3.2f)

**Table 4.3.1: Intermolecular interactions in 6c-1**

| D–B···A | D–B/Å | *D*(D···A )/ Å | *d*(B···A )/Å | ∠D–B···A/º | SYMMETRY |
|---|---|---|---|---|---|
| **C2–H2B···F1** | 1.080 | 3.006(4) | 2.22 | 128 | x, y-1, z |
| **C14–H14···F3** | 1.080 | 3.374(4) | 2.65 | 124 | 1-x, y-½, -z |
| **C7–H7···O1** | 1.080 | 3.456(5) | 2.56 | 140 | 2-x, +y, 1-z |
| **C20–H20···π ($C_{gA}$)** | 1.080 | 3.490(4) | 2.76 | 134 | 1+x, y, z |

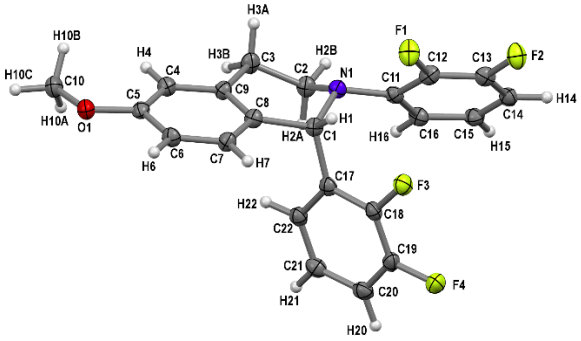


**(a)**

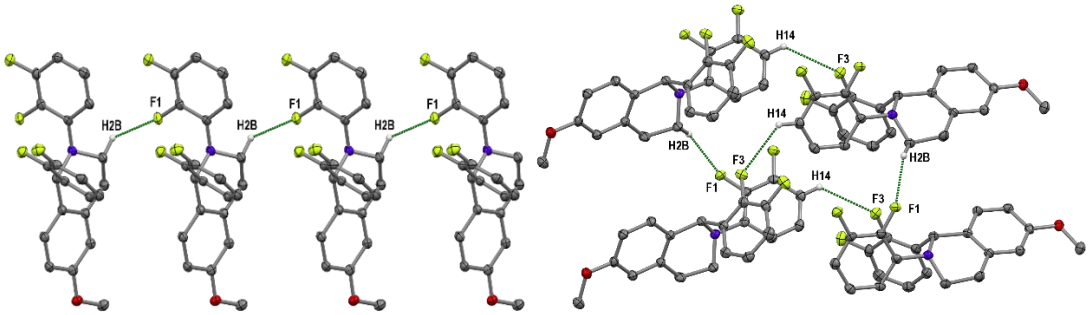


**(b)** **(c)**

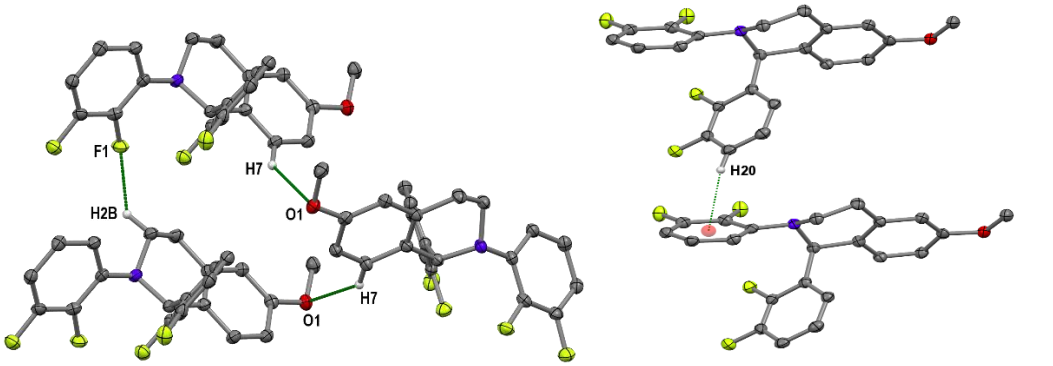


**(d)** **(e)**

**Figure 4.3.1: (a)** ORTEP of **6c-1** drawn with 50% ellipsoidal probability. **(b)** C2-H2B···F1 hydrogen bond generating a 1D catameric chain like structure along the crystallographic *b*-axis. (c) C2-H2B···F1 and C14–H14···F3 hydrogen bonds are generating a tetramer unit by $2_1$ symmetry. **(d)** A trimer formation offering by methoxy oxygen as a weak C7–H7···O1 hydrogen bond by the supporting of C2-H2B···F1 hydrogen bond. **(e)** A C20–H20···π($C_{gA}$) interactions.

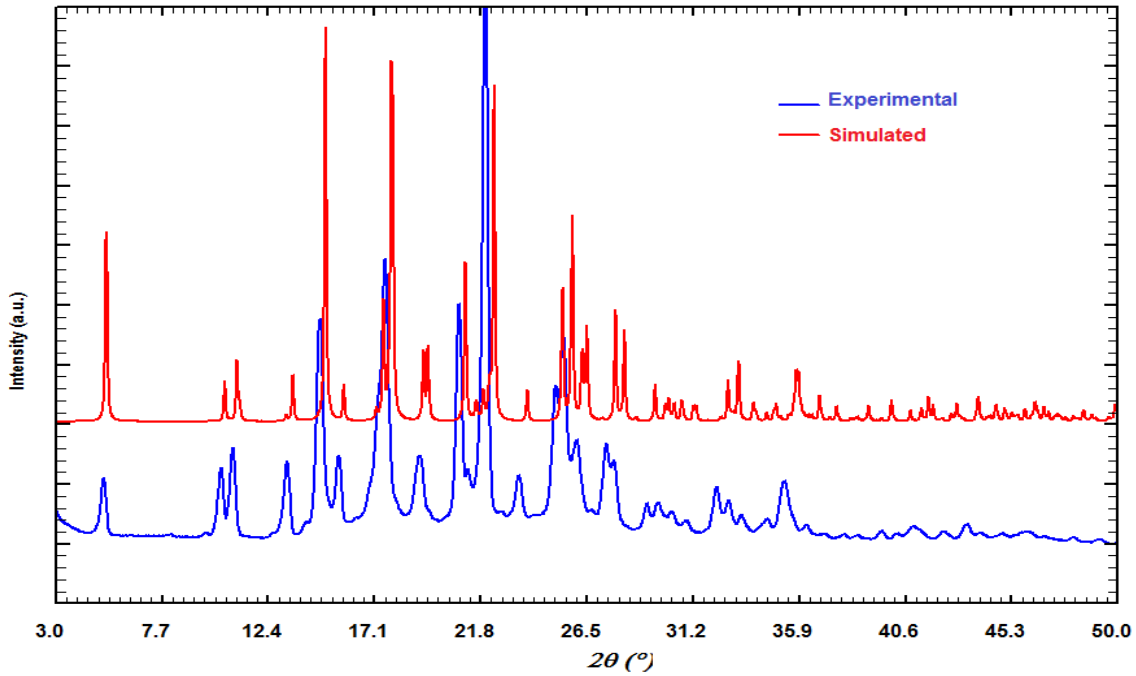


**Figure 4.3.1: (f)** Comparison of experimental and simulated PXRD patterns of **6c-1**

**Table 4.3.2: Intermolecular interactions in 6c-4**

| D–B···A | D–B/Å | *D*(D···A )/Å | *d*(B···A )/Å | ∠D–B···A/º | SYMMETRY |
|---|---|---|---|---|---|
| **C2–H2A···F1** | 1.080 | 3.001(3) | 2.15 | 134 | x, y+1, z |
| **C14–H14···F3** | 1.080 | 3.354(3) | 2.67 | 121 | 1-x, y+½, 2-z |
| **C15–H15···F3** | 1.080 | 3.358(3) | 2.65 | 122 | 1-x, ½+y, 2-z |
| **C7–H7···F4** | 1.080 | 3.657(3) | 2.64 | 157 | x, y-1, z |
| **C7–H7···O1** | 1.080 | 3.490(3) | 2.67 | 133 | -x, y-½, 1-z |
| **C20–H20···π ($C_{gA}$)** | 1.080 | 3.533(3) | 2.79 | 136 | 1+x, y, z |

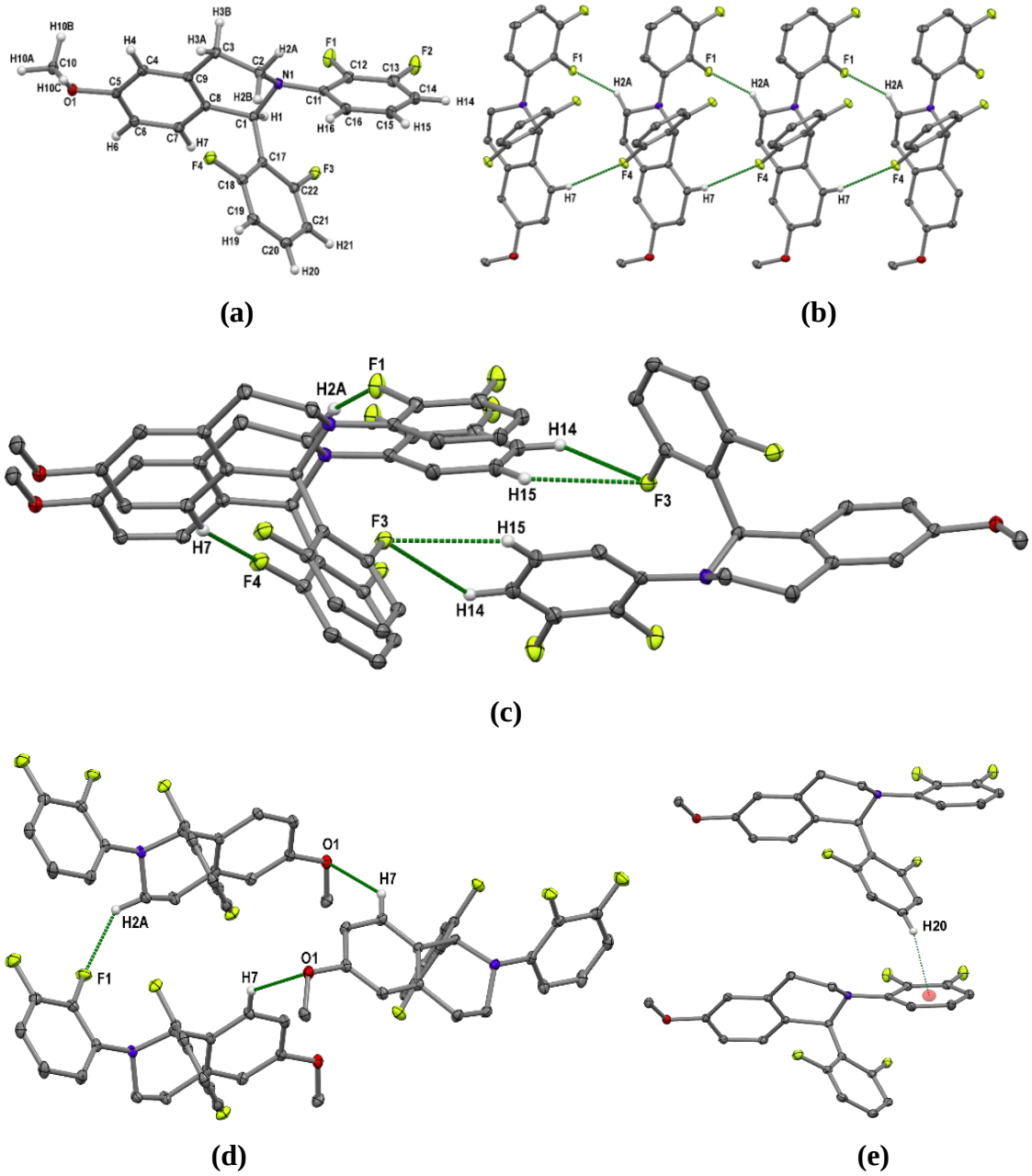


**Figure 4.3.2: (a)** ORTEP of **6c-4** drawn with 50% ellipsoidal probability. **(b)** Two parallel weak C2-H2B···F1 and C7-H7···F4 hydrogen bond generating a 1D catameric chain like structure along the crystallographic *b*-axis. **(c)**All the three fluorine (F1, F3 and F4) are involved in weak C-H···F hydrogen bonds and generating a trimer unit by $2_1$ symmetry. F3 act as a bifurcated acceptor. **(d)** A trimer formation offering by methoxy oxygen as a weak C7–H7···O1 hydrogen bond by the supporting of C2-H2B···F1 hydrogen bond. **(e)** Chain through C20–H20···π($C_{gA}$) interactions.

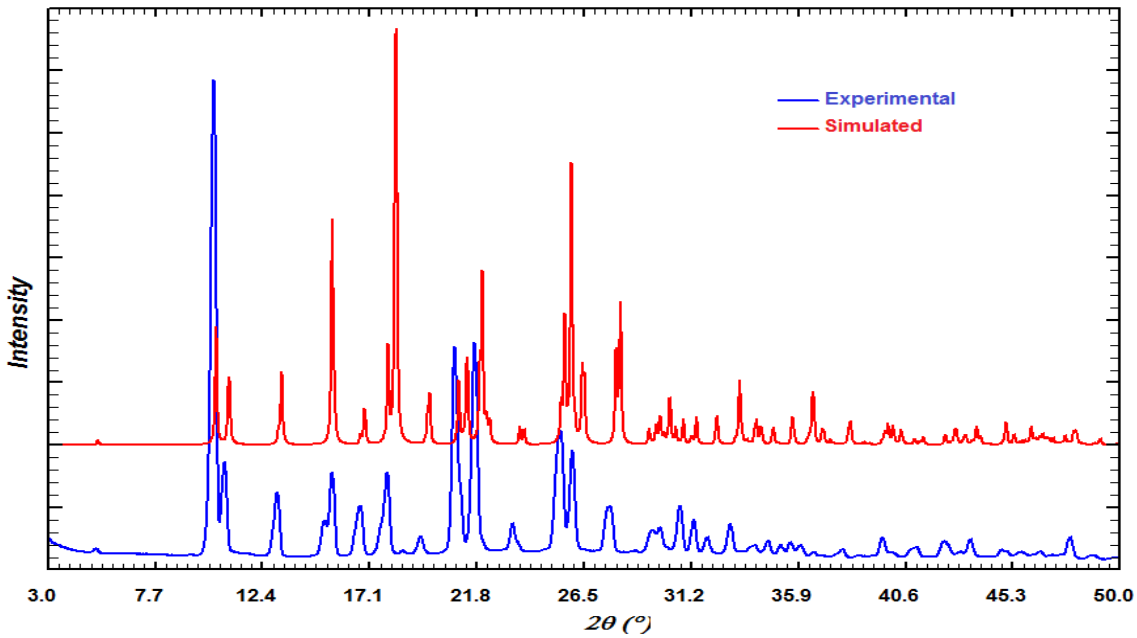


**Figure 4.3.2: (f)** Comparison of experimental and simulated PXRD patterns of **6c-4**

***N*-(2,3-difluorophenyl)-1-(2,4-difluorophenyl)-6-methoxy-1,2,3,4-tetrahydroisoquinoline (6c-2) and *N*-(2,3-difluorophenyl)-1-(2,5-difluorophenyl)-6-methoxy-1,2,3,4-tetrahydroisoquinoline (6c-3):**

The crystal structure of **6c-2** (Figure 4.3.3a) and **6c-3** (Figure 4.3.4a) are found to be isostructural with unit cell similarity index $\pi$ = 0.0043. Both the compounds are crystallised in centrosymmetric monoclinic $P2_1/c$ space group with Z = 4 and Z' = 1 (Figure 4.3.3a and 4.3.4a). In both the compounds, (F1) of the A ring and H6 of the C ring involved in the weak C6–H6···F1 hydrogen bond, which leads to the formation of the cyclic dimer *via* the inversion center (Figure 4.1.3b and 4.1.4b) (Table 4.3.3 and 4.4.4). In the molecule **6c-2**, F4 of the B ring and H21 involved in the formation of the homo dimer synthon by the inversion center and this dimer is further interconnected with another dimer involving a pair of C–H···F hydrogen bonds involving H3A and F2 (Figure 4.3.3c). Whereas, in the crystal structure of **6c-3**, F2 and H3A take part in the formation of hydrogen bond by one unit translational symmetry along the *a*-axis (Figure 4.3.4c). Similarly, C–H···F hydrogen bonds are found to form a linear 1D chain along *y*-axis involving H2 and F3 in both the compounds (Figure 4.3.3d and 4.3.4d). The methoxy oxygen in both are also involved in C14–H14···O1 hydrogen bonds forming a 1D chain in the crystal packing (Figure 4.3.3e and 4.3.4e). Along with these C–H···F and C–H···O hydrogen bonds, the $\pi$ cloud of C ring interacts with the H16 hydrogen leading to

the C16–H16···π($C_{gC}$) interaction in the crystal structure (Figure 4.3.3f and 4.3.4f). The experimental PXRD patterns of **6c-2** and **6c-3** are matching with the corresponding simulated PXRD patterns (Figure 4.3.1f and 4.3.4f)

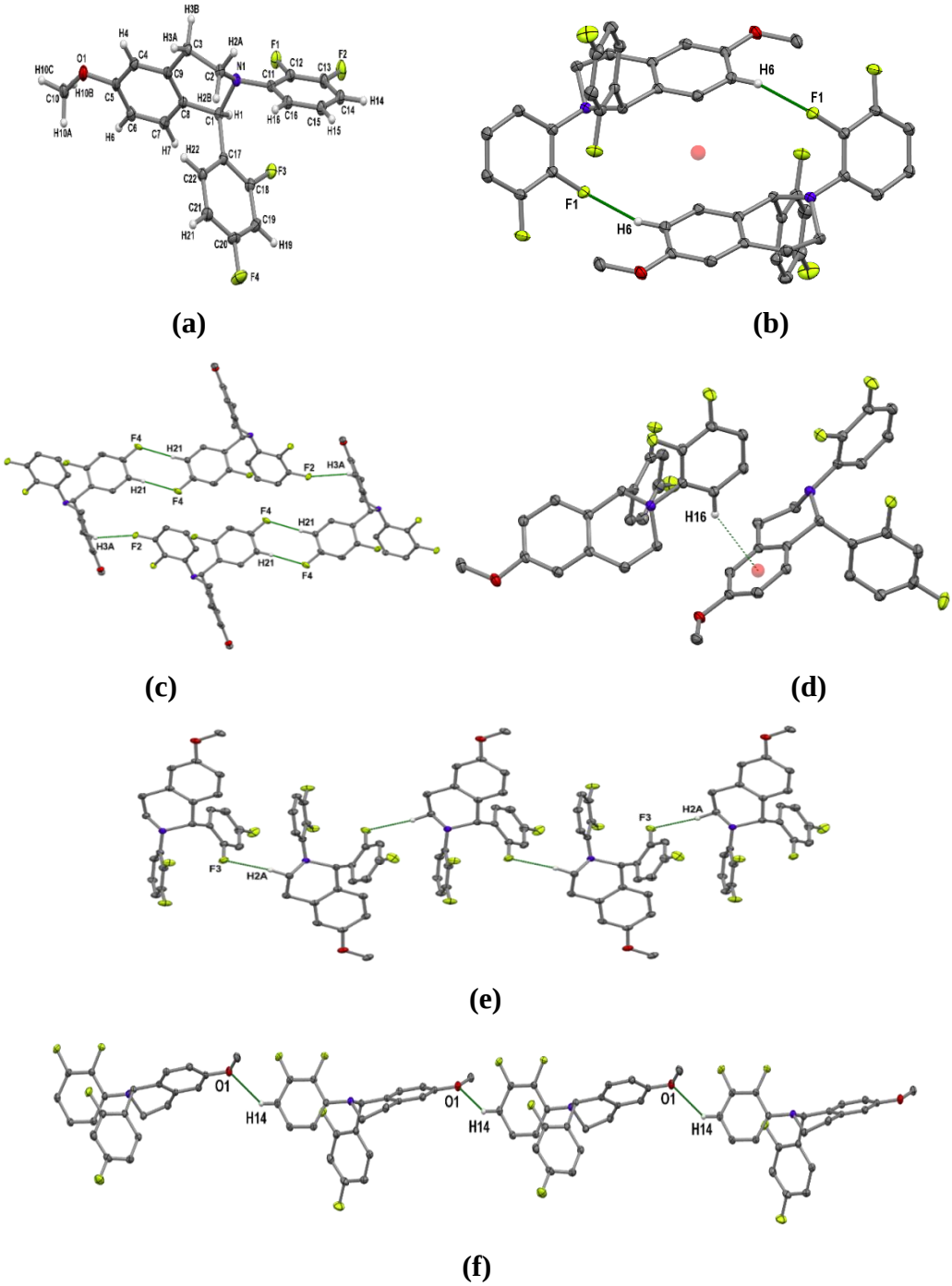


**Figure 4.3.3: (a)** ORTEP of **6c-2** drawn with 50% ellipsoidal probability. **(b)** An inversion center related cyclic dimer synthon by the utilization of C6–H6···F1 hydrogen bond. **(c)** A tetramer unit formation by the combination of C21–H21···F4 and C3–H3A···F2 hydrogen bonds. **(d)** One dimensional linear chain of weak C2–H2A···F3 hydrogen bond. **(e)** A C14–H14···O1 hydrogen bond as a linear 1D

chain in the crystal packing. **(f)** The C16–H16···π($C_{gC}$) interaction in the crystal structure

**Table 4.3.3: Intermolecular interactions in 6c-2**

| D–B···A | D–B/Å | *D*(D···A )/ Å | *d*(B···A )/Å | ∠D–B···A/º | SYMMETRY |
|---|---|---|---|---|---|
| **C6–H6···F1** | 1.080 | 3.500(2) | 2.49 | 155 | -x, 2-y, 1-z |
| **C3–H3A···F2** | 1.080 | 3.337(2) | 2.62 | 123 | x-1, y, z |
| **C2–H2A···F3** | 1.080 | 3.279(2) | 2.28 | 153 | -x, y-½, ½-z |
| **C21–H21···F4** | 1.080 | 3.450(2) | 2.41 | 162 | -x-1, 2-y, -z |
| **C14–H14···O1** | 1.080 | 3.393(2) | 2.59 | 131 | x+1, $^{3}/_{2}$-y, z-½ |
| **C16–H16···π ($C_{gc}$)** | 1.080 | 3.540(2) | 2.71 | 146 | x, ½-y, ½+z |

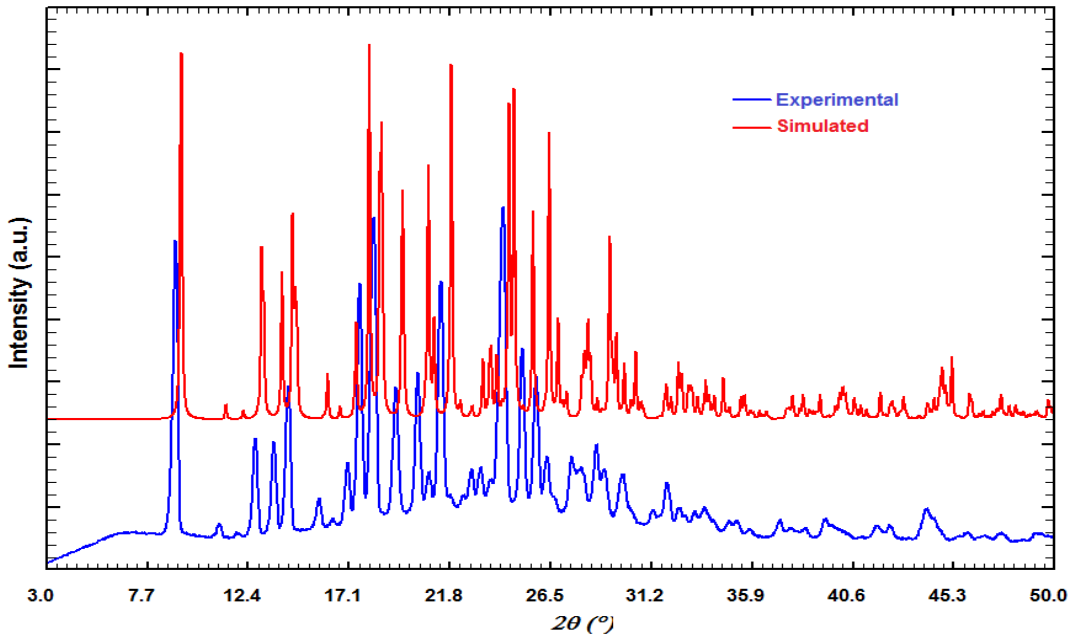


**Figure 4.3.3: (g)** Comparison of experimental and simulated PXRD patterns of **6c-2**

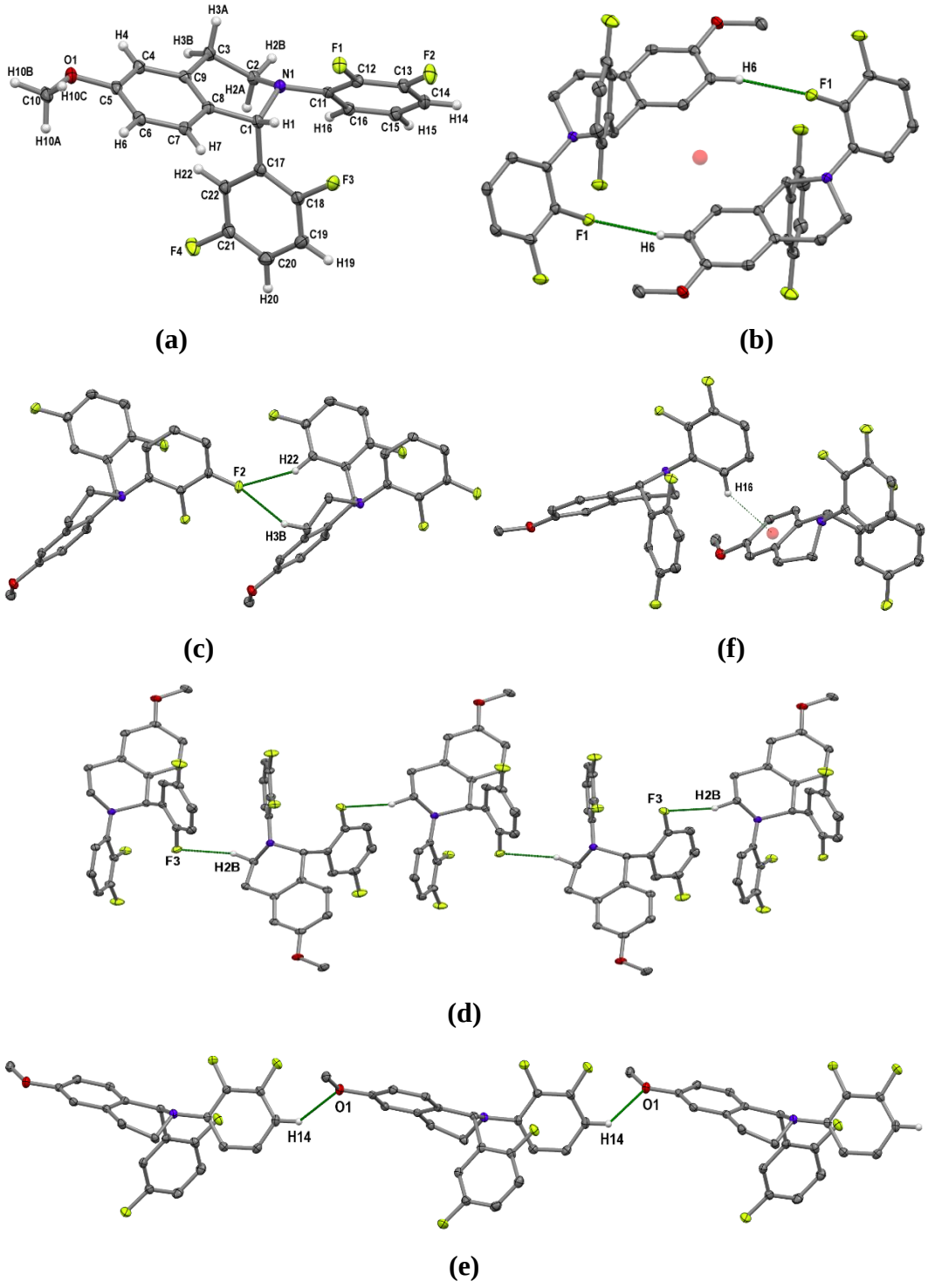


**Figure 4.3.4: (a)** ORTEP of **6c-3** drawn with 50% ellipsoidal probability. **(b)** An inversion center related cyclic dimer synthon by the utilization of C6–H6···F1 hydrogen bond. **(c)** A dimer form in which F2 act as a bifurcated acceptor for the C22–H22···F2 and C3–H3B···F2 hydrogen bonds. **(d)** One dimensional linear chain of weak C2–H2A···F3 hydrogen bond. **(e)** A C14–H14···O1 hydrogen bonds as a linear 1D chain in the crystal packing. **(f)** The C16–H16···π($C_{gC}$) interaction in the crystal structure.

**Table 4.3.4: Intermolecular interactions in 6c-3**

| D–B···A | D–B/Å | *D*(D···A )/ Å | *d*(B···A )/Å | ∠D–B···A/º | SYMMETRY |
|---|---|---|---|---|---|
| **C6–H6···F1** | 1.080 | 3.482(2) | 2.43 | 165 | 1-x, -y, 1-z |
| **C3–H3B···F2** | 1.080 | 3.360(2) | 2.65 | 123 | x-1, y, z |
| **C22–H22···F2** | 1.080 | 3.643(2) | 2.67 | 149 | x-1, y, z |
| **C2–H2B···F3** | 1.080 | 3.233(2) | 2.39 | 134 | 1-x, y+½, ½-z |
| **C14–H14···O1** | 1.080 | 3.333(2) | 2.56 | 128 | x+1, ½-y, z-½ |
| **C16–H16···π ($C_{gC}$)** | 1.080 | 3.566(2) | 2.74 | 146 | x, ½-y, z - ½ |

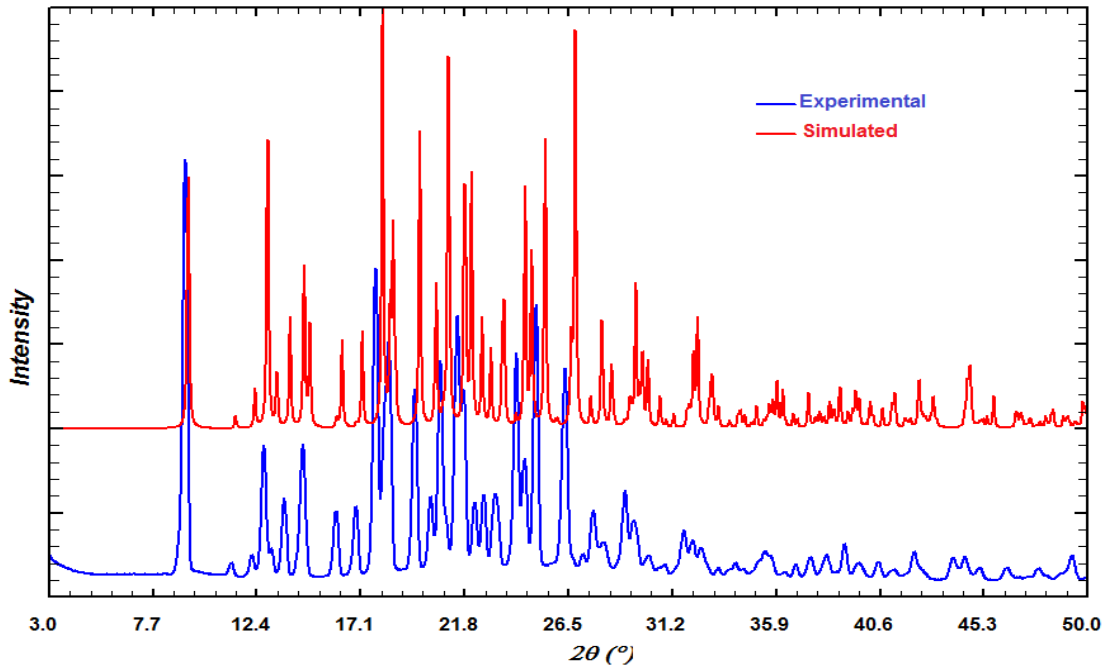


**Figure 4.3.4: (g)** Comparison of experimental and simulated PXRD patterns of **6c-3**

***N*-(2,3-difluorophenyl)-1-(3,4-difluorophenyl)-6-methoxy-1,2,3,4-tetrahydroisoquinoline (6c-5):** This molecule **6c-5** was found to crystallize in $P2_1/c$ space group and the asymmetric unit contained two molecules (Z = 4, Z' = 2) (Figure 4.3.5a) (Table 4.3.5). This asymmetric dimer interacts individually with another asymmetric dimer *via* C18–H18···F3 and C36–H36···F3 hydrogen bonds through the inversion center and thereby creates a tetrameric unit (Figure 4.3.5b). Here F3 acts as a bifurcated acceptor for the C18–H18···F3 and C36–H36···F3 hydrogen bonds. Further F5 of both the molecules of the asymmetric unit individually participates in C22–H22···F5 hydrogen bond by the inversion center and thereby creates a dimer moiety (Figure 4.3.5c). Methoxy oxygen of one molecule of the asymmetric unit is also involved in the weak C26–H26···O2 hydrogen bond through

the inversion center (Figure 4.3.5d). Each molecule of the asymmetric unit also stabilized by C21–H21⋯ π and C43–H43⋯ π interaction in the crystal structure (Figure 4.3.5e). The experimental PXRD pattern of **6c-5** is matching with the corresponding simulated PXRD pattern (Figure 4.3.5f).

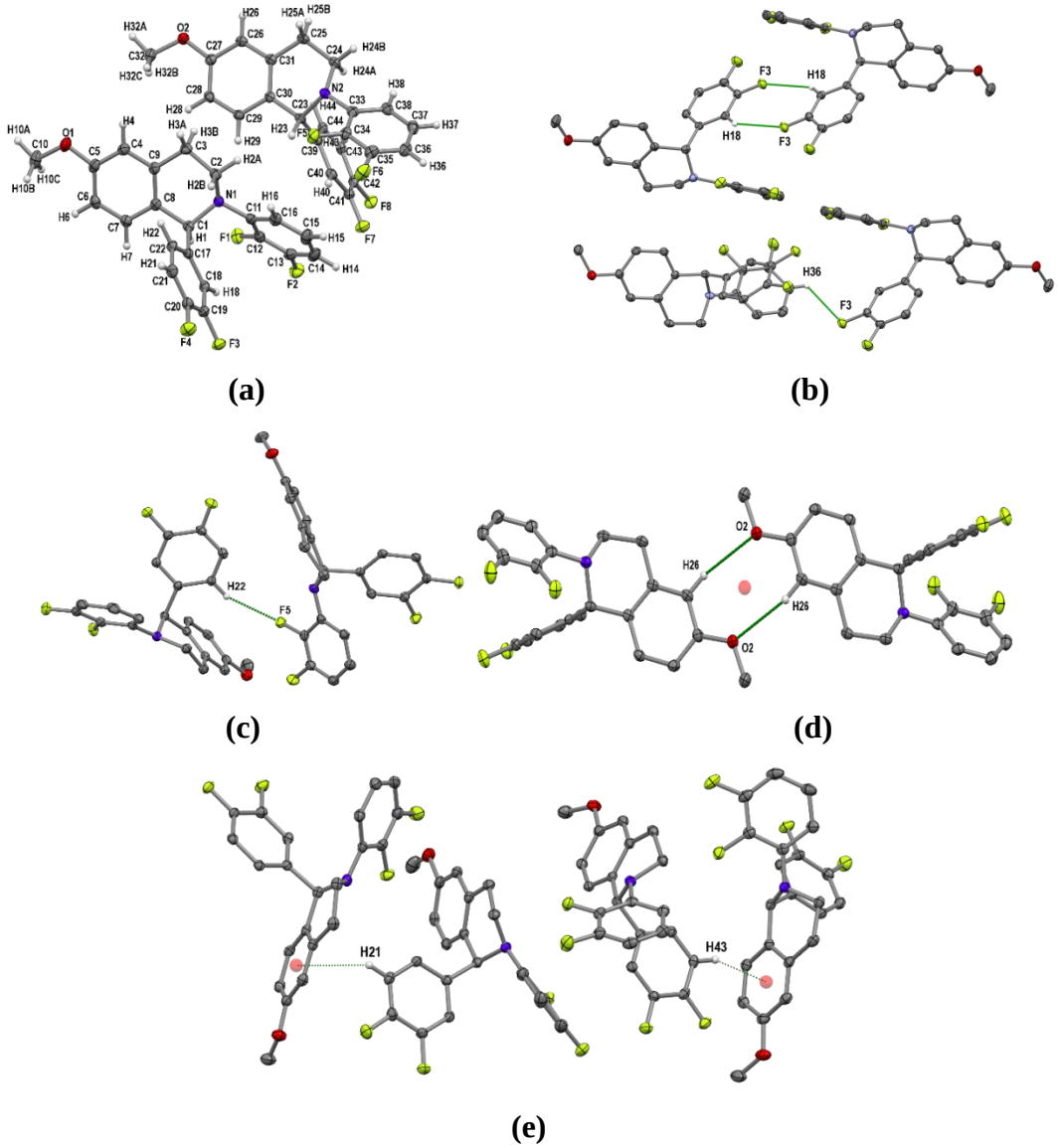


**Figure 4.3.5: (a)** ORTEP of **6c-5** drawn with 50% ellipsoidal probability. **(b)** Inversion center related dimer of asymmetric dimer *via* C18–H18⋯F3 and C36–H36⋯F3 hydrogen bonds. **(c)** Formation of a dimer unit by weak C22–H22⋯F5 hydrogen bond. **(d)** A cyclic dimer synthon offered by C26–H26⋯O2 hydrogen bond through the inversion center. **(e)** C21–H21⋯ π and C43–H43⋯ π interaction in the crystal packing.

**Table 4.3.5: Intermolecular interactions in 6c-5**

| D–B···A | D–B/Å | *D*(D···A )/ Å | *d*(B···A )/Å | ∠D–B···A/º | SYMMETRY |
|---|---|---|---|---|---|
| **C36–H36···F3** | 1.080 | 3.312(2) | 2.54 | 128 | 1-x, 1-y, 1-z |
| **C18–H18···F3** | 1.080 | 3.440(2) | 2.54 | 141 | 1-x, -y, 1-z |
| **C22–H22···F5** | 1.080 | 3.415(2) | 2.40 | 157 | -x, y-½, ½-z |
| **C26–H26···O2** | 1.080 | 3.546(2) | 2.67 | 138 | -x, 1-y, -z |
| **C21–H21···π ($C_{gC}$)** | 1.080 | 3.659(3) | 2.82 | 148 | x -1, y, z |
| **C43–H43··· π ($C_{gC}$)** | 1.080 | 3.446(3) | 2.56 | 156 | x, y, z |

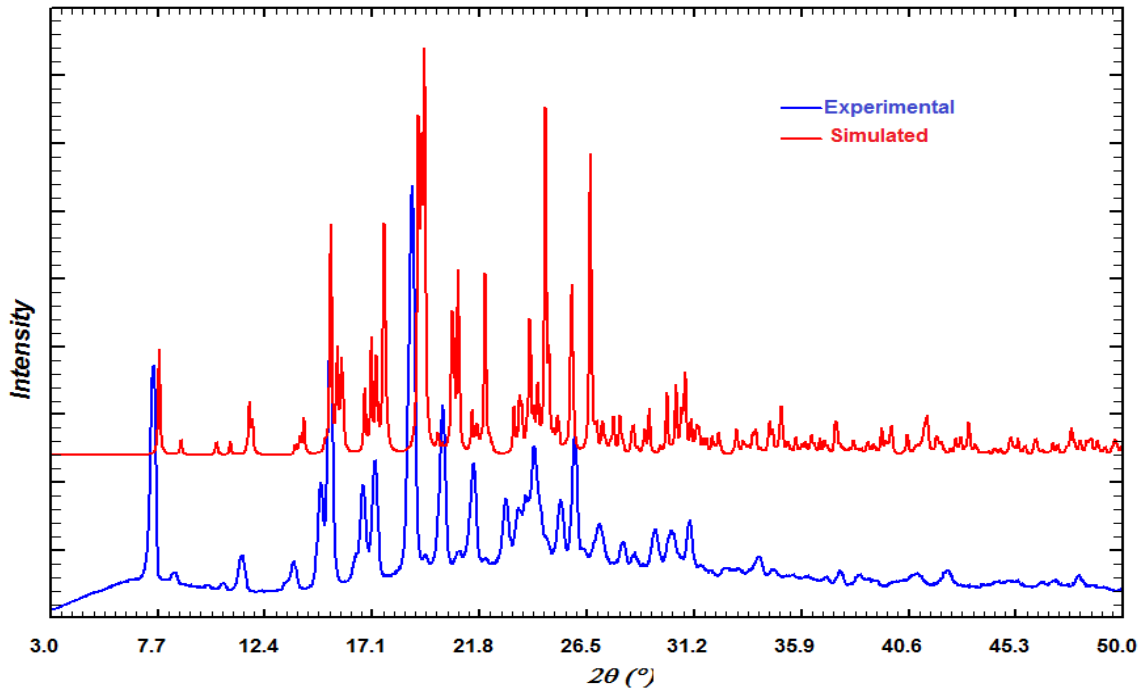


**Figure 4.3.5: (f)** Comparison of experimental and simulated PXRD patterns of **6c-5**

***N*-(2,3-difluorophenyl)-1-(3,5-difluorophenyl)-6-methoxy-1,2,3,4-tetrahydroisoquinoline (6c-6):** The compound **6c-6** was found to crystallize in monoclinic centrosymmetric *C2/c* space group with Z = 8 (Figure 4.3.6a). Out of the four fluorines, three fluorine atoms are involved in the C–H···F hydrogen bonds (Table 4.3.6). The *o*-F on the A ring (F1) contributes to the formation of C3–H3B···F1 by head to tail hydrogen bond and generates a zig-zag catameric chain like structure through the *c*-glide along the crystallographic *c*- direction (Figure 4.3.6b). Similarly *m*-F on the A (F2) ring forms the C15–H15···F2 hydrogen bond and generates 1-D zig-zag chain along the *c*-direction (Figure 4.3.6c). F3 of the B ring and H1 of the $sp^3$ chiral carbon are interconnected by the C1–H1···F3

hydrogen bond through the inversion center (Figure 4.3.6d). F3 behaves as a bifurcated acceptor for C18–H18···F3 hydrogen bond as well. Along with the C–H···F hydrogen bonds, methoxy group also participates in the C14–H14···O1 hydrogen bond to form a 1-D chain in the y-direction by the utilization of translational symmetry (Figure 4.3.6e). The experimental PXRD pattern of **6c-6** is matching with the corresponding simulated PXRD patterns (Figure 4.3.6f).

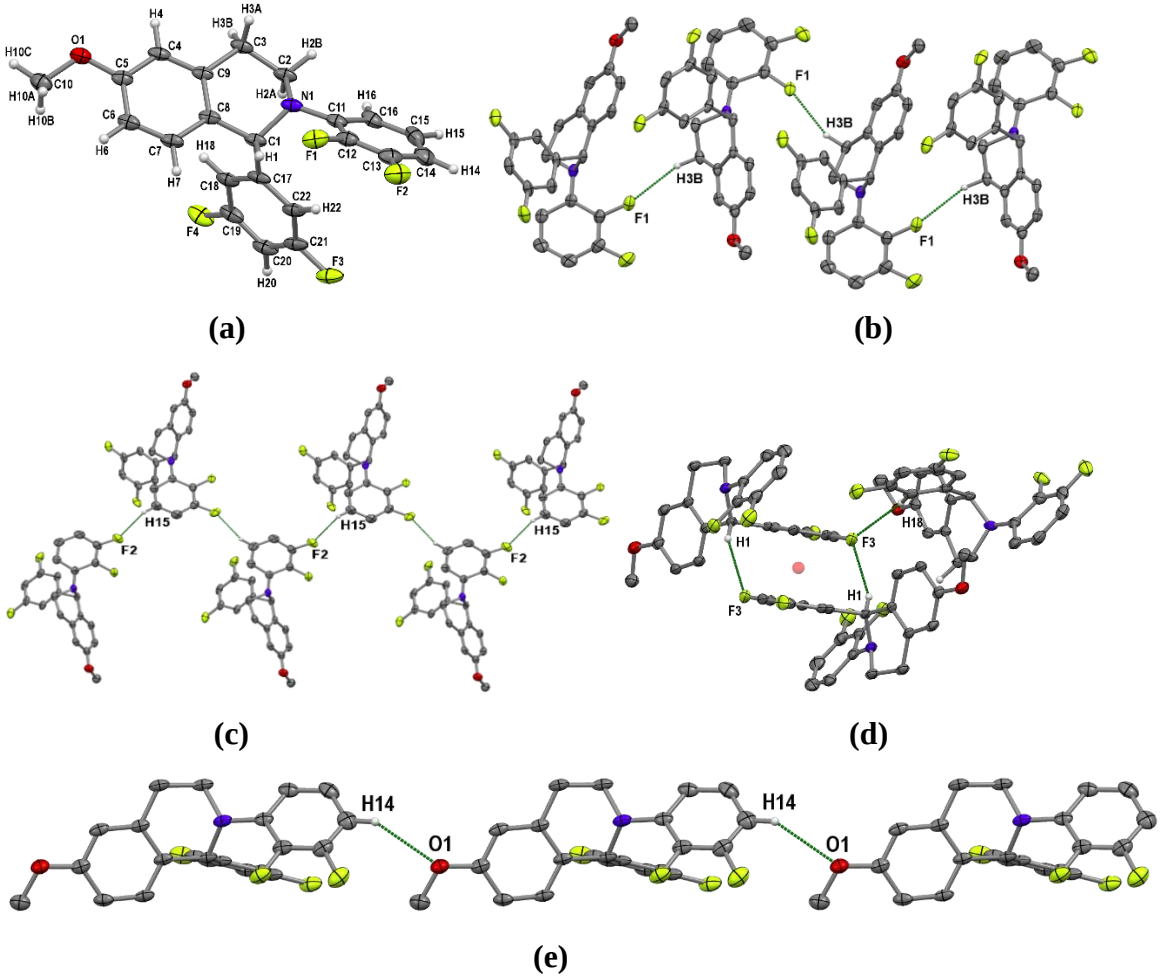


**Figure 4.3.6: (a)** ORTEP of **6c-6** drawn with 50% ellipsoidal probability. **(b)** C3–H3B···F1 hydrogen bond leading to the formation of the zig-zag chai. (c) Another zig-zag chain by C15–H15···F2 hydrogen bond by *c*-glide symmetry. (d) Bifurcated C1–H1···F3 and C18–H18···F3 hydrogen bond *via* inversion center. (e) One dimensional linear chain of the C14–H14···O1 hydrogen bond by translational symmetry.

**Table 4.3.6: Intermolecular interactions in 6c-6**

| D–B···A | D–B/Å | *D*(D···A )/ Å | *d*(B···A )/Å | ∠D–B···A/º | SYMMETRY |
|---|---|---|---|---|---|
| **C3–H3B···F1** | 1.080 | 3.571(3) | 2.55 | 158 | x, 1-y, z+½ |
| **C15–H15···F2** | 1.080 | 3.496(3) | 2.48 | 157 | x, -y, z+½ |
| **C1–H1···F3** | 1.080 | 3.378(3) | 2.45 | 143 | $^{3}/_{2}$-x, ½-y, 1-z |
| **C18–H18···F3** | 1.080 | 3.335(3) | 2.46 | 138 | $^{3}/_{2}$-x, y+½, $^{3}/_{2}$-z |
| **C14–H14···O1** | 1.080 | 3.502(3) | 2.58 | 143 | x, y-1, z |

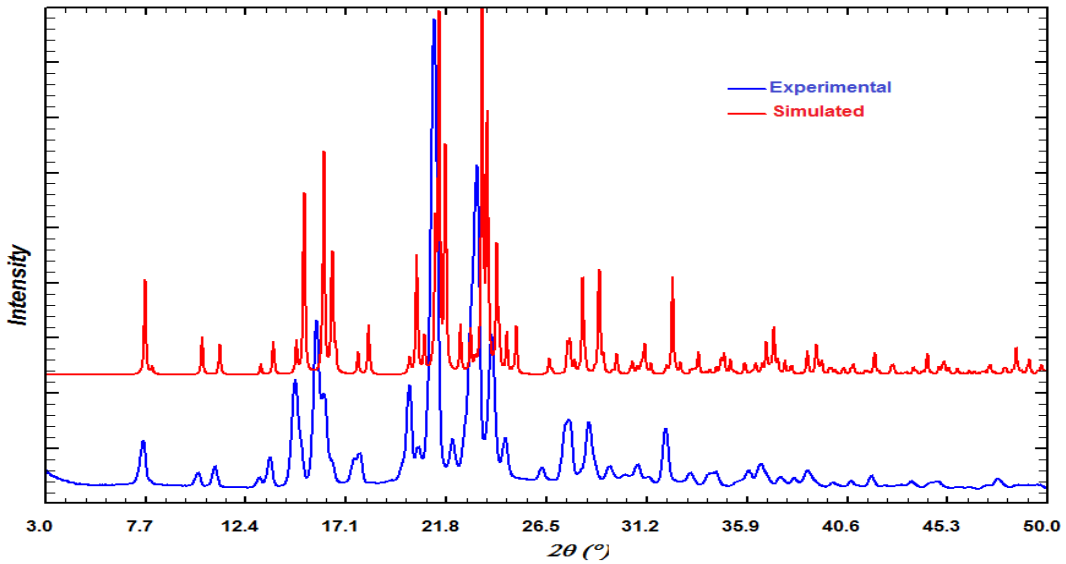


**Figure 4.3.6: (f)** Comparison of experimental and simulated PXRD patterns of **6c-6**

***N*-(2,4-difluorophenyl)-1-(2,3-difluorophenyl)-6-methoxy-1,2,3,4-tetrahydroisoquinoline (6c-7) and *N*-(2,5-difluorophenyl)-1-(2,3-difluorophenyl)-6-methoxy-1,2,3,4-tetrahydroisoquinoline (6c-13):** The crystal of **6c-7** (Figure 4.3.7a) and **6c-13** (Figure 4.3.8a) are found to be isostructural with the unit cell similarity index π = 0.0047. Both the compounds adopted centrosymmetric monoclinic *C*2/*c* space group with Z = 8 and Z' = 1 (Figure 4.3.7a and 4.3.8a). In both the structures, (F1) of the A ring and F3 of the B ring simultaneously involved in the weak C2–H2A···F1 and C16–H16···F3 hydrogen bonds leading to the formation of the one-dimensional ribbon-like structure by the translational symmetry along the *b*-direction (Figure 4.3.7b and 4.3.8b) (Table 4.3.7 and Table 4.3.8). F4 of B ring and H13 involved (C13–H13···F4) in formation of the cyclic dimer by the inversion center, which are further interconnected by another weak C–H···F hydrogen bond in a particular direction (Figure 4.3.7c and 4.3.8c) in both the

structures. Similar to C–H···F hydrogen bonds, methoxy groups are also involved in weak C22–H22···O1 and C21–H21···O1 hydrogen bonds as a bifurcated acceptor and creates a dimer (Figure 4.3.7d and 4.3.8d). Along with these C–H···F and C–H···O hydrogen bonds, the π cloud of C ring interacts with the H20 of the B ring leading to the C20–H20···π($C_{gA}$) interaction in the crystal structure (Figure 4.3.7e and 4.3.8e). In addition to these, C15–F2···F4–C19 interaction results in to a *head-to-trail* dimer across the inversion center in the compound **6c-13** (Figure 4.3.8f). The experimental PXRD pattern of **6c-7** is in agreement with the corresponding simulated PXRD pattern (Figure 4.3.7f) but experimental PXRD pattern of **6c-13** is not matching with the corresponding simulated PXRD pattern (Figure 4.3.8g) indicating the possibility of a second polymorph of **6c-13**.

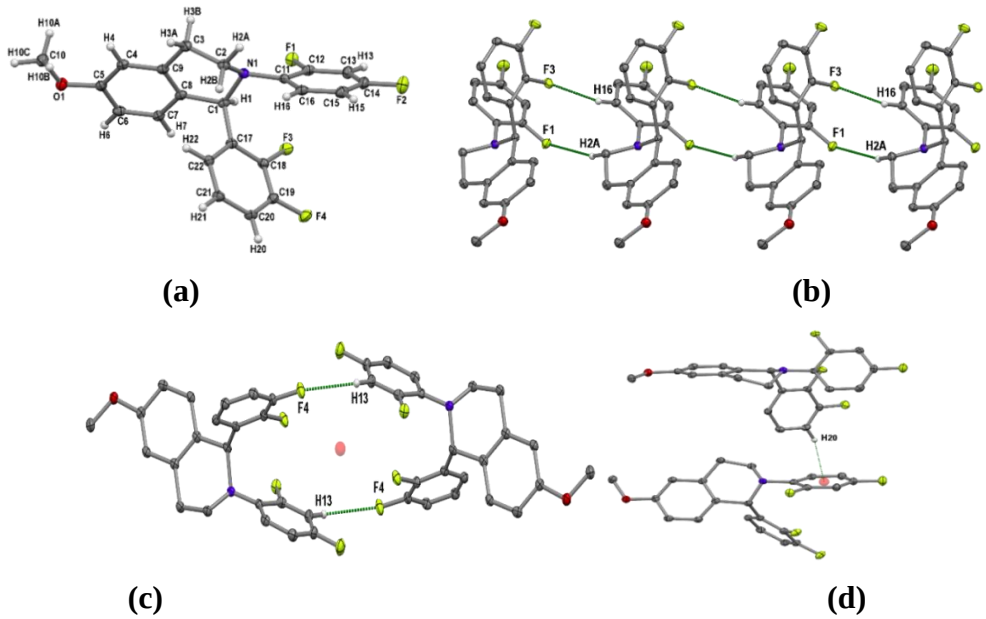


**Figure 4.3.7: (a)** ORTEP of **6c-7** drawn with 50% ellipsoidal probability. **(b)** A 1-D ribbon-like structure in which parallel C2–H2A···F1 and C16–H16···F3 hydrogen bonds are involved. **(c)** A cyclic dimer by the utilization of the C13–H13···F4 hydrogen bond through inversion center. **(d)** C20–H20···π($C_{gA}$) interaction in the crystal structure.

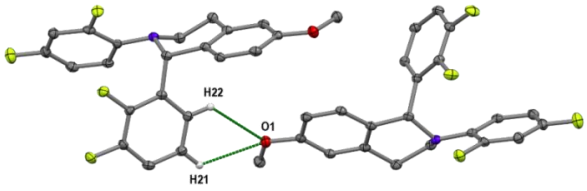


**(e)**

**Figuire 4.3.7: (e)** methoxy group acts as a bifurcated acceptor for weak C22–H22···O1 and C21–H21···O1 hydrogen bonds.

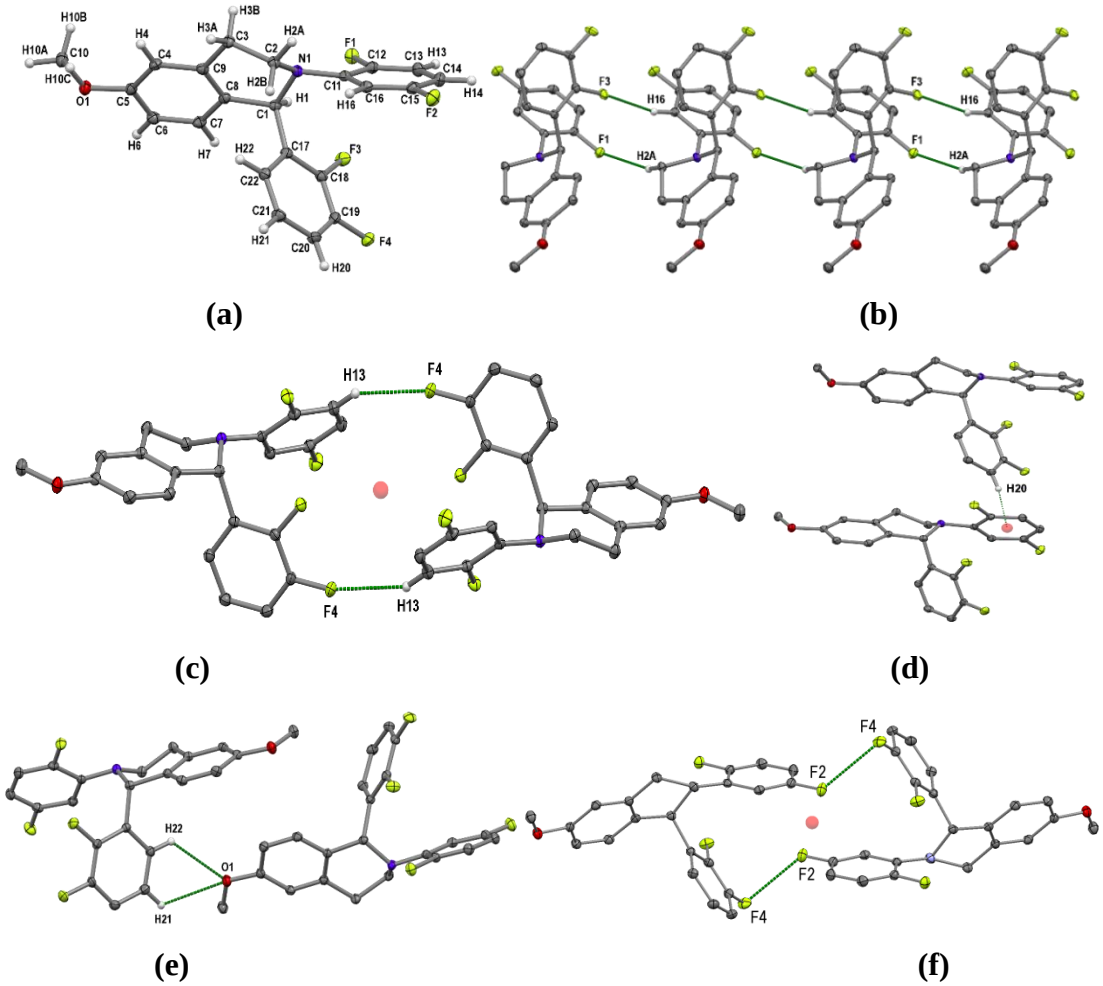


**Figure 4.3.8: (a)** ORTEP of **6c-13** drawn with 50% ellipsoidal probability. **(b)** A 1-D ribbon-like structure in which parallel C2–H2A···F1 and C16–H16···F3 hydrogen bonds are involved. **(c)** A cyclic dimer by the utilization of the C13–H13···F4 hydrogen bond through inversion center. **(d)** C20–H20···π($C_{gA}$) interaction in the crystal structure. **(e)** methoxy oxygen act as a bifurcated acceptor for weak C22–H22···O1 and C21–H21···O1 hydrogen bonds.**(f)** C15–F2···F4–C19 contact *via* inversion center.

**Table 4.3.7: Intermolecular interactions in 6c-7**

| D–B···A | D–B/Å | *D*(D···A )/ Å | *d*(B···A )/Å | ∠D–B···A/º | SYMMETRY |
|---|---|---|---|---|---|
| **C2–H2A···F1** | 1.080 | 3.519(2) | 2.50 | 156 | x, y-1, z |
| **C16–H16···F3** | 1.080 | 3.269(2) | 2.26 | 156 | x, y-1, z |
| **C13–H13···F4** | 1.080 | 3.412(3) | 2.62 | 130 | x, 2-y, z-½ |
| **C22–H22···O1** | 1.080 | 3.332(2) | 2.61 | 123 | $^{3}/_{2}$-x, y-½, $^{3}/_{2}$-z |
| **C20–H20···π ($C_{gA}$)** | 1.080 | 3.486(2) | 2.60 | 156 | x, 2-y, ½+z |

**Table 4.3.8: Intermolecular interactions in 6c-13**

| D–B···A | D–B/Å | *D*(D···A )/ Å | *d*(B···A )/Å | ∠D–B···A/º | SYMMETRY |
|---|---|---|---|---|---|
| **C2–H2A···F1** | 1.080 | 3.408(1) | 2.43 | 150 | x, y-1, z |
| **C16–H16···F3** | 1.080 | 3.289(2) | 2.24 | 163 | x, y-1, z |
| **C13–H13···F4** | 1.080 | 3.146(2) | 2.40 | 125 | 1-x, 2-y, 1-z |
| **C21–H21···O1** | 1.080 | 3.345(2) | 2.67 | 120 | ½-x, y-½, ½-z |
| **C22–H22···O1** | 1.080 | 3.345(2) | 2.67 | 120 | ½-x, y-½, ½-z |
| **C15–F2···F4–C19** | 1.354(2)<br>1.347(1) | 4.104 | 2.902(1) | 130<br>88 | -x, -y, -z |
| **C20–H20···π ($C_{gA}$)** | 1.080 | 3.652(1) | 2.79 | 152 | x, -y, ½+z |

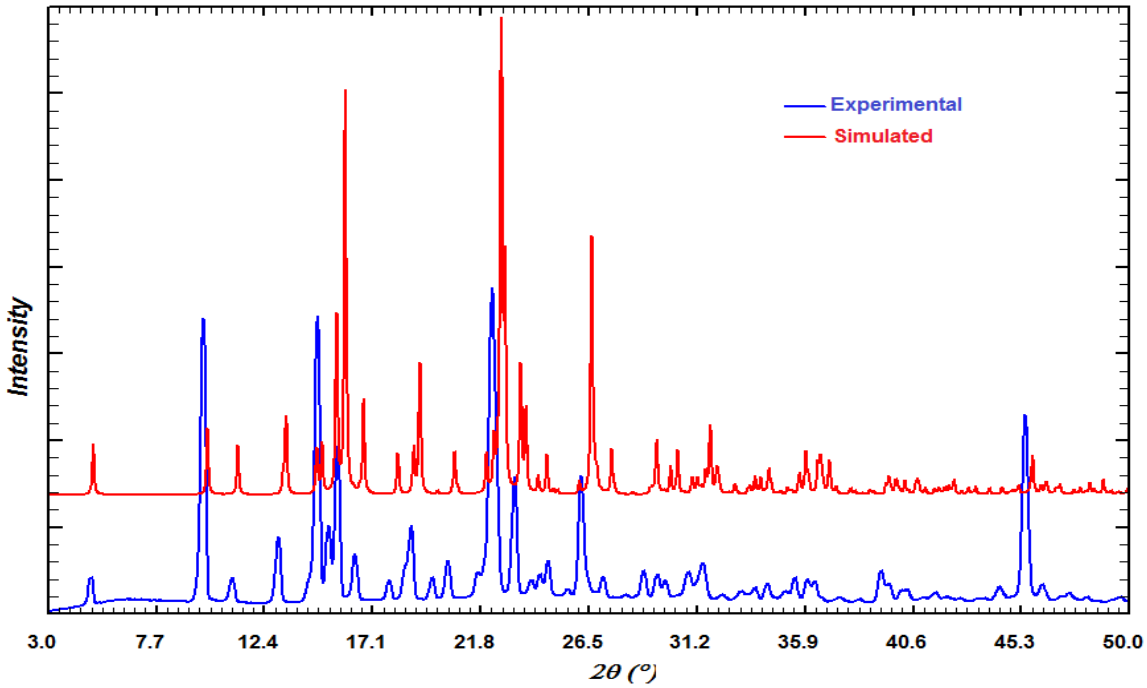


**Figure 4.3.7: (f)** Comparison of experimental and simulated PXRD patterns of **6c-7**

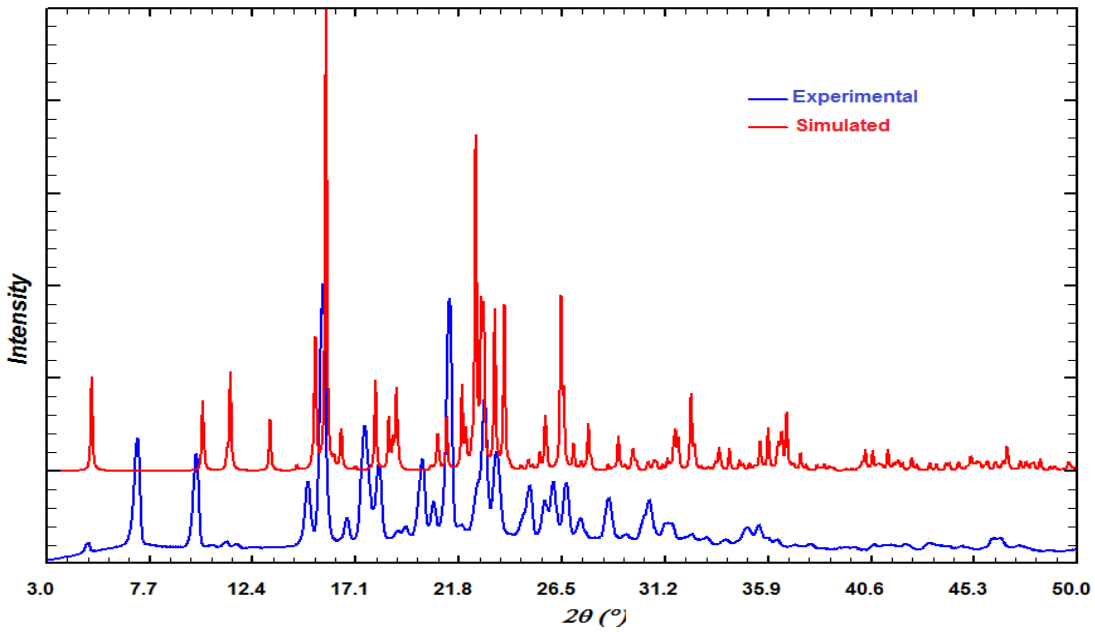


**Figure 4.3.8: (g)** Comparison of experimental and simulated PXRD patterns of **6c-13**

***N*-(2,4-difluorophenyl)-1-(2,4-difluorophenyl)-6-methoxy-1,2,3,4-tetrahydroisoquinoline (6c-8):** The compound **6c-8** adopted orthorhombic $Pca2_1$ space group with Z = 4 and Z' = 1 (Figure 4.3.9a). The *o*-F on both A and B rings contribute to the formation of C2–H2B···F1and C16–H16···F3 hydrogen bond and generate a linear catameric chain like structure along the crystallographic *c*-direction (Figure 4.3.9b) (Table 4.3.9). Another anti-parallel linear chain further interconnects this linear chain by C21–H21···O1 hydrogen bond through the $2_1$ symmetry (Figure 4.3.9c). Again dimer of this chain is also connected by another molecule by C19–H19···F2 hydrogen bonds through the *a*-glide symmetry and creates a trimer unit (Figure 4.3.9d). In this crystal structure, F···F contact and C–H···π interaction have not been observed. The experimental PXRD pattern of **6c-8** is matching with the corresponding simulated PXRD pattern (Figure 4.3.9e).

**Table 4.3.9: Intermolecular interactions in 6c-8**

| D–B···A | D–B/Å | *D*(D···A )/ Å | *d*(B···A )/Å | ∠D–B···A/º | SYMMETRY |
|---|---|---|---|---|---|
| **C2–H2B···F1** | 1.080 | 3.188(3) | 2.20 | 152 | x, +y, z+1 |
| **C19–H19···F2** | 1.080 | 3.321(4) | 2.47 | 135 | 1-x, -y, z-½ |
| **C16–H16···F3** | 1.080 | 3.533(4) | 2.46 | 175 | x, y, z+1 |
| **C21–H21···O1** | 1.080 | 3.347(4) | 2.61 | 125 | 1-x, 1-y, z+½ |

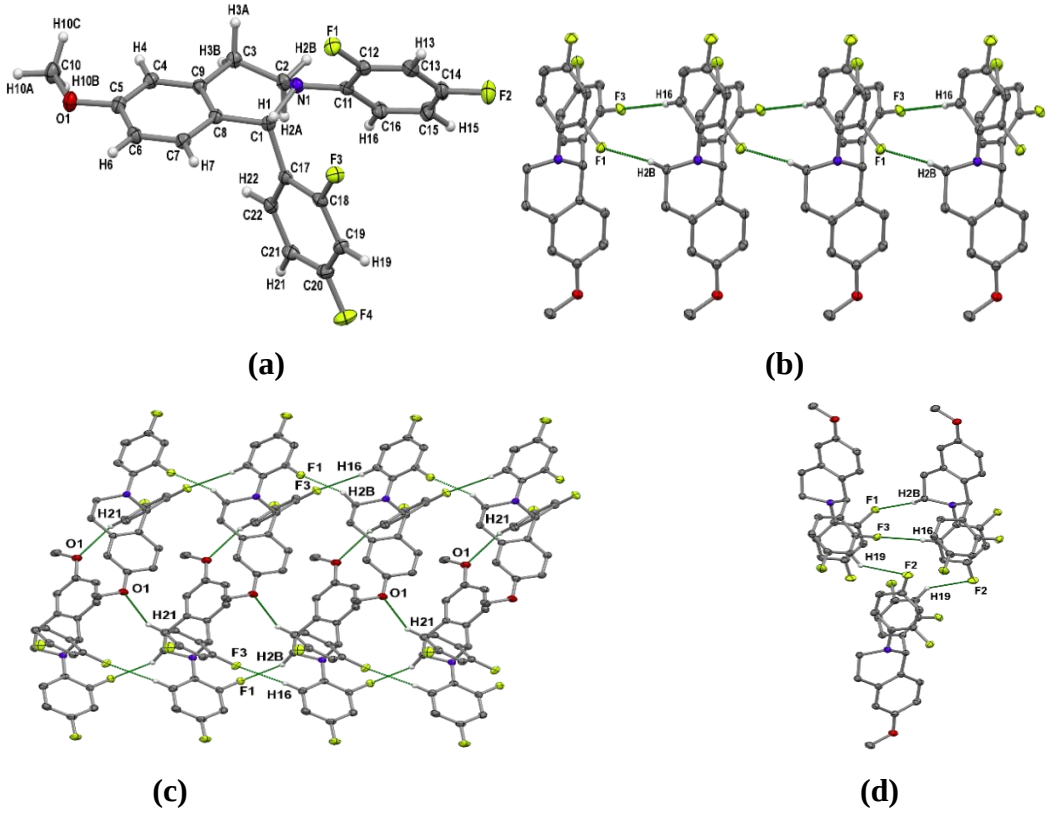


**Figure 4.3.9: (a)** ORTEP of **6c-8** drawn with 50% ellipsoidal probability. **(b)** A 1-dimensional linear chain by two parallel C2–H2B···F1and C16–H16···F3 hydrogen bond. **(c)** Two chains which are anti-parallel are interconnected by C21–H21···O1 hydrogen bond **(d)** A trimer unit in which three fluorines F1, F2 and F3 are involved in C2–H2B···F1, C19–H19···F2 and C16–H16···F3 hydrogen bonds respectively.

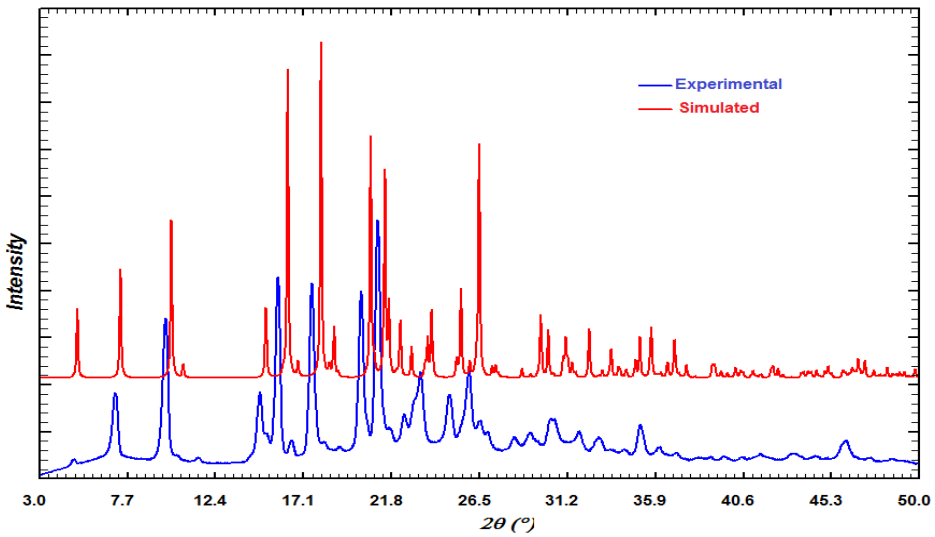


**Figure 4.3.9: (e)** Comparison of experimental and simulated PXRD patterns of **6c-8**

***N*-(2,4-difluorophenyl)-1-(2,5-difluorophenyl)-6-methoxy-1,2,3,4-tetrahydroisoquinoline (6c-9):** The compound **6c-9** crystallized in centrosymmetric monoclinic $P2_1/c$ space group with Z = 4 and Z' = 1 (Figure 4.3.10a). The *o*-F on both A and B ring contributes to the formation of C6–H6···F1and C13–H13···F3 hydrogen bond and generate a linear catameric molecular chain like structure along the crystallographic *c*- direction (Figure 4.3.10b) (Table 4.3.10). The F4 of the B ring acts as a bifurcated acceptor for both H4 and H15 to form C4–H4···F4 and C15–H15···F4 hydrogen bonds respectively. C4–H4···F4 hydrogen bond is utilized to form the dimer through inversion center while C15–H15···F4 hydrogen bond is utilized to propagate the dimer along the crystallographic *c*-direction through *c*-glide symmetry (Figure 4.3.10c). In addition to the C–H···F hydrogen bonds, methoxy group is also involved in the weak C20–H20···O1 hydrogen bond leading to the formation of one-dimensional molecular zig-zag chain *via* screw ($2_1$) operation (Figure 4.3.10d). In this crystal structure C19–H19···$\pi$ ($C_{gA}$) have also been observed, which further stabilizes the crystal packing (Figure 4.3.10e). No F···F contact have been observed in this case. The experimental PXRD pattern of **6c-9** is not matching with the corresponding simulated PXRD pattern indicating the possibility of different polymorphs of this compound (Figure 4.3.10f).

**Table 4.3.10: Intermolecular interactions in 6c-9**

| **D–B···A** | **D–B/Å** | ***D*(D···A )/ Å** | ***d*(B···A )/Å** | **∠D–B···A/º** | **SYMMETRY** |
|---|---|---|---|---|---|
| **C6–H6···F1** | 1.080 | 3.332(4) | 2.54 | 129 | x, y, z-1 |
| **C13–H13···F3** | 1.080 | 3.279(4) | 2.26 | 156 | x, y, z+1 |
| **C4–H4···F4** | 1.080 | 3.393(4) | 2.36 | 159 | -x, 1-y, 1-z |
| **C15–H15···F4** | 1.080 | 3.597(4) | 2.54 | 166 | x+1, $^3/_2$-y, z+½ |
| **C20–H20···O1** | 1.080 | 3.314(4) | 2.42 | 139 | -x, y+½, ½-z |
| **C19–H19···π ($C_{gA}$)** | 1.080 | 3.395(4) | 2.79 | 123 | x, ½-y, ½+z |

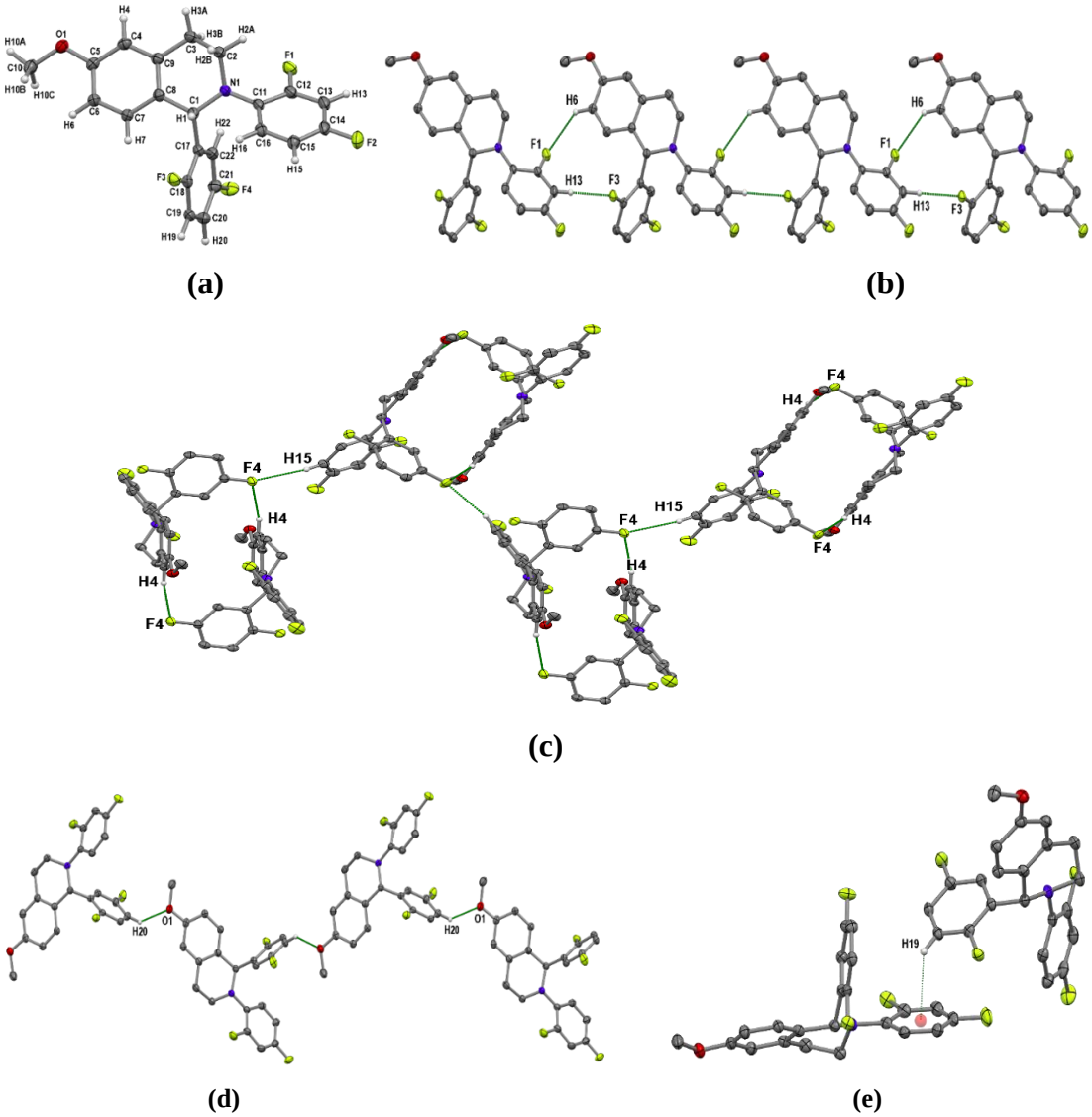


**Figure 4.3.10: (a)** ORTEP of **6c-9** drawn with 50% ellipsoidal probability. **(b)** A 1-D molecular zig-zag chain by the utilization of C6–H6···F1and C13–H13···F3 hydrogen bonds. **(c)** Propagation of the dimer unit along *c*-direction through C15–H15···F4 hydrogen bond. **(d)** A zig-zag molecular chain generated by weak C20–H20···O1 hydrogen bond. **(e)** A C19–H19···π ($C_{gA}$) interaction.

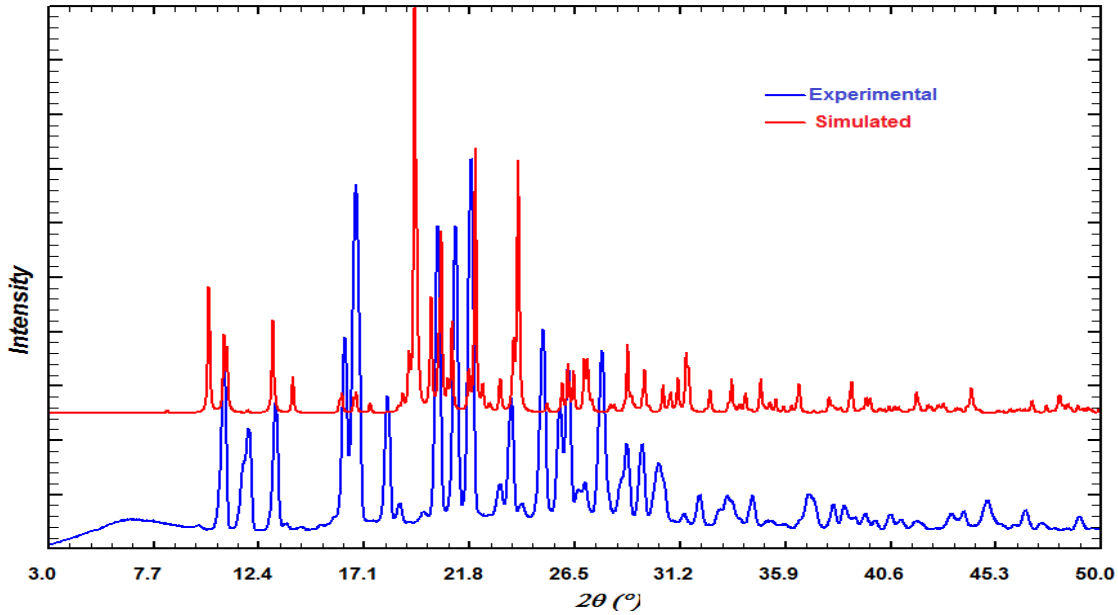


**Figure 4.3.10: (f)** Comparison of experimental and simulated PXRD patterns of **6c-9**

***N*-(2,5-difluorophenyl)-1-(2,6-difluorophenyl)-6-methoxy-1,2,3,4-tetrahydroisoquinoline (6c-16):** This molecule **6c-16** crystallized in monoclinic *Pc* space group two molecules (Z = 4, Z' = 2) in the asymmetric unit, namely molecule A and molecule B (Figure 4.3.11a). These two symmetry independent molecules with different molecular conformation are connected by C4–H4···F8 hydrogen bonds (Figure 4.3.11b) (Table 4.3.11). The molecule A of the asymmetric unit interacts with another "A" molecule *via* C2–H2B···F1, C7–H7···F3 and C16–H16···F4 hydrogen bonds through the translational symmetry and thereby creates one-dimensional tape like structure along the *b*-direction (Figure 4.3.11c). The molecule B of the asymmetric unit also interacts with another B molecule *via* C24–H24B···F5, C38–H38···F7 and C29–H29···F8 hydrogen bonds through the translational symmetry and thereby creating a tape like structure along the *b*-direction (Figure 4.3.11d). Further the molecule A of asymmetric unit interconnected by the molecule B of another asymmetric unit through the C26–H26···F3 and C25–H25···O1 hydrogen bonds by utilization of *c*-glide (Figure 4.3.11e). The C20–H20···π and C42–H42···π interaction also has been observed (Figure 4.3.11f). The experimental PXRD pattern of **6c-16** is in agreement with the corresponding simulated PXRD patterns (Figure 4.3.11g).

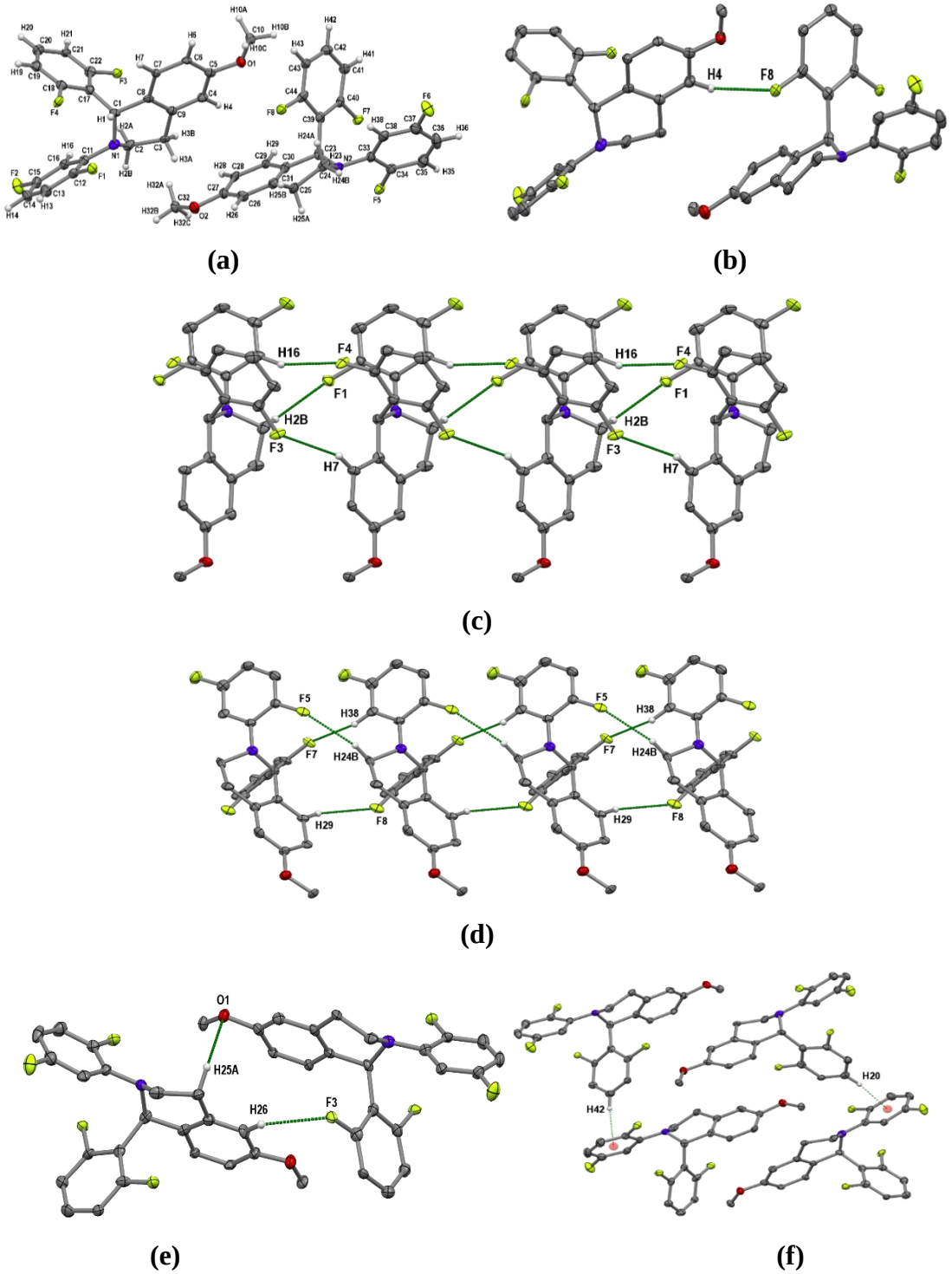


**Figure 4.3.11: (a)** ORTEP of **6c-16** drawn with 50% ellipsoidal probability. **(b)** Symmetry independent two molecules of the asymmetric unit which is interconnected by C4-H4···F8 hydrogen. **(c)** 1-D tap like structure through C2–H2B···F1, C7–H7···F3 and C16–H16···F4 hydrogen bonds. **(d)** Another 1-D tap like structure through *via* C24–H24B···F5, C38–H38···F7 and C29–H29···F8 hydrogen bonds hydrogen bonds. **(e)** A dimer unit *via* c-glide symmetry. **(f)** Both molecules A and B are formed C–H···π interaction.

**Table 4.3.11: Intermolecular interactions in 6c-16**

| D–B···A | D–B/Å | *D*(D···A )/ Å | *d*(B···A )/Å | ∠D–B···A/º | SYMMETRY |
|---|---|---|---|---|---|
| **C4–H4···F8** | 1.080 | 4.40(1) | 2.66 | 134 | - |
| **C16–H16···F4** | 1.080 | 3.233(1) | 2.22 | 156 | x, y-1, z |
| **C29–H29···F8** | 1.080 | 3.570(9) | 2.57 | 153 | x, y-1, z |
| **C2–H2B···F1** | 1.080 | 3.586(1) | 2.63 | 148 | x, y-1, z |
| **C24–H24B···F5** | 1.080 | 3.586(1) | 2.65 | 145 | x, y+1, z |
| **C38–H38···F7** | 1.080 | 3.250(1) | 2.25 | 153 | x, y+1, z |
| **C7–H7···F3** | 1.080 | 3.590(9) | 2.58 | 156 | x, y+1, z |
| **C26–H26···F3** | 1.080 | 3.568(1) | 2.63 | 145 | x, 1-y, ½+z |
| **C25–H25···O1** | 1.080 | 3.542(1) | 2.64 | 140 | x, 1-y, z+½ |
| **C20–H20···π ($C_{gA}$)** | 1.080 | 3.656(9) | 2.79 | 152 | x, 1-y, z-½ |
| **C42–H42···π ($C_{gA}$)** | 1.080 | 3.715(1) | 2.82 | 158 | x, 1-y, z -½ |

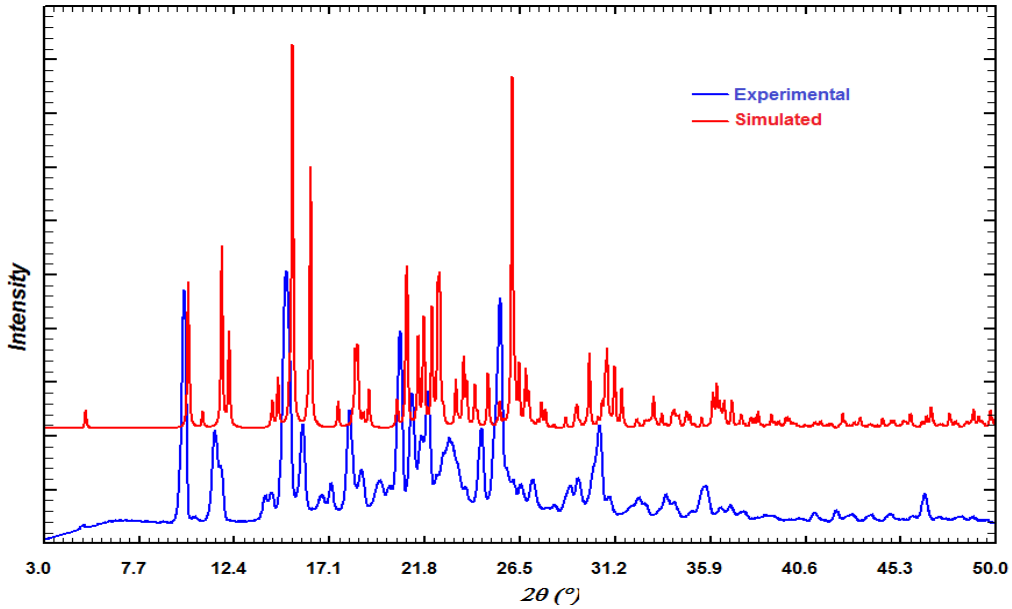


**Figure 4.3.11: (g)** Comparison of experimental and simulated PXRD patterns of **6c-16**

***N*-(2,6-difluorophenyl)-1-(2,3-difluorophenyl)-6-methoxy-1,2,3,4-tetrahydroisoquinoline (6c-19):** This molecule **6c-19** crystallized in monoclinic centrosymmetric $P2_1/c$ space group with (Z = 4, Z' = 1) (Figure 4.3.12a). In this structure only two fluorines *i.e.* F2 and F4 are involved in weak hydrogen bonds. The *m*-F (F4) of the B ring involves *c*-glide to form C13–H13···F4 hydrogen bond and

generates a linear catameric molecular chain like structure along the crystallographic *c*-direction (Figure 4.3.12b) (Table 4.3.12). Similarly *o*-F (F2) of the A ring is interconnected by aliphatic H2B of the another molecule through the C2–H2B···F2 hydrogen bond by the utilisation of translational symmetry and creates 1-D linear chain. These linear chains are further interconnected by another parallel linear chain by bifurcated C21–H21···O1 and C7–H7···O1 hydrogen bonds, which involves the methoxy group (Figure 4.3.12c). Along with C–H···O hydrogen bonds, short F1···F3 contact, and C20–H20···π interaction (Figure 4.3.12e) have been observed. The F1···F3 contact is generated by translational symmetry along *b*-direction (Figure 4.3.12d). The experimental PXRD pattern of **6c-19** is matching with the corresponding simulated PXRD pattern (Figure 4.3.12f).

**Table 4.3.12: Intermolecular interactions in 6c-19**

| **D–B···A** | **D–B/Å** | ***D*(D···A )/ Å** | ***d*(B···A )/Å** | **∠D–B···A/º** | **SYMMETRY** |
|---|---|---|---|---|---|
| **C2–H2B···F2** | 1.080 | 3.270(3) | 2.31 | 147 | x, y-1, z |
| **C13–H13···F4** | 1.080 | 3.260(3) | 2.38 | 137 | x, $^{3}/_{2}$-y, z-½ |
| **C21–H21···O1** | 1.080 | 3.376(3) | 2.63 | 126 | 1-x, y-½, $^{3}/_{2}$-z |
| **C7–H7···O1** | 1.080 | 3.411(3) | 2.63 | 129 | 1-x, y+$^{1}/_{2}$, $^{3}/_{2}$-z |
| **C16–F1···F3–C18** | 1.358(3)<br>1.345(3) | 3.290(4) | 2.66 | 166<br>159 | x, 1+y, z |
| **C20–H20···π ($C_{gA}$)** | 1.080 | 3.581(3) | 2.69 | 162 | x, $^{3}/_{2}$-y, z -½ |

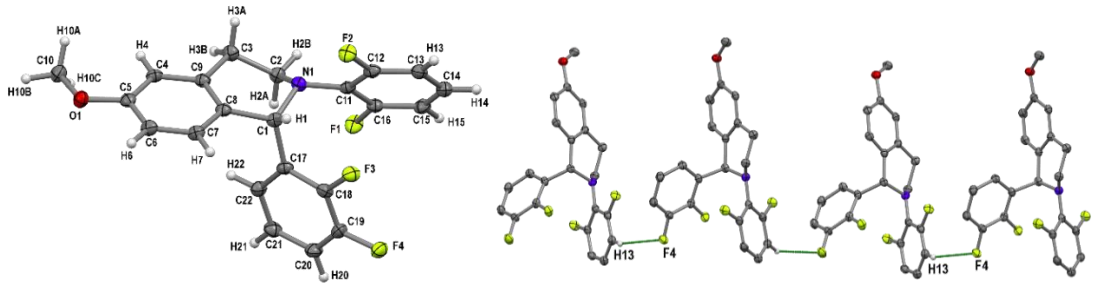


**(a)** **(b)**

**Figure 4.3.12: (a)** ORTEP of **6c-19** drawn with 50% ellipsoidal probability. **(b)** 1-D linear chain of C13–H13···F4 hydrogen bond.

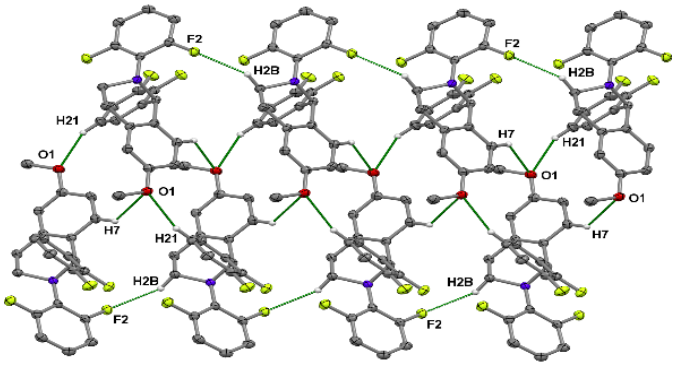


**(c)**

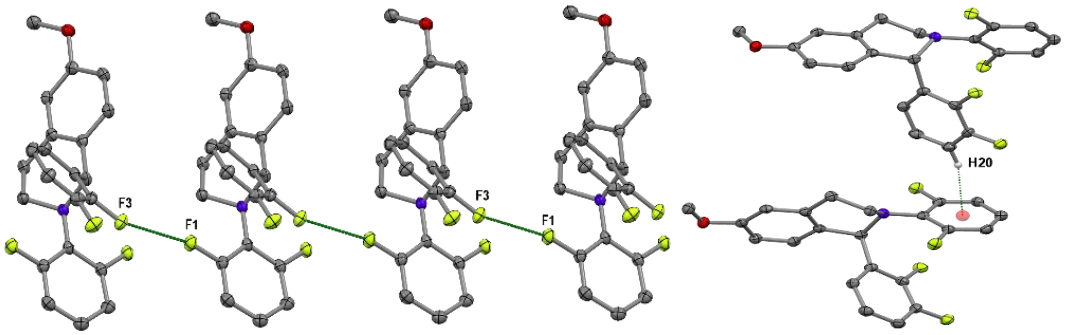


**(d)** **(e)**

**Figure 4.3.12: (c)** The C13–H13···F4 hydrogen bond containing two parallel chain interpenetrated by bifurcated C21–H21···O1 and C7–H7···O1 hydrogen bond. **(d)** A linear chain generated by F1···F3 contact through translational symmetry. **(e)** A *c*-glide related C20–H20···π interaction.

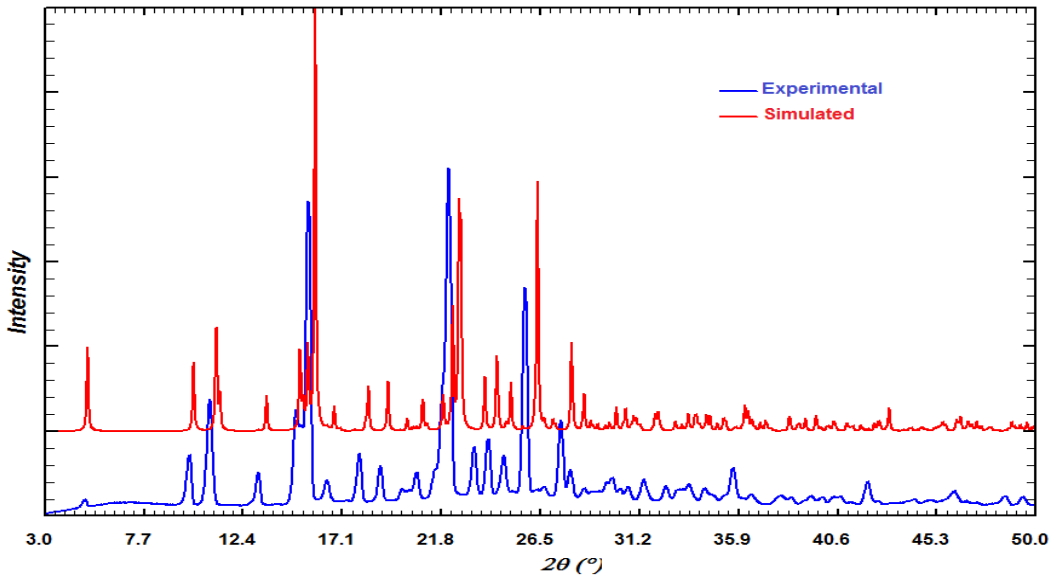


**Figure 4.3.12: (f)** Comparison of experimental and simulated PXRD patterns of **6c-19**

***N*-(2,6-difluorophenyl)-1-(2,5-difluorophenyl)-6-methoxy-1,2,3,4-tetrahydroisoquinoline (6c-21):** The compound **6c-21** was found to crystallize in non-centrosymmetric monoclinic *Pn* space group with Z = 2 and Z' = 1 (Figure 4.3.13a). Both the *o*-F on the A and B rings contribute to the formation of bifurcated C3–H3A···F1 and C3–H3A···F3 hydrogen bonds, which generate a linear catameric molecular chain like structure by utilization of the translational symmetry along the crystallographic *b*-direction (Figure 4.3.13b) (Table 4.3.13). The *m*-F (F4) on B ring is interlinked by a neighbor molecule through C4–H4···F4 hydrogen bond by utilization of the *n*-glide leading to the formation of wave like structure (Figure 4.3.13c). Along with fluorine, oxygen is also involved in the C19–H19···O1 hydrogen bond, which contributes in the crystal packing as a zig-zag one-dimensional molecular chain as well (Figure 4.3.13d). In this crystal structure, the F···F contact and C–H···π interaction have not been observed. The experimental PXRD pattern of **6c-21** is in agreement with the corresponding simulated PXRD pattern (Figure 4.3.13e).

**Table 4.3.13: Intermolecular interactions in 6c-21**

| **D–B···A** | **D–B/Å** | ***D*(D···A )/ Å** | ***d*(B···A )/Å** | **∠D–B···A/º** | **SYMMETRY** |
|---|---|---|---|---|---|
| **C3–H3A···F3** | 1.080 | 3.437(4) | 2.63 | 132 | x, y-1, z |
| **C3–H3A···F1** | 1.080 | 3.236(4) | 2.52 | 123 | x, y-1, z |
| **C4–H4···F4** | 1.080 | 3.536(4) | 2.59 | 146 | x-½, -y, z-½ |
| **C19–H19···O1** | 1.080 | 3.294(5) | 2.57 | 123 | x-½, 1-y, z+½ |

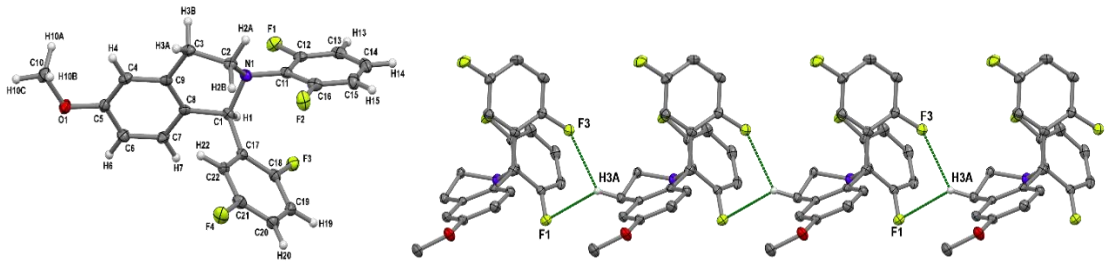


**(a)** **(b)**

**Figure 4.3.13: (a)** ORTEP of **6c-21** drawn with 50% ellipsoidal probability. **(b)** Bifurcated 1-D linear chain of C3–H3A···F1and C3–H3A···F3 hydrogen bond.

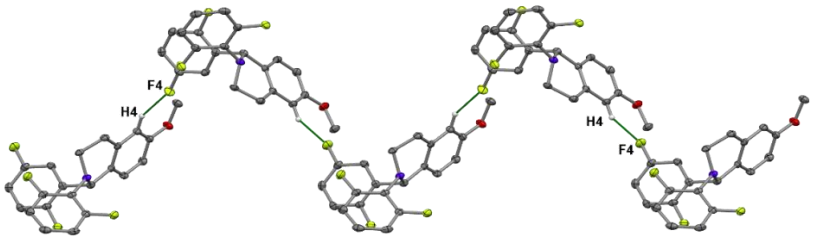


**(c)**

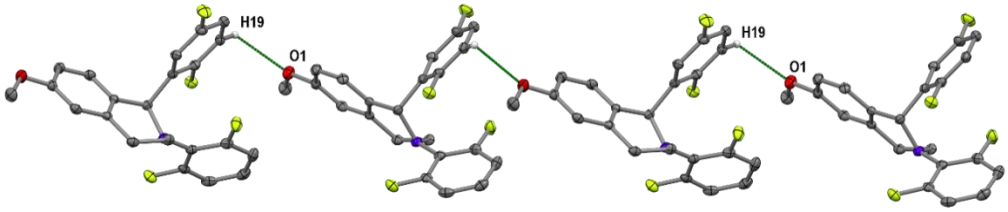


**(d)**

**Figure 4.3.13: (c)** The C4–H4···F4 hydrogen bonded *n*-glide symmetry generates a wavy like structure. **(d)** The one-dimensional molecular chain offered by O1 in the C19–H19···O1 hydrogen bond.

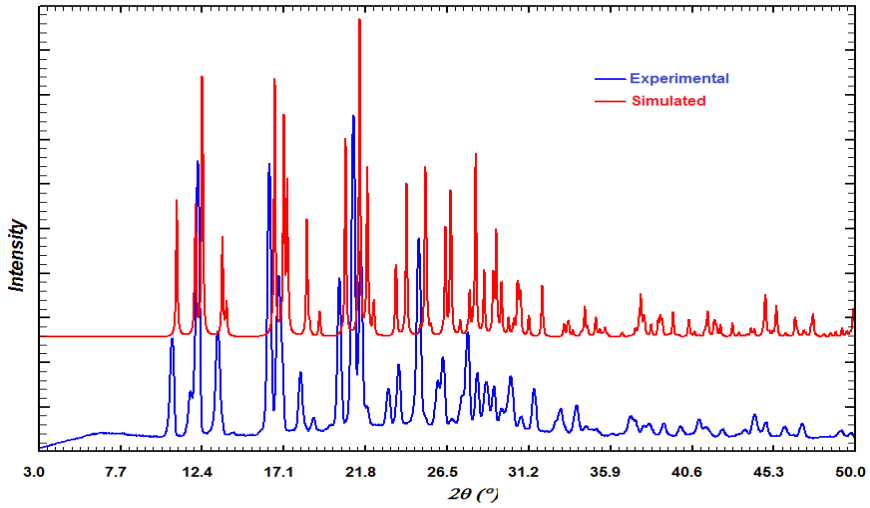


**Figure 4.3.13: (e)** Comparison of experimental and simulated PXRD patterns of **6c-21**

***N*-(2,6-difluorophenyl)-1-(3,4-difluorophenyl)-6-methoxy-1,2,3,4-tetrahydroisoquinoline (6c-23):** The compound **6c-23** was found to crystallize in centrosymmetric monoclinic *Pbca* space group with Z = 8 and Z' = 1 (Figure 4.3.14a). This molecule has a static disordered structure in the B ring by the ratio of 0.65:0.35. The *m*-F (F3A) of part 1 of the B ring and H13 of the A ring involved

in the C13–H13···F3A hydrogen bond in such a way that it creates an inversion center in the dimer synthon (Figure 4.3.14b) (Table 4.3.14). The both *o*-F on the A ring simultaneously takes part in the C2–H2B···F1 and C18A–H18A···F2 hydrogen bonds, which are parallel to each other along the *b*-direction by using translational symmetry (Figure 4.3.14c). In addition to C–H···F hydrogen bonds, F3 and F4 are also involved in C19–F3···F4–C20 contact by the utilization of *b*-glide symmetry, which creates one-dimensional molecular zig-zag chain along the *b*-direction (Figure 4.3.14d). Methoxy group is also involved in the C22A–H22A···O1 weak hydrogen bond, which also contributes to stabilize the crystal packing (Figure 4.3.14e). The experimental PXRD pattern of **6c-21** matches with the corresponding simulated PXRD pattern (Figure 4.3.14f).

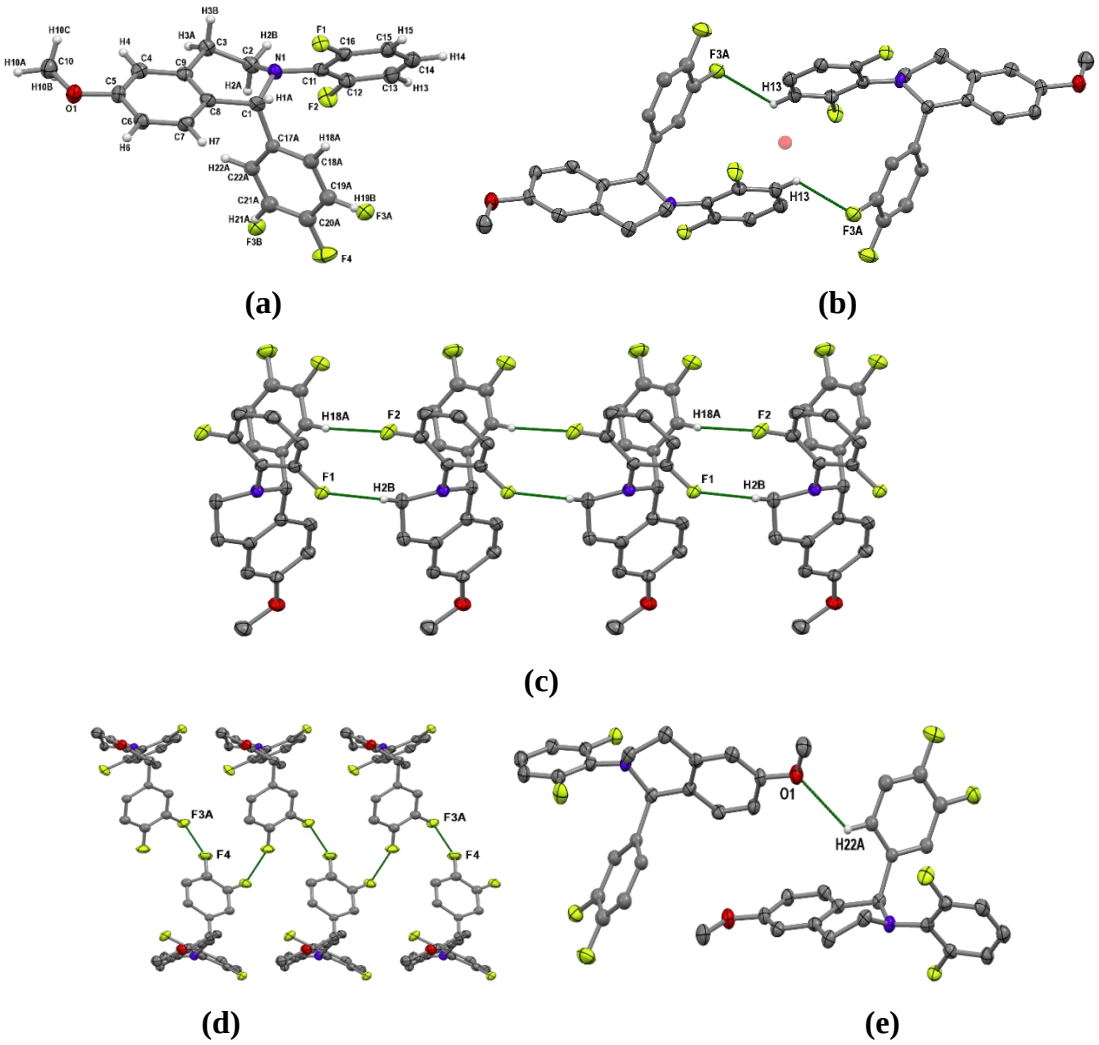


**Figure 4.3.14: (a)** ORTEP of **6c-23** drawn with 50% ellipsoidal probability. **(b)** An inversion center related dimer synthon formation by C13–H13···F3A hydrogen bond. **(c)** Two parallel C2–H2B···F1and C18A–H18A···F2 hydrogen bond

propagating along the *y*-axis. **(d)** A molecular zig-zag chain of F3···F4 contact. **(e)** A C22A–H22A···O1 weak hydrogen bond.

**Table 4.3.14: Intermolecular interactions in 6c-23**

| D–B···A | D–B/Å | *D*(D···A )/ Å | *d*(B···A )/Å | ∠D–B···A/º | SYMMETRY |
|---|---|---|---|---|---|
| **C2–H2B···F1** | 1.080 | 3.297(4) | 2.28 | 157 | x, y-1, z |
| **C18A–H18A···F2** | 1.080 | 3.323(4) | 2.27 | 163 | x, y+1, z |
| **C13–H13···F3A** | 1.080 | 3.274(5) | 2.48 | 130 | 1-x, 1-y, 1-z |
| **C22B–H22B···O1** | 1.080 | 3.416(4) | 2.66 | 127 | 1-x, y-½, ½-z |
| **C19–F3···F4–C20** | 1.307(5)<br>1.367(5) | 4.356(2) | 2.649(4) | 101<br>157 | -½-x, -½+y, z |

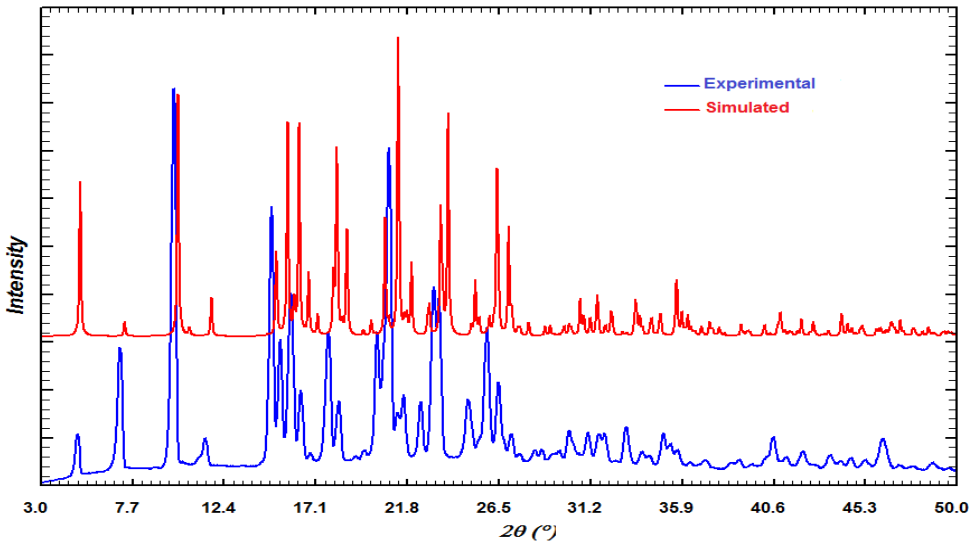


**Figure 4.3.14: (f)** Comparison of experimental and simulated PXRD patterns of **6c-23**

***N*-(3,4-difluorophenyl)-1-(2,3-difluorophenyl)-6-methoxy-1,2,3,4-tetrahydroisoquinoline (6c-25) and *N*-(3,4-difluorophenyl)-1-(3,5-difluorophenyl)-6-methoxy-1,2,3,4-tetrahydroisoquinoline (6c-30):** The crystal structure of **6c-25** (Figure 4.3.15a) and **6c-30** (Figure 4.3.16a) are found to be isostructural with the unit cell similarity index $\pi$ = 0.0034. Both the molecules are crystallized in centrosymmetric monoclinic $P2_1/c$ space group with Z = 4 and Z' = 1. In both the compounds, (F2) of the A ring act as a bifurcated acceptor with H20 and H16 in C20–H20···F2 and C16–H16···F2 hydrogen bond respectively (Table 4.3.15 and Table 4.3.16). The bifurcated C20–H20···F2 hydrogen bond participates in the

formation of symmetrical dimer synthon through the inversion center and this dimer synthon further interconnected by another molecule by two hydrogen bonds, one with bifurcated C16–H16···F2 hydrogen bond and another one through C21–H21···F3 hydrogen bond utilizing the *c*-glide operation (Figure 4.3.15b). But in the compound 6c-30, this symmetrical dimer interconnected by another molecule by four hydrogen bonds, which are offered by the F3 as a trifurcated C7–H7···F3, C22–H22···F3 and C1–H1···F3 hydrogen bond and bifurcated C16–H16···F2 hydrogen bond *via c*-glide symmetry (Figure 4.3.16b). In this isostructural compound, a bifurcated F···F contact also have been observedinvolving C21–F4···F4–C21 and C21–F4···F1–C13 leading to the formation of one-dimensional ribbon-like structure (Figure 4.3.15c) and (Figure 4.3.16c). Since in the 6c-30 structure the position of the F2 group changes from *ortho* to *meta* position, so one additional C20–H20···F4 hydrogen bond is incorporated, which leads to the formation of homo dimer synthon by inversion center (Figure 4.3.16d). Further, C2–H2B···π interaction is also identified in this structure (Figure 4.3.16e). The experimental PXRD pattern of **6c-25** and **6c-30** are in agreement with the corresponding simulated PXRD patterns (Figure 4.3.15d and Figure 4.3.16f).

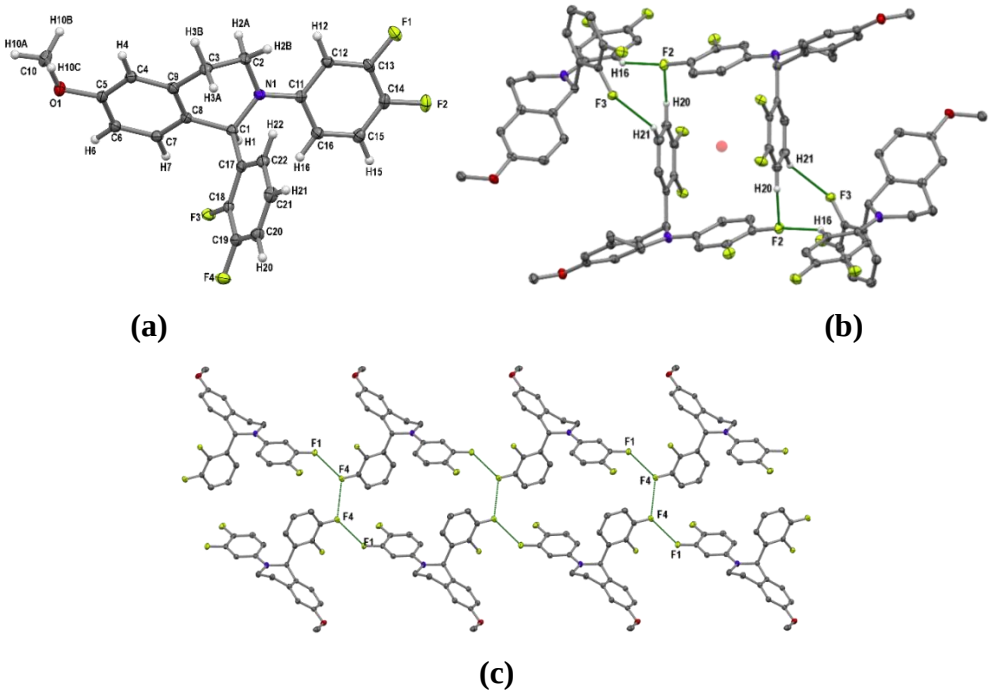


**(a)** **(b)**

**(c)**

**Figure 4.3.15: (a)** ORTEP of **6c-25** drawn with 50% ellipsoidal probability. **(b)** An inversion center related symmetrical dimer synthon formation by one of the

bifurcated C20–H20···F2 hydrogen bond. **(c)** C21–F4···F4–C21 and C21–F4···F1–C13 contact which leads to the formation of one-dimensional ribbon-like structure.

**Table 4.3.15: Intermolecular interactions in 6c-25**

| D–B···A | D–B/Å | *D*(D···A )/ Å | *d*(B···A )/Å | ∠D–B···A/º | SYMMETRY |
|---|---|---|---|---|---|
| **C16–H16···F2** | 1.080 | 3.156(3) | 2.23 | 142 | -x, y+½, $^{3}/_{2}$-z |
| **C20–H20···F2** | 1.080 | 3.226(2) | 2.50 | 123 | 1-x, 1-y, 2-z |
| **C21–H21···F3** | 1.080 | 3.617(2) | 2.63 | 152 | x+1, $^{3}/_{2}$-y, z+½ |
| **C13–F1···F4–C19** | 1.3487(19)<br>1.3506(19) | 5.049(2) | 2.882(1) | 136<br>126 | x, 1+y, z |

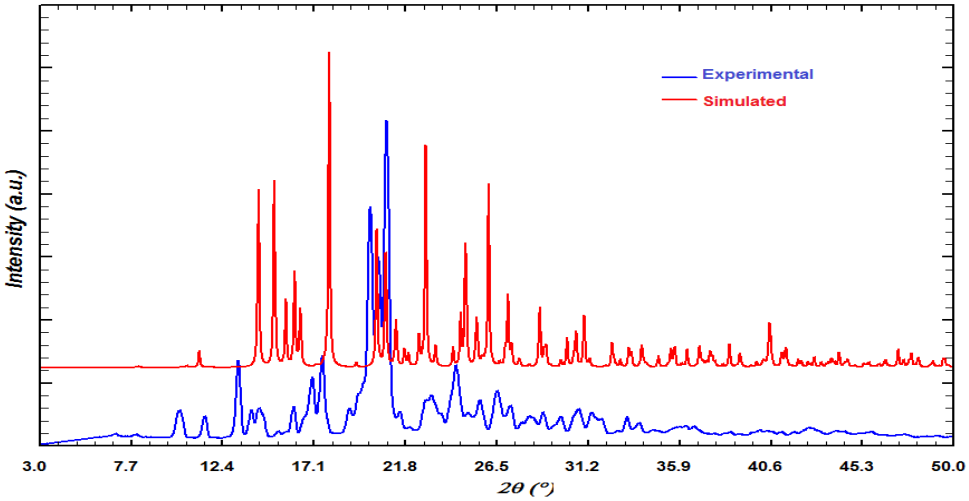


**Figure 4.3.15: (d)** Comparison of experimental and simulated PXRD patterns of **6c-25**

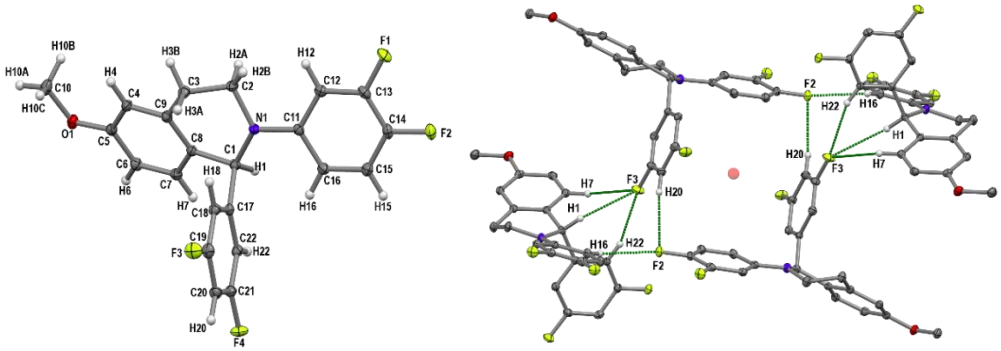

**(a)** **(b)**

**Figure 4.3.16: (a)** ORTEP of **6c-30** drawn with 50% ellipsoidal probability. **(b)** An inversion center related symmetrical dimer synthon formation by one of the bifurcated C20–H20···F2 hydrogen bond.

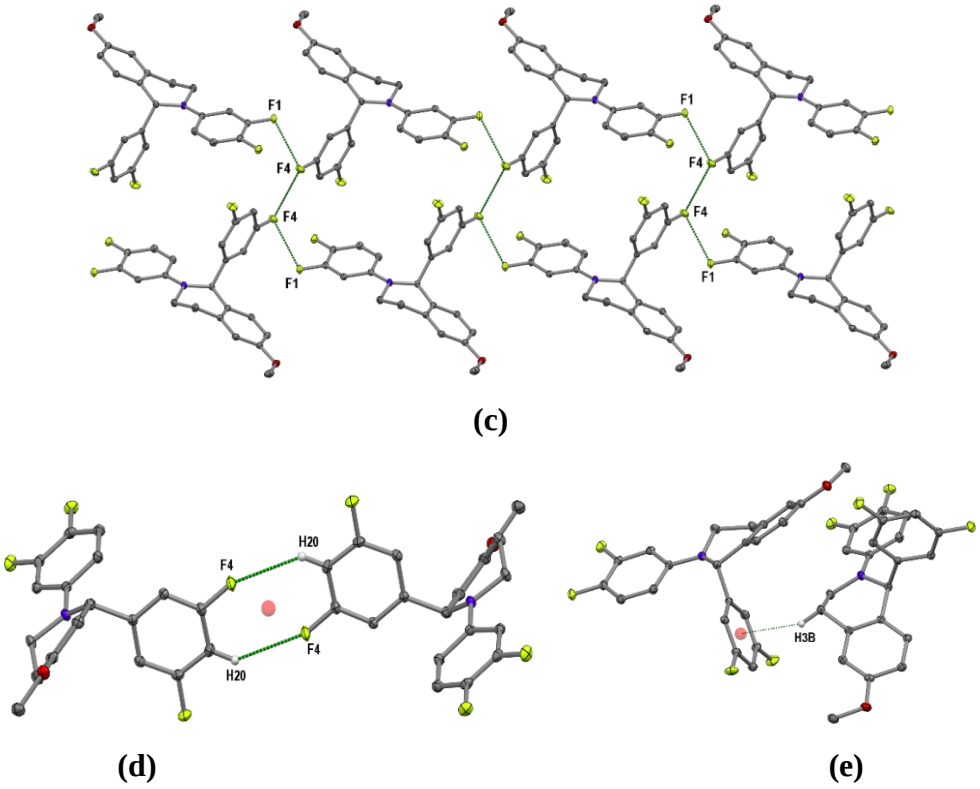


**Figure 4.3.16: (c)** C21–F4···F4–C21 and C21–F4···F1–C13 contact which leads to the formation of one-dimensional ribbon-like structure. **(d)** An inversion center related head to head homo dimer synthon by C20–H20···F4 hydrogen bond. **(e)** A C2–H2B···π ($C_{gB}$) interaction has been observed in 6c-30 structure.

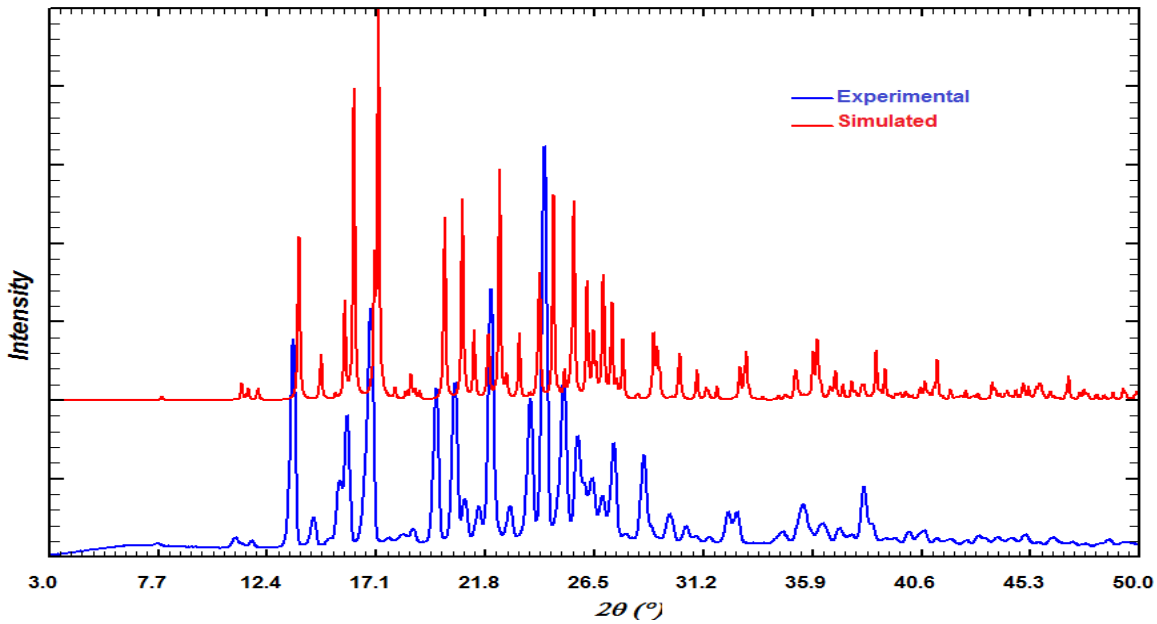


**Figure 4.3.16: (f)** Comparison of experimental and simulated PXRD patterns of **6c-30**

**Table 4.3.16: Intermolecular interactions in 6c-30**

| D–B···A | D–B/Å | *D*(D···A )/ Å | *d*(B···A )/Å | ∠D–B···A/º | SYMMETRY |
|---|---|---|---|---|---|
| **C7–H7···F3** | 1.080 | 3.528(3) | 2.59 | 145 | x-1, $^{3}/_{2}$-y, z-½ |
| **C22–H22···F3** | 1.080 | 3.415(2) | 2.39 | 158 | x-1, $^{3}/_{2}$-y, z-½ |
| **C1–H1···F3** | 1.080 | 3.633(2) | 2.70 | 145 | x-1, $^{3}/_{2}$-y, z-½ |
| **C16–H16···F2** | 1.080 | 3.154(3) | 2.43 | 123 | -x, y+½, ½-z |
| **C20–H20···F2** | 1.080 | 3.351(2) | 2.45 | 140 | 1-x, 1-y, 1-z |
| **C20–H20···F4** | 1.080 | 3.389(2) | 2.54 | 135 | 1-x, 2-y, 1-z |
| **C13–F1···F4–C21** | 1.348(1)<br>1.351(1) | 4.198(2) | 2.871(1) | 109<br>93 | x, y -1, z |
| **C2–H2B···π ($C_{gB}$)** | 1.080 | 3.659(2) | 2.80 | 148 | 1-x, y-½, ½-z |

***N*-(3,5-difluorophenyl)-1-(2,3-difluorophenyl)-6-methoxy-1,2,3,4-tetrahydroisoquinoline (6c-31):** This molecule (**6c-31**) was found to crystallizes in triclinic centrosymmetric *P*-1 space group and the asymmetric unit contained two molecules (Z = 4, Z' = 2), namely molecule A and molecule B (Figure 4.3.17a and Figure 4.3.17b). These two symmetry independent molecules have different molecular conformations. The molecule A of asymmetric unit interacts with another molecule "A" *via* C14–H14···F1, and C16–H16···F2 hydrogen bonds through the inversion center thereby forming two eight-membered dimer synthons (Figure 4.3.17c) (Table 4.3.17). Further the same asymmetric molecule A is interlinked by another molecule of A by C6–H6···F3 hydrogen bond through inversion center creating a dimer unit, which propagates in a particular direction (Figure 4.3.17d). The molecule B of the asymmetric unit also interacts with two molecule B *via* inversion center related as a bifurcated C23–H23···F5, C38–H38···F5 hydrogen bonds and with the molecule A *via* translation symmetry through C25–H25A···F4 hydrogen bond along the *a*-direction (Figure 4.3.17e). Both the molecules of the asymmetric unit offer different F···F contacts. The molecule A of asymmetric unit is linked to another molecule A through the C15–F2···F3–C18 contact across an inversion centre forming a dimer unit, and this dimer unit is further interconnected by another dimer unit by utilization of C13–F1···F4–C19 contact through another inversion centre. Hence the combination of both the C15–F2···F3–C18 and C13–F1···F4–C19 contacts creates 1-D tape like structure along the *a*-direction (Figure 4.3.17f). Similarly, B molecule of the asymmetric unit also generates 1-D tape like structure by the combination of the

bifurcated C37–F5···F7–C40 and C35–F6···F7–C40 contacts along the *a*-direction (Figure 4.3.17g). The experimental PXRD pattern of **6c-31** is matching with the corresponding simulated PXRD pattern (Figure 4.3.17h).

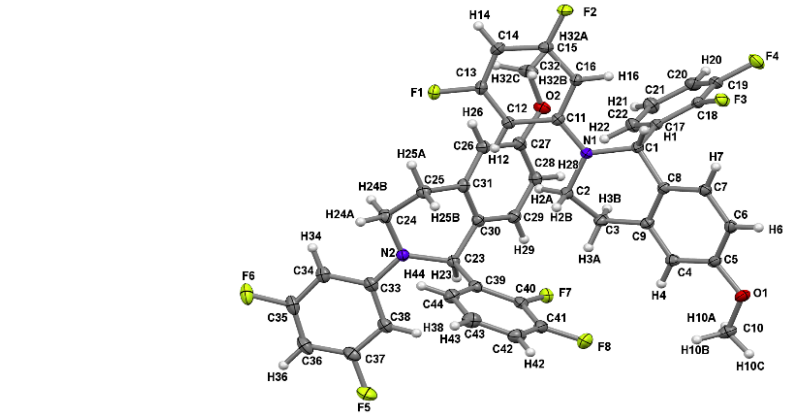


**(a)**

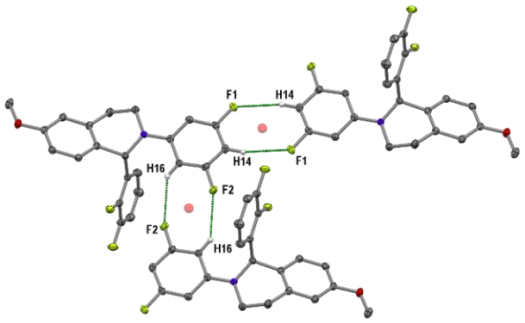


**(b)**

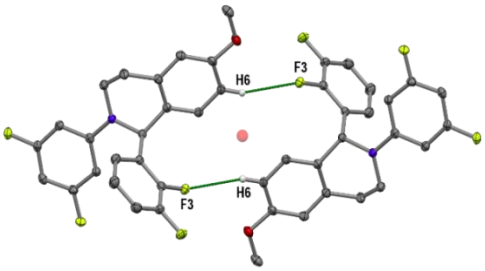


**(c)**

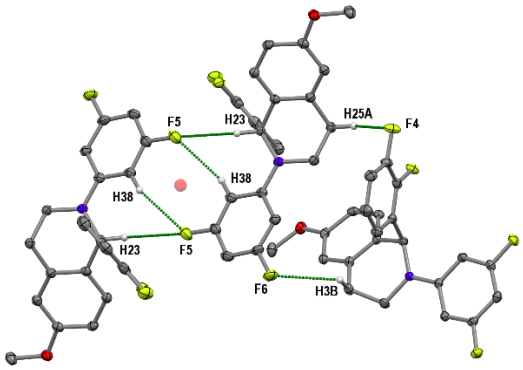


**(d)**

**Figure 4.3.17: (a)** ORTEP of **6c-31** drawn with 50% ellipsoidal probability. **(b)** Eight members double dimer synthon which offered by molecule A of the asymmetric unit. **(c)** Another dimer unit of molecule A by C6–H6···F3 hydrogen bond *via* again inversion center. **(d)** Inversion center related bifurcated C23–H23···F5 and C38–H38···F5 hydrogen bond which offered by the molecule B of the asymmetric unit.

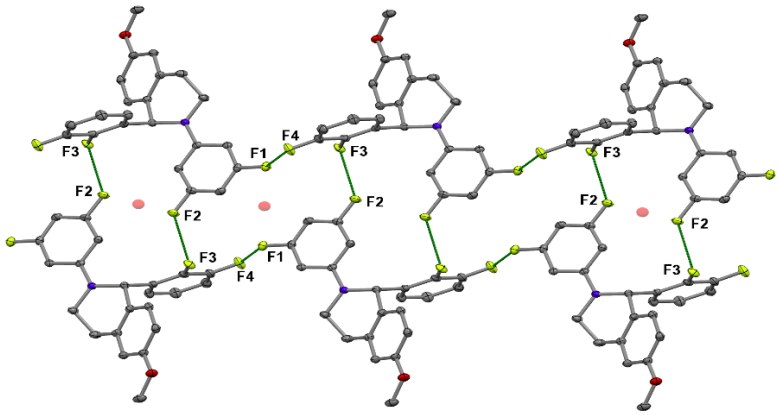


**(e)**

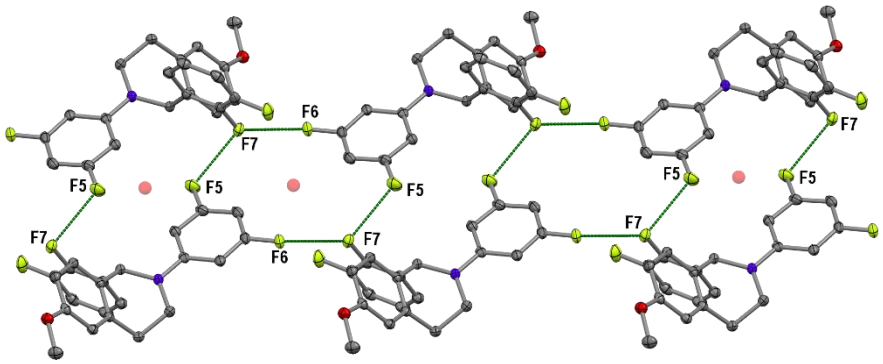


**(f)**

**Figure 4.3.17: (e)** Combination of C15–F2···F3–C18 and C13–F1···F4–C19 contacts leading to the formation of 1-D tape like the structure of molecule A along *a*-direction. **(f)** The B molecule of the asymmetric unit also generates 1-D tape like structure by C37–F5···F7–C40 and C35–F6···F7–C40 contact.

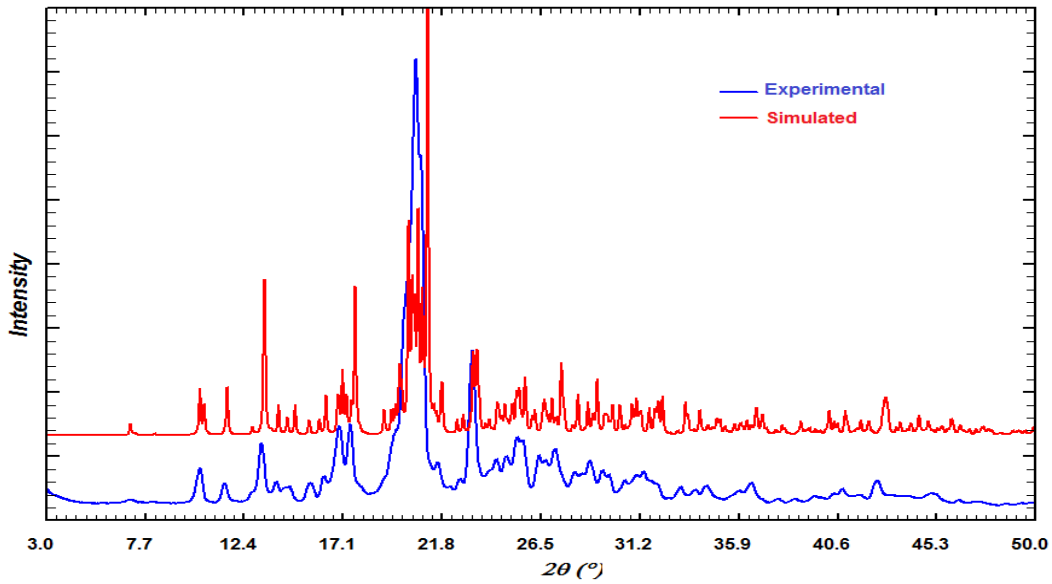


**Figure 4.3.17: (g)** Comparison of experimental and simulated PXRD patterns of **6c-31**

**Table 4.3.17: Intermolecular interactions in 6c-31**

| D–B···A | D–B/Å | *D*(D···A )/Å | *d*(B···A )/Å | ∠D–B···A/º | SYMMETRY |
|---|---|---|---|---|---|
| **C38–H38···F5** | 1.080 | 3.304(2) | 2.38 | 142 | 1 - x, 2 - y, - z |
| **C23–H23···F5** | 1.080 | 3.464(2) | 2.60 | 136 | 1 - x, 2 - y, - z |
| **C16–H16···F2** | 1.080 | 3.336(2) | 2.44 | 139 | - x, - y, 1 - z |
| **C14–H14···F1** | 1.080 | 3.476(2) | 2.43 | 163 | 1 - x, - y, 1 - z |
| **C25–H25A···F4** | 1.080 | 3.467(2) | 2.52 | 146 | x + 1, y, z |
| **C6–H6···F3** | 1.080 | 3.608(2) | 2.58 | 159 | - x - 1, 1 - y, 1 - z |
| **C13–F1···F4–C19** | 1.362(1)<br>1.352(1) | 5.185(2) | 2.921(13) | 140<br>131 | 1 - x, 1 - y, 1 - z |
| **C15–F2···F3–C18** | 1.363(1)<br>1.357(1) | 4.277(2) | 2.950(1) | 127<br>85 | - x, 2 - y, 1 - z |
| **C37–F5···F7–C40** | 1.363(1)<br>1.350(1) | 3.977(2) | 2.804(15) | 120<br>90 | 1 - x, 2 - y, - z |
| **C35–F6···F7–C40** | 1.364(1)<br>1.350(1) | 4.953(2) | 2.889(15) | 134<br>137 | x - 1, y, z |

***N*-(3,5-difluorophenyl)-1-(2,5-difluorophenyl)-6-methoxy-1,2,3,4-tetrahydroisoquinoline (6c-33):** This molecule **6c-33** adopted triclinic centrosymmetric *P*-1 space group, and the asymmetric unit contained two molecules (Z = 4, Z' = 2), namely molecule A and molecule B (Figure 4.3.18a). These two symmetry independent molecules are connected by weak C29–H29···F4 hydrogen bond. The molecule A of asymmetric unit interacts with another molecule A *via* C2–H2B···F1 hydrogen bond through the inversion center and this dimer further interconnected at both sides by C36–H36···F2 and C23–H23···F3 hydrogen bonds thereby creating 1-D molecular chain (Figure 4.3.18b). The molecule B of the asymmetric unit also interacts with a molecule A through C41–H41···F2 and C19–H19···F5 hydrogen bonds *via* translation symmetry and creates a dimer. This dimer is further connected to another dimer by C14–H14···F6 hydrogen bond to form a molecular chain along the *a*-direction (Figure 4.3.18c). Simultaneously the molecule B is also involved in the formation of homo dimer by *head-to-head* contact through the inversion center by C34–H34···F5 hydrogen bond (Figure 4.3.18d). The molecules are connected by the F···F contact (Figure 4.3.18e) as well. The molecule A of asymmetric unit interacts with the molecule B through the C13–F2···F7–C40 and C21–F4···F8–C43 contacts, which leads to the formation of a (Figure 4.3.18e).

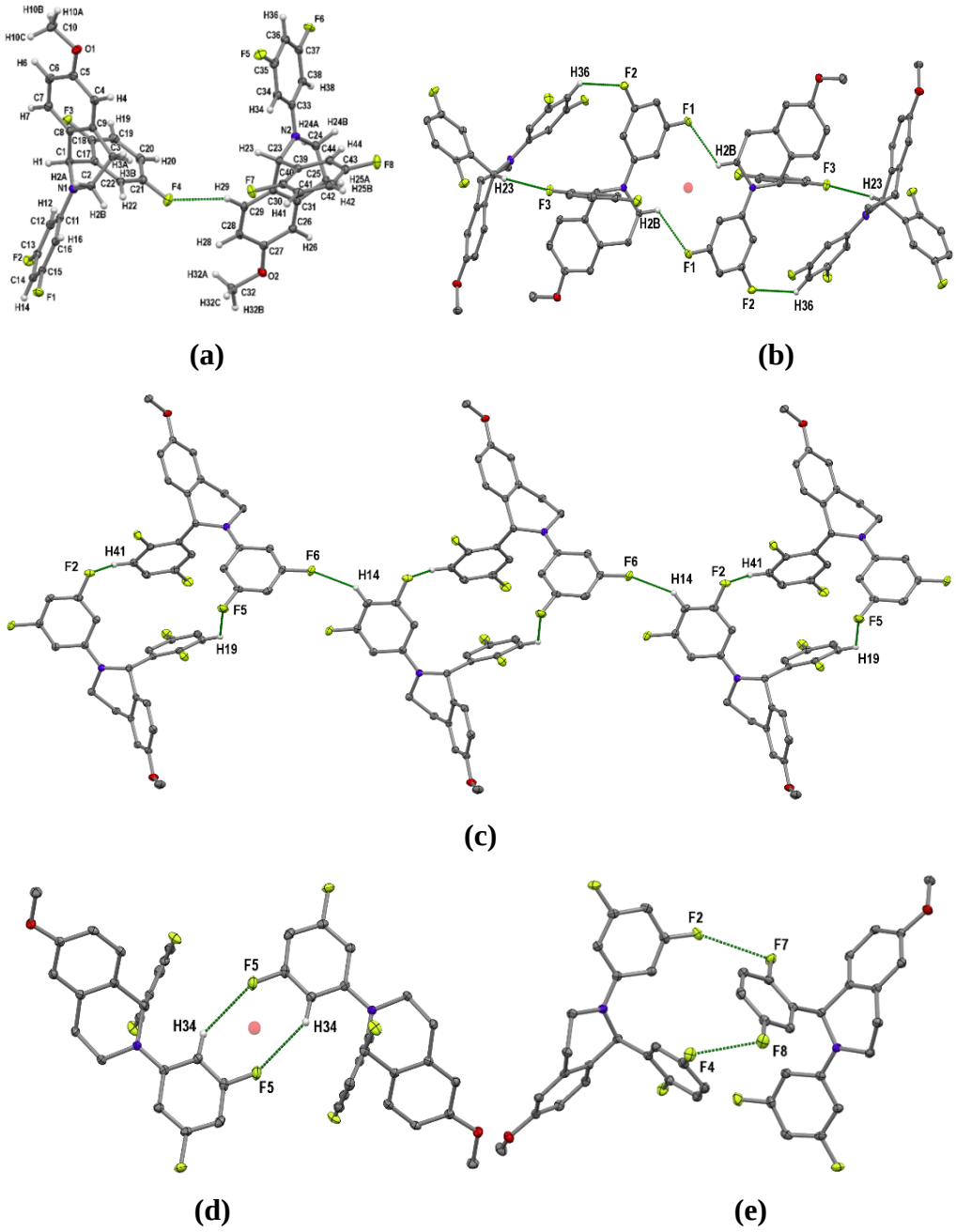


**Figure 4.3.18: (a)** ORTEP of **6c-33** drawn with 50% ellipsoidal probability. **(b)** An inversion center related symmetrical dimer which propagates in both direction by another C36–H36···F2 and C23–H23···F3 hydrogen bond. **(c)** A propagation of dimer unit by C14–H14···F6 hydrogen bond along the *a*-direction. **(d)** Inversion center related C34–H34···F5 and hydrogen bond which offered by the molecule B of the asymmetric unit. **(e)** The combination of C13–F2···F7–C40 and C21–F4···F8–C43 contact leading to the formation of dimer form.

**Table 4.3.18: Intermolecular interactions in 6c-33**

| D–B···A | D–B/Å | *D*(D···A )/Å | *d*(B···A )/Å | ∠D–B···A/º | SYMMETRY |
|---|---|---|---|---|---|
| **C2–H2B···F1** | 1.080 | 3.965(2) | 2.56 | 121 | - |
| **C34–H34···F5** | 1.080 | 3.472(2) | 2.64 | 133 | 2 - x, - y, 1 - z |
| **C36–H36···F2** | 1.080 | 3.202(2) | 2.36 | 133 | 1 - x, - y, 1 - z |
| **C23–H23···F3** | 1.080 | 3.624(2) | 2.63 | 152 | 1 - x, - y, 1 - z |
| **C14–H14···F6** | 1.080 | 3.314(2) | 2.45 | 137 | x - 1, y + 1, z - 1 |
| **C41–H41···F2** | 1.080 | 3.195(2) | 2.41 | 128 | x + 1, y, z |
| **C21–F4···F8–C43** | 1.363(1)<br>1.363(1) | 3.527(2) | 2.841(1) | 106<br>96 | - x, 1 - y, 1 - z |
| **C13–F2···F7–C40** | 1.363(1)<br>1.362(1) | 4.395(2) | 2.841(1) | 145<br>101 | - x,1 - y, 1 - z |

***N*-(3,5-difluorophenyl)-1-(2,6-difluorophenyl)-6-methoxy-1,2,3,4-tetrahydroisoquinoline (6c-34):** The molecule **6c-34** adopted monoclinic $P2_1/c$ space group with Z = 4 and Z' = 1 (Figure 4.3.19a). F2 of the A ring acts as a bifurcated acceptor to form C3–H3B···F2 and C21–H21···F2 hydrogen bonds and offer stabilization to the crystal packing (Figure 4.3.19b) (Table 4.3.19). The C3–H3B···F2 hydrogen bond is also supported by C14–H14···O1 hydrogen bond to make a zig-zag molecular chain by utilization of *c*-glide along the *c*-direction (Figure 4.3.19c). Further the π cloud of the C ring interacts with the H1 hydrogen leading to the C1–H1···π($C_{gC}$) interaction in the crystal structure (Figure 4.3.19d). The experimental PXRD pattern of **6c-34** matcches with the corresponding simulated PXRD pattern (Figure 4.3.19e).

**Table 4.3.19: Intermolecular interactions in 6c-34**

| D–B···A | D–B/Å | *D*(D···A )/ Å | *d*(B···A )/Å | ∠D–B···A/º | SYMMETRY |
|---|---|---|---|---|---|
| **C3–H3B···F2** | 1.080 | 3.470(4) | 2.64 | 133 | x, ½ - y, z - ½ |
| **C14–H14···F1** | 1.080 | 3.427(5) | 2.69 | 125 | 1 - x, - y, 1 - z |
| **C21–H21···F2** | 1.080 | 3.239(4) | 2.42 | 132 | 1 - x, 1 - y, 1 - z |
| **C14–H14···O1** | 1.080 | 3.377(3) | 2.67 | 123 | x, ½ - y, z + ½ |
| **C1–H1··· π ($C_{gC}$)** | 1.080 | 3.629(2) | 2.71 | 154 | 2 - x, 1 - y, 1 - z |

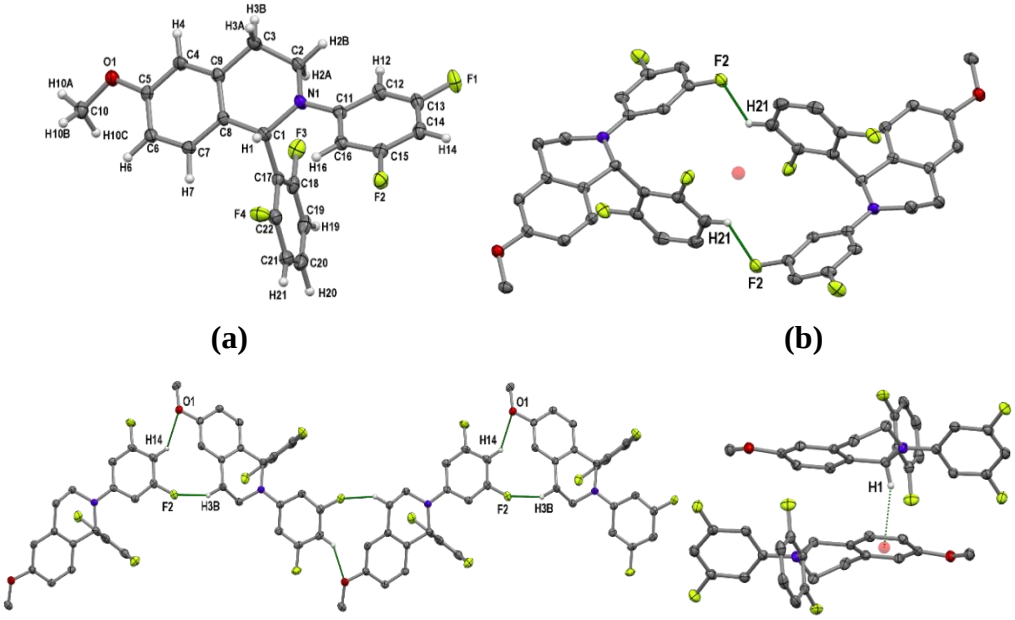


**Figure 4.3.19: (a)** ORTEP of **6c-34** drawn with 50% ellipsoidal probability. **(b)** An inversion center related symmetrical dimer of C21–H21···F2 hydrogen bond. **(c)** The combination of C–H···F and C–H···O hydrogen bonds which leads to the formation of the 1-D molecular chain. **(d)** A C1–H1···π ($C_{gC}$) interaction.

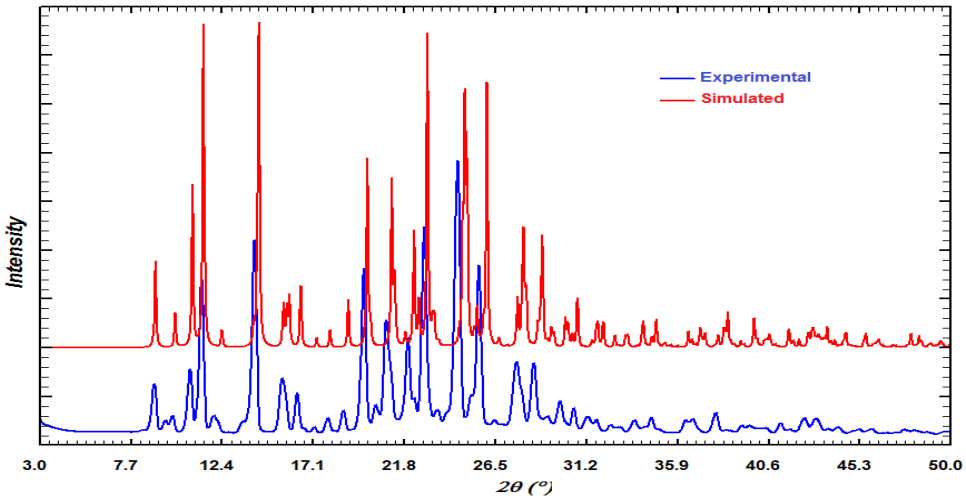


**Figure 4.3.19: (e)** Comparison of experimental and simulated PXRD patterns of **6c-34.**

***N*-phenyl-1-phenyl-6-methoxy-1,2,3,4-tetrahydroisoquinoline (6c-37):** The molecule **6c-37** adopted centrosymmetric monoclinic *Pbca* space group with Z = 8 and Z' = 1 (Figure 4.3.20a). This molecule does not have any fluorine atom so there is no possibility of C–H···F hydrogen bonds. Only the methoxy group acts as a

bifurcated acceptor for weak hydrogen bonds involving H19 of the B ring (C19–H19···O1 hydrogen bond) *via* the *b*-glide leading to the formation of wave like structure along the *b*-direction (Figure 4.3.20b) (Table 4.3.20) and with H15 of the A ring (C15–H15···O1 hydrogen bond) through *b*-glide and creates one-dimensional zig-zag molecular chain along the *b*-direction (Figure 4.3.20c). Both C19–H19···O1 and C15–H15···O1 hydrogen bonds are parallel to each other. Along with the C–H···O hydrogen bond, C7–H7··· $\pi(C_{gA})$ interaction have also been observed in in this crystal structure (Figure 4.3.20d). The experimental PXRD pattern of 6c-37 matches with the corresponding simulated PXRD patterns (Figure 4.3.20e).

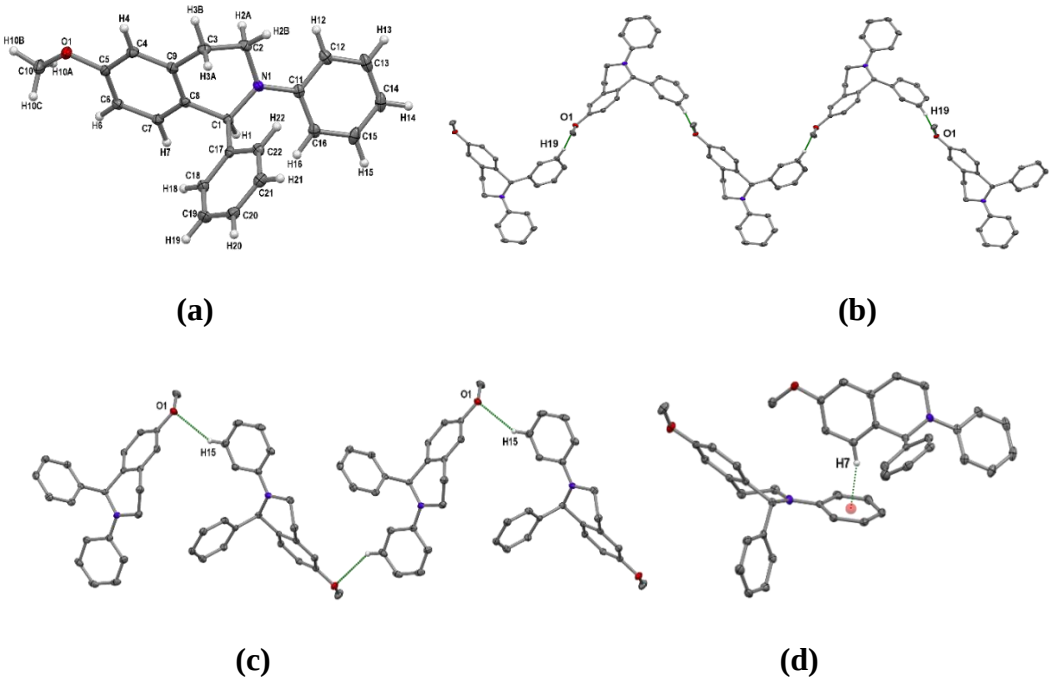


**Figure 4.3.20: (a)** ORTEP of **6c-37** drawn with 50% ellipsoidal probability. **(b)** A wave like structure offered by C19–H19···O1 hydrogen bond. **(c)** C15–H15···O1 hydrogen bond leads to the formation of 1-D zig-zag molecular chai. **(d)** C7–H7···$\pi(C_{gC})$ interaction.

**Table 4.3.20: Intermolecular interactions in 6c-37**

| **D–B···A** | **D–B/Å** | ***D*(D···A )/Å** | ***d*(B···A )/Å** | **∠D–B···A/º** | **SYMMETRY** |
|---|---|---|---|---|---|
| **C15–H15···O1** | 1.080 | 3.270(2) | 2.41 | 135 | ½ - x, y - ½, z |
| **C19–H19···O1** | 1.080 | 3.508(2) | 2.47 | 161 | $^{3}/_{2}$ - x, y - ½, z |
| **C7–H7··· π ($C_{gA}$)** | 1.080 | 3.3345(16) | 2.48 | 150 | x - ½, y, ½ - z |

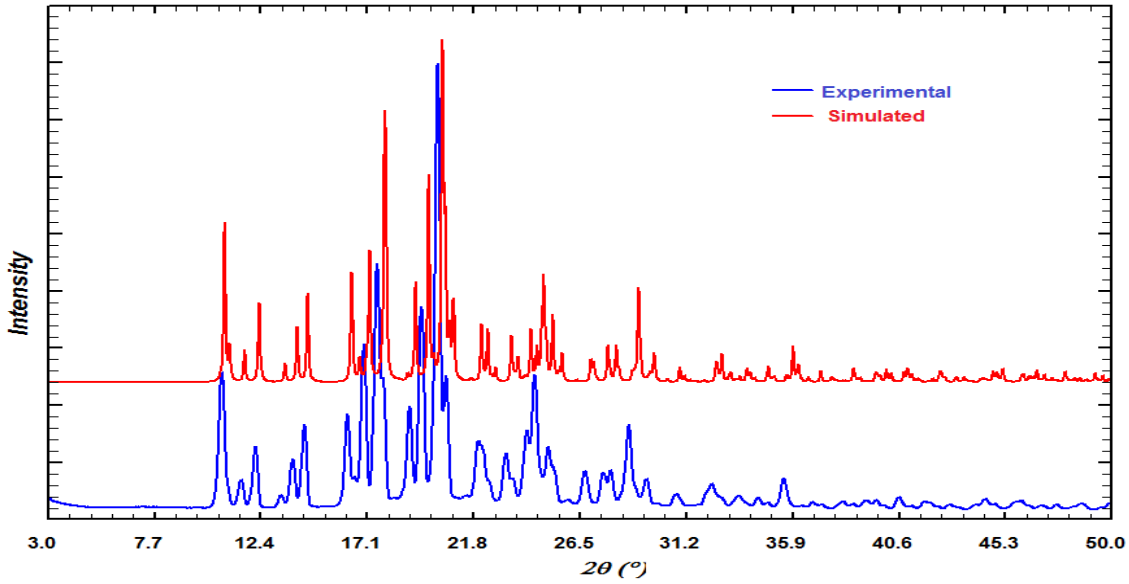


**Figure 4.3.20: (e)** Comparison of experimental and simulated PXRD patterns of **6c-37**

## 4.4 Discussion

The structures of the tetrafluorinated isoquinoline derivatives reported in this chapter display a library of supramolecular assemblies involving mostly the C–F group, which were historically refuted in stabilizing the crystal structures. It is noted that the crystal density of the non-fluorinated analogue (**6c-37**) is the lowest (1.242 g/cm$^3$, like that of **4a-37**) among all the compounds reported here. The density of the fluorinated molecules is found to be between 1.438 g/cm$^3$ and 1.492 g/cm$^3$, comparable to those found for compounds reported in the Chapter 3.

As all these isoquinoline based compounds do not have any strong hydrogen bonding sites, the interaction of these molecules with all types of solvents is through very weak van der Waal's interactions and hence, the solute-solvent interaction in solution is not strong enough to yield different structural variations when these compounds are crystallized from various solvents. Therefore, we did not encounter any polymorphism in these compounds. Fluorine mediated interactions are responsible for building different crystalline architecture in these molecules. The structures of these compounds revealed that the aromatic C–F acceptor groups not only form hydrogen bonds with aromatic C–H donors, but also form hydrogen bonds with –$CH_2$– groups present in the molecule. Aromatic fluorine is seen to form dimers through the 8 membered synthon (I) and through 5 membered synthon (II) involving bifurcated C–F acceptor and in one case a bifurcated C–H donor (III)

(Figure 4.4.1). The synthon (I) has been the most common in all the structures reported in this thesis and the other two synthons have also been observed frequently.

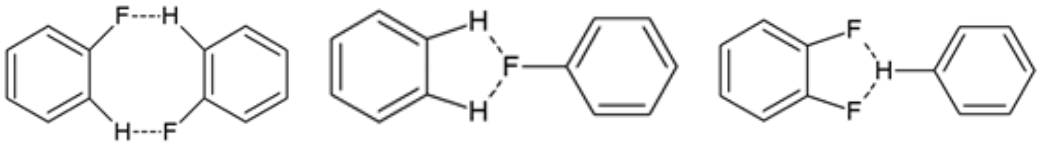


(I) (II) (III)

**Figure 4.4.1:** Supramolecular dimer synthons involving C–F groups

The Table 4.4.1 lists a statistical summary of weak hydrogen bonds observed in this chapter. This table indicates that the fluorine mediated interactions preferentially lie between 120-150$^{o}$ for the ∠C–H···F and the H···F distance ranges from 2.2-2.7 Å. It is also evident from this table that the frequency of fluorine mediated interaction is more than those involving the methoxy group.

**Table 4.4.1: Statistical Summary of C–H···F and C–H···O hydrogen bonds**

| **H···F Distance Range** | **Number of C–H···F hydrogen bonds** | **Angle Range ∠C–H···F** | **Number of C–H···F hydrogen bonds** |
|---|---|---|---|
| **2.2≥d>2.0Å** | 0 | **130≥θ>120.0** | 17 |
| **2.3≥d>2.2Å** | 10 | **140≥θ>130.0** | 16 |
| **2.4≥d>2.3Å** | 8 | **150≥θ>140.0** | 14 |
| **2.5≥d>2.4Å** | 18 | **160≥θ>150.0** | 20 |
| **2.6≥d>2.5Å** | 16 | **170≥θ>160.0** | 6 |
| **2.7≥d>2.6Å** | 20 | **180≥θ>170.0** | 1 |
| **H···O Distance Range** | **Number of C–H···O hydrogen bonds** | **Angle Range ∠C–H···O** | **Number of C–H···O hydrogen bonds** |
| **2.2≥d>2.0Å** | 0 | **130≥θ>120.0** | 9 |
| **2.3≥d>2.2Å** | 0 | **140≥θ>130.0** | 7 |
| **2.4≥d>2.3Å** | 0 | **150≥θ>140.0** | 1 |
| **2.5≥d>2.4Å** | 3 | **160≥θ>150.0** | 0 |
| **2.6≥d>2.5Å** | 5 | **170≥θ>160.0** | 1 |
| **2.7≥d>2.6Å** | 10 | **180≥θ>170.0** | 0 |

It is evident from the structural analysis that the position of C–F group in an aromatic ring does not have any particular preference for the formation of a particular synthon but the change in the position of the C–F group from *ortho*- to *meta*- or from *meta*- to *para*- maintains the same supramolecular synthon as is seen in many cases. In addition to the formation of weak C–H···F hydrogen bond, the molecules have been seen to offer plenty of C–F···F–C interactions in the structure

of many molecules. A careful investigation of these C–F···F–C interactions indicate that these interactions can also be classified as one of Type I, Type II or quasi Type I/Type II, just like the same was done for other C–X···X–C (X = Cl, Br and I) interactions by Thodadi *et al.*[39] It is also noted that the C–F···F–C interactions can also be bifurcated in nature and hence. This observation indirectly indicates that the electron density distribution around the F atom in a C–F bond is non-uniformly distributed; hence there are electron rich and electron deficient regions, which can either donate or accept electrons simultaneously from another similar C–F group. This can only be established by an accurate experimental charge density analysis of these molecules, which is beyond the scope of the current thesis.

We have also compared these tetrafluorinated compounds with their di and mono fluorinated analogues reported earlier.[50a,b,d] It was observed that the compounds having the fluorine substitution at the *ortho*- position of the phenyl ring (A or B ring) had intramolecular C–H···F–C hydrogen bond. If the F atom was present at the *ortho*- position in the A ring then the C–H···F–C hydrogen bond was found involving either C1–H1 and/or C2–H2(A/B) forming a six membered intramolecular hydrogen bond thereby restricting the rotation of N1–C11 bond. On the other hand, if the F atom was present at the *ortho*- position in the B ring then the C–H···F–C hydrogen bond was found involving either C1–H1 and/or C7–H7 and/or C2–H2(A/B) forming a five or seven membered intramolecular hydrogen bond thereby restricting the rotation of C1–C17 bond. The same trend has been observed in the molecules reported in this chapter. For the compounds having F at the *ortho*- position of the A or B ring, the corresponding intramolecular hydrogen bond was inevitable and hence the rotation of the A or B ring was restricted for those molecules about the N1–C11/C1–C17 bond (Figure 4.4.2).

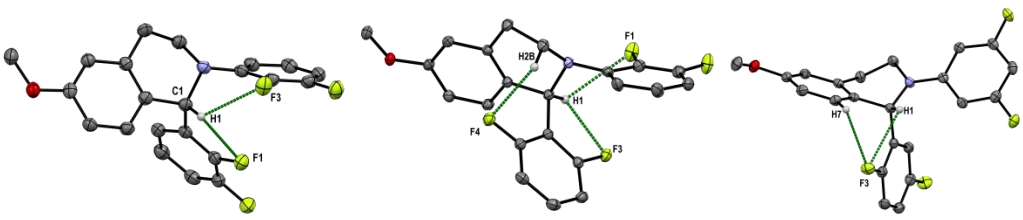


**(a)** **(b)** **(c)**

**Figure 4.4.2:** Representative molecules having intramolecular C–H···F–C hydrogen bond(s) (a) **6c-1**, (b) **6c-4**, (c) **6c-33**.

The compounds containing the fluorine at the *meta*- position only in the earlier reported structures indicated the appearance of disorder in the fluorophenyl ring about the N1–C11 bond or the C1–C17 bond. This disorder was earlier attributed to the competition between the weak C–H···F–C hydrogen bond and C–F···F–C interaction. In our current study, if the molecule has a F atom at the *ortho*-position then the corresponding fluorophenyl ring is conformationally locked and hence the fluorine at the *meta*- position either enjoies C–H···F–C hydrogen bond or opts for C–F···F–C interaction. But, if the A or B ring is not conformationally locked by the intramolecular hydrogen bond and there is F atom at the *meta*-position of the A or B ring then the said disorder becomes possible due to the free rotation of A/B ring about N1–C11 bond and/or the C1–C17 bond. In reality, this has been observed in only structure (**6c-23**). A careful observation of other such molecules revel that the fluorine at the *meta*- position of the A ring in **6c-25** and **6c-30** is responsible for the formation of C–F···F–C interaction. In other similar compounds show the preference of the fluorine at the *meta*- position for C–H···F–C hydrogen bond against the possible C–F···F–C interaction.

The reported mono or difluoro analogues containing fluorine at the *para*-position were found to offer either C–H···F–C hydrogen bond and/or C–F···F–C interaction. In the structures reported here we observed that the fluorine at the *para*-position either formed C–H···F–C hydrogen bond or not participated in any intermolecular interaction.

## 4.5 Conclusion

The structural analyses of the fluorinated isoquinoline derivative have been carried out at low temperature (100.0K) to analyse the weak intermolecular interactions involving organic fluorine in these molecules. Some of the purified compounds were found to be dense liquid and hence their structural study could not be conducted. The compounds, which produced good quality crystals were structurally studied. Some of the molecules have shown static orientational disorder of the fluorophenyl ring(s) but none of them resulted into polymorphism. All the molecules were packed in 3D lattices with different unit cell parameters and in a variety of space groups. The packing of these molecules was guided by weak intermolecular interactions involving fluorine, thereby generating different

supramolecular architecture through three different supramolecular synthons in addition to a simple C–H···F–C hydrogen bond between the two molecules. C–F···F–C interactions of all the types were found to play a significant role in the packing.

**References:**


1. Desiraju, G. R.; Steiner, T. *The Weak Hydrogen Bond in Structural Chemistry and Biology*; Oxford University Press: Oxford, **1999**
2. Pauling, L. *The nature of the chemical bond and the structure of molecules and crystals*; Cornell University Press: Ithaca, NY, 1939.
3. (a) Pauling, L. *The nature of the chemical bond and the structure of molecules and crystals: an introduction to modern structural chemistry*; Cornell University Press: Ithaca, NY, 1960, Vol. 18. (b) Pauling, L.; Delbrück, M. *Science* **1940**, *92*, 77−79.
4. (a) Jeffrey, G. A.; Saenger, W., *Hydrogen bonding in biological structures*; Springer−Verlag: Berlin, 1991. (b) Jeffrey, G. A. *An Introduction to Hydrogen Bonding*; Oxford University Press: Oxford, 1997.
5. Pimentel, G. C.; McClellan, A. L. *Hydrogen bonding*: *Annual Review of Physical Chemistry* **1971**, *22*, 347−385.
6. (a) Steiner, T.; Saenger, W. *Journal of the American Chemical Society*, **1993**, *115*, 4540–4547. (b) Steiner T. *Angew chem. Int. Ed. Engl*. **2002**, *41*, 48−76.
7. (a) Arunan, E.; Desiraju, G. R.; Klein, R. A.; Sadlej, J.; Scheiner, S.; Alkorta, I.; Clary, D. C.; Crabtree, R. H.; Dannenberg, J. J.; Hobza, P.; Kjaergaard, H. G.; Legon, A. C.; Mennucci, B.; Nesbitt. D. *J. Pure Appl. Chem.* **2011**, *83*, 1637−1641. (b) Desiraju, G. R. *Angew. Chem., Int. Ed.* **2011**, *50*, 52−59.
8. (a) Seto, C. T.; Whiteside, G. M. *J. Am. Chem. Soc.* **1993**, *115*, 905−916. (b) Zimmerman, S. C.; Corbin, P. S. *Struct. Bonding* **2000**, *96*, 63−94. (c) Prins, L. J.; Reinhoudt, D. N; Timmerman, P. *Angew. Chem. Int. Ed*. **2001**, *40*, 2382–2426. (d) Yamauchi, K.; Lizotte, J. R.; Long, T. E. *Macromolecules* **2002**, *35*, 8745−8750. (e) Park, P.; Zimmerman, S. C. *J. Am. Chem. Soc*. **2006**, *128*, 11582−11590. (f) Bouteiller, L. *Adv. Polym. Sci*. **2007**, *27*, 79−112; (g) Wua, Y. -C.; Kuo, S. -W. *J. Mater. Chem.* **2012**, *22*, 2982−2991.
9. (a) Atwood, J. L.; Steed, J. W. *Encyclopedia of Supramolecular Chemistry, Volume 1*; CRC Press: 2004; pp 357−363. (b) Hamilton, A. D. *Supramolecular control of structure and reactivity, Perspectives in supramolecular chemistry*; Wiley: Chichester, 1996, Vol. 3.

10. Aakeröy, C. B.; Fasulo, M. E.; Desper, J. *Mol. Pharmaceutics.* **2007**, *4*, 317-322.
11. (a) Etter, M. C.; *Acc. Chem. Res*. **1990**, *23*, 120–126. (b) Etter, M. C.; Admond, D. A. *J. Chem. Soc. Chem. Commun.* **1990**, 589−591. (c) Ermer, O.; Eling, A. *J. Chem. Soc. Perkin Trans. 2.* **1994**, 925−944. (d) Aakeroy, C. B.; Desper, J.; Fasulo, M.; Hussain, I.; Levin, B.; Schultheiss, N. *CrystEngComm* **2008**, *10*, 1816−1821. (e) Aakeroy, C. B.; Salmon, D. J.; *CrystEngComm* **2005**, *7*, 439–448. (f) Choudhury, A. R.; Yufit, D. S.; Howard, J. A. K. *Z. Kristallogr*. **2014**; *229,* 625-634.
12. (a) Glasstone, S. *Trans. Faraday Soc.* **1937**, 200−214. (b) Desiraju, G. R.; Steiner, T. *The Weak Hydrogen Bond in Structural Chemistry and Biology*; Oxford University Press: Oxford, 1999; pp 30. (b) Gordy, W. J. *Chem. Phys.* **1939**, *7*, 163−166. (c) Dougill, M. W.; Jeffrey, G. A. *Acta Crystallogr*. **1953**, *6*, 831−837. (d) Jones, G. P.; Cornell, B. A.; Horn, E.; Tieklink, E. R. T. *J. Cryst. Spectro. Res.* **1989**, *19*, 715−723. (e) Sutor, D. J. *Acta Crystallogr.* **1958**, *11*, 453–458. (a) Sutor, D. J. *Nature* **1962**, *195*, 68–69. (f) Sutor, D. J. *J. Chem. Soc.* **1963**, 1105−1110. (g) Taylor, R.; Kennard, O. *J. Am. Chem. Soc.* **1982**, *104*, 5063−5070. (h) Allen, F. H.; Kennard, O.; Taylor, R. *Acc. Chem. Res.*, **1983**, *16,* 146–153. (i) Pedireddi, V. R. *Cryst. Growth Des.*, **2001**, *1*, 383−385. (j) Boryczka, S.; Rozenberg, M. S.; Schreurs, A. M. M.; Kroon, J.; Starikov, E. B.; Steiner, T. *New J. Chem.* **2001**, *25*, 1111−1113. (k) Pedireddi, V. R. *CrystEngComm* **2002**, *4*, 315−317. (l) Domagała, M.; Grabowski, S. J.; Urbaniak, K.; Mloston´, G. *J. Phys. Chem. A* **2003**, *107*, 2730−2736. (m) Steiner, T. *Crystallography Reviews*, **2003**, *9*, 177−228. (n) Dev, S.; Maheswari, S.; Choudhury, A. R. *RSC Adv.* **2015,** *5,* 26932-26940.
13. (a) Desiraju, G. R. *Acc. Chem. Res*. **1991**, *24*, 290−296. (b) Steiner, T. *Angew. Chem. Int. Ed.* **2002**, *41*, 48−76.
14. Desiraju, G. R. *Acc. Chem. Res.* **2002**, *35*, 565–573.
15. Allen, F. H.; Kennard, O.; Taylor, R. *Acc. Chem. Res.* **1983**, *16*, 146–153.
16. (a) Desiraju, G. R. *Acc. Chem. Res*. **1991**, *24*, 290−296. (b) Pedireddi, V. R. *Crystal Growth & Design*, **2001**, *1*, 383−385. (c) Boryczka, S.; Rozenberg, M. S.; Schreurs, A. M. M.; Kroon, J.; Starikov, E. B.; Steiner, T. *New J. Chem.*

**2001**, *25*, 1111−1113. (d) Pedireddi, V. R. *CrystEngComm* **2002**, *4*, 315−317. (e) Steiner, T. *Angew. Chem. Int. Ed.* **2002**, *41*, 48−76. (f) Domagała, M.; Grabowski, S. J.; Urbaniak, K.; Mloston´, G. *J. Phys. Chem. A* **2003**, *107*, 2730−2736. (g) Steiner, T. *Crystallography Reviews*, **2003**, *9*, 177−228.

17. (a) Sarma, J. A. R. P.; Desiraju, G. R. *Acc. Chem. Res*. **1986**, *19*, 222−228. (b) Desiraju, G. R. *Acc. Chem. Res*. **1996**, *29*, 441−449. (c) Langley, P. J.; Hulliger, J.; Thaimattam, R.; Desiraju, G. R. *New J. Chem.* **1998**, *22*, 1307−1309. (d) Foces-Foces, C.; Jagerovic, N.; Elguero, J. *Acta Crystallogr., Sect. C* **2000**, *56*, 215−218. (e) Wolstenholme, D. J.; Weigand, J. J.; Cameron, E. M.; Cameron, T. S. *Phys. Chem. Chem. Phys*. **2008**, *10*, 3569−3577.
18. (a) Etter, M. C. *Acc. Chem. Res*. **1990**, *23*, 120−126. (b) Aakeroy, C. B.; Evans, T. A.; Seddon, K. R.; Palink, I´. O´. *New J. Chem*. **1999**, *23*, 145−152. (c) Jeffrey, G. A. *Crystallogr. Rev*. **2003**, *9*, 135−176. (d) Steiner, T. *Crystallogr. Rev*. **2003**, *9*, 177−228. (e) Virdo, J. D.; Crandall, L.; Dang, J. D.; Fulford, M. V.; Lough, A. J.; Durfee, W. S.; Bender, T. P. *CrystEngComm* **2013**, ***15***, 8578−8586.
19. (a) Pascard, C. *Acta Cryst*. **1995**, *D51*, 407−417. (b) Glusker, J. P. *Acta Cryst*. **1995**, *D51*, 418−427. (c) Pierce, A. C.; Sandretto, K. L.; Bemis G. W. *Proteins Struct. Funct. Bioinf*. **2002**, *49*, 567−576. (d) Pierce, A. C.; Haar, E.; Binch, H. M. *J. Med. Chem*. **2005**, *48*, 1278−1281. (e) Nayak, S. K.; Mallik, S. B.; Kanaujia, S. P.; Sekar, K.; Ranganathan, K. R.; Ananthalakshmi, V.; Jeyaraman, G.; Saralaya, S. S.; Rao, K. S.; Shridhara, K. *CrystEngComm* **2013**, *15*, 4871−4884.
20. Malone, J. F.; Murray, C. M.; Charlton, M. H.; Docherty, R.; Lavery, A. J. *J. Chem. Soc. Faraday Trans*. **1997**, *93*, 3429–3436. (b) Perutz, M. F. *Philos. Trans. R. Soc. London Ser. A* **1993**, *345*, 105–112.
21. Desiraju, G. R.; Steiner, T. *The Weak Hydrogen Bond in Structural Chemistry and Biology*; Oxford University Press: Oxford, 1999; pp 155.
22. (a) Nishio, M.; Hirota, M. *Tetrahedron* **1989**, *45*, 7201–7245. (b) Nishio, M.; Umezawa, Y.; Hirota, M.; Takeuchi, Y. *Tetrahedron* **1995**, *51*, 8665–8701.
23. Nishio, M.; Hirota, M.; Umezawa, Y. *The CH/πInteraction. Evidence, Nature, and Consequences*; Wiley-VCH: New York, USA, 1998.
24. Nishio, M. *CrystEngComm.* **2004**, *6*, 130–158.
25. Tatko, C. D.; Waters, M. L.; *J. Am. Chem. Soc*. **2004**, *126*, 2028−2034.

26. (a) Brandi, M.; Weiss, M. S.; Jabs, A.; Suhnel, J.; Hilgenfeld, R. *J. Mol. Biol.* **2001**, *307*, 357−377. (b) Steiner, T.; Koellner, G. *J. Mol. Biol.* **2001**, *305*, 535–557. (c) Bhattacharya, R.; Chakrabarti, P. *J. Mol. Biol*. **2003**, *331*, 925−940.
27. (a) Muller, K.; Wegner, G. *Electronic Materials: The Oligomer Approach*; Wiley-VCH: Weinheim, 1998. (b) Österbacka, R.; An, C. P.; Jiang, X. M.; Vardeny, Z. V. *Science* **2000**, *287*, 839–842.
28. (a) Liu, C. -S.; Sun, G. -H.; Li, M.; Guo, L. -Q.; Zhou, L. -M.; Fang, S. -M. *Open Crystallography Journal* **2008**, *1*, 24−30. (b) Goel, M.; Jayakannan. M. *Chem. Eur. J*. **2012**, 1*8*, 11987–11993.
29. (a) Ozawa, T.; Tsuji, E.; Ozawa, M.; Handa, C.; Mukaiyama, H.; Nishimura, T.; Kobayashi, S.; Okazaki, K. *Bioorganic & Medicinal Chemistry* **2008**, *16*, 10311−10318. (b) Kumari, M.; Balaji, P. V.; Sunoj, R. B. *Phys. Chem. Chem. Phys*. **2011**, *13*, 6517−6530. (c) Sogawa, K.; Okuda, R.; In, Y.; Ishida, T.; Taniguchi, T.; Minoura, K.; Tomoo, K. *J. Biochem.* **2012**, *152*, 221−229.
30. Saraogi, I.; Vijay, V. G.; Das, S.; Sekar, K.; Guru Row, T. N. *Cryst. Engg.* **2003**, *6*, 69−77.
31. Hassel, O.; Romming, C. *Quart. Rev. Chem. Soc*. **1962**, *16*, 1−18.
32. Auffinger, P.; Hays, F. A.; Westhof, E.; Shing Ho, P. *Proc. Natl. Acad. Sci. U. S. A.* **2004**, *101*, 16789−16794.
33. (a) Robinson, J. M. A.; Kariuki, B. M.; Harris, K. D. M.; Philip, D. *J. Chem. Soc., Perkin Trans. 2* **1998**, *11*, 2459−2470. (b) Moorthy, J. N.; Natarajan, R.; Mal, P.; Venugopalan, P. *J. Am. Chem. Soc*. **2002**, *124*, 6530−6531. (c) Gonnade, R. G.; Bhadbhade, M. M.; Shashidhar, M. S.; Sanki, A. K. *Chem. Commun*. **2005**, *47*, 5870−5872. (d) Reddy, C. M.; Kirchner, M. T.; Gundakaram, R. C.; Padmanabhan, K. A.; Desiraju, G. R. *Chem. Eur. J*. **2006**, *12*, 2222−2234. (e) Gonnade, R. G.; Shashidhar, M. S.; Bhadbhade, M. M. *J. Indian Inst. Sci.* **2007**, *87*, 149−165. (f) Berger, R.; Resnati, G.; Metrangolo, P.; Weberd, E.; Hulliger, *J. Chem. Soc. Rev*. **2011**, *40*, 3496-3508.
34. (a) Aakeröy, C. B.; Evans, T. A.; Seddon, K. R.; Palink, I. *New J. Chem*. **1999**, *23*, 145−152. (b) Gibb, C. L. D.; Stevens, E. D.; Gibb, B. C. *J. Am. Chem. Soc*. **2001**, *123*, 5849−5850.
35. van den Berg, J. A.; Seddon, K. R. *Cryst. Growth Des*. **2003**, *3*, 643−661.

36. Sakurai, T.; Sundaralingam, M.; Jeffrey, G. A. *Acta Crystallogr*. **1963**, *16*, 354−363.
37. Ramasubbu, N.; Parthasarathy, R.; Murray-Rust, P. *J. Am. Chem. Soc*. **1986**, *108*, 4308−4314.
38. (a) Desiraju, G. R.; Partasarathy, R. *J. Am. Chem. Soc.* **1989**, *111*, 8725−8726; (b) Hathwar, V. R.; Roopan, S. M.; Subashini, R.; Khan, F. N.; Guru Row, T. N. *J. Chem. Sci*. **2010**, *122*, 677–685.
39. Tothadi, S.; Joseph, S.; Desiraju, G. R. *Cryst. Growth Des*. **2013**, *13*, 3242–3254.
40. (a) Taylor, R.; Kennard, O. *J. Am. Chem. Soc.* **1982**, *104*, 5063−5070. (b) Han, Z.; Zhao, Y.; Peng, J.; Tian, A.; Liu, Q.; Ma, J.; Wang, E.; Hu, N. *CrystEngComm* **2005**, *7*, 380−387. (c) Wei, H. -Q.; Jin, W. -J. *Fenxi Huaxue* **2007**, *35*, 1381−1386. (c) Takemura, A.; McAllister, L. J.; Karadakov, P. B.; Pridmore, N. E.; Whitwood, A. C.; Bruce, D. W. *CrystEngComm* **2014**, *16*, 4254−4264. (d) Baldrighi, M.; Bartesaghi, D.; Cavallo, G.; Chierotti, M. R.; Gobetto, R.; Metrangolo, P.; Pilati, T.; Resnati, G.; Terraneo, G. *CrystEngComm* **2014**, *16*, 5897−5904. (e) Metrangolo, P.; Meyer, F.; Pilati, T.; Resnati, G.; Terraneo, G. *Angew. Chem. Int. Ed.* **2008**, *47*, 6114–6127.
41. (a) Thalladi, V. R.; Weiss, H. C.; Bla1ser, D.; Boese, R.; Nangia, A.; Desiraju, G. R. *J. Am. Chem. Soc.* **1998**, *120*, 8702−8710. (b) Politzer, P.; Lane, P.; Concha, M. C.; Ma, Y.; Murray, J. S. *J. Mol. Model*. **2007**, *13*, 305–311. (c) Clark, T.; Hennemann, M.; Murray, J. S.; Politzer, P. *J. Mol. Model*. **2007**, *13*, 291–296. (d) Herlitzke, B. J.; Ojala, W. H. Abstracts of Papers, *247th ACS National Meeting & Exposition*, Dallas, TX, United States, March 16−20, **2014** (2014), CHED−1113.
42. (a) Schlosser, M. *Angew. Chem. Int. Ed*. **1998**, *110*, 1496−1513 and references therein. (b) Smart, B. E. *J. Fluorine Chem*. **2001**, *109*, 3−11 and references therein.
43. (a) Dunitz, J. D.; Taylor, R. *Chem. Eur. J.* **1997,** *3,* 89–98. (b) Dunitz; J. D. *ChemBioChem* **2004**, *5*, 614–621.
44. Zhou, P.; Zou, J.; Tian, F.; Shang, Z. *J. Chem. Inf. Model*. **2009**, *49*, 2344–2355
45. O'Hagon, D. *Chem. Soc. Rev.* **2008**, *37*, 308-319.
46. Shimoni, L.; Glusker, J. P. *Struct. Chem.* **1994**, *5*, 383– 397.

47. Howard, J. A. K.; Hoy, V. J.; O'Hagan, D.; Smith, G. T. *Tetrahedron* **1996**, *52*, 12613–12622.
48. Thalladi, V. R.; Weiss, H. C.; Bläser, D.; Boese, R.; Nangia, A.; Desiraju, G. R. *J. Am. Chem. Soc.* **1998**, *120*, 8702–8710.
49. Choudhury, A. R.; Nagarajan, K.; Guru Row, T. N. *Acta Crystallogr. Sect. C: Cryst. Struct. Commun.* **2004**, *60*, o644−o647.
50. (a) Choudhury, A. R.; Urs, U. K.; Guru Row, T. N.; Nagarajan, K. *J. Mol. Struct.* **2002**, *605*, 71–77. (b) Choudhury, A. R.; Guru Row, T. N. *Cryst. Growth Des.* **2004**, *4*, 47–52. (c) Choudhury, A. R.; Nagarajan, K.; Guru Row, T. N. *Cryst. Eng.* **2003**, *6*, 43–55. (d) Choudhury, A. R.; Guru Row, T. N. *CrystEngComm* **2006**, *3*, 265–274.
51. (a) Chopra, D.; Guru Row, T. N. *CrystEngComm* **2008**, *10*, 54– 67. (b) Nayak, S. K.; Reddy, M. K.; Guru Row, T. N.; Chopra, D. *Cryst. Growth Des.* **2011**, *11*, 1578–1596. (c) Nayak, S. K.; Reddy, M. K.; Guru Row, T. N.; Chopra, D. *CrystEngComm.* **2012**, *14,* 200-210.
52. (a) Panini, P.; Chopra, D. *CrystEngComm* **2012**, *14*, 1972–1989. (b) Panini, P.; Chopra, D.; *CrystEngComm*. **2013**, *15*, 3711–3733.
53. Karanam, M.; Choudhury, A. R. *Cryst. Growth Des.* **2013**, *13*, 4803– 4814.
54. (a) Kaur, G.; Panini, P.; Chopra, D.; Choudhury, A. R. *Cryst. Groth Des*. **2012**, *12*, 5096–5110. (b) Kaur, G.; Choudhury, A. R. *Cryst. Growth Des.* **2014**, *14*, 1600–1616. (c) Kaur, G.; Choudhury, A. R. *CrystEngCom.* **2015**, *17*, 2949–2963. (d) Kaur, G.; Singh, S.; Sreekumar, A.; Choudhury, A. R. *J. Mol. Struct*. **2016**, *1106*, 154–169.
55. *The Cambridge Structural Database, version 5.38. ConQuest 1.19*; Cambridge Crystallographic Data Centre: Cambridge, U.K., Nov 2016,
56. (a) Schwarzer, A.; Seichter, W.; Weber, E.; Stoeckli-Evans, H.; Losada, M.; Hulliger, J. *CrystEngComm*, **2004**, *6*, 567−572. (b) Schwarzer, A.; Weber, E. *Cryst. Growth Des*. **2008**, *8*, 2862−2874. (c) Asensio, G.; Medio-Simon, M.; Alema´n, P.; Arellano, C. R. de *Cryst. Growth Des*. **2006**, *6*, 2769−2778. (d) Schwarzer, A.; Bombicz, P.; Weber, E. *J. Fluorine Chem*. **2010**, *131*, 345−356.
57. Prasanna, M. D.; Guru Row, T. N. *Cryst. Eng*. **2000**, *3*, 135−154.
58. Chopra, D.; Guru Row, T. N. *CrystEngComm.* **2011**, *13*, 2175–2186.
59. Chopra, D. *Cryst. Growth Des.* **2012**, *12*, 541–546.

60. Parsch J.; Engels J. W.; *J. Am. Chem. Soc*., **2002**, *124*, 5664–5672
61. Frohlich, R.; Rosen, T. C.; Meyer, O. G. J.; Rissanen, K.; Haufe, G. *J. Mol. Struct*. **2006**, *787*, 50−62.
62. (a) Lee H.; Knobler C. B.; Hawthorne M. F.; *Chem. Commun*. **2000**, 2485–2486. (b) Abad A.; Agullo C.; Cunat A. C.; Vilanova C.; Arellano M. C. R.; *Cryst. Growth Des*. **2006**, *6*, 46–57. (c) Mehta G.; Sen S.; *Eur. J. Org. Chem*. **2010**, 3387–3394.
63. Shukla, R.; Chopra, D. *CrystEngComm*. **2015**, *17*, 3596–3609.
64. Koch, U.; Popelier, P. L. *J. Phys. Chem*. **1995**, *99*, 9747–9754
65. Nagarajan, K.; Talwalker, P. K.; Kulkarni, C. L. *Ind. J. Chem.* **1985**, *24B*, 83−97.
66. Chopra, D.; Row, T. N. G. *J. Mol. Struct.* **2005**, *733*, 133-141.
67. Chopra, D.; Thiruvenkatam, V.; Row, T. N. G. *J. Mol. Struct.* **2006**, *6*, 843−845.
68. Lai, C.; Brain, G. Cox, *J. Org. Chem.* **2007**, *72*, 8863−8869.
69. CrystalClear2.0, Rigaku Corporation, Tokyo, Japan.
70. Dolomanov, O.V.; Bourhis, L.J.; Gildea, R. J.; Howard, J. A. K.; Puschmann, H. *J. Appl. Cryst*. **2009**, *42*, 339-341.
71. Sheldrick, G.M.; *Acta Cryst.* **2008**, *A64*, 112-122.
72. Sheldrick, G.M.; *Acta Cryst*. **2015**. *A71*, 3-8.
73. Macrae, C. F.; Bruno, I. J.; Chisholm, J. A.; Edgington, P. R.; McCabe, P.; Pidcock, E.; Rodriguez-Monge, L.; Taylor, R.; Streek, J.; Wood, P. A *J. Appl. Crystallogr.* **2008**, *41*, 466–470.
74. Nardelli, M. *J. Appl. Crystallogr*. **1995**, *28*, 569.
75. Spek, A. L. *Acta Crystallogr.* **2009**, *D65*, 148–155.
76. (a) Prasad, A. S. B.; Bhaskarkanth, J. V.; Periasamy, M. *Tetrahedron* **1992**, *48*, 4623–4628
(b) Harrison, C. R.; Hodge, P.; Hunt, B. J.; Khoshdel, E.; Richardson, G. *J. Org. Chem.* **1983**, *48*, 3721- 3728.

**Publications from PhD thesis**

1. "Can C–H···F–C hydrogen bonds alter crystal packing features in the presence of N–H···O=C hydrogen bond?" **Yadav**, **H. R.** and Choudhury, A. R. (manuscript under review).

2. "How important are fluorine mediated interactions in controlling the crystal packing in the presence of C–H···O=C hydrogen bonds?" **Yadav, H. R.** and Choudhury, A. R. (manuscript submitted).

3. "Structural variations invoked by fluorine mediated interactions in fluorinated tetrahydroisoquinoline derivatives" **Yadav, H. R.** and Choudhury, A. R. (manuscript under preparation).

**Publications from collaborations**

1. Mondal, P. K.; **Yadav, H. R.**; Choudhury, A. R. Chopra, D. *Acta Crystallogr. Sect. B* (in press).

2. Dey, D.; Das, S.; **Yadav, H. R**.; Ranjani, A.; Gyathri, L.; Roy, S.; Guin, P. S.; Dhanasekaran, D.; Choudhury, A. R.; Akbarsha, M. A.; Biswas, B., *Polyhedron* **2016,** *106*, 106-114.

3. Dey, D.; Pal, S.; **Yadav, H. R**.; Sengupta, P. S.; Choudhury, A. R.; Kole, N.; Biswas, B. *RSC Adv.* **2015,** *5* (53), 42681-42688.

4. Dey, D.; **Yadav, H. R**.; De, A.; Chatterjee, S.; Maji, M.; Choudhury, A. R.; Kole, N.; Biswas, B. *J. Coord. Chem.* **2014,** *68* (1), 169-180.

5. Ghosh, A. K.; Mitra, M.; Fathima, A.; **Yadav, H**. **R**; Choudhury, A. R.; Nair, B. U.; Ghosh, R. *Polyhedron* **2016,** *107*, 1-8.

6. Dey, D.; **Yadav, H. R**.; De, A.; Sengupta, P. S.; Choudhury, A. R.; Kole, N.; Biswas, B. *Chemistry select* **2016,** *1*, 1910-1916.

7. Mal, S. K.; Mitra, M.; **Yadav, H. R.**; Purohit, C. S.; Choudhury, A. R.; Ghosh, R., *Polyhedron* **2016**, *111*, 118-122.

8. De, A.; Garai, M.; **Yadav, H. R.;** Choudhury, A. R.; Biswas, B.; *Appl. Organometal. Chem*. **2017**, *31*, e3551.

**9.** Garai; M.; Dey, D.; Kole, N.; **Yadav, H. R.**; Choudhury, A. R.; Biswas, B. (Manuscript Submitted).

**10.** Kachwal, V.; Parvej, A.; **Yadav, H. R.;** Sheik, P.; Choudhury, A. R.; Inamur, L. (Manuscript Submitted)